An Integrated Study of $CaCO_3$ Formation and Inhibition

Aurélie Charlotte Martinod

Submitted in accordance with the requirements for the degree of
Doctor of Philosophy

The University of Leeds
School of Mechanical Engineering

October, 2008

The candidate confirms that the work submitted is his/her own and that appropriate credit has been given where reference has been made to the work of others.

Acknowledgements

First I would like to express my gratitude to Professor Anne Neville. I would like to thank her for giving me the opportunity to work with her and for trusting me and supporting me during this project. The scientific knowledge and the supervision of my work and most of all the motivation she kept sharing with me for the last three years were a valuable help.

A special thank to Myriam Euvrard for assisting my work in Besancon University and for the time she spent on my project. Many thanks to all the team from Besancon University for their help and their warm welcome (Alexandra, Cedric, Claudine...).

I would like to thank the FAST team from Edinburgh for their financial support, their advice and their involvement in this project. A special thank to Ken, Eric, Christine, Lorraine, Mike, Oscar and Robin, for the entertainment during the trips in Heriot Watt University.

I appreciate the work done from the technicians from Leeds and Heriot-Watt Universities: Keith, Graham, Tony and Walter. Many thanks to Jackie, always available and helpful. Thank you to all the Coserg team for their support and it was very pleasant to work and to share the everyday life with them. A very special thank to the Scale team. It has been great to work with you and to share special moments, thanks to Eleftheria for listening, Violette for her daily good mood and to Wendy for her friendliness. Thank you to Helene for her help in the electrodeposition study.

I would like to tell my family (my parents, siblings and grand parents) and my friends that without their support and their kindness this journey would not have been the same. Thanks to Violette, Eleftheria, Rob, Bertram, Juan, Diego, Kosta, Natalia, Rock, Cecilia, Georgio, Olivier, Michele, Thibaut, Hélène, Francky, Emerick, Anne-lise V, Dorothée, Christian, Raf, Manu, Florent, Stéphanie, Greg, Elsa, Fanny, Emilie, Sandrine, Anne-lise T. Laëtitia, Mélanie B., Florian., Antoine S., Caroline, Ismaël, Cecile, Yverain, Maude, Laurent and Mélanie H..

Last but not least, I would like to express a thousand thanks to Antoine for his support, his trust in me and his eternal positivism. Thank you.

Abstract

The management of mineral scale is a challenge in many industrial fields and environmental issues relating to eutrophication are leading industry to develop environmentally-friendly solutions to scale control. The determination of the strategy of inhibition is a real challenge as many factors influence the formation of calcium carbonate formation and affect the performance of scale inhibitors.

The processes of $CaCO_3$ formation on a surface have been studied. The mechanisms of inhibition of three green (Carboxymethyl Inulin, CMI, Polymaleic acid, PMA and Polyaspartic acid, PA) and one conventional (Polyphosphinocarboxylic acid, PPCA) scale inhibitors of calcium carbonate nucleation and growth have been investigated. The interactions between the chemicals and the surface have been studied by chronoamperometry. The use of surface analysis enabled these interactions to be characterised. The *in-situ* electrochemical flow cell permitted the characterisation of the crystals formed (size, number and surface coverage of the electrode) and the affinity of the chemicals to inhibit the nucleation and/or the growth to be determined. Important information on the different effects of scale inhibitors on $CaCO_3$ polymorphs has been found by use of Synchrotron X-Ray Diffraction (SXRD) as an *in-situ* method for crystal characterisation.

The inhibitors partly inhibit the deposition of $CaCO_3$ by forming a film on the deposition surface. The interactions between the inhibitors and the metal surface occur via the cations Ca^{2+} and/or Mg^{2+}. The adsorption of the chemicals on the crystals of $CaCO_3$ has been investigated and it appears that the PPCA, PMA and PA act by blocking the growth sites of the crystals. Each inhibitor exhibits an affinity to the surface of deposition and with the $CaCO_3$ crystals but to a different extent resulting in different inhibition efficiencies. The PPCA affected greatly the deposition of $CaCO_3$ and PA and PMA exhibited similar effects. Nevertheless the PA is more efficient when it is present during the nucleation step or early crystallisation whereas PMA acts more during the growth process. The SXRD permitted three steps of growth to be detected in the non-inhibited case and PMA, PA, CMI act by reducing the growth of the different planes whereas the PPCA totally inhibited two main crystal planes (the aragonite (032) and the vaterite (300)) and an acceleration of the growth of the calcite C(006) and of the aragonite A(111) was observed.

Contents

Figures

Tables

List of publications

- A. Martinod, H. Job. A. Neville, K. Sorbie. *Electrodeposition of $CaCO_3$ and the effects of Inhibitors/Surface Interactions.* Chemistry in the Oil Industry X, Royal Society of Chemistry (RSC), November 2007, Manchester, UK

- A Martinod, M. Euvrard, A. Foissy, A. Neville. *Progressing the understanding of chemical inhibition of mineral scale by green inhibitors.* Desalination, 220 (1-3), 345-352, 2008.

- A. Martinod, A. Neville, K. Sorbie. *Synchrotron X-ray diffraction: in-situ study of $CaCO_3$ formation and inhibition by a green polymer (PMA)*, to be published in Desalination 2008.

- A Martinod, A. Neville, M. Euvrard. *Experimental investigation of scaling control by a non-phosphorous polymer: polyaspartic acid*, to be published in Desalination 2008.

- A. Martinod, A. Neville, K. Sorbie, Z. Zhong. *Assessment of $CaCO_3$ inhibition by the use of Synchrotron X-Ray Diffraction on a metallic substrate.* NACE International, CORROSION 2008, March 2008, New Orleans, USA,

- A. Martinod, A. Neville, K. Sorbie. *Electrodeposition of a calcareous layer: Effects of green inhibitors.* Submitted to Chemical Engineering Sciences.

Nomenclature

ΔG: Free energy ($kJ.mol^{-1}$)

Δf: Changes in oscillating frequencies

γ: Free surface energy (J)

σ: Surface energy

ρ: Density of a particle ($g.\mu m^{-3}$)

Γ: Amount of a chemical adsorbed ($mg.m^{-2}$)

ν: Kinematic viscosity ($cm^2\ s^{-1}$)

ω: Angular velocity ($rad\ s^{-1}$)

[Ca]: Molar concentration of calcium ($mol.l^{-1}$)

a: Ionic activity

A(t): Surface area of a crystal (cm^2)

A: Electrode area (cm^2)

A: Nucleation rate constant (s^{-1})

C: Concentration of reactant ($mol.l^{-1}$)

C^b: Bulk concentration ($mol\ dm^3$)

D: Diffusion coefficient of the electroactive species ($cm^2\ s^{-1}$).

E: Potential (V)

F: Faraday's constant (96487 $C\ mol^{-1}$)

f: Shape factor

g: Kinetic order of growth

i_L: Limiting current density ($mA.cm^{-2}$)

IP: Activity product

K'_s: Solubility product

k_v: Volume shape factor

k_l: Lateral growth rate ($mol/\mu m/s$)

K: Constant of affinity

M: Molecular weight ($g.mol^{-1}$)

m: Molar concentration ($mol.l^{-1}$)

m_0 : Solubility

m_{adh}: Mass of solid adhered (g)

N: Number of crystals

N_0: Active nucleation sites (μm^{-2})

n: Number of electrons involved in the reaction

P: Perimeter of a crystal

r: equivalent radius of the crystal

r_c : Critical radius

Ra: Surface roughness

S: Supersaturation ratio

S: Surface area of a crystal

S(t): Surface coverage (%)

$S_{ext}(t)$: Extended surface coverage (%)

T: Temperature

t: Time

t_{ind}: Induction time

t_s: Scaling time

R_g: Gas constant (8.3143 $J.mol^{-1}K^{-1}$).

V(t): Volume of the crystal at time t

W(t): Total mass of crystals at time t

$W_{No\ SI}$: Mass of the calcareous deposit formed in absence of inhibitor

W_{SI}: Mass of the calcareous deposit formed in the presence of inhibitor

Chapter 1
Introduction

1.1 Oil and gas: the major energetic source

The emergence of new technology and the changes in living habits have lead to high and increasing energy consumption. Figure 1.1 illustrates the increase of energy consumption according to the energetic source from 1990 and this increasing requirement for energy will keep increasing until 2030 according to prediction models. The energy based on oil and gas is the major energetic source.

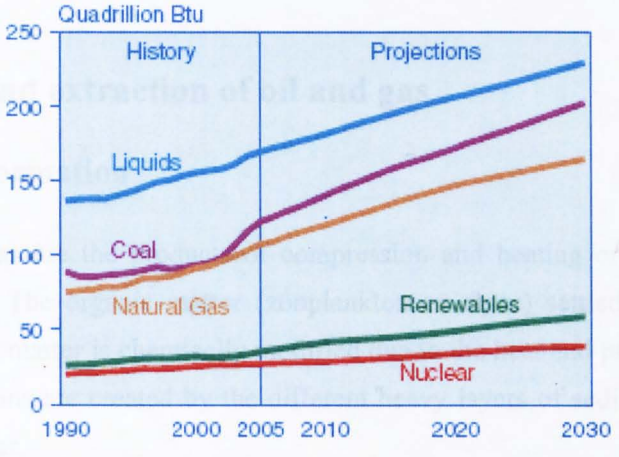

Liquid fuels and other petroleum include petroleum-derived fuels and non-petroleum-derived fuels, such as ethanol and biodiesel, coal-to-liquids, and gas-to-liquids. Petroleum coke, which is a solid, is included. Also included are natural gas liquids, crude oil consumed as a fuel, and liquid hydrogen.

Figure 1.1: World marketed energy use by fuel type, 1990-2030 [1]

The greatest oil consumers are Saudi Arabia with 27.4 barrels per year per inhabitant, Canada with 25.9, the United States with 25.4, Belgium with 22.5 and the Netherlands with 21.2. The United Kingdom, France, Italy and Germany consume between 11 and 12 barrels per year per inhabitant. Brazil and China only used 4.2 and 1.8 barrels per year per inhabitant respectively but their consumptions increased by 28 and 102% respectively during the last ten years.

The production of oil and gas needs to follow the trend of their consumption. Saudi Arabia, Russia, the United States, Iran, Mexico, China, Norway, and Canada produced more than 3,000,000 barrels per day in 2004 with production of 10411, 9261, 7228, 4106, 3825, 3485, 3189 and 3056 10^3 barrels a day respectively. It is important to note that some countries like Brazil, Kazakhstan and Qatar increased their oil production by 220%, 280% and 87% in 10 years.

The oil and gas reserves have been estimated and calculations were realised based on the consumption in 2005 and the needs in oil are covered for the next 40 years and the gas reserves are greater and should provide an energetic source for the next 60 years.

1.2 Formation and extraction of oil and gas

1.2.1 Oil and gas formation

Crude oil and gas are the products of compression and heating organic matter over geological time scale. The organic matter (zooplankton or algae) settled to a sea or lake bottom and the organic matter is chemically modified due to the heat and pressure conditions. These extreme conditions are created by the different heavy layers of sediment accumulated above the organic matter.

Uren defined a reservoir as a body of porous and impermeable rock containing oil and gas, through which fluids may move toward recovery opening under the pressures existing or that may be applied [2]. An oil reservoir is composed of the hydrocarbon material, a porous and permeable reservoir rock in which the crude oil and the gas accumulates and an impermeable seal to block the oil and gas to reach the surface. The oil and gas can migrate with the underground water flows for hundred of kilometres horizontally until the liquid is trapped in a reservoir. The water is heavier than oil and the gas is lighter than oil thus the three component liquid when trapped in a reservoir is organised according to a three layer model: water at the bottom, oil and then gas on the top.

1.2.2 Process of extraction

Wells are drilled in the reservoir for the extraction phase. The primary recovery occurs if the pressure in the reservoir is sufficient to force the oil to the surface. Usually 20% of the oil can be extracted by primary recovery.

The second recovery is used when the underground pressure drops stopping the primary recovery. In that case pumps can be used to extract the remaining oil. Techniques which increase the reservoir pressure are also used in the secondary recovery. The injection of water in the wells leads to an increase of the pressure and the water displace the oil from the reservoir to a production well. 35% of the oil of a reservoir can be extracted by primary and secondary extraction.

The tertiary recovery improves the oil extraction by gas injection, chemical injection and thermal recovery. 30 to 60% of the oil can be recovered by tertiary recovery. The viscosity of the oil is decreased during this process of extraction to improve the flow rate of the oil. The techniques aiming to heat the oil to reduce its viscosity are called Thermally Enhanced Oil Recovery method (TEOR) (steam can be injected). 5 to 15% of the oil present in the reservoir can be recovered by this technique.

1.3 Scale formation: problems and remedies

1.3.1 Problems encountered

Salts precipitation occurs when a system is not at the ionic equilibrium. This can be promoted by the changes of temperature and pressure or by introducing a brine which is not at equilibrium with the system. The formation of scale can occur in the reservoir which can lead to the blocking of the pores of the porous media. Thus oil can be trapped in the substrate and its extraction becomes impossible. During the extraction process the extreme conditions of temperatures and pressures lead to scale formation on the installation surfaces. The formation of scale in the pipes can lead to a large reduction of the flow as shown in Figure 1.2. The damage of safety valves can also be a consequence of the presence of scale on the installation. These blockages can lead to unscheduled shutdown and deferred oil production [3].

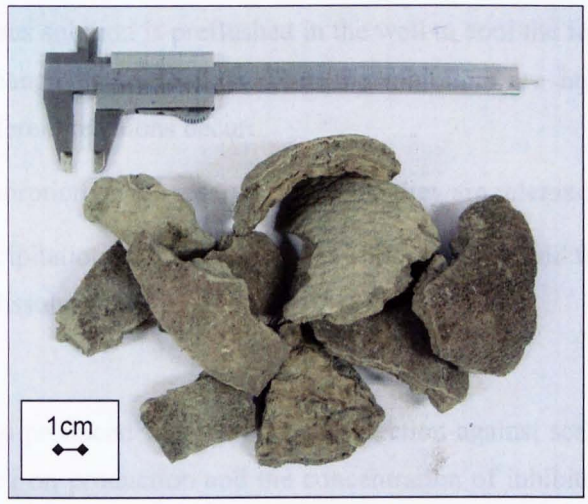

Figure 1.2: Fouling material (calcium carbonate) that has been cleared from a pipe [4]

1.3.2 Current remedies

The addition of chemicals is the common method to reduce scale formation. The additives are injected during a squeeze treatment. The principles of the squeeze treatment are summarised in Figure 1.3. The scale inhibitors are injected in the production well (opposed to the injection wells). The well is then shut in during the treatment.

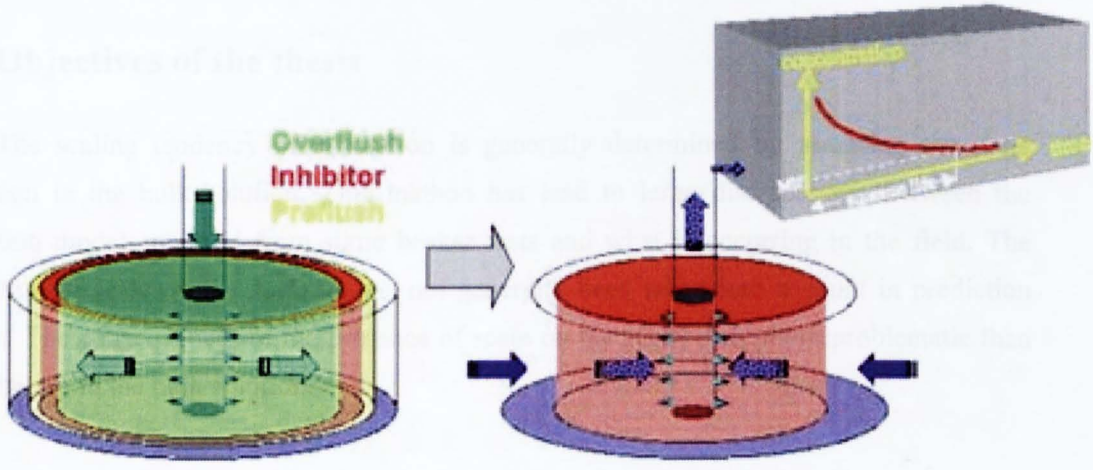

Figure 1.3: Principle of the squeeze treatment [5]

First a dilute aqueous solution is preflushed in the well to cool the formation in the near wellbore area and to change its wettability. Then the inhibitors are injected and retained within the rock. Two different reactions occur:

- Adsorption on the reservoir rock and they are released by desorption,
- Precipitation in the formation as solid or liquid and they are released by re-dissolution

Their release in the produced water provides protection against scaling. After the shut in the well is placed back on production and the concentration of inhibitors in the produced water is assessed and when this concentration is below the threshold level for effective inhibition (Minimum Inhibition Concentration), the treatment is repeated [3, 6].

The scale inhibitors used are then released in the environment. The discharge of these chemicals has an impact on the environment. Green chemistry has come to be the focus of some industry, primarily due to introduction of legislation to control the discharge of chemicals which are likely to have an effect on the biological cycle.

1.4 Objectives of the thesis

The scaling tendency of a solution is generally determined by assessing the scale formation in the bulk solution. This method has lead to large discrepancies between the prediction models realised from static beaker tests and what is occurring in the field. The deposition of scale on the surfaces has not generally been taken into account in prediction models. The consequences of the presence of scale on the surface are more problematic than precipitation in the bulk solution.

This study is focused on the deposition of calcium carbonate onto a metal surface and its inhibition by different chemicals. The mechanisms of inhibition have been investigated for four different scale inhibitors: the phosphinopolycarboxylic acid (PPCA), the polymaleic acid (PMA), the polyaspartic acid (PA) and the carboxymethyl inulin (CMI). The PPCA is a commercial inhibitor widely used in the oil and gas field and it has been taken as a reference in this study. The PMA, the PA and the CMI are environmental friendly (green) and are seriously considered as alternatives to current non-green technologies.

The main aim of the thesis is to provide a new understanding of $CaCO_3$ formation and inhibition at a surface. The specific objectives of the thesis are described below:

- *To quantify the efficiency of selected chemicals to inhibit $CaCO_3$.* Four chemicals have been tested and their ability to reduce $CaCO_3$ deposition has been studied. The aim is to compare in which extent different molecules slow down the deposition of calcium carbonate.

- *To determine the mechanisms of inhibition.* $CaCO_3$ deposition occurs under different steps and the inhibitors can act on one or several steps. The aim is to assess the different mechanisms of inhibition and to link it with the efficiency in order to determine the most efficient strategy of inhibition.

- *To use an innovative in-situ SXRD technique to probe the mechanisms of growth and inhibition.* The laboratory conditions are often very different from the field conditions therefore this project (SXRD study) is focused on the study of $CaCO_3$ deposition and inhibition in realistic conditions in terms of nature of the substrate, temperature and pressure. An important objective of this study was to determine the mechanism of inhibition at the crystal plane level to point out any affinity between the chemicals and some specific crystals.

1.5 Thesis layout

A brief introduction of the oil and gas extraction and the problems generated by scale formation during the extraction process is presented in Chapter 1 as well as the objectives of this thesis.

Chapter 2 gives background on the different types of scale encountered in the oil and gas field and on the formation of calcium carbonate. The literature review is presented. A review of the different methodologies to study $CaCO_3$ formation and the different parameters influencing this process is given. Then the mechanisms of inhibition and the different inhibitors used in the industry are reported. This chapter ends with a presentation of different principles of green chemistry and its application in the oil and gas industry.

The principles of the methodology (Electrodeposition and Synchrotron X-Ray Diffraction, SXRD) used in this study are explained in Chapter 3. The set-up used with these different methods are described as well as the mathematical model used to extract the data from the electrochemical *in-situ* study. The analysis techniques (contact angle measurement and Fourier Transform Infra-Red spectroscopy) are also described.

Chapters 4, 5 and 6 present the results obtained in this study.

The electrodeposition tests conducted in static conditions under non-inhibited and inhibited conditions are presented in Chapter 4. The surface of deposition has been characterised by contact angle measurements and infra-red spectroscopy.

Chapter 5 gives the results obtained with the *in-situ* electrochemical cell. The morphology of the crystals of $CaCO_3$ has been investigated.

The effects of the scale inhibitors on the different crystal planes during the nucleation and growth process of $CaCO_3$ are described with the SXRD study.

In Chapter 7 the results are discussed. The contribution made by the thesis is presented through reference to the current work in the field.

Chapter 8 presents the conclusions raised from this thesis and Chapter 9 introduces some recommendations for future work.

Chapter 2
Background on calcium carbonate formation and literature review

2.1 Introduction

In the oil and gas sector, mineral scale formation is a major flow assurance problem. The scale tendency and the type of scale depends on the water chemistries and the mineralogy of the environment.

Table 2.1 presents a summary of the common carbonate and sulphate scales encountered in the oil and gas field and their relative solubilities. It is interesting to note the large range of solubility concerning the sulphate scales. The sulphate scales are harder to remove as they are not acid soluble scales [7].

Table 2.1: Common scale mineral, their composition, their relative solubility and physical conditions that cause their formation [8].

Mineral type	Composition	Relative solubility (mg/L)	Causes of solubility change
Calcite	$CaCO_3$	196	pCO_2, Total pressure, TDS, Temperature
Siderite	$FeCO_3$	100	pCO_2, Total pressure, TDS, Temperature
Barite	$BaSO_4$	44	Pressure, TDS, Temperature
Celestite	$SrSO_4$	520	Pressure, TDS, Temperature
Anhydrite	$CaSO_4$	3270	Pressure, Temperature
Gypsum	$CaSO_4.H_2O$	6300	Pressure, Temperature

Conditions 100°C, solution 1m of NaCl, pH7, Anhydrite present at over 100°C, Gypsum present at less than 100°C. TDS: Total Dissolved Salts

The two main encountered mineral scales in the oil and gas field are calcium carbonate ($CaCO_3$) and barium sulphate ($BaSO_4$). The calcium ions and the bicarbonate ions present in the produced water are responsible for the formation of calcium carbonate. When the water passes through the carbon dioxide bubble point (due to the decrease of the pressure), CO_2 is lost into the gas phase and as seen with the equilibrium presented in Equation 2.1 for the case of calcium carbonate, the precipitation of carbonate scale occurs.

$$Ca^{2+}\ (aq) + 2HCO_3^-\ (aq) \leftrightarrow CaCO_3\ (s) + CO_2\ (g) + H_2O\ (l) \qquad \textbf{Equation 2.1}$$

Moreover a consequence of the loss of carbon dioxide is the increase of the pH (as illustrated in the Equation 2.2) resulting in a reduction of the solubility of calcium carbonate [9].

$$CO_2\ (g) + H_2O\ (l) \leftrightarrow H_2CO_3\ (aq) \leftrightarrow HCO_3^-\ (aq) + H^+\ (aq) \qquad \textbf{Equation 2.2}$$

The sulphate scales can form when the injection water containing sulphate ions is mixed with the formation water containing barium ions. Thus according to Equation 2.3 precipitation of barium sulphate occurs. It is likely to find barium sulphate scale when barium ions are present in the formation water and sulphate in the injection as the solubility of this scale is vey low (Table 2.1).

$$Ba^{2+} + SO_4^{2-} \leftrightarrow BaSO_4 \qquad \textbf{Equation 2.3}$$

This study was focused only on one scale: calcium carbonate. The aim of this chapter is to present a theoretical background on calcium carbonate formation. Firstly the basic principles of crystallography as well as the characteristics of calcium carbonate are presented. A review of all the different methods used to generate and to study $CaCO_3$ in the bulk solution and on the surface is given. Then the focus is on the different chemical and physical parameters influencing the formation of calcium carbonate. The mechanisms of inhibition are described in the fourth part as well as the four chemicals used in this study as scale inhibitors. Finally a complete definition of the green chemistry and of the legislation related to the release of chemicals in the marine environment ends this chapter.

2.2 Background on $CaCO_3$ formation

The precipitation of $CaCO_3$ occurs if the system has reached some degree of supersaturation. The degree of supersaturation (the deviation from the equilibrium saturated conditions) is the essential factor to permit the deposition to occur.

The general scheme of a crystallization process is as follow:

- Achievement of supersaturation,
- Formation of crystal nuclei,
- Growth of the crystals.

2.2.1 Driving force

Calcium carbonate formation is governed by the following equilibria [10]:

$$CO_{2(g)} + H_2O \leftrightarrow H_2CO_3 \qquad \textbf{Equation 2.4}$$

$$H_2CO_3 \leftrightarrow HCO_3^- + H^+ \qquad \textbf{Equation 2.5}$$

$$HCO_3^- \leftrightarrow CO_3^{2-} + H^+ \qquad \textbf{Equation 2.6}$$

$$Ca^{2+} + CO_3^{2-} \leftrightarrow CaCO_3 \qquad \textbf{Equation 2.7}$$

The reaction occurs when the thermodynamic conditions are favourable [11]. Water can be characterized by the supersaturation ratio, S. S is defined as follow:

$$S = (a_{Ca^{2+}} \times a_{HCO_3^-}) / K'_s \qquad \textbf{Equation 2.8}$$

where $a_{Ca^{2+}}$ and $a_{HCO_3^-}$ are the activity of calcium ions and bicarbonate ions and K'_s is the solubility product depending on the temperature and the pressure. According to the value of S, the water has different properties:

S<1 (undersaturated), the solution is aggressive,

S=1, the solution is in thermodynamic equilibrium,

S>1, (supersaturated), the solution is calcifying and calcium carbonate precipitation occurs.

In an undersaturated solution and a solution at the equilibrium, homogenous spontaneous nucleation cannot occur and if a crystal is added it will dissolve in a undersaturated solution. The saturated conditions do not allow the nucleation or the growth of a crystal but a seeding crystal added would not be dissolve. The supersaturated domain can be divided in three parts. The metastable zone does not permit a homogenous spontaneous nucleation but crystals added will grow. The labile zone is the region in which spontaneous homogenous nucleation occurs. The third zone is the precipitation zone. This zone is many times supersaturated and an amorphous precipitate is formed (Figure 2.1)[12]. In the $CaCO_3$ case, the crystallizing agents are the calcium and carbonate ions and the crystals of $CaCO_3$ are the macromolecules.

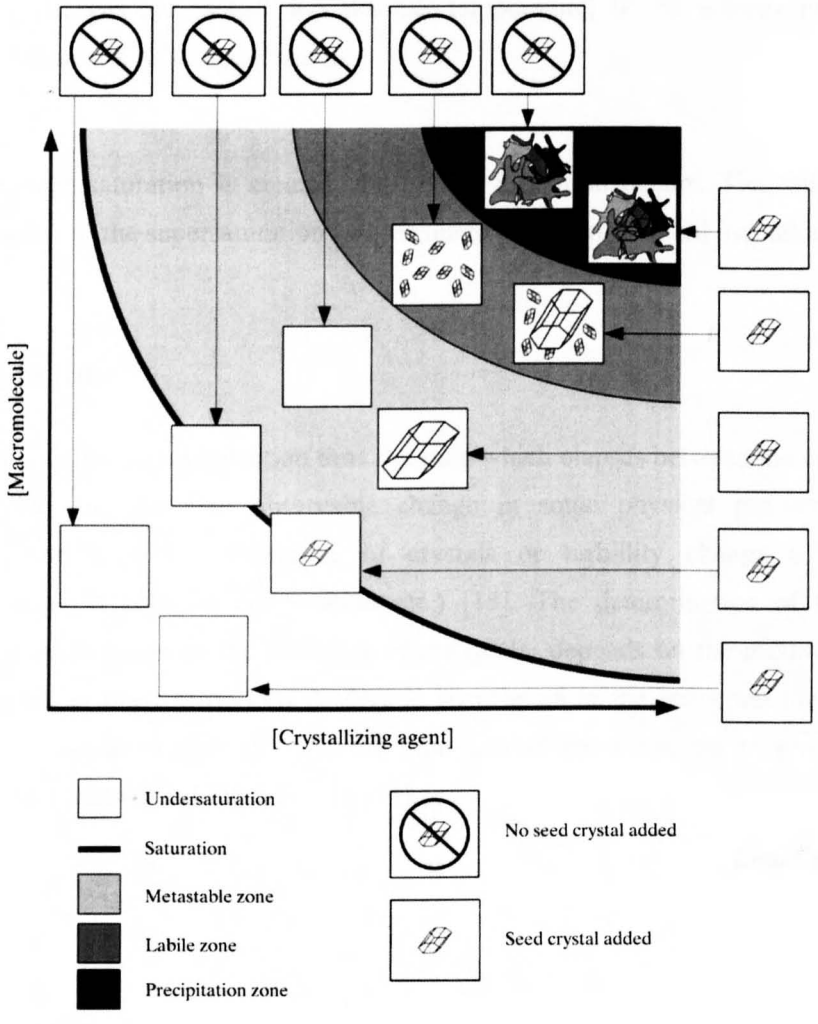

Figure 2.1: A two-dimensional representation of the three major saturation zones: *undersaturation*, *saturated* and *supersaturated* [12]

When $1 < S < 40$, the solution is metastable and the precipitation is possible when S is close to 40. The solution is completely unstable when S is above 40; spontaneous precipitation occurs [11].

During the process of precipitation the driving force are changing. The driving force for calcium carbonate formation is the change in Gibbs free energy for going from the supersaturated solution to equilibrium [13]. The Equation 2.9 illustrates the variations in the Gibbs free energy during a nucleation process:

$$\Delta G = -\frac{1}{2} R_g T \ln(\frac{IP}{K_s^0}) \qquad \textbf{Equation 2.9}$$

with R_g as the gas constant, T the absolute temperature, IP the activity product of $CaCO_3$ in the solution and K_s° at equilibrium.

When the supersaturation is created, the crystal formation occurs. The time elapses between the creation of the supersaturation and the nucleation start is called induction time.

2.2.2 Induction time

Söhnel and Mullin called induction time the time which elapses between the creation of the supersaturation and the first observable change in some physical property of the precipitating system (ie. the appearance of crystals or turbidity change of solution conductivity change in solution composition etc.) [14]. The determination of the exact induction time is a challenge as the detection of the nuclei depends on the accuracy of the method used: a nuclei must grow to a detectable size therefore the induction time (t_{ind}) is composed of the nucleation time (t_n) and the time needed for a nucleus to grow until a detectable size (t_g) as shown in Equation 2.10 [15].

$$t_{ind} = t_n + t_g \qquad \textbf{Equation 2.10}$$

The induction period can be defined as described by Equation 2.11 when homogeneous nucleation is followed by a diffusional growth [14]:

$$\log t_{ind} = C + \frac{\alpha_t}{(\log S_\alpha)^2} \qquad \textbf{Equation 2.11}$$

where t_{ind} is the induction time, C is a constant, α_t is the slope of log t_{ind} versus $(\log S)^{-2}$ function and S_α the supersaturation of the solution.

Gill *et al.* showed the relation between the induction time and the supersaturation [16].

$$K = T_{Ca}^{(p-1)} t \qquad \textbf{Equation 2.12}$$

where K is a constant, T_{Ca} is the molar concentration of ions, p the apparent number of ions in the critical nucleus, t the induction time.

2.2.3 Nucleation process

A stable nucleus is composed of several molecules and the number of molecules varies according to the nature of the crystals: from 10 to several thousands (water ice for example contains 80 to 100 molecules). The formation of a nucleus is a complex process and depends on several conditions. The constituents molecules have to coagulate, to be stable (to avoid being dissolved) and to be orientated into a fixed lattice. The collision of two molecules usually starts the process of nucleation and then a third molecules participates to the formation of the nucleus and so on [17]. Ion pairing and clusters are formed by electrostatic interactions between dissolved anions and cations (Figure 2.2). Then the clusters grow step by step by the addition of ions until a critical size [18].

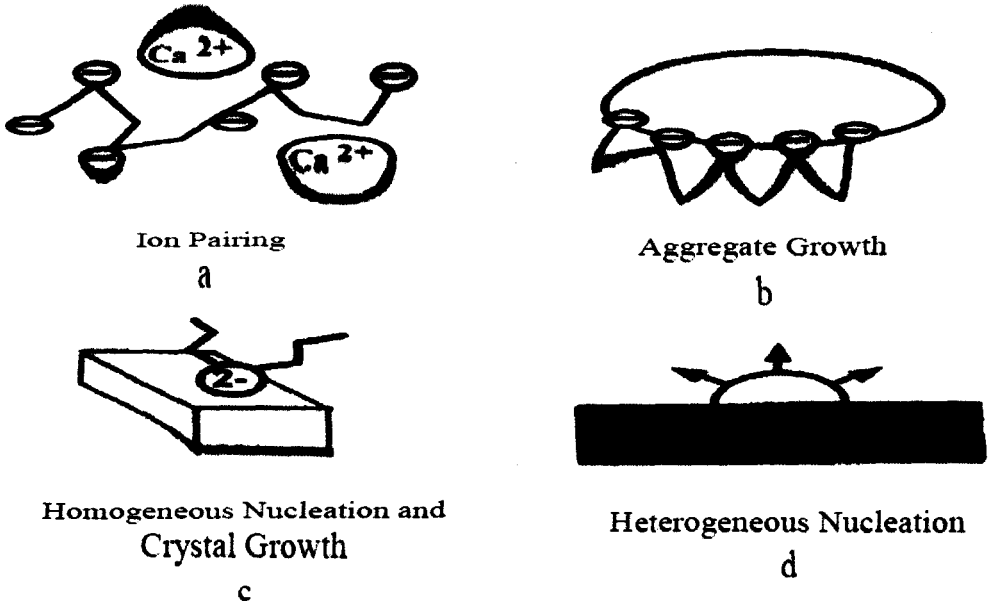

Figure 2.2: Schematic representations of processes involved in initial stages of scale formation: (a) ion pairing, (b) prenucleation aggregate growth, (c) and (d) particle nucleation and growth [19]

The nucleation process occurs in very high supersaturated region and very rapidly [17]. In case of the formation of calcium carbonate the electrostatic interactions between the calcium cations and the bicarbonate anions lead to the formation of the nucleus of $CaCO_3$.

Three kinds of nucleation are observed according to the characteristics of the environment where the nucleation takes place [20]:

Primary homogeneous nucleation: it occurs in the absence of solid phase (foreign particles, crystals already formed). The number of crystals formed during the homogeneous nucleation following by diffusional growth can be determined by [14]

$$\log N = D - \frac{\alpha_N}{(\log S_\alpha)^2} \qquad \textbf{Equation 2.13}$$

where N is the number of crystals, D a constant, α_N the slope of log N versus $(\log S)^{-2}$ function and S_α the supersaturation.

Primary heterogeneous nucleation: it takes place when a solid interface of a foreign seed (like ions or impurities) is present in the solution. Most of the primary nucleation are heterogeneous induces by other surface. The homogeneous and heterogeneous nucleation do not take place at the same time so the nucleation rate is the sum of these two nucleation rates.

Secondary nucleation: it is initiated by the presence of the crystalline suspension itself.

An homogeneous nucleation occurs when the local supersaturation is about 40 whereas a much lower supersaturation is enough to observe an heterogeneous nucleation [21]

Primary and secondary nucleation take place at different time during the crystallization process as shown in Figure 2.3.

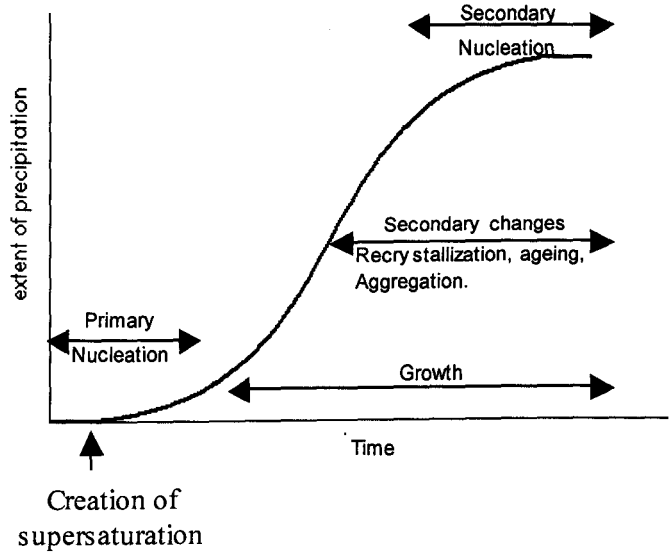

Figure 2.3: Kinetic processes involved in precipitation [22]

The excess of the free energy variation during a homogenous nucleation process is described as shown in Equation 2.14. The surface excess free energy (ΔG_s) is the free energy between the surface of the particle and the bulk of the particle and the volume free energy (ΔG_v) is the excess free energy between a very large particle and the solute solution [17].

$$\Delta G = \Delta G_s + \Delta G_v \qquad \textbf{Equation 2.14}$$

The surface excess free energy is a positive quantity proportional to r^2 and the volume free energy is a negative quantity proportional to r^3 in a supersaturated solution, r being the radius of the particle. Figure 2.4 shows the existence of a critical size, r_c, when ΔG reaches a maximum, ΔG_{crit}. Equation 2.15 presents the relationship between ΔG_{crit} and the critical size where σ is the surface energy of droplet per unit area.

$$\Delta G_{crit} = \frac{4}{3}\pi\sigma r_c^2 \qquad \textbf{Equation 2.15}$$

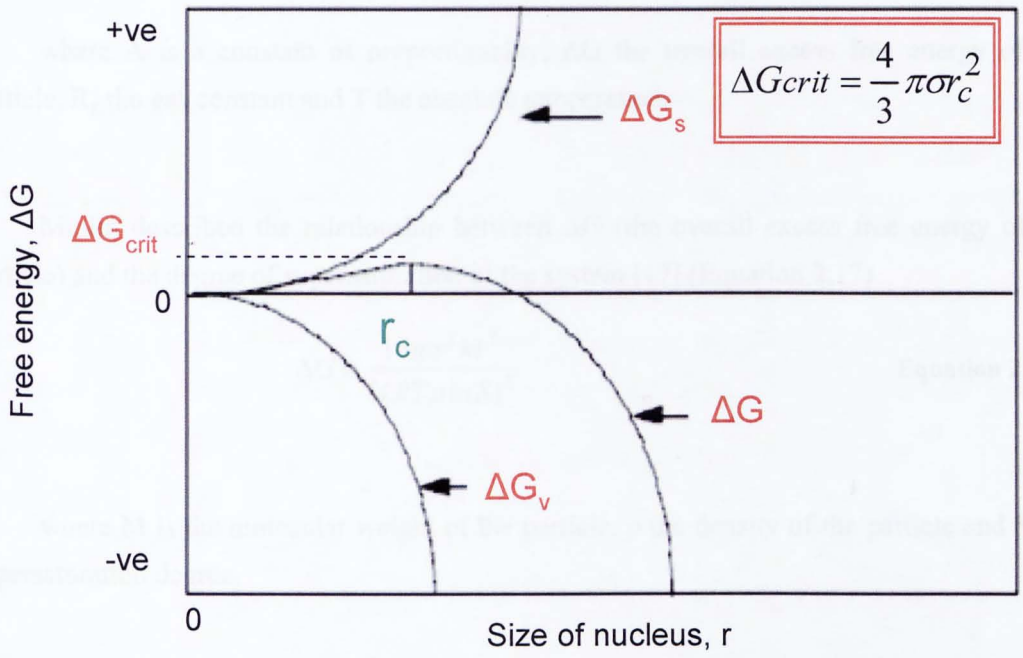

Figure 2.4: Free energy diagram for nucleation explaining the existence of a 'critical' nucleus [17]

The behaviour of a nucleus in a supersaturated solution depends on its size. In any case, the system would go for a decrease of the free energy of the particle. Therefore a particle with a smaller radius than r_c will dissolve in the solution and a particle with a size exceeded r_c will grow. Thus r_c is the minimum size of a stable nucleus. Packter showed that the critical radius for a crystal of calcium carbonate was 10Å in his experimental conditions [23]. ΔG_{crit} is necessary to form stable nuclei. The energy of a solution at constant temperature and pressure is constant but the distribution is not homogenous. There is statistical distribution of the energy in the solution in the molecules constituting the system and then nucleation occurs in the supersaturated regions where ΔG_{crit} has been reached. In case of heterogeneous the free energy required to form a stable nuclei is smaller than for the homogeneous nucleation, the surface or foreign particle present in the supersaturated solution inducing the nucleation [17].

This last point illustrates the significance of studying the process of crystallisation on a surface as less energy is required to form a precipitate thus the industrial systems containing surfaces (potential nucleation sites) will encountered problems due to the formation of a precipitate much more easily.

The rate of nucleation, N, is the number of nuclei formed per unit time per unit volume and can be described by Equation 2.16.

$$N = A.\exp^{(-\frac{\Delta G}{R_g T})} \qquad \textbf{Equation 2.16}$$

where A is a constant of proportionality, ΔG the overall excess free energy of the particle, R_g the gas constant and T the absolute temperature.

Mullin described the relationship between ΔG (the overall excess free energy of the particle) and the degree of supersaturation of the system [17] (Equation 2.17)

$$\Delta G = \frac{16\pi\sigma^3 M^2}{3(RT\rho \ln S)^2} \qquad \textbf{Equation 2.17}$$

where M is the molecular weight of the particle, ρ the density of the particle and S the supersaturation degree.

Combining Equation 2.16 with Equation 2.17, the nucleation rate is governed by three main variables the supersaturation degree, the interfacial tension and the temperature (Equation 2.18).

$$N = A.\exp[-\frac{16\pi\sigma^3 M^2}{3R^3T^3\rho^2(\ln S)^2}] \qquad \textbf{Equation 2.18}$$

Many factors (like the pH, the dissolved $CaCO_3$ [10], the nature of the substrate [24] etc.) influence the nucleation rate thus the nucleation process. These different factors will be reviewed and studied in the section 2.4 of this chapter.

2.2.4 Growth process

Once the nuclei are stable (when they are larger than the critical size), the growth process occurs to lead to the formation of a crystal of visible size. The growth is controlled by three general headings: the surface energy, the adsorption-layer and the dislocation theories.

2.2.4.1 Surface energy

The surface energies theory is based on the fact that a crystal is more stable when its surface free energy is low and hence its area is minimum. If a crystal grows in a solution, the growth of the different faces will grow with respect that the whole crystal has a minimum total surface free energy for a given volume [17]. It has been suggested that the growth of the faces is proportional to the surface energy and that it is inversely proportional of the reticular density (number of lattice points per unit area) of the lattice plane meaning that the growth of the face with a low reticular density is greater than the other faces and that it can disappear as illustrated in Figure 2.5. A crystal which grows and keeps its geometry during the growth process is called "invariant". The growth of the crystal leading to a modified geometry is called "overlapping".

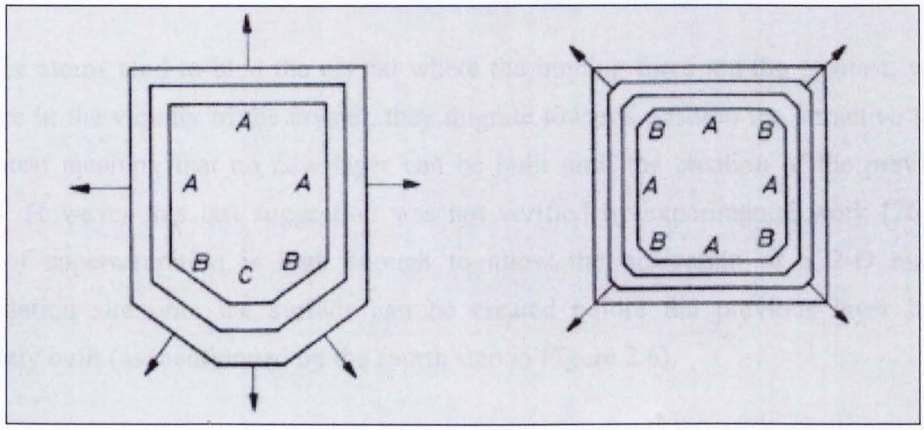

Figure 2.5: Velocities of crystal growth faces: (a) invariant crystal: (b) overlapping [17]

2.2.4.2 Adsorption layer theory

The adsorption theory is known as well as the Kossel, Stranski, Volmer theory (KSV) [25]. They pointed out that the crystal surface is not homogenous in terms of growth sites. The surface of a crystal is composed of smooth surfaces, steps and kink sites (1, 2 and 3 in Figure 2.6). The growth occurs first in the kink site as with three faces in contact with the crystal surface, the binding energy is the highest compared to the step site and the flat surface [26].

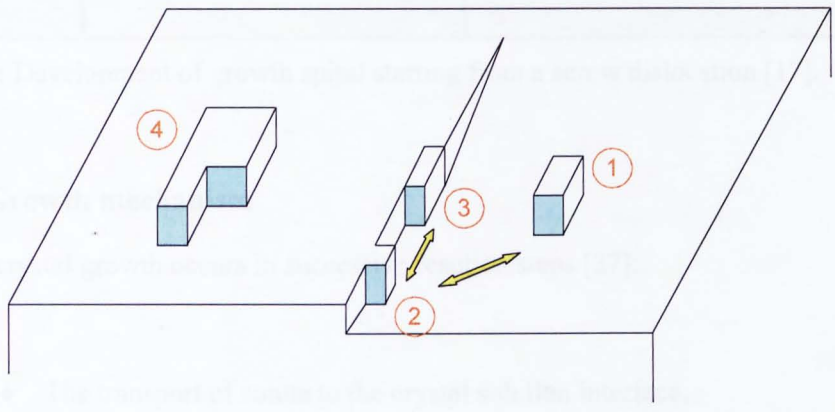

Figure 2.6: Representation of a crystal surface showing the development of an emerging growth step [26].

The atoms tend to bind the crystal where the binding force are the greatest; when the atoms are in the vicinity of the crystal, they migrate towards position the attractive force are the greatest meaning that no new layer can be built until the creation of the previous has finished. However this last suggestion was not verified by experimental work [26]. If the degree of supersaturation is high enough to allow the nucleation of a 2-D nucleus, a crystallization site onto the surface can be created before the previous layer has been completely built (as mentionned by the fourth step in Figure 2.6).

2.2.4.3 Dislocation

A dislocation is an irregularity in the crystal lattice. It is likely for a crystal to grow with some imperfections due to the presence in the solution of impurities or foreign atoms or ions. The screw dislocation has been characterized by the Burton, Cabrera, Franck (BCF) theory [17, 25]. During the growth process, sometimes a step may develop on the surface leading to an excessive development of one part of the crystal.

Figure 2.7 shows the spiral growth generated onto the surface of a crystal by the emergence of a step. As no 2-D nucleation is needed for the growth of the following layer (because of the spiral growth), the crystal growth occur at very low supersaturation degree.

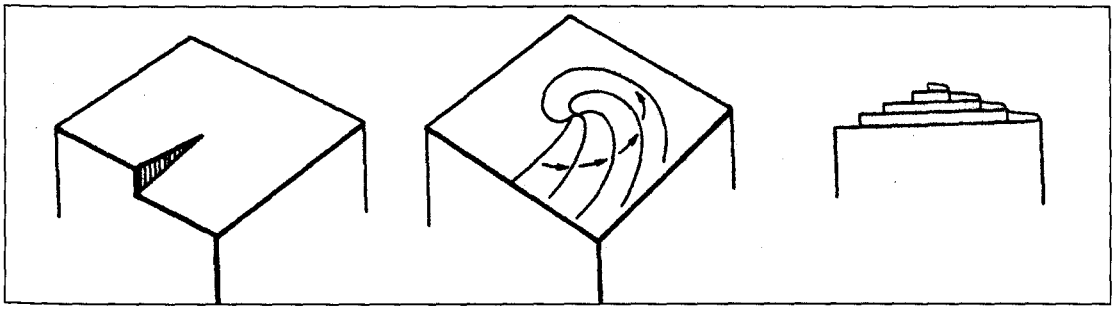

Figure 2.7: Development of growth spiral starting from a screw dislocation [17].

2.2.4.4 Growth mechanism

The crystal growth occurs in successive reaction steps [27]:

- The transport of solute to the crystal solution interface,
- The adsorption of solute at the surface,
- The incorporation of the crystal constituents into the lattice.

The presence of a laminar film of liquid in contact with the growing face, through which the solutes need to diffuse to reach the surface of the crystal is assumed. The thickness of this film varies according to the agitation of the system: it decreases with the increase of the agitation. There are two main steps in the growth process. First the molecules of solutes are transported from the bulk solution to the crystal face by diffusion and then they are incorporated in the crystal lattice. Figure 2.8 illustrates the driving forces in crystallization. It is important to note that the driving forces will rarely be equal and the variation of the concentration in the laminar film is not necessarily linear [17].

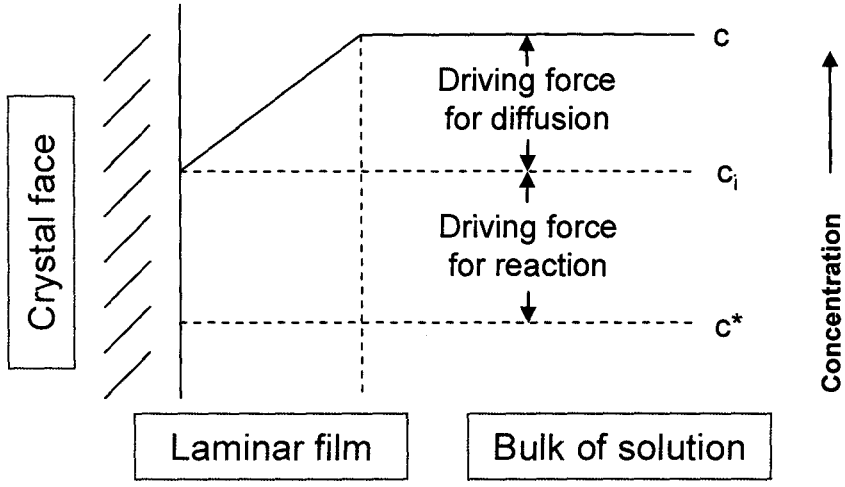

Figure 2.8: Concentration driving forces in crystallization from solution [17]

Nancollas *et al.* showed that the growth rate could be expressed as a decrease of the molar concentration of the constituents of the crystals (m) with time (Equation 2.19)

$$-\frac{dm}{dt} = ks(m - m_0)^2 \qquad \textbf{Equation 2.19}$$

where k is the rate constant for growth, m_0 the solubility and s is some function of the number of growth sites available for deposition [28].

From Equation 2.19, Nancollas described the crystallization rate of sparingly soluble electrolyte and in the case of calcium carbonate it gives (Equation 2.20) [14, 29],

$$-\frac{d[Ca]}{dt} = k_c A(t)([Ca\ ][Ca]_{eq})^g \qquad \textbf{Equation 2.20}$$

where k_c is the crystal growth constant, A(t) the surface area of the crystals, g is the kinetic order of growth, [Ca] the molar concentration of calcium, $[Ca]_{eq}$ the molar concentration of calcium at the equilibrium.

An important factor in the determination of the growth rate is that the surface area of the crystals in contact with the solution increases with time. Thus Söhnel and Mullin proposed a way to include this fact in Equation 2.20 [14] (considering that the number of crystals is constant and that the crystals are the same shape).

$$W(t) = NV(t)\rho = N\rho k_v r(t)^3 \qquad \textbf{Equation 2.21}$$

where W(t) is the total mass of crystals in 1 litre of solution at time t, N the number of crystals, V(t) the volume of the crystal at time t, ρ the density of the crystal, k_v the volume shape factor, r the equivalent radius of the crystal. The surface area of the crystal is

$$A(t) = Nk_a r(t)^2 \qquad \textbf{Equation 2.22}$$

where k_a is the area shape factor.

Combining Equation 2.21 and Equation 2.22 gives

$$A(t) = [\frac{k_a}{(\rho k_v)^{2/3}}][W(t)^2 N]^{1/3} \qquad \textbf{Equation 2.23}$$

The total mass of crystals in 1litre of solution can be described with

$$W(t) = ([Ca]_i - [Ca])M \qquad \textbf{Equation 2.24}$$

where M is the molecular weight of $CaCO_3$.

By combining Equation 2.20, Equation 2.21 and Equation 2.24 the variation of the calcium concentration can be expressed by

$$-\frac{d[Ca]}{dt} = k_c \frac{k_a}{(\rho k_v)^{2/3}} M^{2/3} N^{1/3} \times ([Ca]_i - [Ca])^{2/3} ([Ca] - [Ca]_{eq})^g \qquad \textbf{Equation 2.25}$$

Equation 2.26 gives the crystal growth rate,

$$\frac{dr}{dt} = K_g ([Ca] - [Ca]_{eq})^g \qquad \textbf{Equation 2.26}$$

The relationship between K_g in Equation 2.26 and K_c in Equation 2.25 is given by Equation 2.27,

$$K_g = \frac{K_c M}{\rho} = 10^B \left(\frac{M k_v^{\ 2}}{\rho k_a^{\ 3} N}\right)^{1/3} \qquad \textbf{Equation 2.27}$$

Where B is the intercept of the $\log\left(\frac{d[Ca]}{dt}\right)$ versus $\log([Ca]_i - [Ca])^{2/3}([Ca] - [Ca]_{eq})^g$.

2.2.5 Crystallography of $CaCO_3$

According to Barrett, "a crystal consists of atoms arranged in a pattern that repeats periodically in three dimensions" [30]. The important feature of a crystal is the regularity of the arrangements of the elements constituting the crystals. A crystal is composed of the repetition of identical templates. A single template is the unit cell and Figure 2.9 illustrates the three vectors and the three angles characterising the size and the shape of a unit cell.

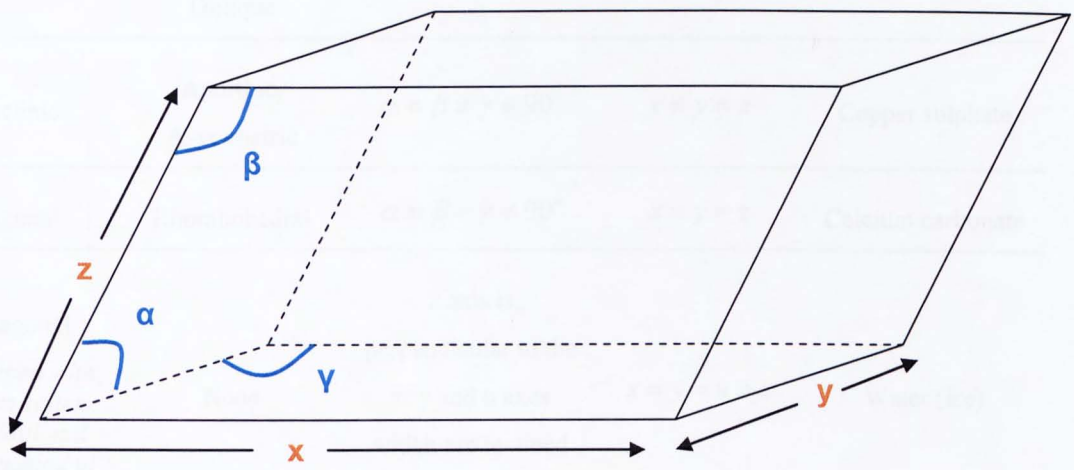

Figure 2.9: Characteristics of a unit cell

A unit cell is defined by the length of the axes (x, y and z)) and the angle between the axes x and y (γ), the axes y and z (α) and the axes x and z (β). According to these characteristics, Mullin defined the 7 crystal systems presented in Table 2.2 [17].

Table 2.2: The seven crystal systems [17]

System	Other names	Angles between axes	Length of axes	Examples
Regular	Cubic, Octahedral, Isometric, Tesseral	$\alpha = \beta = \gamma = 90°$	$x = y = z$	Sodium chloride
Tetragonal	Pyramidal, Quadratic	$\alpha = \beta = \gamma = 90°$	$x = y \neq z$	Nickel sulphate
Orthorhombic	Rhombic, Prismatic, Isoclinic, Trimetric	$\alpha = \beta = \gamma = 90°$	$x \neq y \neq z$	Silver nitrate
Monoclinic	Monosymmetric, Clinorhombic, Oblique	$\alpha = \beta = 90° \neq \gamma$	$x \neq y \neq z$	Sucrose
Triclinic	Anorthic, Asymmetric	$\alpha \neq \beta \neq \gamma \neq 90°$	$x \neq y \neq z$	Copper sulphate
Trigonal	Rhombohedral	$\alpha = \beta = \gamma \neq 90°$	$x = y = z$	Calcium carbonate
Hexagonal *(described with a 4-axes system, the additional axe is named u)*	None	z axis is perpendicular to the x, y and u axes which are inclined at 60° to each other	$x = y = u \neq z$	Water (ice)

The crystal planes can be described by their axial intercept, the axes being chosen according to the parametral plane (reference plane), face ABC in Figure 2.10. The axial intercepts of the parametral plane are AO=a, BO=b and CO=c. The intercepts of the face considered are named X, Y and Z on the respective axes x, y and z. Miller determined a way to represent each face of the crystal according to the indices *h*, *k* and *l* defined by

$$h=\frac{a}{X}\ ;\ k=\frac{b}{Y}\ ;\ l=\frac{c}{Z} \qquad \textbf{Equation 2.28}$$

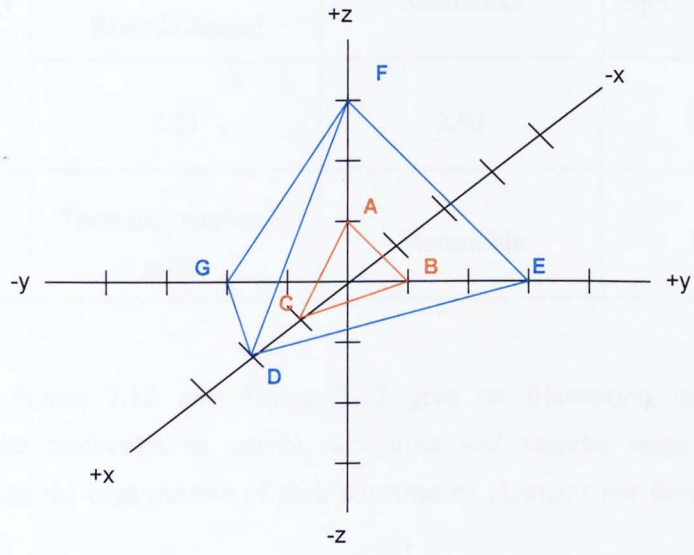

Figure 2.10: Intercepts of planes on the crystallographic axes [17]

In the example presented in Figure 2.10, the Miller indices of the face DEF are

$$h=\frac{a}{X}=\frac{a}{2a}=\frac{1}{2}\ ;\ k=\frac{b}{Y}=\frac{b}{3b}=\frac{1}{3}\ ;\ l=\frac{c}{Z}=\frac{c}{3c}=\frac{1}{3} \qquad \textbf{Equation 2.29}$$

By convention, the value of *b* is unity therefore the Miller indices of the face DEF are *h*:*k*:*l*=3:2:2. The Miller indices are inversely proportional to its axial intercepts [17].

Calcium carbonate exhibits a polymorphism. It can crystallize into different forms but these forms are chemically identical. The properties of the calcium carbonate crystalline forms are summarized in Table 2.3.

Table 2.3: Properties of calcium carbonate crystalline forms

	Calcite	**Aragonite**	**Vaterite**
Crystal system	Trigonal [31]	Orthorombic [32]	Hexagonal [33]
Crystal morphology	Cubical or Rhombohedral	Needlelike	Spherical or disclike
Density (g/cm^3)	2.71	2.93	2.66
Stability	Thermodynamically stable	Metastable	Unstable

Figure 2.11, Figure 2.12 and Figure 2.13 give an illustration of a schematic representation of the molecules of calcite, aragonite and vaterite respectively. These molecules differs from the organization of their constituting elements not from the nature of these elements.

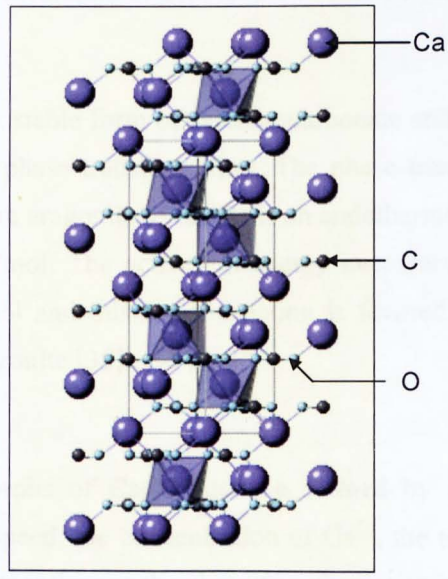

Figure 2.11: Schematic representation of a molecule of calcite [31, 34]

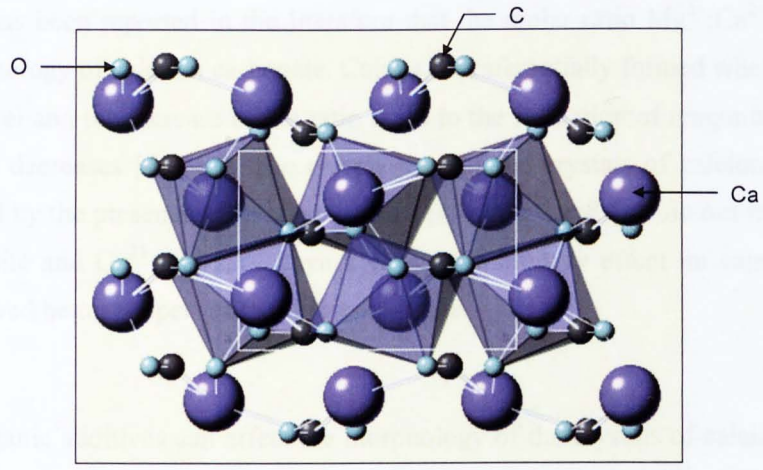

Figure 2.12: Schematic representation of a molecule of aragonite [32, 34]

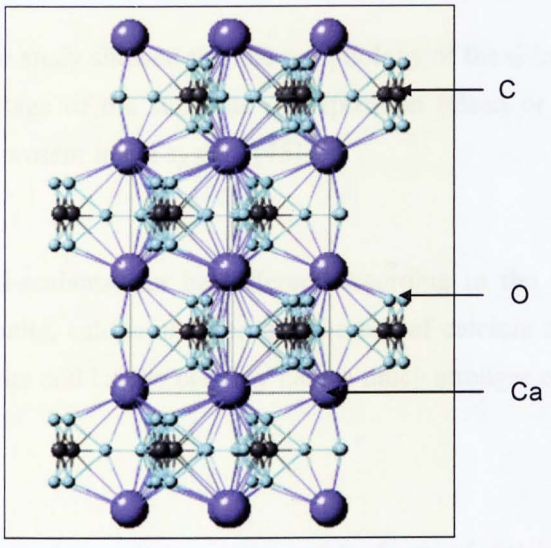

Figure 2.13: Schematic representation of a molecule of vaterite [33, 34]

The calcite is the most stable form of calcium carbonate and Perić *et al.* determined the energy of activation of the phase transformation. The phase transformation, in the specific experimental conditions, from aragonite to calcite is an endothermal process and the energy of activation was 234.5±5.6kJ/mol. The activation energy necessary to transform vaterite into calcite was 252.8±48.7kJ/mol and this transformation is favored by the presence of calcite and slightly inhibited by aragonite [35].

The different polymorphs of $CaCO_3$ can be formed by changing the experimental conditions like the stirring speed, the concentration of Ca^{2+}, the temperature, the pH and the flow rate. The crystals defects influence the phase transformation as well [36-40].

It has been reported in the literature that the molar ratio Mg^{2+}:Ca^{2+} influences greatly the morphology of calcium carbonate. Calcite is preferentially formed when the magnesium is at low level and the increase of the ratio leads to the formation of aragonite while the content of calcite decreases [41, 42]. The morphology of the crystals of calcium carbonate can be controlled by the presence of divalent cations [43]. Mg^{2+} and Fe^{2+} do not influence the growth of aragonite and Cu^{2+} and Zn^{2+} have a stronger inhibitory effect on calcite, while Sr^{2+} and Ba^{2+} showed better properties to inhibit aragonite.

Organic additives can affect the morphology of the crystals of calcium carbonate and a wide range of morphology can be formed by adding organic additives [41, 42, 44]. This point is developed later in this chapter.

An electrochemical study showed that the morphology of the calcium carbonate crystals depends on the initial stage of the substrate of deposition (clean or damaged) and on the concentration of $CaCO_3$ present in the system [45].

The action of anti-scalants can be different according to the nature of the calcium carbonate deposit (aragonite, calcite or vaterite). The use of calcium complexing substances retards growth of aragonite and calcite but they have a much stronger effect on aragonite than on calcite [46].

Calcite is the most thermodynamically stable form of calcium carbonate but the presence of certain impurities or a high temperature, above 60°C, leads to the formation of aragonite [10, 14]. For a fast nucleation rate calcite is mainly deposited on the surface whereas for a slower rate vaterite in generally formed [21, 47].

The adherence of the calcareous layer on the surface depends on the polymorph of the crystals [47]. Wang *et al.* showed that the deposit formed on a surface at 20°C was harder to remove than a deposit formed at 90°C. SEM investigations demonstrated that the deposit was composed of calcite at 20°C whereas it was aragonite at 90°C. The authors pointed out the role of the polymorph on the adhesion of the deposit. The build-up of a top-layer of aragonite onto aragonite does not provide strong adhesion (because of their needle morphology) so it is easier to remove than when the layers of $CaCO_3$ are composed of calcite [48].

The role of suspended minerals in a scaling solution has been investigated and it has been found that the nature of the mineral influences the morphology of the crystals formed. The addition of montmorillonite ((Na, Ca)(Al, Mg)$_6$ $(Si_4O_{10})_3(OH)_6$ – nH_2O) leads to the formation of calcite whereas in absence of this mineral and under the same conditions vaterite was formed. Quartz had no influence on the precipitation whereas kaolinite ($Al_2Si_2O_5(OH)_4$) inhibited the precipitation process to some extent [49].

2.3 Review of the methodologies to study $CaCO_3$

The different methodologies to study the scale formation in the bulk solution and onto a surface are reviewed and a particular focus is on the methods used in this thesis. It is essential to study the mechanisms of scale formation and inhibition both in the bulk and on the surface as it has been seen that the mechanisms of scale formation are different according to the nature of the nucleation. Moreover the mechanisms of scale inhibition can be different according to where the inhibition occurs (in the bulk solution or on a surface) [50].

2.3.1 Scale precipitation in the bulk solution

Bulk precipitation is usually studied with a beaker test with a supersaturated scaling solution. The measurements made to determine the kinetics of scale precipitation are various.

The assessment of the pH variations has been often used to study the kinetics of $CaCO_3$ precipitation. According to Equation 2.2, the formation of $CaCO_3$ generates a drop of the pH. The decrease of the pH can be measured and the kinetics of calcium carbonate determined [51] or the pH can be kept constant and the kinetics of scale formation are determined from the volume of the titration solution added [52-54]. The last method is referred as the pH-stat method.

As calcium carbonate is formed the concentrations of calcium and bicarbonate are depleted from the solution. Ross *et al.* determined the effects of polyaspartic acids by quantifying the concentration of calcium left in the solution by atomic absorption spectroscopy [55]. Nancollas has studied the growth of calcium carbonate crystals which were already characterized (length and surface area known) by adding them in a stable supersaturated solution. The inoculated solution has been filtrated during the growth step and the filtrate has been analyzed by Atomic Absorption Spectroscopy [29].

In order to generate secondary nucleation, calcium carbonate seeds crystals can be added in the bulk solution in order to provide nucleation sites [53, 54, 56, 57]. The use of a calcium-selective electrode has been used as well to assess the drop of the Ca^{2+} concentration [51, 56, 58].

Tantayakom *et al.* studied the barium sulphate scale inhibition by assessing the changes of the turbidity of the bulk solution. They determined the critical supersaturation ratio for which barium sulphate precipitates for different experimental conditions [59]. He *et al.* studied the induction period of calcium carbonate formation at 25 and 90°C by turbidity measurements [60]. Sohnel *et al.* measured the turbidity of the solution to study the effects of magnesium, manganese, chromium and fluorine on the kinetics of scale precipitation [14].

Euvrard *et al.* developed a test based on the evaluation of the number of crystals present in a supersaturated solution. The solution has been evaporated and filtrated and a chemical analyses has been carried out to determine the mass of the precipitate and a morphometric analysis has permitted to define the mean characteristics of the crystals [61].

2.3.2 Scale deposition on a surface

The review of the methods specific to the study of scale deposition on a solid surface study is divided in to two categories: non-electrochemical and electrochemical methods.

2.3.2.1 Non-electrochemical methods

The Quartz Crystal Microbalance (QCM) is a very accurate set-up allowing the detection of a very small quantity of deposit. Changes of 0.5ng can be determined according to the model of the QCM [62]. Deposition of a thin film on the surface of a quartz crystal disc oscillator plated with gold decreases the frequency in proportion to the mass of the film. The thickness of the crystals determines the resonant frequency so the mass sensitivity. The Sauerbrey equation gives the relationship of the mass of solid adhered (m_{adh}) on the quartz crystal with the changes in oscillating frequencies (Δf) (Equation 2.30). K_s is the proportionality constant determined by calibration.

$$m_{adh} = -K_s \Delta f \qquad \textbf{Equation 2.30}$$

The adhesion mechanism of calcium carbonate has been studied by using the quartz microbalance technique (QCM). Calcium carbonate precipitates firstly as an amorphous compound and then as a stable crystalline form. They found that at high supersaturation ratio calcite was the predominant crystal observed whereas at low supersaturation ratio leaf-like vaterite is obtained. They also showed that the contribution of the indirect adhesion of crystals precipitated in the bulk is less important than the direct adhesion. The significant role of the stirring rate and the inclination of the surface on the rate and the amount of scale formed has been demonstrated [63, 64].

A calcium carbonate cooling water scaling system permits the deposition of scale layers under well-known conditions on heat transfer surfaces. The measurement of the temperature before and after the test section enables the calculation of the scaling resistance (Rf) which is proportional to the thickness of the scale deposit. It is assumed that the thermal conductivity of the scale remains constant [65].

Hasson *et al.* examined the effects of anti-scalants using a falling film system. The system simulates the operation of a water-cooling tower. A hot aqueous solution of $Ca(HCO_3)_2$ flow down the outer surface of a vertical pipe and the falling film released CO_2 due to the evaporative air-cooling of the film creating the supersaturation regarding $CaCO_3$ [66].

The tube blocking test is the most common method to study scale deposition. The scaling flow is going through a thin tube and the building up of scale on the surface of the tube generates changes in the pressure between the inlet and outlet of the tube. The increase of the differential pressure illustrates the building-up of scale in the thin tube. This method has been used by Dyer and Graham to study the effects of the temperature and the pressure on barium sulphate and calcium carbonate precipitation. They pointed out the greater effects of the temperature on the scaling tendency [67].

Some comparative studies of green [68] and non-green [69] inhibitors have been realised by dynamic tube blocking tests. Bazin *et al.* compared the effects of different CMI on $CaCO_3$ and $BaSO_4$ inhibition on the time at which the blockage of the tube occurs. The MIC (Minimum Inhibiting Concentration) of various inhibitors have been determined in different conditions (inhibited, addition of iron, calcium and barium free brines) [70].

Tube blocking tests have been used by Zhang *et al.* to build a kinetic model to predict the scale formation. The results obtained are in a good agreement with the measurements realised downhole. They also found that the most probable crystals in an oilfield reservoir is calcite [71].

Hennessy *et al.* developed an *in-situ* flow cell allowing the application of high pressure and high temperature. They studied the formation of $BaSO_4$ under non ambient conditions with a Synchrotron X-Ray Diffraction [72]. The substrate of deposition used was silicon for its good X-Ray diffraction properties. This cell permits the effects of the brines compositions, the effects of scale inhibitors, temperature, pressure, flow rate to be determined. Chen *et al.* used this cell to study the influence of the magnesium ions of $CaCO_3$ formation and the effects of scale inhibitors. For this work, the substrate of scale deposition was silicon and PMMA (polymethylmetacrylate). It has been found that the scale formation can be divided in two steps. The first one is unstable: various vaterite and aragonite polymorphs emerge from the solution and then disappear. This unstable phase is followed by a stable phase in which the crystals adhere on the surface and then grow [73].

In this thesis the *in-situ* flow cell has been used with Synchrotron X-Ray Diffraction as the means of analysing the scale. Full details of the cell and of the conditions of the experiments are described in Chapter 3.

Synchrotron X-Ray diffraction have been already used to study $BaSO_4$ formation and inhibition by a carboxylic acid and a phosphonate [74]. They revealed the formation of $BaSO_4$ on an electrode surface despite the small mass of the deposit. The SXRD spectra showed the trend of the crystals size and the authors pointed out the corrosion inhibition properties of the phosphonate inhibitor with the absence of iron sulphate.

2.3.2.2 Electrochemical methods

Ledion *et al.* proposed the first electrochemical method (chronoamperometry) in 1985. It is based on promoting the oxygen-reduction reaction by polarising a metallic electrode at a negative potential. The reduction of the oxygen leads to a local increase of the pH resulting in $CaCO_3$ formation onto the metal surface [75]. Full details of the principles of the electrochemical method are presented in Chapter 3. A review of the various electrochemical based approaches which have been used to study calcium carbonate formation and inhibition is presented.

- *Chronoamperometry*

The current is proportional to the flow of oxygen moving towards the electrode and decreases when the active surface decreases, blocked by the scale formation. The current i_L reaches a final value close to zero when the surface is completely covered and isolated by scale. The morphology of the scale deposit is related to the residual current: the more compact and isolating, the lower the residual current. Ledion defined the scaling time t_s as the intersection between the tangent at the inflexion point of the chronoamperometric curve and the time axis (it is a rough approximation of the scaling potentiality of water) [11].

The effects of the sulphates, the calcium concentration and the potential on the nature of the deposit has been studied by chronoamperometry [76, 77]. Calcium carbonate was found for a potential between -0.9 and -1.1V whereas brucite ($Mg(OH)_2$) was the only forming for a potential up to -1.3V. At potential -1.2V brucite and calcium carbonate are found, only aragonite crystals have been detected by XRD analyses or *ex-situ* SEM. But the impedance technique shown the presence of a porous film on the surface. This film may be the precursor of the brucite

Chronoamperometry is very often combined with the impedance technique and the electrogravimetry especially when scale inhibitors are used as the residual current often increases when the quantity of additives increases [10, 21, 47, 76-82].

➢ *Impedance*

The impedance technique permits to determine two quantities C_{HF} and R_{HF} obtained from its high frequency behaviour. C_{HF}, the capacitance (measure of the amount of electric charge stored (or separated) for a given electric potential), depends on the surface coverage and R_{HF}, the resistance (measure of the degree to which an object opposes an electric current through it), on the morphology of the deposit [80]. Gabrielli *et al.* showed when non-scaling conditions (e.g potential too low to enable oxygen reduction) are applied on a surface already covered by scale that C_{HF} do not vary whereas R_{HF} increased with time.

Therefore with this technique they shown that the thickness of the deposit do not change and the porosity change with time (the pores narrow with time) [83].

Devos *et al.* developed a novel technique combining EIS (Eletrochemical Impedance Spectroscopy) with microscope to allow *in-situ* observations [79]. Deslouis *et al.* combined the impedance technique with the EHD (Electrohydrodynamic Impedance, based on flow modulation technique) to study the formation of $Mg(OH)_2$ without $CaCO_3$ [81].

➢ *EQCMB*

The electrochemical method can be coupled with a QCM. This technique is called chronoelectrogravimetry and has been used by Gabrielli *et al.* to determine the effects of the degree of hardness, a surface pre-treatment and oxygen concentration. This method enables the determination of the nucleation time and the total mass deposited on the surface as a function of time [21].

The EQCM has been inserted in a flow cell to study the effects of the hydrodynamic conditions on the scale formation and inhibition [84]. The authors demonstrated that the scaling rate increased with the flow rate in the laminar regime and a higher inhibition efficiency was found at the turbulent regime when inhibitors were added.

The nucleation process has been studied with an EQCM by Devos *et al.* and they showed that the nucleation rate increases with the dissolved $CaCO_3$ and the pH and not the growth process. Moreover they pointed out that the convection does not influence the nucleation rate only the growth process [10, 82].

➢ *RDE*

Neville *et al.* developed an electrochemical-based method, the Rotating Disc Electrode (RDE) to study the extent of surface coverage on scaled electrode [85, 86]. This technique permits to obtain precisely the coverage by having uniform controlled hydrodynamic conditions over the surface of the electrode.

A relation between the limiting current (i_L) and the rotational speed enables the determination of the percentage of surface coverage in accordance of the Levich equation (Equation 2.31).

$$i_L = 0.62nFAC^bD^{2/3}\nu^{-1/6}\omega^{1/2} \qquad \textbf{Equation 2.31}$$

where i_L is the limiting current (mA), ω the angular velocity of the RDE (rad s^{-1}), C^b the bulk concentration of electroactive species (mol dm^3), ν the kinematic viscosity (cm^2 s^{-1}), F the Faraday's constant (96487 C $equiv^{-1}$), A the electrode area (cm^2), n the number of electrons involved in the reaction, and D the diffusion coefficient of the electroactive species (cm^2 s^{-1}).

By plotting i_L against $\omega^{1/2}$, the percentage of the coverage can be determined.

$$\text{coverage} = [(m_1-m_2)/m_1] \text{ x}100 \qquad \textbf{Equation 2.32}$$

where m_1 and m_2 are the gradient of the i_L against $\omega^{1/2}$ plot for the unscaled (initial) and scaled (final) respectively.

A good correlation is observed between results obtained with electrochemical monitoring and image analysis [85]. Morizot *et al.* showed by using RDE the role of Ca^{2+} and Mg^{2+} in the inhibitor film formation mechanism [87] and Neville *et al.* studied the film promoted by magnesium and found that there is no calcium in this thin layer even if calcium is present in the solution [88].

Chen *et al.* studied the calcium carbonate precipitation in the bulk solution by assessing the concentration of Ca^{2+} by ICP (Induced Coupled Plasma) and the deposition on a surface by RDE and illustrated the need of studying both surface and bulk scale formation as the mechanisms differ [50].

- *Other applications*

Gabrielli *et al.* developed an electrode which allows the use of isolating materials. They successfully determined the scaling susceptibility of a material. They tested various material and they pointed out the lower scaling susceptibility of the PTFE (Polytetrafluoroethylene) compared to the Plexiglas® and PVC (polyvinyl chloride) [89].

In-situ observations and in real-time have been done by Euvrard *et al.* by using a transparent electrode connected to a video set-up. The analyses of the images of the electrode covered by scale allow them to study nucleation and growth of electrodeposited calcium carbonate and to determine the morphometric characteristics (diameter, surface, shape) of the crystals of $CaCO_3$ [90]. A full description of this set-up is presented in Chapter 3 as it has been used in this study to determine the effects of the scale inhibitors. Devos *et al.* used a microscope coupled with a EQCMB. The whole thickness of the EQCMB have been made optically transparent by spraying a thin layer of a transparent and conductive semi-conductor [10].

Analyses were done with a laser beam reflected on a surface covered where crystallization of calcium carbonate takes place. Three substrates were studied; stainless steel, copper and soft steel (XC38 (98.7% of Fe, 0.4% of C, 0.6% of Mn, 0.3% of Si)) and it has been found that the nature of the substrate has an impact on the nucleation and growth process and they do not act on the nature of the crystals [24, 91]. The nature of the substrate has a significant effect on the scaling process both by acting on the number of nucleation sites and by acting on the nucleation rate.

Electrochemical methods have not only been used in the study of scale deposition. These technique can be applied in water treatment to recover phosphonates, magnesium and azote by electrodepositing a mineral named struvite ($MgNH_4PO_4.6H_2O$) and to decrease the degree of hardness of a hard water [92].

2.4 Parameters influencing $CaCO_3$ formation

2.4.1 Effects of the supersaturation

Chen *et al.* studied the effects of the degree of supersaturation on the induction time and the growth of the crystals in the bulk solution and on the surface. They found that the supersaturation degree has an important impact on the induction, growth, morphology of the crystals and rate of scale formation: at high supersaturation, the induction time is short and the growth of $CaCO_3$ is rapid for both crystals nucleated in the bulk or on the surface whereas the decrease of the supersaturation leads to the increase of the induction time and to a slow down of the growth only for the crystals nucleated in the bulk solution [50].

The effects of the degree of supersaturation on the induction time was confirmed by Ben Armor *et al.*. The study focused on the heterogeneous nucleation and the influence of different parameters pointed out that the type of nucleation (heterogeneous or homogeneous) is highly dependent on the supersaturation state of the solution as heterogeneous nucleation occurs at low supersaturation and both heterogeneous and homogeneous occurs at higher supersaturation [93]. This finding illustrates the need of higher driving forces for homogeneous nucleation to occur [17]. Tend *et al.* showed that increasing the supersaturation resulted in a faster nucleation rates and in a development of 2-D nuclei [94].

Moreover Pina *et al.* worked on the effects of the supersaturation on the growth of $BaSO_4$ and $SrSO_4$ and determined that the supersaturation influences the model of growth: 2-D nucleation occurs at high supersaturation and spiral growth at low supersaturation [95].

Moreover the supersaturation not only influences the kinetics of $CaCO_3$ formation but also the morphology of the crystals. The decrease of the supersaturation leads to an increase of the aragonite fraction and to some extent to the disappearance of the calcite crystals in the deposit formed [96, 97].

2.4.2 Effects of the pH

As seen previously the formation of calcium carbonate is controlled by the calco-carbonic equilibrium presented in Equation 2.4-Equation 2.7. These equilibria are highly dependent on the pH as shown on the repartition diagram of the C-species (Figure 2.14).

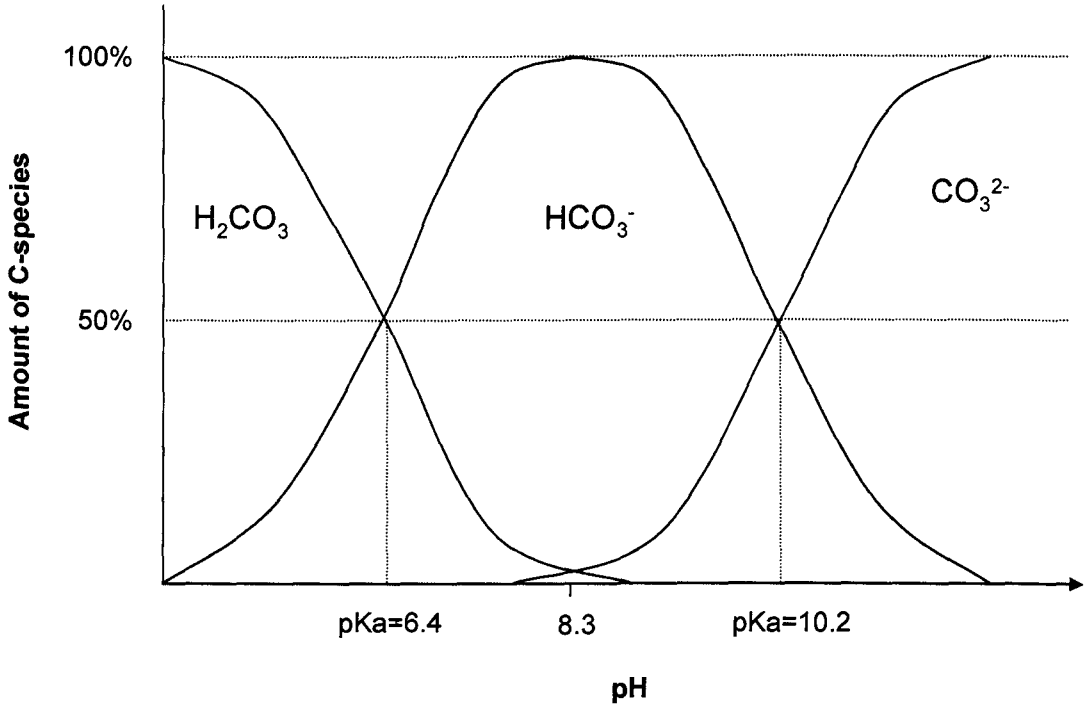

Figure 2.14: Distribution of carbonic ions as a function of pH

The formation of $CaCO_3$ is favoured at high pH due to the hydrocarbonate/carbonate buffer equilibrium.

The pH affects the morphology of the crystal as determined by Cheng *et al.* [98]. The influence of the pH was strong at high pH. The particle size seems to be in correlation with the pH: a high pH means a small average size of the particles [99, 100]. At high pH the nucleation rate is increased as the supersaturation increases leading to a change in the morphology of the crystals. Moreover, the induction time decreases with the increase of the pH as seen with the increase of the supersaturation [50, 101].

2.4.3 Effects of the temperature

The temperature is one of the most important factors to consider for a study of calcium carbonate formation and especially in oil and gas field as the temperature varies strongly during all the oil extraction process and can reach some extreme values.

The temperature has different effects on the supersaturation of a solution according to the elements taking into account; the temperature increases the supersaturation relative to calcium carbonate resulting in a higher scale tendency at high temperature whereas the temperature decreases the supersaturation with respect of $BaSO_4$ leading to a decrease of $BaSO_4$ precipitation [67].

The higher scale tendency for calcium carbonate at high temperature have been checked as well by chronoamperometry study for a potential applied of -1V/SCE (Saturated Calomel Electrode) [77]. Barchiche *et al.* have found by using electrochemical tests that the temperature can be in favour in aragonite when a moderate potential (-1.0V/SCE) is applied whereas brucite ($Mg(OH)_2$) is observed at higher potential (-1.2V/SCE) (Figure 2.15)[77].

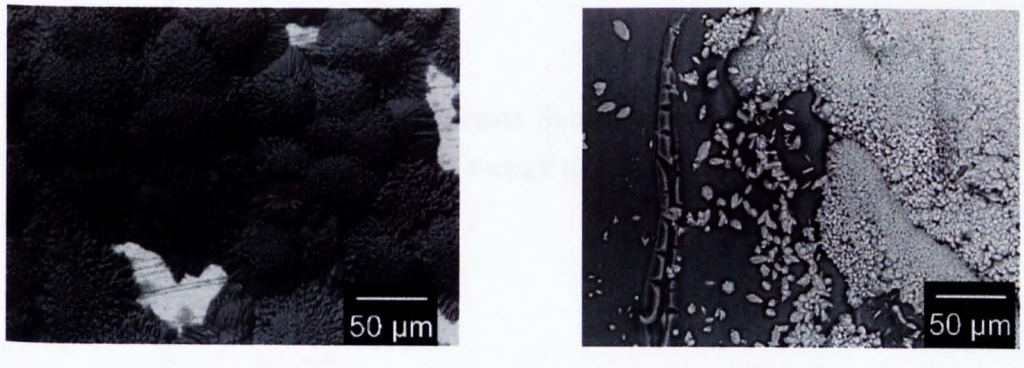

Figure 2.15: SEM pictures of (a) aragonite and (b) brucite ($Mg(OH)_2$) formed at 30°C at a potential of -1.0V/SCE and -1.2V/SCE respectively

The influence of the substrate of deposition on the kinetics of precipitation is lost with the increase of the temperature showing the increase of the homogeneous nucleation with the temperature [93].

The morphology of the crystals of calcium carbonate can be modified according to the temperature as the increase of the temperature leads to the decrease of the solubility of the aragonite and the calcite but in a different extent [102, 103]. It has been determined that calcite is the most stable crystals at 30°C whereas aragonite is observed at higher temperature (~35°C) [104, 105]. Lin and Dexter explained this difference of solubility with the incorporation of Mg^{2+} into calcite [106, 107].

2.4.4 Effects of calcium concentration

Devos *et al.* and Barchiche *et al.* studied by electrodeposition the effects of calcium concentration on the process of scale formation. The chronoamperometric curves show the decrease of the scaling power with the decrease of the calcium concentration [10, 77]. Moreover the calcareous deposit is thinner but more compact at high calcium concentration. The nucleation rate increases with calcium concentration (for concentrations ranged from 120mg/L to 200mg/L) whereas the growth rate does not vary [10]. It has been shown by assessing the drop of the concentration of calcium in a pure calco-carbonically water that the rate of nucleation and the crystalline growth rate decrease with the water hardness [93].

Euvrard *et al.* pointed that at low degree of hardness (10°F) the nucleation was progressive and vaterite was formed whereas it was instantaneous for a higher degree of hardness (30°F and 50°F) and calcite was observed. This show a strong correlation between nucleation and crystalline form [90].

The general trend of calcium carbonate formation with the increase of $[Ca^{2+}]$ is the increase of the number of crystals and the average size of each crystal [108].

2.4.5 Effects of Magnesium

The influence of Mg^{2+} on calcium carbonate formation has been widely studied as strong effects on calcite have been pointed out.

Magnesium is adsorbed onto the surface of calcite and incorporated in the crystal lattice. The magnesian calcite is more soluble than pure calcite, resulting in an inhibition of calcite whereas Mg^{2+} is not incorporated in aragonite crystal. That is why magnesium inhibits nucleation and growth of calcite.

The magnesium ions does not affect the nucleation and the growth of the aragonite [107, 109]. The inhibition of the calcite growth is greater when the growth occurs according to the 2-D growth model [109]. As the calcite is preferentially formed at low temperature, the inhibition of effects of Mg^{2+} on calcium carbonate are greater [106].

The amount of Mg^{2+} incorporated in the calcite lattice increases with the initial concentration of Mg^{2+} in the solution. Moreover the nature of the magnesium salt as a source of Mg^{2+} influences its incorporation into the crystal lattice [110].

With the non uniformly incorporation of magnesium in the crystal lattice of calcite, the properties of the new calcite formed have changed: the growth rate is lower than the one observed with the original calcite due to the developing new crystal faces with a high Mg^{2+} density and lower growth rate [111].

Chen *et al.* has studied the effects of magnesium on the early stages of calcium carbonate formation by electrochemical method (RDE). It has been found that magnesium is incorporated in $CaCO_3$ nuclei and a thin layer of Mg-$CaCO_3$ is formed and adsorbed on the metal surface at the initial stage of scale formation. This layer is the main contribution of the coverage of the surface [112]. The percentage of the Mg/Ca ratio in the deposit is proportional to the Mg concentration in the scaling solution. The inhibiting effects of magnesium are greater in the bulk precipitation than on the surface deposition [113].

Magnesium affects the morphology of the crystals of calcite: Mg^{2+} leads to distorted crystals and increases the roughness of the surface [114].

2.4.6 Effects of foreign ions

The presence of foreign ions or impurities influences the crystallisation mechanism and the nature of the precipitate. These compounds act by adsorbing the surface of the crystals or by inserting the crystal lattice as seen with the magnesium ions.

Roques demonstrated that the effects of foreign ions on $CaCO_3$ formation depend on the size of the ions (the ionic radius) and on the hydration energy (as dehydration is necessary to integrate the crystal structure) [115]. Table 2.4 summarises the required conditions for a foreign ion to integrate the crystal lattice of $CaCO_3$. Ions smaller than Ca^{2+} (to be able to insert themselves into the crystal lattice) and with a much higher hydration energy tend to lead to the formation of aragonite under conditions where calcite would be preferentially formed.

The size of the ion is not the only conditions required as a smaller ion than Ca^{2+} with similar hydration energy would not lead to any change of the morphology of the crystals. An ion bigger than Ca^{2+} is not able to integrate the crystal lattice and generally the hydration energy of these ions is lower than Ca^{2+} [115].

Table 2.4: Necessary conditions for a foreign ion to incorporate into the crystal lattice of $CaCO_3$

Ionic radius	Hydration energy	Variation of the morphology
$R_x<R_{Ca2+}$	$E_x>>E_{Ca2+}$	Calcite to Aragonite
$R_x<R_{Ca2+}$	$E_x\approx E_{Ca2+}$	Calcite
$R_x>R_{Ca2+}$	$E_x<E_{Ca2+}$	Calcite

The sorption behaviours of the ions on $CaCO_3$ crystals is a determining factor in the effects of these ions on the properties of the precipitate. Cadmium (Cd) is preferentially incorporated into the step structures of the crystals whereas lead (Pb) forms a precipitate onto the surface of the crystals. Hausner *et al.* studied the effects of Pb and Cd in similar experimental conditions on the dissolution of $CaCO_3$ and the authors showed the dissolution inhibiting effects of Cd on calcite whereas Pb does not inhibit the dissolution of calcite [116].

The inhibiting effects of the zinc (Zn^{2+}) and the copper (Cu^{2+}) have been pointed out by Meyer *et al.* and confirmed by Guizellaoui and Lopez [117-119]. The addition of Zn^{2+} leads to a decrease of the size of the crystals of $CaCO_3$ with a more significant number of crystals. The use of the allotropic cell device demonstrated the $CaCO_3$ inhibiting effects of Cu^{2+} and Zn^{2+} by changing the morphology of the crystals from calcite to aragonite suspensions which act as nuclear centres of crystalline growth in solution; the presence of Zn^{2+} and Cu^{2+} leads to the formation of crystals in the bulk rather than onto the surface [118].

It was found that the iron (Fe) reduces the scaling risks. Fe^{2+} acts on the crystallization process and leads to an increase of the formation of fine particles in the bulk solution. Iron could precipitate in the form of ferric hydroxides which could act as nucleation sites. A comparative study of the effects of Fe^{2+} and Mn^{2+} and the effects generated by Mn^{2+} on $CaCO_3$ formation are less significant [120].

The kinetics of formation are only slowed down at the initial step of $CaCO_3$ but after this step, Mn^{2+} does not affect the crystallisation of $CaCO_3$ in a significant way [120].

Sulphate ions have been studied by an electrochemical method and it has been found that SO_4^{2-} seem to hinder the aragonite formation by acting directly on the crystallization or by promoting the gel-like Mg-containing layer that forms usually in the experimental conditions used [77].

2.4.7 Effects of dissolved oxygen

Gabrielli *et al.* have studied the effects of oxygen concentration on calcium carbonate deposition by electrochemical method. The scaling rate and the amount of calcium carbonate increase with oxygen concentration. Observations with a SEM permit to determine that the nucleation rate is very fast at high concentration whereas it is slow at low concentration. Moreover the microscopic observations confirmed that the crystal morphology is dependent on oxygen concentration [21].

2.4.8 Effects of the nature of the substrate of deposition

Calcium carbonate formation occurs onto different substrates and its mechanism of formation may vary according to the surface of deposition.

Dalas *et al.* studied the effects of the nature of the material added into a scaling solution as substrate of $CaCO_3$ formation. Calcite may nucleate and grow onto chitin and cellulose [121, 122]. Vaterite is preferentially formed onto cholesterol and calcium carbonate monohydrate onto polymeric substrates [123, 124]. It has been seen that the vaterite and the $CaCO_3$ monohydrate were transforming into calcite. These studied have been realised under the same temperature and pH conditions so the formation of calcite might be due to the experimental conditions and not specific to the substrate.

Nevertheless the formation of vaterite and $CaCO_3$ monohydrate show the different mechanisms of $CaCO_3$ deposition regarding to the substrate. Sabbides and Koutsoukos demonstrated that the addition of calcite, aragonite or vaterite seeds in a scaling solution leaded only to aragonite overgrowth pointing out that the substrate is not the key factor controlling the nature of the overgrowth [125].

The nature of the substrate has an important effect on the nucleation process and the scaling rate of $CaCO_3$. Electrochemical tests have been realised with different type of working electrode (differing by the nature of the material) and it has been found that gold surface permits a quick scale deposition compared to bronze and stainless steel surfaces which allow a slower scale deposition [47]. The first steps of the nucleation are influenced by the nature of the substrate but not the lateral growth [24].

A difference of the amount of $CaCO_3$ formed onto metal substrates has been pointed out, copper permitting a greater deposition than stainless steel [126] and struvite ($MgNH_4PO_4.6H_2O$) precipitates in a greater extent onto a stainless steel surface compared to a teflon surface [127].

The morphology of the precipitate does not seem to depend on the nature of the metallic substrate used. The morphology of the calcium carbonate formed onto stainless steel 316L, teflon and copper was similar regardless the substrate of deposition [105]. A comparative study of the metallic and the plastic substrates pointed out that the nature of the substrate influences the kinetics of precipitation [93].

2.4.9 Effects of the surface roughness

Mantel *et al.* did not show any influence of the surface roughness on $CaCO_3$ deposition by studying the current density variations by electrodeposition [128] but it is well known that the surface finish plays a great role in scale precipitation. Gunn showed that the rate of crystallisation of $CaSO_4$ is highly affected by the surface conditions. The greatest deposition of $CaSO_4$ was obtained with rougher surfaces [129]. This has been verified with $CaCO_3$ precipitation by MacAdam and Parsons: the scaling rate increases with the degree of roughness. A high rough surface provides favourable nucleation sites [126]. This is also supported by Doyle *et al.* who studied the effects of the surface roughness on struvite precipitation [127].

The roughness of a surface influences the adhesion of a calcite precipitate onto the surface: the disbonding stress of a deposit adhering to a smooth surface (Ra=0.1μm) is 30 times smaller than that required for a deposit adhering to a rough surface (Ra=18-24μm) [130].

This is probably due to the increase of surface of deposition area in the case of a rough surface and a rough surface offers more hooking sites promoting a mechanical interlocking effect [130].

2.4.10 Effects of the hydrodynamic conditions

Recent works on the influence of the hydrodynamic conditions on the deposition of $CaSO_4$ scale on aluminium and stainless steel showed the increase of the deposition rate with the Reynolds number. This is due to the higher supply of scaling elements onto the surface and it also provides the necessary activation energy needed for the nucleation or epitaxial growth of the crystals. Moreover these works demonstrated that the mass transport was diffusion controlled [131, 132]. Similar studies have been realised on $BaSO_4$ and the same conclusions have been raised [133]. These results are in a good agreement with previous studies done on $CaCO_3$. The scale growth rate is dependent on the flow velocity containing the scaling elements. Hasson *et al.* assessed the growth of $CaCO_3$ onto a surface (grams of $CaCO_3$ per hour per square meter) as a function of the Reynolds number and the authors found that the amount of $CaCO_3$ formed is a linear function of the Reynolds number. This is due to the dependence of the mass transfer on the Reynolds number [134].

The flow rate affects the morphology of the deposit: for low flow rate, bigger crystals of $CaCO_3$ are formed and the layer are more compact [103].

The flow system can affect the scale deposition in different extent according to the flow system considered. Hasson *et al.* studied the effects of scale inhibitors in two different flowing system: a flow pipe system and a falling film system [135]. The main difference between these two systems comes from the fact that the solution is not in contact with a gaseous phase in a flow pipe system. It is a closed system whereas the falling film system is an opened system. The main consequence of this difference is the supersaturation: it is almost constant inside the pipe whereas the supersaturation is much higher at the liquid/air interface in the opened system (due to CO_2 desorption from the liquid to the gas phase). Hasson determined the higher scale tendency in the falling system compared to the flow pipe system and different inhibition properties for scale inhibitors according to the system considered.

2.4.11 Effects of the pressure

During the oil and gas extraction process, the pressure varies extremely and can reach 100MPa. The pressure decreases with the increase of the supersaturation for carbonates and sulphates scaling solutions. The effects of the pressure is more significant at high temperature [67].

2.5 Mechanisms of inhibition

According to Freedman, three empirical processes are involved in scale inhibition: threshold effects, crystal distortion and dispersancy [136]. The different mechanisms of inhibition are summarised in Figure 2.16. Inhibitors act according to their own mechanisms. They can act on the nucleation step, the crystal growth, on the agglomeration of the fine scale particles. The effectiveness of an inhibitor is its ability to maintain scaling ions in solution. The MIC (Minimum Inhibitor Concentration) is a measurement of the efficiency. It is the concentration which prevents scale formation over the test period [137].

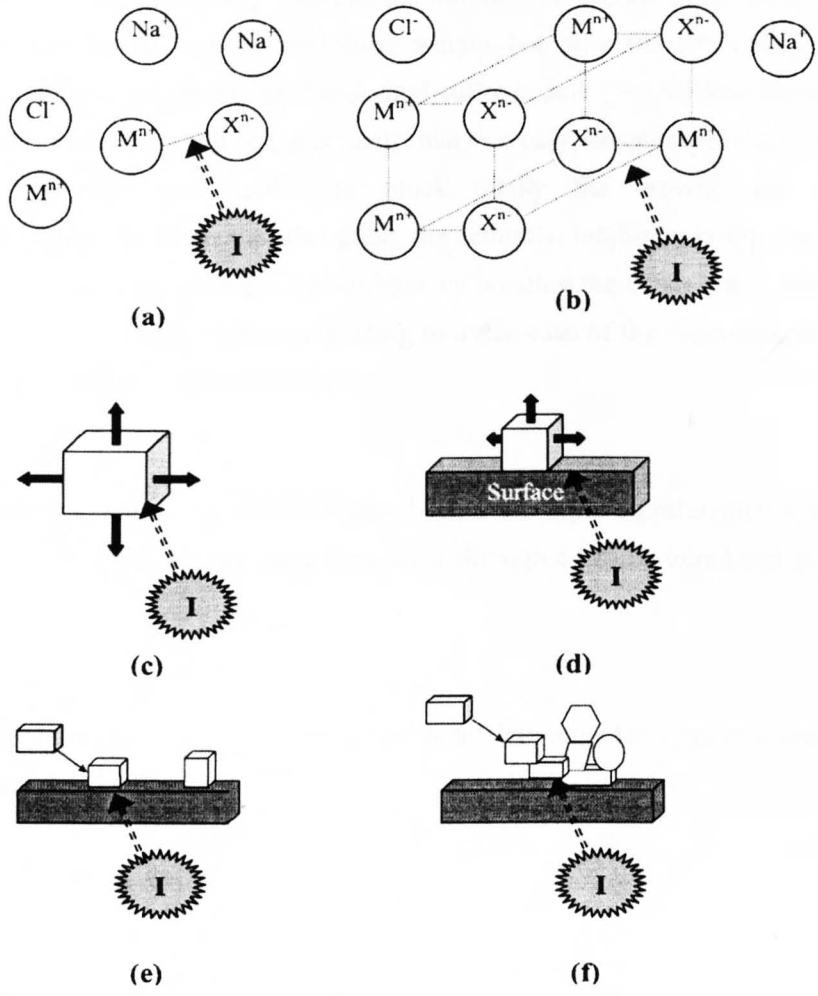

Figure 2.16: Main mechanisms of scale formation and inhibition : (a) ion pairing formation, (b) prenucleation cluster, (c) homogeneous nucleation and crystal growth, (d) heterogeneous nucleation, (e) crystal adsorption, (f) particles agglomeration, I: Site of possible inhibitor action [138].

2.5.1 Threshold effect

It is in the 1930's the principle of threshold was discovered when it has been noticed that a large quantity of insoluble material can be held in solution by a small quantity of inhibitors (a few ppm) [139]. The threshold effect refers to the ability of organic chemicals at sub-stoichiometric levels to prevent or delay scale formation [136]. Threshold level of chemicals are often used to avoid scale formation [18].

The adsorption behaviour of polyelectrolytes on $BaSO_4$ crystals has been study and it has been pointed out the relationship between the inhibitor effect, the maximal coverage of the inhibitor on the crystal and the molecular weight but only for structurally identical compounds. A copolymer of maleic acid and vinyl sulfonic acid (PMA-PVS) showed better inhibition properties of the growth of the crystals than two polyphosphinoacrylates whereas a lower surface coverage was needed to block totally the growth. For the two polyphosphinoacrylates, the better the adsorption, the better the inhibition [140]. Benton *et al.* showed the phosphonates act as threshold inhibitor by bonding the crystals and blocking the growth sites and by promoting nucleation leading to a decrease of the supersaturation of the solution and the generation of small nuclei [141].

The phosphorus containing inhibitor adsorb onto the crystal preferentially at growth sites such as steps and kinks. Growth may then occur through a less favoured and slower way [19].

The type and thus the strength of the formed bond determine the final attachment of the inhibitor to the crystal [140].

2.5.2 Crystal distortion

When minerals precipitate from a solution containing scale inhibitors, the crystals are often distorted which can be less adherent on a surface and have less tendency to agglomerate [136]. Davis *et al.* shown the use of an inorganic phosphonate inhibitors generates calcium carbonate crystals completely distorted [19].

Benton *et al.* demonstrated that organic additives can generate large modifications of the crystal habit. Phosphonate compounds have been studied on $BaSO_4$ formation and the crystals formed appeared to be spheroid and 15-20 times smaller than the crystals obtained with no additive [141]. This was in good agreement with Van der Leeden *et al.* who illustrated the variations of the morphology of $BaSO_4$ with the addition of a copolymer (PMA-PVS) [140]. Davis *et al.* showed the drastic changes of the morphology of $CaCO_3$ by addition of organic phosphate inhibitor [19].

Polymers act on the morphology of the crystals and can lead to the distortion of the crystals especially the polymers with carboxylate functional groups as they interact with Ca^{2+} of the crystals stabilizing the suspension and so preventing the crystalline formation [142].

2.5.3 Dispersancy

It is the ability to minimize agglomeration and settling of suspended solids. It is a charge repulsion process. The negative charge density is increased on the surface of the particle by the attachment of active chemicals so that the particles repel each other [136]. The polymers with sulfonate functional groups are excellent at enhancing the negative charge of crystal formations thus repulsion occurs. This inhibition mechanism is based on a adsorption/desorption equilibrium of the polymer [142].

Schwamborn studied the effects of the chemical synthesis of polyaspartic acid on their ability to inhibit calcium carbonate. Their inhibition properties has been determined by their calcium carbonate dispersing capacity. The four aspartic acids studied showed good dispersion properties (more than 130mg $CaCO_3$/g) [143].

2.6 Scale inhibitors

The type of scale inhibitors used in the oil and gas sector is various: phosphonates [18, 19, 60, 139] ,polyphosphates [18, 51, 52, 57], polyelectrolytes and carboxylic acids.

2.6.1 Phosphonates

The efficiency of phosphonates (Figure 2.17) to inhibit calcium carbonate formation has been widely demonstrated and their stability at high temperature is a significant advantage for the industry [144]. The DETPMP for example is widely used in the oil and gas sector.

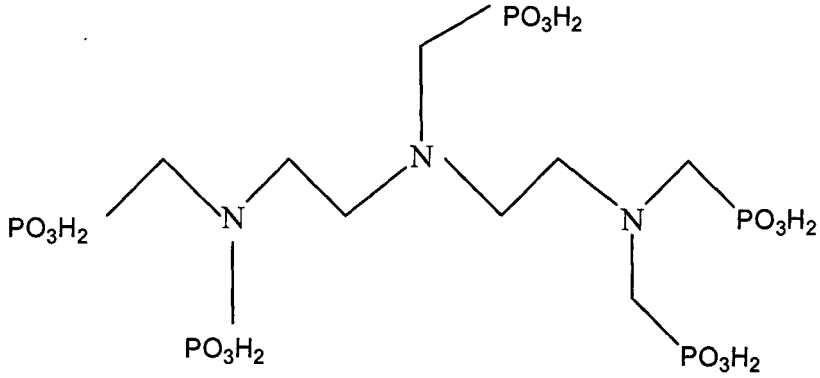

Diethylenetriaminepenta(methylenephosphonic acid) (DETPMP)

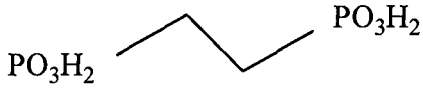

Ethane-1,2-diphosphonic acid
(1,2 EDPA)

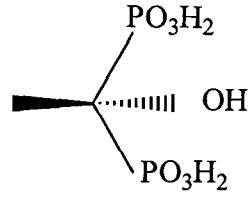

Hydroxyethylidenediphosphonic acid (HEDP)

Figure 2.17: Schematic representation of phosphonates used as scale inhibitors

The mechanism of inhibition of $CaCO_3$ of the phosphonates involves blockage of crystal growth sites [144]. They act on the morphology of $BaSO_4$ and the presence of phosphonates in a scaling brines leads to distorted crystals. It has been shown that the phosphonates interact with Mg, Ca, Sr and Ba (following the ionic radius of the ions). Benton *et al.* showed the greater efficiency of the phosphonates when calcium is present in the scaling solution.

The calcium phosphonate complexes inhibit the growth of the crystals of $BaSO_4$ by being involved in the crystallisation process [141]. It has been proposed that calcium phosphonates inhibit $BaSO_4$ according to two mechanisms; by inducing the nucleation and by blocking the growth sites.

The number of phosphonates functional groups improves the inhibition property of a molecule but it is not the most important conditions. The molecular structure plays a crucial role in the inhibition efficiency of the phosphonates has demonstrated by Davis *et al.* [19].

HEDP (Hydroxyethylidenediphosphonic acid) (Figure 2.17) affects $CaCO_3$ formation with two different mechanisms according to the temperature; at low temperature, HEDP acts at a threshold level and at higher temperature HEDP by reducing the rate of CO_2 evolution indirectly increasing the pH [139]. Its efficiency to inhibit $BaSO_4$ has been illustrated by He *et al.* [60].

DETPMP is a common scale inhibitor and it has been widely study. It acts mainly as a crystal growth retardation by blocking the growth site of the crystals [145]. Its efficiency is not enhanced by addition of EDTA and citric acid [69] but it is increased with the presence of Ca^{2+} in a low barium sulphate scaling brine [145]. Moreover it has been proved that phosphonates (in particular EDTMP, ethylenediaminetetrakis(methylenephosphonic acid) inhibit strongly $CaCO_3$ formation onto a surface by adsorbing on this surface and EDTMP inhibits growth of $CaCO_3$ in the bulk solution by bonding the kink and step sites growth of the crystals [58].

2.6.2 Polyphosphates

In the RO (Reverse Osmosis) desalination plants, SHMP (sodium hexametaphosphate, Figure 2.18) was used to control sulphate-based scales and to prevent any residual alkalinity from depositing $CaCO_3$. Its use was combined with acid to control alkaline scale. Major problems where due to the use of this combination of products like acid-induced corrosion and reversion of SHMP to the sludge-forming orthosphosphate.

Butt *et al.* showed that a replacement by a commercial phosphonate was possible as it exhibited better inhibition properties (regarding $CaCO_3$, $SrSO_4$ and $CaSO_4$) than the SHMP [57].

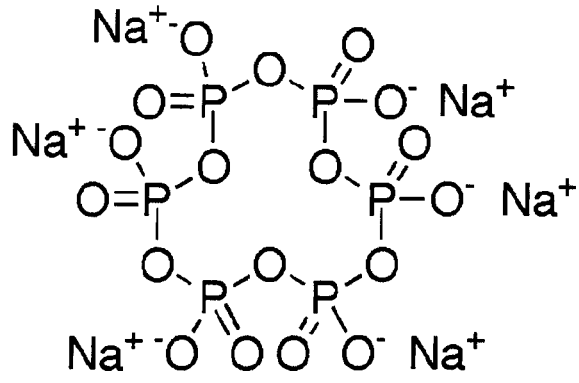

Figure 2.18: Sodium hexametaphosphate

A comparative study showed the relative efficiency of different polyphosphates. The tripolyphosphate is seen to inhibit $CaCO_3$ in a greater extent than pyrophosphate and hexametaphosphate (Figure 2.18 and Figure 2.19). The Langmuirian adsorption of the polyphosphates on the crystals of calcium carbonate has been pointed out as their mechanism of inhibition [52]. Hasson *et al.* studied by freely falling film method a ring structured hexametaphosphate and a linear chained polyphosphate and did not find any difference in the $CaCO_3$ inhibition: both inhibitors increased the induction time and the scale growth reached an asymptotic limiting thickness [66].

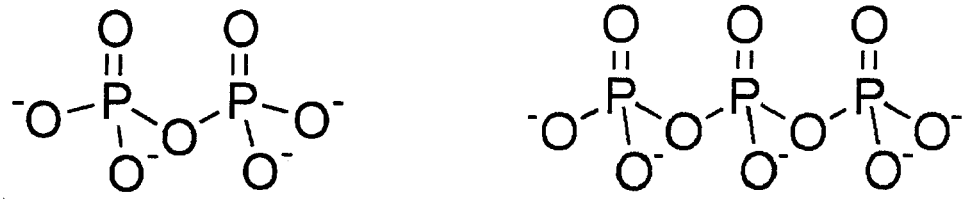

(a) (b)

Figure 2.19: General molecular structure of (a) pyrophosphates and (b) tripolyphosphates

The morphology of the crystals present in the solution could influence the adsorption properties of the phosphonates but Grases and March by adding different types of crystal seeds (with different morphology) did not show any difference of the inhibition of $CaCO_3$ [51].

2.6.3 Polyelectrolytes

Figure 2.20 shows various types of polymers used as scale inhibitors in the industry.

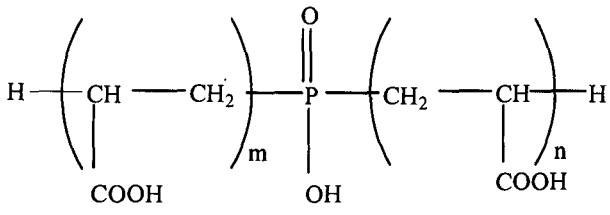

Polyphosphinocarboxylic acid (PPCA)

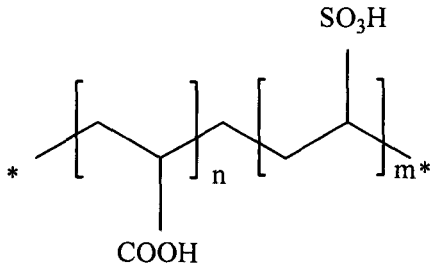

Polyvinyl sulfonate and Polyacrylic acid copolymer (PVS)

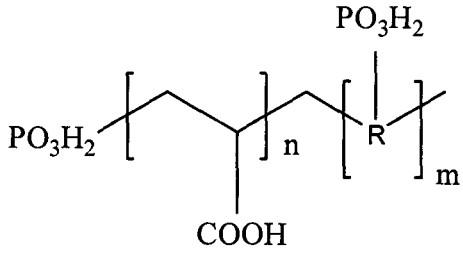

Phosphonocarboxylic acid (POCA)

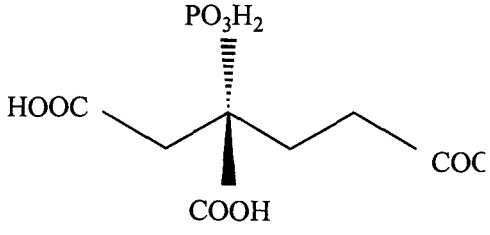

2-phosphono-butane-1,2,4-tricarboxylic acid (PBTC)

Figure 2.20: Schematic representation of polyelectrolytes used as scale inhibitors

2.6.3.1 Phosphinopolycarboxylic acid (PPCA)

The PPCA acts as a nucleation inhibitor and it has a great affinity with calcium ions. Graham *et al.* showed that contrary to what was seen with the DETPMP, Mg^{2+} do not poison the efficiency of PPCA. As observed with the DETPMP, the Ca^{2+} enhances the efficiency of the PPCA in a low barium sulphate scaling brine but in a medium scaling solution the efficiency of the PPCA decline with the addition of Ca^{2+}. This last remark is due to the incompatibility between the concentration of Ca^{2+} used (between 657 and 2257ppm) and the PPCA. The precipitation of PPCA with Ca^{2+} (or Mg^{2+}) limits the amount of PPCA available to inhibit $BaSO_4$ [145].

The effects of 5 and 10ppm of different types of scale inhibitors (DETPMP, Phosphonates and phosphate ester) have been showed to be the strongest at 5ppm for the PPCA by tube blocking tests. At 10ppm all the inhibitors presented similar inhibition properties [70].

2.6.3.2 Polymers

Yuan *et al.* studied two different polymers: a sulphonated carboxylic acid copolymer (S-PCA) and a sulphonated phosphinocarboxylic acid copolymer (S-PPCA) [69]. Both inhibitors inhibit $BaSO_4$ crystallisation partially by a dispersion mechanism. A main finding from this study was the different evolution of their inhibition properties: after 10 minutes of tests the inhibition of these two chemicals were similar whereas after 3 hours a large difference was observed (S-PPCA lost completely its inhibition whereas S-PCA still has 50% of efficiency).

The effects of a copolymer of maleic acid and vinyl sulfonic (PMA-PVS) [140] or acrylamide [141] on the growth inhibition of $BaSO_4$ has been demonstrated. These polymers interact with the crystals resulting in a change of the morphology.

2.6.4 Carboxylic acids

2.6.4.1 Polyacrylic acids

Polyacrylic acids (Figure 2.21) affect strongly the morphology of the crystals of $CaCO_3$ and leads to the formation of distorted calcite [100].

Polyacrylic acid can be found under polymers forms like phosphinopolyacrylic acid [146] (widely used in the oil and gas sector) or under acrylic polymer used in RO (reverse osmosis) desalination process [66]. The efficiency of two acrylic polyelectrolytes to prevent the formation of $CaCO_3$ has been compared with polyphosphate and polyphosphonates has been studied and similar efficiency has been seen for a range of concentration 0.2 to 0.5ppm [66].

A significant difference of efficiency between the polyacrylic acid and a phosphonate based polymer (2-phosphonobutane-1,2,4-tricarboxylic acid, PBTCA) has been found in favour of the PBTCA (it is important to note that the concentration (5ppm) and the methods used were different) [65].

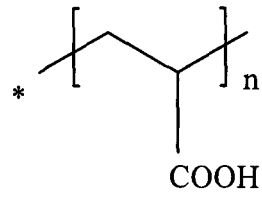

Figure 2.21: Schematic representation of Polyacrylic acid (PAA)

2.6.4.2 Polymaleic acid

Some characteristics of polymaleic acid (Figure 2.22) are similar to aquatic fulvic acids (size, elemental composition, FT-IR spectra). Physical and chemical properties of the polymaleic acid are similar to aquatic and terrestrial fulvic acids but contrary to these acids the polymaleic acid exhibits a low molecular absorptivity (measurement of how strongly a chemical absorbs the light at a given wavelength) [147].

The anti-scaling properties of the fulvic acid has been studied. A complete inhibition of nucleation of $CaCO_3$ has been observed by the authors when the fulvic acid was present in the system at the beginning of the test and when vaterite was present in the system first, a concentration between 1.5 and 4ppm of fulvic acid generated a large decrease of the supersaturation of the solution. They pointed out that the fulvic acid adsorbs on the vaterite surface to block the growth sites and that the high affinity between the calcium carbonate and the fulvic acid is due to electrostatic interactions [148].

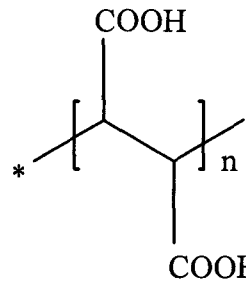

Figure 2.22: Schematic representation of Polymaleic acid (PMA)

PMA has been studied as a surface treatment to protect calcite from acid attack. It has been found that a protective film is formed on the surface which appears to be stable and non porous [149] but a comparison between the polymaleic acid and the phosphoric acid shown that phosphoric acid is more suitable to protect calcite stone material [150].

2.6.4.3 Polyaspartic acid

The mechanism of polyaspartic acid (Figure 2.23) scale inhibition has been studied by electrochemical method [151]. It appears that they act on both nucleation and growth of calcium carbonate. All polyaspartates act as threshold inhibitors i.e. the concentration at which they are efficient is below the stoechiometric value with calcium carbonate. The study of the changes in the crystal morphology allowed the authors to understand how polyaspartates act. It is a combined model of complexation, adsorption and dispersion.

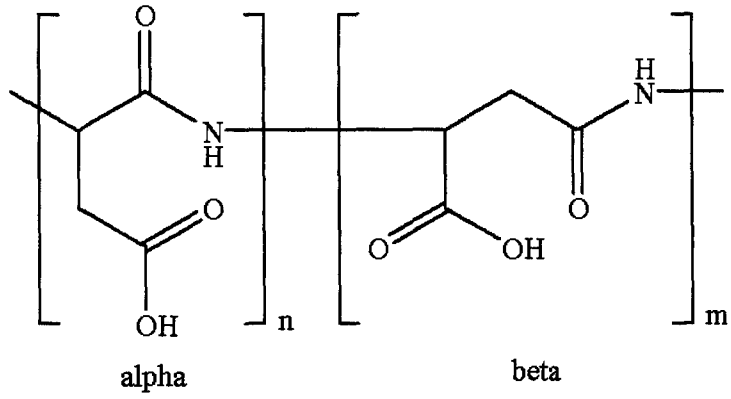

Figure 2.23: Schematic representation of a Polyaspartic acid

The morphology of calcium carbonate deposit formed in presence of polyaspartic acid is vaterite dominant leading to a more porous and less adherent deposit onto a metal surface [151]. Their adsorption on a metallic surface depend on their molecular weight but not on their level of ramification. The amount of adsorbed polyaspartate decreases with the increase of the molecular weight [151]. The optimum molecular weight for polyaspartate inhibition on calcium carbonate and barium sulphate is in the range of 3000-4000Mw [55].

Different pathways exist to produce polyaspartates. The choice of the production way is important because it has an effect on the structure of the molecule (molecular weight, molecular geometry) and so on its properties like biodegradability, sequestring and dispersing activities [143, 152]. The initial molecule used to synthetise polyaspartic acid influences greatly the properties of the final molecule. Estievenart *et al.* studied four polyaspartic acids all synthesized from aspartic acid according to different pathway. The polyaspartic acids obtained presented specific calcium carbonate inhibition efficiency and biodegradability. Schwamborn *et al.* used maleic acid anhydre as initial molecule and they showed that the polyaspartic acid is a biodegradable alternative to currently homo and copolymers with the same efficiency.

Moreover maleic acid anhydre is available in large quantity without additional new investment. As the reactants, the reaction conditions, the reaction techniques and the reaction equipment during the synthesis play a role in the properties of the final molecule, there is not only one specific polyaspartic acid produced from one pathway but the combinations of all the parameters leads to a wide range of molecules with different properties [143].

The efficiency to inhibit calcium and magnesium containing scale of a polyaspartic acid produced from maleic acid anhydre has been tested [153]. The authors showed the influence of the pH on the ability of the polyaspartic acid to inhibit scale. Under their specific experimental conditions 100% efficiency was reached with 3ppm of inhibitor at pH 3 whereas a concentration of 9ppm at pH 9 was needed to reach 97.24% and 98.63% for the calcium and magnesium containing scale respectively.

Likewise having interesting inhibition properties on calcium carbonate, polyaspartic acids present a high biodegradability and they could be an alternative to existing chemistry as the inhibition efficiency of polyaspartic acids regarding $CaCO_3$ and $BaSO_4$ is comparable or even better as the efficiency measured under similar experimental conditions of polyacrylic acids [3, 55].

2.6.4.4 Carboxymethyl inulin

Carboxymethyl inulin (Figure 2.24) is formed by carboxylation of a natural carbohydrate obtained from the chicory plant. A study on the toxicological profile of this inhibitor shown that CMI does not present significant toxicological and genotoxical characteristics. The biopolymer backbone is a polysaccharide composed of D-fructose units linked at the 1 and 2 position and end-capped with a D-glucose [154].

Static and dynamic adorption/desorption tests have been done with CMI (Carboxymethyl inulin) on limestone core material. Its behaviour is similar to polyacrylic acids and CMI presents superior adsorbing properties [68].

The degree of substitution has a significant role in the inhibition properties of CMI. When the degree of substitution and the polymerization degree are high, inhibitory activity is optimum [56, 155]. Others carboxymethyled polysaccharides (dextrine, cellulose) show good inhibition properties whereas a carboxymethyled disaccharide has no influence on the calcium carbonate crystallization [56].

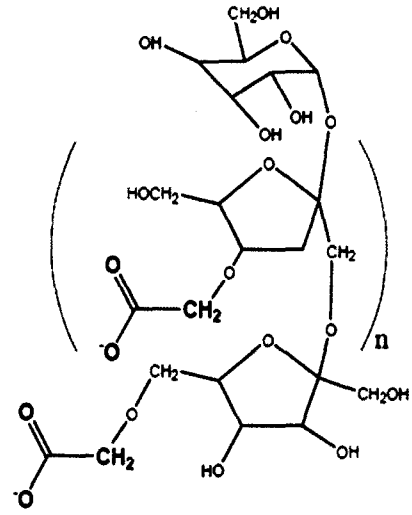

Figure 2.24: Schematic representation of carboxymethyl inulin

Moreover, CMI was used as a dissolver of silica and calcium carbonate scale deposits and it is a good cations sequestrants [154]. It is capable to inhibit a variety of scale deposit (calcium sulphate, barium sulphate) [155]. CMI prolongs the induction time of $CaCO_3$ formation. Demadis *et al.* showed that the addition of 300ppm of CMI delay the precipitation by 50 minutes and by 20 minutes for an addition of 100ppm.

The addition of 10,000ppm of CMI has a dramatically cleaning effect and very rapid (within 6 minutes) on $CaCO_3$ already formed [156] illustrating the dissolvent effects mentioning previously.

The polymaleic acid, the polyaspartic acid and the carboxymethyl inulin present not only scale inhibition properties but good ecotoxicological characteristics as well.

2.7 Green chemistry and legislation

2.7.1 Principles of Green Chemistry

Green chemistry is the utilization of a set of principles that reduces or eliminates the use or generation of hazardous substances to human health or environment in the design, manufacture and application of chemical products [157].

Pioneering scientists have defined twelve principles of green chemistry [157]:

1. It is better to prevent waste than to treat or clean up waste after it is formed.

2. Synthetic methods should be designed to maximise the incorporation of all materials used in the process into the final product.

3. Wherever practicable, synthetic methodologies should be designed to use and generate substances that possess little or no toxicity to human health and the environment.

4. Chemical products should be designed to preserve efficacy of function while reducing toxicity.

5. The use of auxiliary substances (e.g. solvents, separation agents, etc.) should be made unnecessary wherever possible and, innocuous when used.

6. Energy requirements should be recognized for their environmental and economic impacts and should be minimized. Synthetic methods should be conducted at ambient temperature and pressure.

7. A raw of material of feedstock should be renewable rather than depleting wherever technically and economically practicable.

8. Unnecessary derivization (blocking group, protection/deprotection, temporary modification of physical/chemical processes) should be avoided whenever possible.

9. Catalytic reagents (as selective as possible) are superior to stoichiometric reagents.

10. Chemical products should be designed so that at the end of their function they do not persist in the environment and break down into innocuous degradation products.

11. Analytical methodologies need to be further developed to allow for real-time, in-process monitoring and control prior to the formation of hazardous substances.

12. Substances and the form of a substance used in a chemical process should be chosen so as to minimize the potential for chemical accidents, including releases, explosions, and fires.

Green chemistry has come to the focus of governments and industries and development efforts are conducted with the goal being to reduce emissions and waste with zero emissions, to develop safer products and process, to conduct life-cycle assessments of the processes and increase efficiency in use of materials, energy and water [158].

The oilfield industry worked in agreement with green chemistry principles in order to find green chemicals, especially green inhibitors, to reply to the demand of the legislation.

2.7.2 Strategy to protect marine environment

The OSPAR Commission is the international body responsible for the harmonisation of strategies and legislation in the North-East Atlantic region. One of the objectives of this committee with regard to hazardous substances is to prevent pollution of the maritime area by continuously reducing discharges, emissions and losses of hazardous substances, with the ultimate aim of achieving concentrations in the marine environment near background values for naturally occurring substances and close to zero for man-made synthetic substances [159].

The eutrophication is the accumulation of chemical nutrients, generally nitrogen and phosphorous compounds in an ecosystem. The main consequence of this accumulation of nutrients is the massive development of primary productivity (excessive growth of plant like algae, called algal bloom) resulting to a decrease of oxygen level and severe reductions of the water quality leading to the death of the animals from the ecosystem.

Regarding eutrophication, OSPAR's objective is to achieve, by the year 2010, and maintain a healthy marine environment where eutrophication does not occur [159].

2.7.3 Legislation

A Harmonised Mandatory Control System (HMCS), implemented of OSPAR Decision 2000/2 defines the parameters chosen for the North-East Atlantic area [160, 161].

The aim of HMCS is to protect the marine environment by identifying chemicals used in offshore oil and gas operations. A legislation drives the development and selection of chemicals which have the lowest impact on the marine environment

The HMCS system has four aspects Figure 2.25:

- Environmental data of the chemical,
- HOCNF (Harmonised Offshore Chemical Notification Form),
- Pre-screening scheme,
- Chemical Hazard Assessment and Risk Management.

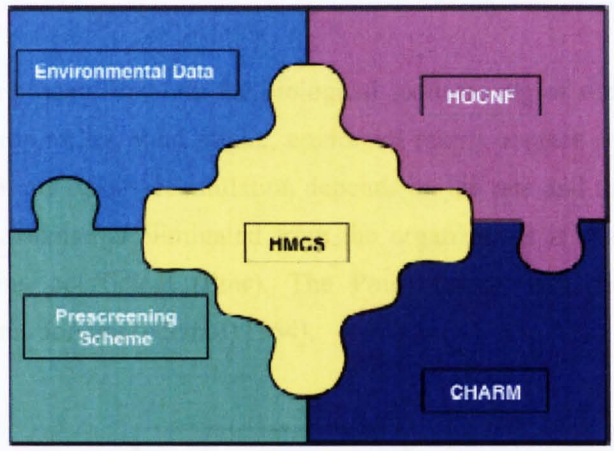

Figure 2.25: Different element of the HMCS system [160]

2.7.3.1 Environmental data

Information on the volume discharged, discharge patterns, environmental fate and ecotoxycological data are required in this step. The ecotoxycological data concern three characteristics [162]:

- **Toxicity**

The toxicity is the degree to which a chemical can harm humans or animals. It is determined by the Effect Concentration (EC) and the Lethal Concentration (LC) which will affect 50% of the population tested.

EC_{50} or LC_{50}>1mg/L for inorganic substances
EC_{50} or LC_{50}>10mg/L for organic substances

- **Biodegradation**

The biodegradation is the breakdown of organic contaminants by microbial organisms into smaller compounds. The microbial organisms transform the contaminants through metabolic or enzymatic processes. Biodegradation processes vary greatly, but frequently the final product of the degradation is carbon dioxide or methane. Biodegradation is a key process in the natural attenuation of contaminants at hazardous waste sites [163].

>60% in 28 days
If <20% the chemical is candidate for substitution

- **Bioaccumulation**

The accumulation process involves the biological sequestering of substances that enter the organism through respiration, food intake, epidermal (skin) contact with the substance, and/or other means. The rate of bioaccumulation depends on the rate and the mode of uptake and how quickly the substance is eliminated from the organism. It is characterized by the octanol/water partitioning coefficient (*Pow*). The *Pow* characterises the affinity of the chemicals with the organic solvent (octanol) [164].

Log *Pow*<3

To enter the PLONOR List (Pose Little Or NO Risk), a chemical must pass two of these three criteria with a biodegradability at least up to 20%. The details of the tests required are given Table 2.5.

Table 2.5: Environmental Tests required under HMCS [165]

	Test Required	**Test Protocol**
Toxicity	Algae	72hr EC_{50}: *Skeletonema costatum* ISO/DIS 10253
	Crustacean	48hr LC_{50} : *Acartia tonsa* ISO TC 147/SC5/WG2
	Fish	96hr LC_{50}: *Schophthalamus maximus*, juvenile OECD 203 modified for marine species
	Crustacean-Sediment reworker	10 day LC_{50}: *Corophium valutator* PARCOM
Biodegradation	Water soluble substances	28 day aerobic, marine OECD 306
	Water insoluble substances	28 day aerobic, marine BODIS (BOD for Insoluble Substances)
Bioaccumulation	Bioaccumulation potential	Octanol/water partition co-efficient (log P_{ow}) OECD 117 or 107

2.7.3.2 HOCNF

The data are reported to the respective authority governing the waters in which the activities will take place, using a Harmonised Offshore Chemical Notification Form document. This document aims to summarise some characteristics of the chemical in terms of compositions, use, discharge in the environment and details of the supplier [166].

2.7.3.3 Pre-screening scheme

The scheme presented in Figure 2.26 is used to analyse the HOCNF. There are five outcomes:

- Permission,
- Refusal of permission,
- Substitution,
- Temporary permission with the aim of seeking hazardous alternatives,
- Ranking (according to CHARM).

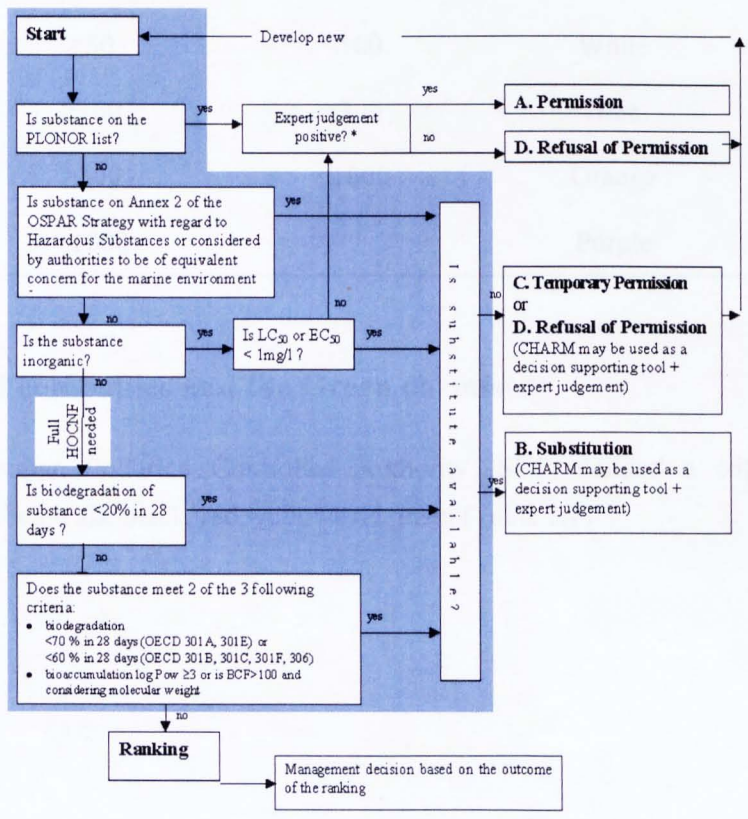

Figure 2.26: HSMC Harmonised pre-screening scheme [167]

2.7.3.4 CHARM

It is a tool to characterize the degree of harm that a chemical can generate. PEC (Predicted Environmental Concentration), related to chemical properties such as bioaccumulation, biodegradation, concentration, and PNEC (Predicted No Effect Concentration), related to the toxicity of a product, are calculated and HQ (Hazard Quotient) is determined (PEC/PNEC). If HQ>1, the chemical has a great potential to harm the environment (Table 2.6) [160].

CHARM is a model and some offshore activities do not enable easily the use of this model like for example the scale inhibitor squeeze treatment [165].

Table 2.6: The Offshore Chemical Notification Scheme HQ range and colour banding (lower values represent least potentially hazardous) [168].

Minimum value	Maximum value	Category
>0	<1	Gold
≥1	<30	Silver
≥30	<100	White
≥100	<300	Blue
≥300	<1000	Orange
≥1000		Purple

2.7.4 The Oil companies and the Green chemistry

The Norwegian Pollution Controlled Authority (SFT) defined a colour label to characterise the chemicals: black, red, yellow and green (Table 2.7).

The black chemicals are the substances with a biodegradability less than 20% after 28 days and a bioaccumulation potential of log P*ow* more than 5 or a high toxicity (LC-50 or EC-50 more than 10mg/l). The red substances are inorganic substances with a toxicity level of EC50 or LC50 <1 mg/l, organic substances with a biodegradability less than 20 % or a substance with two of the following characterisitics:

•biodegradability BOD28 < 60 %

•bioaccumulation potential log Pow> 3

•acute toxicity LC50 or EC50 < 10 mg/l.

The yellow substances are the substances not classified in the black and red list and that are not on the PLONOR list. The green substances are on the PLONOR list and they are not harmful for the environment.

Table 2.7: Substitution criteria SFT (Norwegian Pollution Controlled Authority) [169]

PLONOR list			
BOD≥60%	If toxic→ Red	If toxic→ Red	
BOD<60%			If toxic→ Red
BOD<20%		If toxic→ Black	If toxic→ Black
	Log Pow>5	Log Pow>3	Log Pow≤3
Black: Disposal to sea not allowed			
Red: To be replaced			
Yellow: Acceptable			
Green: PLONOR List or water			
"If toxic": Measured toxicity in an EC-50 or LC-50 test is less than 10mg/l			

BOD;Biodegradability

The legislation became more strict with the nature and the quantity of the chemicals discharged in the environment and a goal of zero discharge was aimed for 2005 in Norway and the Government's environmental policy and environmental state of the nation (2006-2007) says: "the zero discharge target for added chemicals is considered to be achieved" [170] and Figure 2.27 and Figure 2.28 illustrate the decrease of the quantity of black and red substances released in the sea since 1998.

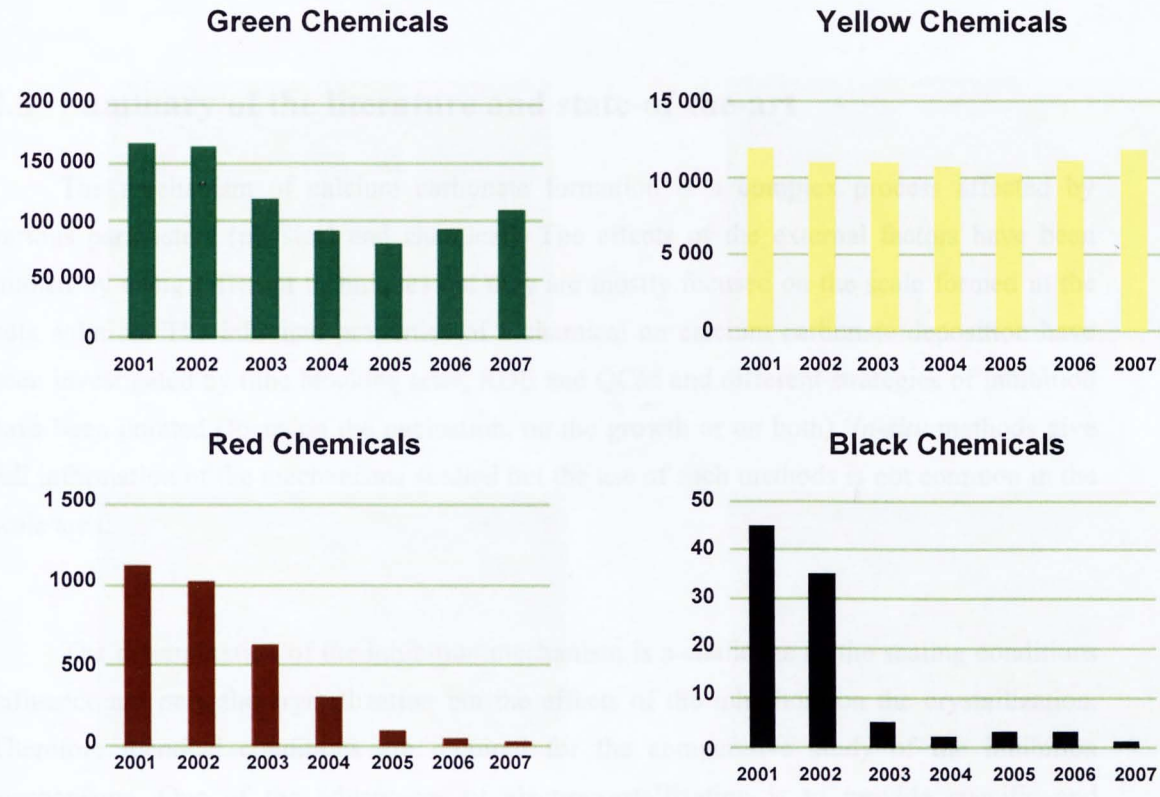

Figure 2.27: Discharge of Green, Yellow, Red and Black chemicals in tonnes from the Norwegian Oil Industry [170]

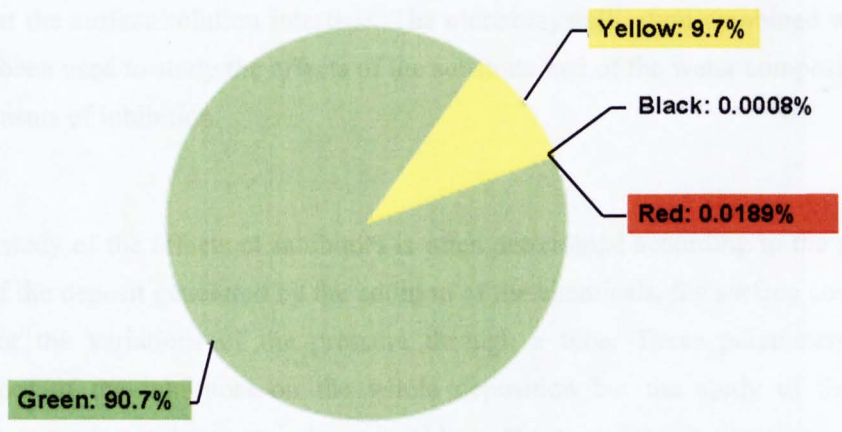

Figure 2.28: Distribution of the total chemicals discharged in 2007 [170]

The environment concerns lead the research to develop new environmental friendly chemicals, currently named "Green" as scale inhibitors. The challenge is to determine the mechanisms of action of these chemicals against scale deposition to optimise their use (environmental conditions i.e pH, temperature, brines composition etc., nature of the scale they inhibit, bulk or surface active). An understanding of their mechanisms of inhibition could lead to the syntheses of more efficient green scale inhibitors.

2.8 Summary of the literature and state-of-the-art

The mechanism of calcium carbonate formation is a complex process affected by various parameters (physical and chemical). The effects of the external factors have been studied by using different techniques but they are mostly focused on the scale formed in the bulk solution. The inhibited properties of a chemical on calcium carbonate deposition have been investigated by tube blocking tests, RDE and QCM and different strategies of inhibition have been pointed (focus on the nucleation, on the growth or on both). *In-situ* methods give full information of the mechanisms studied but the use of such methods is not common in the scale area.

The determination of the inhibition mechanism is a challenge as the scaling conditions influence not only the crystallization but the effects of the inhibitors on the crystallization. Therefore identical conditions are required for the comparative study of the inhibition mechanisms. One of the advantages of electrocrystallization is to provide specific and constant scaling conditions at the vicinity of the electrode. The chronoamperometry has been widely used to determined the scaling potential of a solution but not to study the interactions occurring at the surface/solution interface. The electrocrystallization combined with a video set-up has been used to study the effects of the substrate and of the water composition but not the mechanisms of inhibition.

The study of the effects of inhibitors is often determined according to the reduction of the mass of the deposit generated by the addition of the chemicals, the surface coverage of an electrode or the variations of the pressure through a tube. These parameters are direct consequences of the inhibitors on the whole deposition but the study of the inhibition mechanism occurring at the crystal planes level has not received much attention.

The use of environmental friendly inhibitors in the industry becomes more and more a necessity. Comparative study of the mechanisms of one conventional inhibitor and different green inhibitors has not been realised with calcium carbonate. Some sparse information is found in the literature on the polymaleic acid, the carboxymethylin inulin and especially the polyaspartic acid but a comparison of their mechanisms and efficiency on calcium carbonate deposition on a metal surface has not been investigated yet.

Chapter 3
Methodology

3.1 Introduction

This thesis is focused on several objectives reported in Chapter 1 and therefore different methods have been used to study the formation of calcium carbonate and the mechanisms of inhibition of scale inhibitors.

Static tests under polarization conditions (electrodeposition) (Chapter 4) have been conducted with a 3-electrode cell to study the current density variations as a function of time as scale deposits. The effects of some scale inhibitors on the properties of the calcareous deposit and on the interactions between the inhibitors and a metal surface are assessed.

The physical characteristics of the crystals of calcium carbonate (shape, size and number) have been studied with an *in-situ* flow cell under polarization conditions (Chapter 5). The set-up used made possible *in-situ* and real time measurements of parameters like the mean diameter of the crystals of calcium carbonate and the surface coverage of the electrode.

The crystallography of the calcium carbonate crystals formed was studied by Synchrotron X-Ray Diffraction with an *in-situ* cell (Chapter 6). The determination of the effects of the inhibitors on the different crystal planes were studied as well as the kinetics of formation of specific crystal planes.

These methods are described in this chapter in addition to some general information which is important for all aspects of the study.

3.2 Brine preparation

The composition of the brines was different according to the method used to create a supersaturation environment. The details of the composition of the brines are presented in the experimental part of each results chapter. All the brines were prepared from the chemicals listed in Table 3.1: (Prolabo, BDH®).

Table 3.1: Details of the salts used for the preparation of the brines

Brine 1	NaCl; KCl; $SrCl_2$; $MgCl_2$, $6H_20$; $CaCl_2$, $6H_20$
Brine 2	NaCl; $NaHCO_3$

Brine 1 (containing calcium ions) and Brine 2 (containing bicarbonate ions) were prepared separately. The appropriate quantity of the specific salts were weighed and mixed with distilled water. The brines used for electrodeposition tests (Chapter 4 and 5) were not buffered as the pH was largely increased due the appliance of a potential therefore creating the supersaturated environment.

3.3 Scale inhibitors properties

The details of the four scale inhibitors studied are presented in Table 3.2 and the molecular structures can be found in Chapter 2. One commercial non green scale inhibitor (PPCA, polyphosphinocarboxylic acid) has been taken as a reference to compare its inhibition mechanism to three green inhibitors. The ecotoxicological properties of the green inhibitors are summarized in Table 3.3.

Table 3.2: Description of the scale inhibitors studied

Inhibitor description/ Reference	Details	Supplier	Active content (%)	Molecular weight
Non-green PPCA/ Bellasol S40	Phosphino polycarboxylic acid	BWA	42	~3600
CMI/ Dequest 11625	Sodium Carboxymethyl inulin	Champion Technologies	17.5	>2000
PMA/ DP5006	Polymaleic acid	BWA	47	n.a
PA/ T/1120	Poly-α-β-D,L-aspartic acid	Champion Technologies	39	Low

Table 3.3: Ecotoxicological properties of the inhibitors used in this study

Inhibitors	Toxicity	Bioaccumulation	Biodegradability
PPCA	low	Log P_{ow}<<3	Not readily biodegradable
CMI	$EC_{50\ 48hrs\ Daphnia}$: 2000mg/L $LC_{50\ 96hrs\ zebra\ fish}$ > 10000mg/L	Not known	25%
PMA	$EC_{50\ 72hrs\ Algae}$: 380mg/L $LC_{50\ 96hrs\ Fish}$ > 1000mg/L $LC_{50\ Brown\ Shrimp}$ > 2160mg/L	Log P_{ow}<0	29%
PA	$EC_{50\ 48hrs\ Daphnia}$: 1798mg/L $LC_{50\ 96hrs\ Fish}$: 2117mg/L	Log P_{ow}<0	41%

3.4 Substrate for deposition

For the electrodeposition tests (Chapter 4 and 5), the substrate was stainless steel, UNS S31603. The composition of the metals used as a substrate for calcium carbonate deposition is presented in Table 3.4. The active surface was polished to 1200grit and then the surface finished of 6μm was achieved with a diamond polishing compound.

Two different capillary cells were used with the synchrotron X-ray diffraction: stainless steel (UNS 31603) and hastelloy C-276 (UNS N10276). The diameter was 2mm bore and the surface finish was less than 1.6μm Ra.

Table 3.4: Composition of the metals used as substrate of scale deposition [171].

Composition	Hastelloy UNS N10276	Stainless steel UNS 31603
Ni	55%	8.0 – 12.0 %
Mo	16 – 18%	2.0 – 3.0%
Cr	15.5 – 17.5%	17.0 – 21.0%
Fe	4.5 – 7.0%	BAL.
Mn	1%	<1.5%
Si	1%	<2.0%
C	0.12%	<0.03%

3.5 Static tests

The static tests have been conducted under polarization conditions with a simple 3-electrode cell. Electrodeposition is a method to promote specific electrochemical reactions at the active surface and the solution at the surface, as a result of these reactions, becomes supersaturated. Deposition onto the surface then occurs. The conditions at the interface are well controlled and the scale deposition occurring at the surface is reproducible.

3.5.1 Background on electrochemistry associated with scale formation

Calcium carbonate formation by electrodeposition occurs by a sequence of chemical reactions at the interface. By imposing a cathodic potential in the oxygen-reduction regime (Figure 3.1) the reaction as in Equation 3.33 occurs.

$$O_2+2H_2O+4e^- \rightarrow 4OH^- \qquad \textbf{Equation 3.33}$$

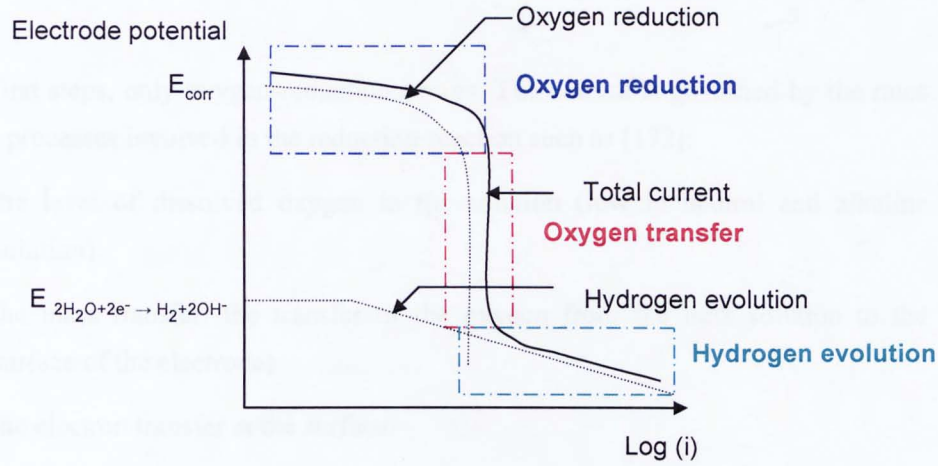

Figure 3.1: Polarization diagram showing the contribution of oxygen and hydrogen evolutions on the total cathodic current (in dotted line), semi logarithmic scale [138]

The diagram (Figure 3.1) shows the assessment of the total current with the variation of the electrode potential. Two cathodic reactions can occur at the surface of the electrode: the oxygen-reduction (Equation 3.33) and the hydrogen evolution (Equation 3.34). The black line represents the variations of the total current and the dot lines shows the current variations due to the oxygen-reduction and the hydrogen evolution.

$$2H_2O+2e^- \rightarrow H_2+2OH^- \qquad \textbf{Equation 3.34}$$

At the free corrosion potential (E_{corr}) the cathodic reaction rate balances the anodic reaction rate as the rates are equal but with the opposite sign (i.e all the electrons produced during the anodic reaction are consumed during the cathodic reaction). The variation of the total current when the potential is displaced from E_{corr} is a measure of the reaction rate. Three steps control the total current variations:

- The first step is characterised by an increase of the current. The total current is only composed of the current generated by the oxygen-reduction reaction. This step is controlled by the oxygen-reduction rate.
- The second step is characterised by a constant current with the variations of the potential. This step is controlled by the oxygen mass transfer (the transfer of the oxygen from the bulk solution to the surface).
- The third step is controlled by the hydrogen evolution reaction rate.

In both first steps, only oxygen-reduction occurs. The current is governed by the rates of the different processes involved in the reduction-reaction such as [172]:

- the level of dissolved oxygen in the solution (low in neutral and alkaline solution)
- the mass transfer: the transfer of the oxygen from the bulk solution to the surface of the electrode)
- the electron transfer at the surface.

The two last processes are illustrated in Figure 3.2. Chemical reactions might occur before or after the electron transfer but this not the case with the reduction of the oxygen.

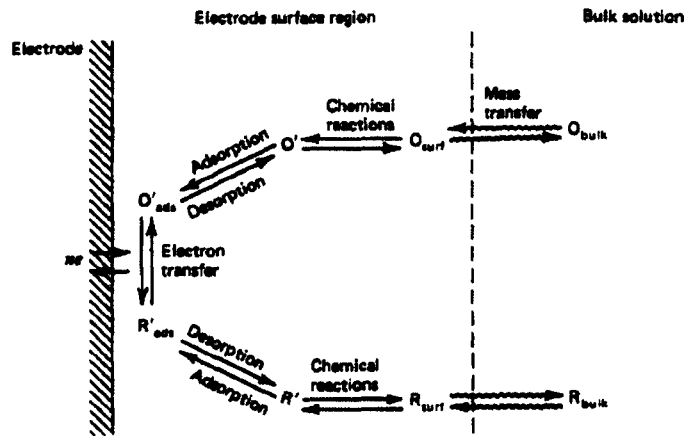

Figure 3.2: Pathway of a general electrode reaction [172]

During the first step, the interface is characterised by low potentials and low currents. The rate of the electron-transfer is smaller than the rate of the oxygen mass transfer. This step is controlled by the rate of the oxygen-reduction as the limiting factor is not the availability of oxygen at the interface. Higher currents are involved in the second step and the electron-transfer rate becomes higher than the mass transfer rate. In this step the limiting factor is the availability of oxygen as the oxygen consumption (by reduction) is high and the stock of oxygen at the interface can not be replenished quickly enough (by mass transfer). The slowest process in the reduction-reaction is the transfer of oxygen from the bulk to the surface. This step is controlled by mass transfer.

Three different modes of mass transfer (movement of material from one location in a solution to another) can occur in a solution [172]:

- Migration: movement of a charged body under the influence of an electric field (a gradient of electrical potential)
- Diffusion: movement of a species under the influence of a gradient of chemical potential (i.e concentration gradient).
- Convection: stirring or hydrodynamic transport.

In this study, only the diffusion mass transfer is relevant.

3.5.2 Chronoamperometry

The production of OH^- at the interface shifts the pH and hence the equilibria of the CO_2-H_2O system (Figure 2.14). As a result the interface becomes supersaturated with respect to $CaCO_3$ and the deposition of $CaCO_3$ can occur as in Equation 3.35.

$$Ca^{2+} + CO_3^{2-} \rightleftharpoons CaCO_3 \qquad \textbf{Equation 3.35}$$

Magnesium hydroxide can be formed (Equation 3.36) on the surface as a gel-like film at a minimum pH value 9.3 [81]

$$Mg^{2+} + 2OH^- \rightarrow Mg(OH)_2 \qquad \textbf{Equation 3.36}$$

The current density is proportional to the consumption of oxygen at the electrode surface and decreases when the active surface area decreases (due to the reduction access on the surface); when it is blocked by the scale formation. The residual current density reaches a final value close to zero when the surface is completely covered by scale. The morphology of the scale deposit (and in particular the porosity) is related to the residual current [11].

The formation of calcium carbonate by electrodeposition was summarised by Ledion *et al.* in 1985 [75] and the different parts of a typical chronoamperometric curve was explained (Figure 3.3):

- I_O to I_M: the increase of the current is due to the increase of the pH at the interface. At the beginning, the current variations are under reaction rate control and not mass transfer control. After the establishment of the oxygen diffusion layer, the pH maintains a uniform value at the electrode surface [173]. During this step the first crystals of calcium carbonate are formed.
- I_M to I_R: this step is characteristic of the progressive coverage of the electrode surface by the calcareous deposit.
- After I_R is reached: the filling-up of the discontinuities occurs during this last step.

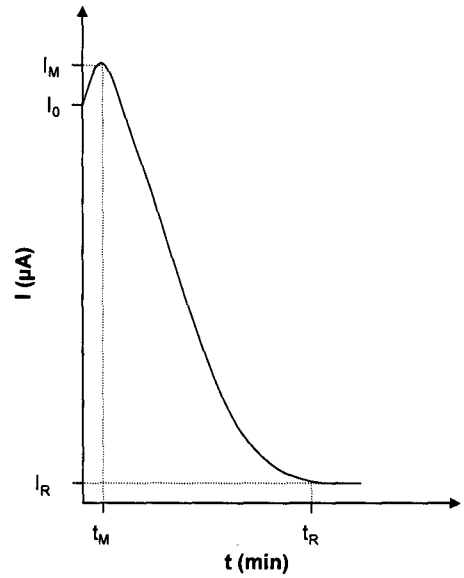

Figure 3.3: Typical chronoamperometric curve, I=f(t) [75]

3.5.3 Electrochemical set-up

3.5.3.1 3-electrode cell

A 3-electrode cell was used in these electrodeposition tests. The potential was applied with a EG&G VersaStatTM II® (Figure 3.4).

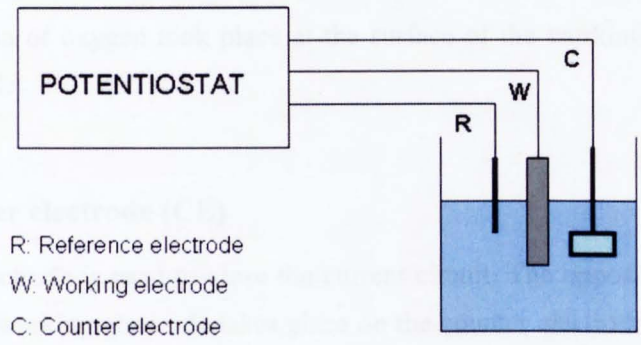

Figure 3.4: 3-electrode cell used for the potentiostatic tests. Applied potential -0.8V (Ag/AgCl)

The potential -0.8V (Ag/Ag/Cl) was applied as it corresponds to the O_2-diffusion plateau as shown on Figure 3.5.

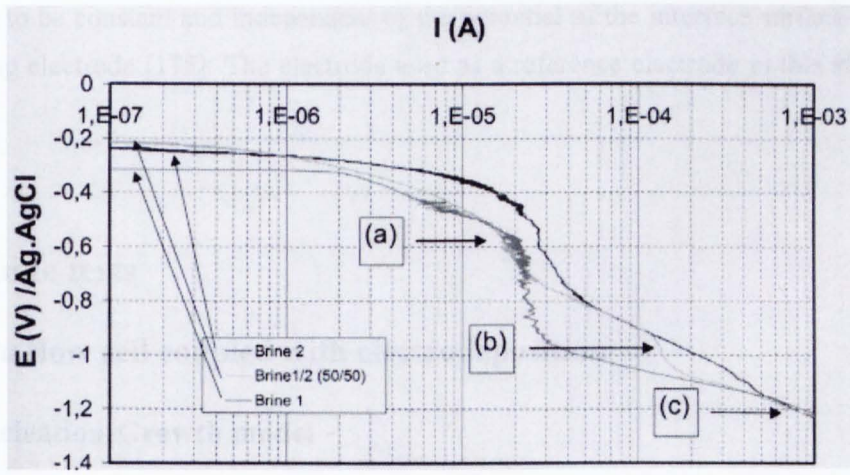

Figure 3.5: Cathodic polarization: determination of the O_2-diffusion plateau [174]

Three electrodes are necessary to apply a potential and to record the current density variations: the working electrode (WE), the counter electrode (CE) and the reference electrode (RE).

3.5.3.2 The working electrode (WE)

The working electrode is an electronic conductor in contact with an electrolyte solution. In this study the working electrode was a cylinder of stainless steel UNS 31603 and the active surface in contact with the bulk was $1 cm^2$ (the rest of the electrode was covered with isolation tape). As the reduction of oxygen took place at the surface of the working electrode it was considered as a cathode.

3.5.3.3 The counter electrode (CE)

The counter electrode is used to close the current circuit. The opposite reaction of the one occurring on the working electrode takes place on the counter electrode. In this study an oxidation takes place on the counter electrode (made of an inert metal, platinum).

3.5.3.4 The reference electrode (RE)

The absolute value of the difference of the potential at the metal-solution interface can not be measured, only its changes. The reference electrode is the electrode against which the difference of potential is measured. The potential of the surface-solution of the reference electrode has to be constant and independent of the potential of the interface surface-solution of the working electrode [175]. The electrode used as a reference electrode in this study was Ag/AgCl.

3.6 Dynamic tests

3.6.1 *In-situ* flow cell coupled with electrodeposition

3.6.1.1 Nucleation-Growth model

The data in this part of the study have been analysed using the nucleation and growth model proposed by Beaunier *et al.* [173] and modified by Euvrard *et al.* [91] which assumes that crystallization is controlled by diffusion.

It is assumed that the unit area of the substrate has a finite number of active nucleation sites N_0 (μm^{-2}) and that all nucleation events are independent to each other. So, at a time t, the probability of nucleation depends only on the number of free sites. For non-growing crystals, the number density of nuclei follows the Poisson law:

$$N(t) = N_0 [1-\exp(-At)] \qquad \textbf{Equation 3.37}$$

Where A (s^{-1}) is the nucleation rate constant (conversion of a site into a nucleus); in our approach the density of active sites N_0 is the detected number of crystals. Two different cases exist according to the nucleation rate constant value:

- When $At >> 1$, N(t) is close to N_0, it means that all active sites have generated nuclei in the very early stage (first seconds) of the process; this is instantaneous nucleation.
- When $At << 1$, it indicates progressive nucleation; $N(t)$ is close to N_0At, the number of converted sites increases linearly with time.

A difficulty in the analysis of the data is that the coalescence (or overlap) of crystals may occur and the actual covered surface area S(t) is different from the extended surface area $S_{ext}(t)$ that would be covered by all the nuclei at time t without effects of overlap. The relationship between S(t) and $S_{ext}(t)$ is given by Equation 3.38 and Equation 3.39.

$$S(t) = 1-\exp(-S_{ext}(t)) \qquad \textbf{Equation 3.38}$$

$$S_{ext}(t) = (M k_l N_0 / \rho).[t-1/A + \exp(-At)/A] \qquad \textbf{Equation 3.39}$$

A is the nucleation rate, k_l the lateral growth rate (mol/μm/s), M is the molar mass of $CaCO_3$ (100g/mol) and ρ is the density of the crystals ($\rho = 2.71\ 10^{-12}$ g/μm^3 for calcite).

From Equation 3.38 and Equation 3.39, the surface coverage S(t) is :

$$S(t) = 1- \exp[-(M k_l N_0 / \rho).[t- 1/A + \exp(-At)/A]] \qquad \textbf{Equation 3.40}$$

For an extended time, S(t) is simplified as follows:

$$S(t) = 1- \exp[-(M k_l N_0 / \rho).[t- 1/A]] \qquad \textbf{Equation 3.41}$$

In case of instantaneous nucleation, if $At>>1$, i.e. for sufficiently long observation times, e.g. t>1s, Equation 3.39 is simplified as follow:

$$S_{ext}(t) = - Ln(1- S(t)) = M k_1 N_0 t / \rho \qquad \textbf{Equation 3.42}$$

$$k_1 = - Ln(1- S(t)) \rho / M N_0 t \qquad \textbf{Equation 3.43}$$

In case of progressive nucleation, the value of S_{ext} is quantified as follows:

$$S_{ext}(t) = - Ln(1- S(t)) = M k_1 N_0 A t^2 / \rho \qquad \textbf{Equation 3.44}$$

Using the model above, the experimental data allows the determination of:

- *the type of nucleation*: if $S_{ext}(t)$ is a linear function of t, nucleation is instantaneous, whereas if it is a linear function of t^2, the nucleation is progressive,
- *the mean lateral growth rate of crystals* k_1.

In using this electrochemical cell the objectives are the characterisation of the crystals of calcium carbonate generated by electrodeposition in presence of scale inhibitors and to determine either the inhibitor action by inhibiting the growth (lateral growth k_1 constant) and/or the nucleation of the crystallization.

3.6.1.2 Parameters studied and definition

The number of particles, the shape factor (f) and the diameter of the particles and the surface coverage were determined by image analysis. The image of the surface and the crystals was analysed at different times. For each image, the crystals have been selected on the screen with a specific image analysis software (ARIES, software ESILAB).

The surface and the diameter of the single crystals, the surface coverage and the shape factor were calculated directly by the software. The shape factor (f) is defined as follows:

$$f=P/4\pi S \qquad \textbf{Equation 3.45}$$

where P is the perimeter and S is the surface area of the crystal. The value of the shape factor range from 0 to 1. A circle crystal is characterised by a shape factor close to 1 and a rod-shape crystal is characterised by a shape factor close to 0.

The extended surface area and the lateral growth were calculated according to Equation 3.42 and Equation 3.43.

3.6.1.3 Experimental set-up

- **Electrochemical cell**

The electrochemical cell integrated 3 electrodes in 2 parallel PMMA (poly(methyl methacrylate) plates (Figure 3.6). One plate contains a removable plug comprising a circular stainless steel electrode. The opposite plate contains a window that was made electrochemically conducting by deposition of tin oxide. The electrode was connected to a power supply. The electrical potential of the working electrode was measured relative to a silver wire inserted through the plug and immersed in the solution which flows by gravity (40ml/min) in a rectangular channel. The silver wire was pre-treated with diluted solution of hydrochloric acid so it worked as Ag/AgCl electrode. The potential applied was -0.8V Ag/AgCl And each test was run for 60 minutes.

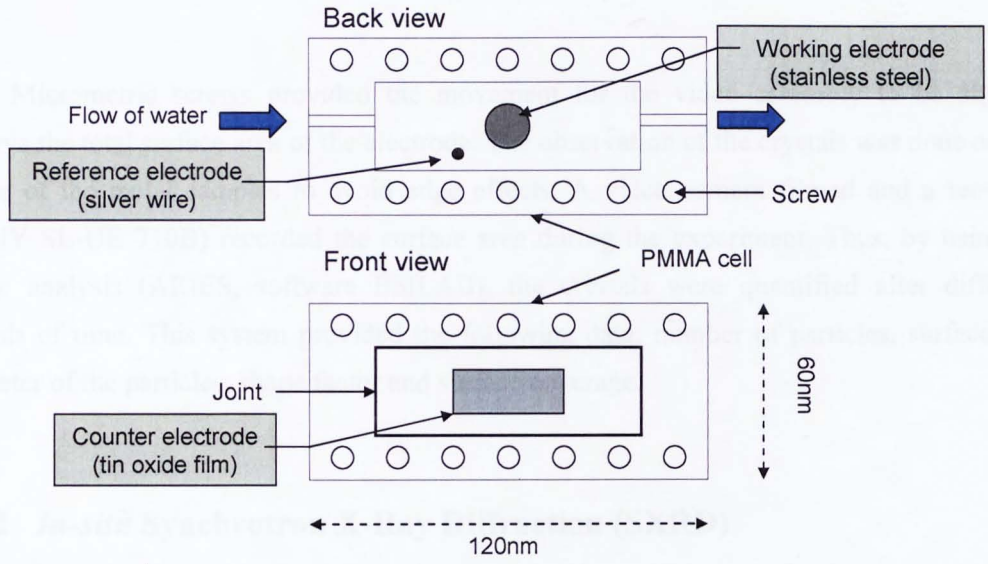

Figure 3.6: *In-situ* electrochemical flow cell

- **Optical and measurement set up**

The video assembly contained a 20x long working distance objective, a video tube, a lighting system, a camera (SONY SSC-DC38P) and an image monitor (SONY PVM 1450). The magnification power (1000x) monitored the particles (crystals and inhibitor) on the working electrode as soon as their size reached 1µm. The crystals smaller than 1µm were not detected. A Scanning Electron Microscope (SEM) has been used to analyse some surfaces in order to have a better accuracy in the detection of crystals.

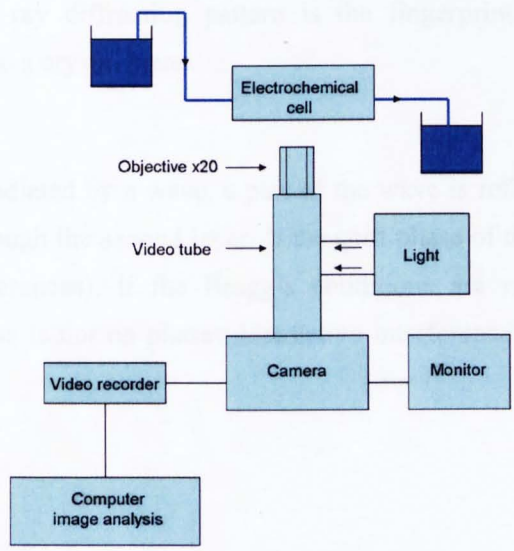

Figure 3.7: Experimental set-up of the *in-situ* polarization tests

Micrometric screws provided the movement for the video assembly to be able to observe the total surface area of the electrode. The observation of the crystals was done on the centre of the metal samples to avoid edge effects. A video camera filmed and a recorder (SONY SL-UE 710B) recorded the surface area during the experiment. Thus, by using an image analysis (ARIES, software ESILAB), the crystals were quantified after different periods of time. This system provided the following data: number of particles, surface and diameter of the particles, shape factor and surface coverage.

3.6.2 *In-situ* Synchrotron X-Ray Diffraction (SXRD)

The use of X-ray diffraction to study crystallography of compounds is widely used. The use of synchrotron radiations allows the study of very small amounts of scattering matter. Moreover the wavelengths available are much shorter and therefore the accuracy of the determination of the characteristics of a compound increases. In principle a very good time resolution can be achieved allowing a quick data collection [176]. The charged particles are accelerated in a curve path device (synchrotron) to a vey high speed through magnetic fields. The synchrotron radiations thus produced, hit a metal target and X-ray are generated.

3.6.2.1 Powder X-ray diffraction

The general principles of X-ray diffraction have been demonstrated with the irradiation of single crystals. The X-ray diffraction pattern is the fingerprint of a crystal as each diffraction ring is specific to a crystal plane.

When an atom is irradiated by a wave, a part of the wave is reflected by the first layer and the rest is diffused through the second layer. If the shift phase of the reflected beam is on phase (constructive interferences), if the Bragg's conditions are respected, the beam is diffracted. If the shift phase is not on phase (destructive interferences), diffraction does not occur (Figure 3.8).

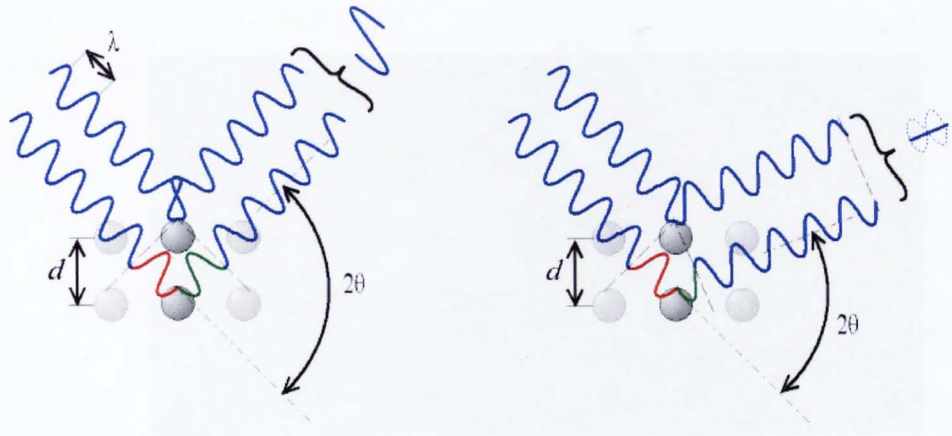

Constructive interferences *Destructive interferences*

Figure 3.8: Illustration of the Bragg's conditions

In other term the beam is diffracted if the difference of the pathway of the different waves (corresponding to the distance AB+BC in Figure 3.9) is equal to an integer multiple of the wavelength.

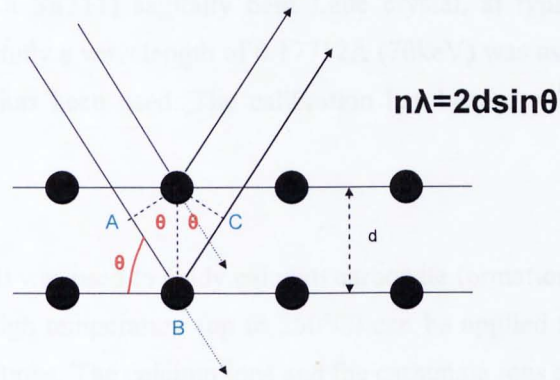

Figure 3.9: Determination of the Bragg's law

The study of a polycrystalline sample increases the chance to detect crystals as the chance to find a crystal in the Bragg's conditions increases with the increase of the number of crystals. For the study of a single crystal, the sample can be rotated in order to increase the chance to detect the crystal; at some point the correct Bragg angle will be reached and thus a diffracted beam will be generated.

When a powder sample is irradiated by a X-ray and if the crystals are orientated randomly, the diffraction beams resulting are lying on the surface as diffraction cones. These cones can be diffracted in all directions (forwards and backwards). The intersection between the diffracted cones and the detector gives a line of diffraction specific to the 2-theta angle.

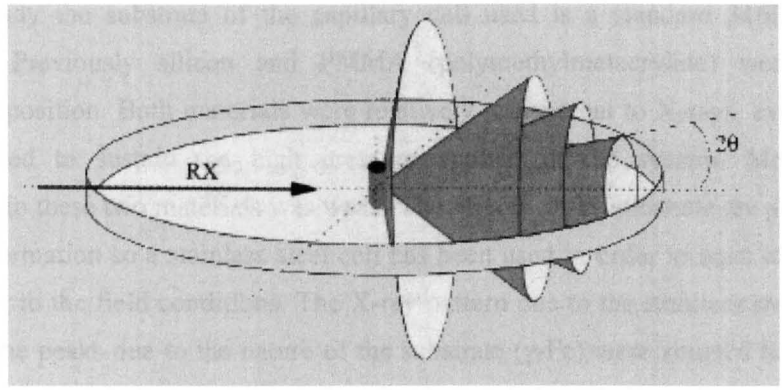

Figure 3.10: Debye-Scherrer and Hull diagram [177]

3.6.2.2 Experimental set up

The experiments have been carried out in Brookhaven National Laboratory in the National Synchrotron Light Source departement (US) in collaboration with Dr Zhong Zhong. The beam X17B1 has been used. Monochromatic beams with energies tunable from 55 to 80 keV are provided with a Si(311) sagitally bent Laue crystal, at typical flux rate of 10^{11} photons/s [178]. In this study a wavelength of 0.17712Å (70keV) was used. A 2-dimensionnal Siemens CCD detector has been used. The calibration has been done with NIST standard Al_2O_3.

An *in-situ* flow cell was used to study calcium carbonate formation and inhibition. High pressure (34MPa) and high temperature (up to 250°C) can be applied to the cell in order to reproduce realistic conditions. The calcium ions and the carbonate ions are kept separated and pumped into the system. The two different brines are heat up with an oven and then mixed in the mixing chamber. Calcium carbonate formation occurs in a 2mm bore capillary cell and the X-ray beam passes through this cell (Figure 3.11).

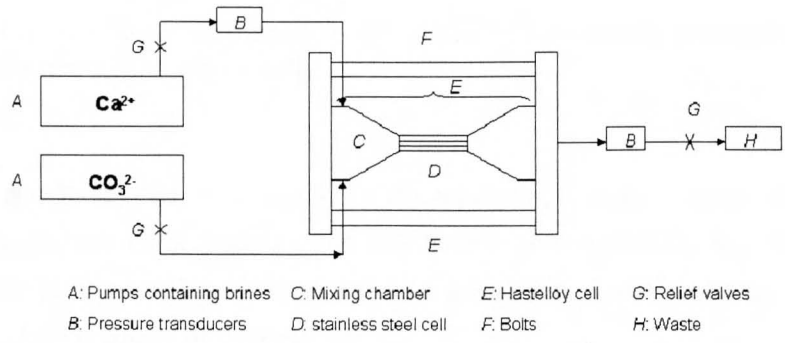

Figure 3.11: *In-situ* flow cell used with the synchrotron X-Ray Diffraction

In this study the substrate of the capillary cell used is a standard 316L austenitic stainless steel. Previously silicon and PMMA (polymethylmetacrylate) were used as substrates for deposition. Both materials were relatively transparent to X-rays, even with the thickness required to sustain the high pressure applied in the system. Moreover the background due to these two materials was weak. The effects of the substrate are an important factor in scale formation so a stainless steel cell has been used in order to have experimental conditions closer to the field conditions. The X-ray pattern due to the stainless steel is strong (Figure 3.12). The peaks due to the nature of the substrate (γ-Fe) were situated between 4.6° and 4.8° and between 5.2° and 5.7°. It has been decided to ignore these two regions. Nevertheless the results obtained give important information on calcium carbonate formation and inhibition and the effects of the substrate.

Stainless steel was chosen as substrate for deposition of $CaCO_3$ for the SXRD as it is a relevant material. Most of the equipments in the oil and gas extraction process are steel. Therefore despite the inconvenience of the significant diffraction background, stainless steel was chosen. The results obtained gives information on $CaCO_3$ formation and inhibition mechanisms closer to what is occurring in real conditions.

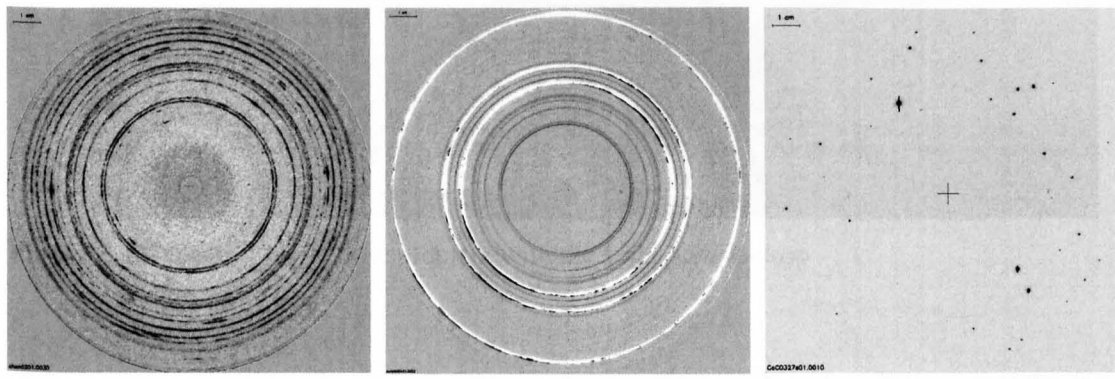

(a) PMMA cell (b) Stainless steel cell (c) silicon cell

Figure 3.12: The X-ray diffraction rings of calcium carbonate scale formed in PMMA, stainless steel and silicon cell

The data have been processed by Dr Zhong Zhong with an in-house program at X17B1 in Brookhaven National Laboratory and they have been converted to the appropriate format. The FullProf [179] suite has been used for the initial data analysis like the determination of the peaks, of the intensity of the peak, etc.

The Inorganic Crystals Structure Database (ICSD) [180] has been used to identify the XRD peaks and assign them to crystal planes of the three polymorphs corresponding to the d-space values obtained after analysis with FullProf suite.

3.7 Adsorption of scale inhibitors

3.7.1 Adsorption on a metal surface

3.7.1.1 Contact Angle measurements

The chemical affinity that a liquid has with a solid has been determined by measuring the contact angle between two of the interfaces at the three-phase line in contact (in this case the metal surface and a droplet of water) (Figure 3.13). This has been used to assess the adsorption of the inhibitors and their effects on the metal surface.

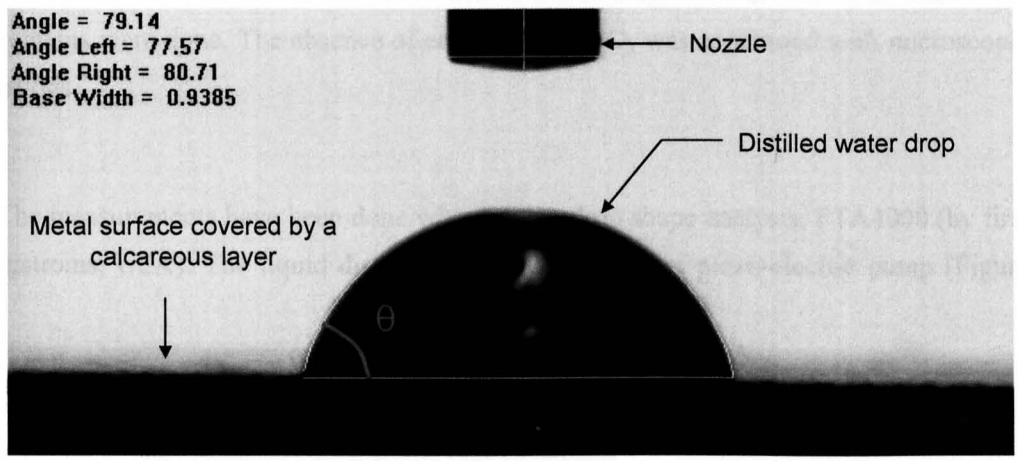

Figure 3.13: Contact angle measurement with the static sessile drop

Young's equation (Equation 3.46) relates the contact angle taking into account the free energies of the surface, the liquid and the solid/liquid interfacial free energy:

$$\gamma_{SV} - \gamma_{SL} - \gamma . \cos\theta = 0 \qquad \textbf{Equation 3.46}$$

where γ_{SV} , γ_{SL} and γ are the free surface energies of the solid/vapour interface, of the solid/liquid interface and of the interface liquid/vapour respectively and θ the contact angle (Figure 3.14).

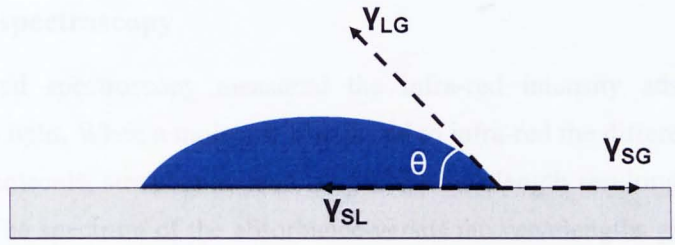

Figure 3.14: Representation of a contact angle and of the three components of the Young's equation

The changes in the surface properties (due to the changes of the calcareous layer present onto the surface) can be underlined by the changes in the value of the contact angle. A flat drop indicates a high affinity with the surface and on the contrary a more rounded drop indicates lower affinity. The contact angle measurement have been done to look the effects of the inhibitor film potentially formed onto the metal surface. A concentration of inhibitor sufficient to inhibit $CaCO_3$ formation (to avoid any effects of the roughness of the calcareous deposit on the contact angle value) was added in the scaling brine and some contact angle measurements were done. The absence of crystals of $CaCO_3$ was confirmed with microscopic observations.

The measurements have been done with a video drop shape analysis, FTA4000 (by first ten Angstroms, USA). The liquid dispensing is controlled by a piezo-electric pump (Figure 3.15).

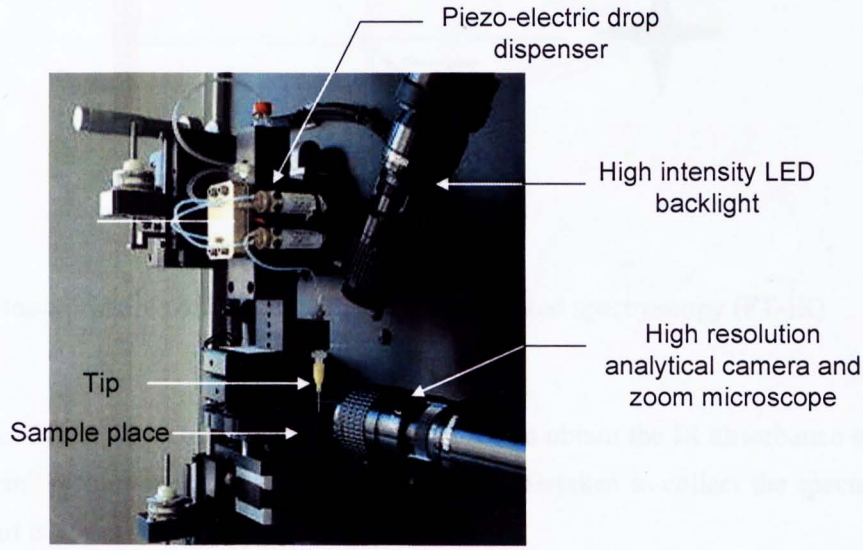

Figure 3.15: Details of the apparatus used to realise the contact angle measurements (FTA4000)

3.7.1.2 FT-IR spectroscopy

The infra-red spectroscopy measured the infra-red intensity adsorbed versus the wavelength of the light. When a molecule is exposed to infra-red the different chemical bonds constituting the molecule, stretch and bend at specific wavelength resulting in the absorbance of the infra-red. The spectrum of the absorbance versus the wavelengths gives the fingerprint of the molecule. In this study the Fourier Transform Infra Red (FT-IR) was used to determine this spectrum.

A light from the IR source travels to the beam splitter. The beam is divided into two beams: one reflected on a fixed mirror and the other one is reflected on a translating mirror. Both lights travels back on the beam splitter before passing through the sample and then to the detector.

The consequence of the movement of the translating mirror is the reflection of different frequencies in different way which creates an interferogram. A spectrum is deduced from this interferogram with a Fourier transform (Figure 3.16).

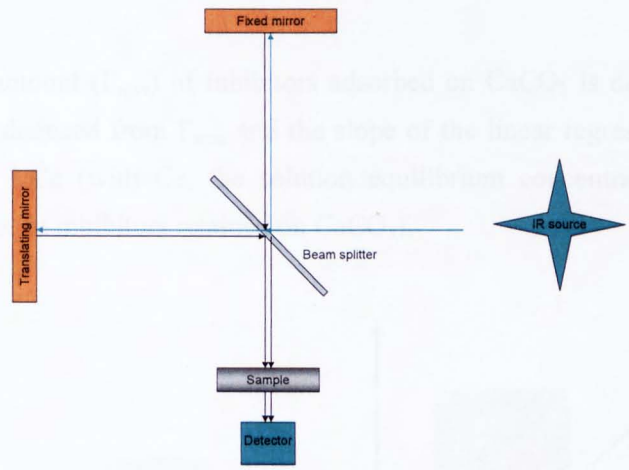

Figure 3.16: Basic principle of a Fourier Transform Infra Red spectroscopy (FT-IR)

A Perkin-Elmer® Spectrum SpotLight™ was used to obtain the IR absorbance spectra. 50 scans at $8cm^{-1}$ resolution, from 4000-$700cm^{-1}$ were undertaken to collect the spectra. The diffraction limit is 10µm.

The Spectrum SpotLight™ is coupled with an imaging system which permits optical images of the surface to be collected.

3.7.2 Adsorption isotherms

The interactions between the chemicals and the crystals of calcium carbonate have been studied. 5mg/L of crystals of calcium carbonate with a specific surface area of $70m^2/g$ (Solvay, France) was mixed in water until stabilisation of the pH (48 hours). Then different concentrations of scale inhibitors were added and then the solution was centrifuged after 24 hours. The supernatant was kept and the CO_3^{2-} present in the supernatant has been removed by N_2-bubbling. Then the Total Organic Carbon (TOC analyzer, Schimadzu) was measured to estimate the quantity of additive still present in the solution, not fixed to the $CaCO_3$ [181]. Finally, the amount of organic carbonate that had been lost through adsorption on the separated calcium carbonate was calculated from the difference between the initial and final concentrations.

The adsorption isotherm of Langmuir equation allowed the determination of the constant of affinity (K) between the inhibitors and $CaCO_3$:

$$1/\Gamma = (1+KCe)/\Gamma_{max}KCe \qquad \textbf{Equation 3.47}$$

The maximum amount (Γ_{max}) of inhibitors adsorbed on $CaCO_3$ is determined and the constant of affinity is deduced from Γ_{max} and the slope of the linear regression of the graph $1/\Gamma$ as a function of 1/Ce (with Ce, the solution equilibrium concentration of the scale inhibitors, Γ the amount of inhibitors retained on $CaCO_3$).

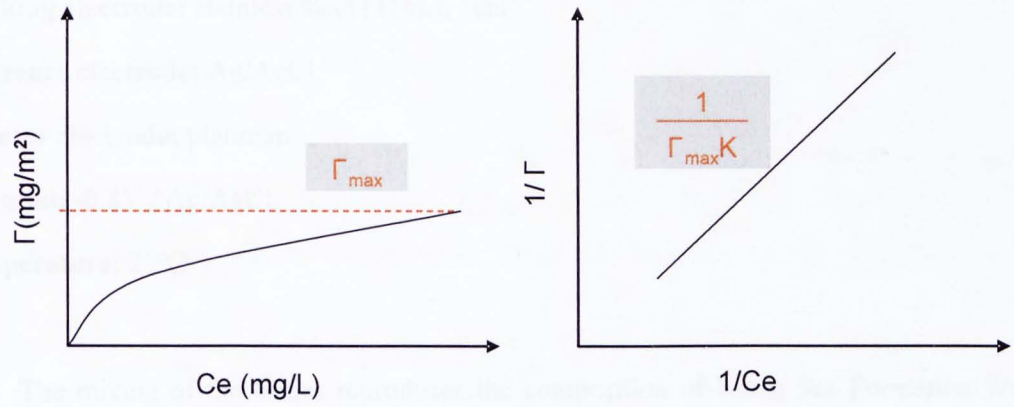

Figure 3.17: Illustration of the determination of the constant of affinity between calcium carbonate and the scale inhibitors in case of Langmuir adsorption.

Chapter 4
Effects of the scale inhibitors on $CaCO_3$ formed by electrodeposition and determination of the interactions between the metal surface and the scale inhibitors

In this chapter calcium carbonate was generated by electrodeposition and the effects of scale inhibitors were studied by chronoamperometry. The variations of the current were recorded on 4 and 24 hour duration tests for the four inhibitors studied (Phosphinocarboxylic acid, PPCA, Polymaleic acid, PMA, Polyaspartic acid, PA and Carboxymethyl inulin, CMI) at three different concentrations (1, 4 and 10ppm or 15ppm for the CMI) to determine the effects of these inhibitors on calcium carbonate formation. A high concentration of inhibitor (30ppm) was tested and contact angle measurements and Fourier Transform Infra Red spectroscopy (FT-IR) have been made in order to assess the changes in the surface properties and to detect the presence of inhibitors, as an adsorbed layer, on the metal surface. In order to determine the efficiency of the different scale inhibitors the weight of the calcareous deposit has been determined for various concentrations of inhibitors.

4.1 Experimental details

4.1.1 $CaCO_3$ deposition

In this chapter calcium carbonate has been electrodeposited on a metal surface using a 3-electrode cell in static conditions. The cell comprised the following:

Working electrode: stainless steel (316L), $1cm^2$

Reference electrode: Ag/AgCl

Counter electrode: platinum

Potential: -0.8V / Ag/AgCl

Temperature: 23°C

The mixing of the brines reproduces the composition of North Sea Formation Water (Banff reservoir). The composition of the brines used is summarized in Table 4.1. 200ml of brine 2 is added to 200ml of brine 1 at t=0 min. The brine is just saturated as the supersaturation index of the final brine is 1.02 and it has been determined with ScaleSoftPitzerTM version 4.

Table 4.1: Composition of the different brines used in this study (NSB=Non Scaling Brine)

	NaCl	KCl	SrCl	$MgCl_2$	$CaCl_2$	$NaHCO_3$
Brine 1	64.10g/L^{-1}	2.25g/L^{-1}	0.80g/L^{-1}	5.75g/L^{-1}	28.45g/L^{-1}	0
Brine 2	63.00g/L^{-1}	0	0	0	0	1.55g/L^{-1}
Brine 2 NSB	63.00g/L^{-1}	0	0	0	0	0

A non scaling brine (mix of brine 1 and brine 2 NSB) has been used in order to study the current variation at the interface metal surface/solution when no calcium carbonate layer was formed.

Each test (for each inhibitor at all concentrations) has been run for 14400 seconds (4 hours) and 86400 seconds (24 hours). These are the baseline data to compare inhibition efficiencies and mechanisms.

The residual current was determined for each experiment. It is a good indicator of the nature of the deposit (thickness and porosity). A low current means the oxygen access on the surface is partially blocked and the oxygen reduction is limited. The higher the residual current, the thinner and more porous the deposit [11, 75, 182].

4.1.2 Scale inhibitors

Four inhibitors (presented in Chapter 3) have been tested in this study: one non green (Phosphinopolycarboxylic acid, PPCA) and three green (Carboxymethyl Inulin, Polymaleic acid and Polyaspartic acid). The inhibitors are added in brine 1 prior to mixing with Brine 2.

4.1.3 Weight measurement

The weight of the sample has been measured before and after the experiment with a balance (OHAUS Analytical+) with a precision of 0.01mg.

At the end of a test the sample is rinsed with distilled water and dry with compressed air (the tip of the compressed air equipment is far enough not to remove the calcareous layer on the surface). The weight of the calcareous deposit has been determined for the tests run with a scaling brine uninhibited and for each inhibitors at the concentration 1 and 4ppm as for the concentrations 10ppm and 15ppm, the weight was reduced by such an extent that weight measurement was no longer accurate.

4.1.4 Microscopic observations

The surface of the sample have been observed with a light microscope and/or with a SEM (Philips® xl30 ESEM).

4.1.5 Experimental overview

The experimental overview is presented in Table 4.2.

Table 4.2: Experimental overview of the static electrodeposition tests

	CA for 24 hours	**CA for 4 hours** Contact angle and FT-IR analyses	
PPCA	1, 4, 10ppm	10, 30ppm	30ppm*
CMI	1, 4, 15, 30ppm	15, 30ppm	30ppm*
PMA	1, 4, 10ppm	10, 30ppm	-
PA	1, 4, 10ppm	10, 30ppm	-

*CA: Chronoamperometry; *Mg^{2+} or Ca^{2+} free brines*

4.2 Effects of 4 scale inhibitors on electrodeposited calcium carbonate on a metal surface

5 different chronoamperometric curves are presented on each graph:

- 3 concentrations of each inhibitor were tested, 1, 4 and 10ppm and 4 for CMI (1, 4, 15 and 30ppm).
- 2 reference solutions were used in this study: a scaling brine (SB) with no inhibitor and a non scaling brine (NSB) with no inhibitor (free from carbonate ions).

The current density variation has been assessed over a 24 hour period. The chronoamperometric curve obtained in absence of inhibitors is presented in Figure 4.1. A large increase of the current was observed in the early stages for the scaling brine with no inhibitor (Figure 4.1). The initial increase of the current was due to the formation of the diffusion layer [173] as mentioned in Chapter 3.

4.2.1 Polyphosphinocarboxylic acid

Chronoamperometric curves are presented in Figure 4.1 for 5 different solutions. Two different categories of behaviour were observed. For 1ppm of PPCA and the non inhibited scaling brine their curves were comparable. With 4 and 10ppm of PPCA the curves were comparable to the non scaling brine trend. The extent of the increase of the magnitude of the current observed at the beginning of the curve was less with 1ppm of PPCA and a small and short increase was observed with 4ppm but with 10ppm there was no increase.

The decrease of the current density observed after the initial increase was due to the progressive coverage of the active surface by crystals of $CaCO_3$. The crystals blocked the access of O_2 to the surface resulting in a slow down of the rate of the oxygen-reduction reaction leading to the decrease of the kinetics of $CaCO_3$ formation. It is clear that 1ppm of PPCA did not affect the oxygen-reduction rate so the mechanism of calcium carbonate formation occurred with 1ppm was probably similar to the non-inhibited case.

The residual current density (value of the current density reached in the final steady stage) is characteristic of the scale deposit formed on the surface in terms of porosity and thickness.

The residual current was much higher with 4 and 10ppm of PPCA with values of 0.023, 0.018mA/cm^2 respectively compared to 0.0082mA/cm^2 at 1ppm. The calcareous deposit obtained with 1ppm of PPCA and no inhibitor were similar (Figure 4.2 and Figure 4.3). The deposit present on the surface at 4ppm did not generate a decrease of the residual current compared to that seen in the non scaling brine but the absence of the progressive decrease showed that the mechanisms of $CaCO_3$ formation has been strongly modified. The same was observed with 10ppm but this time a difference in the baseline current was recorded with the non-scaling case indicating that greater interactions between the inhibitors and the surface were occurring.

At 1ppm the principal mechanism occurring on the surface was calcium carbonate deposition and at 10ppm there was no scale on the surface so the variation of the current was due to the interactions between the inhibitors and the surface. At 4ppm there was still calcium carbonate formation and the film of inhibitors on the surface was probably more extensive than for 1ppm. Nevertheless the residual current is higher for 4ppm. The interactions occurring for this concentration on the surface have less effect on the oxygen access than calcareous layer formation (observed at 1ppm) and the film formation (observed at 10ppm).

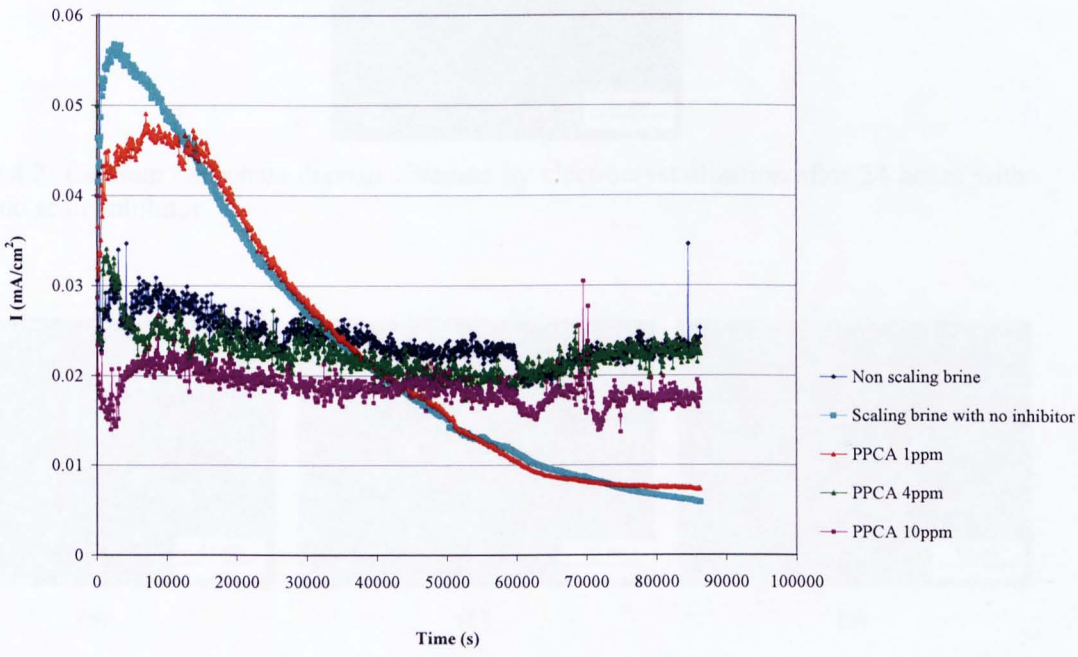

Figure 4.1: Assessment of the variation of the current density for a 24 hour duration in presence of PPCA during calcium carbonate electrocrystallization.

The oscillations of the current signal are due to the adherence of the deposit on the surface: the less adherent, the more the signal oscillates [75]. The oscillations were greater for the non-scaling brine compared to the non-inhibited scaling brine.

It has been found previously that the addition of PPCA leads to the formation of vaterite [73] and the crystals in this current work were more rounded than the ones observed with no inhibitor. No significant difference was observed in the crystal morphology when 1ppm of PPCA was added (Figure 4.2 and Figure 4.3). The crystals were probably distorted with no inhibitor as they grew in close contact with each other but the crystals were generally well defined and rounded. The distortions appeared from 4ppm of PPCA : 4ppm of PPCA generated a large decrease in the size and the number of crystals as expected from the chronoamperometric curve (Figure 4.1). No deposit was observed with 10ppm of PPCA but the residual current was slightly different from that observed with a non-inhibited brine. This was probably due to the presence of an inhibitor film on the surface. This last remark will be examined in the discussion chapter (Chapter 7).

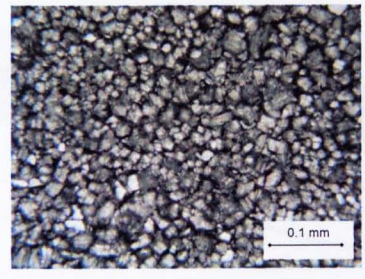

Figure 4.2: Calcium carbonate deposit obtained by electrocrystallization after 24 hours with no scale inhibitor.

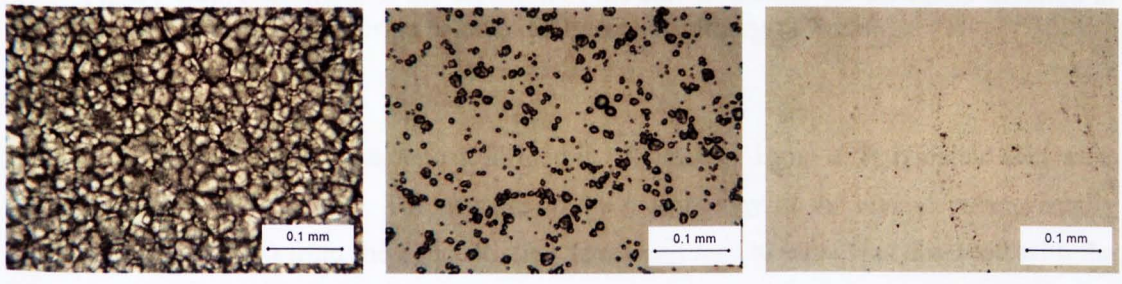

(a) (b) (c)

Figure 4.3: Calcium carbonate deposit obtained by electrocrystallization after 24 hours with 1ppm (a), 4ppm (b) and 10ppm (c) of PPCA

4.2.2 Polymaleic acid

The chronoamperometric curves obtained with Polymaleic acid were modified even at low concentration (Figure 4.4). None of the concentrations tested gave a curve similar to the one obtained with no inhibitor. The progressive drop of the current was reduced with 1ppm of Polymaleic acid whereas with the same concentration of PPCA no difference was observed. Polymaleic acid decreased the kinetics of calcium carbonate deposition. The residual current was modified from 1ppm of Polymaleic acid (0.0051 and 0.0132 mA/cm^2 for the scaling brine with no inhibitor and 1ppm of Polymaleic acid respectively). The first values of the current density (between 0 and $0.015mA/cm^2$) were artefact (they were not present in similar tests).

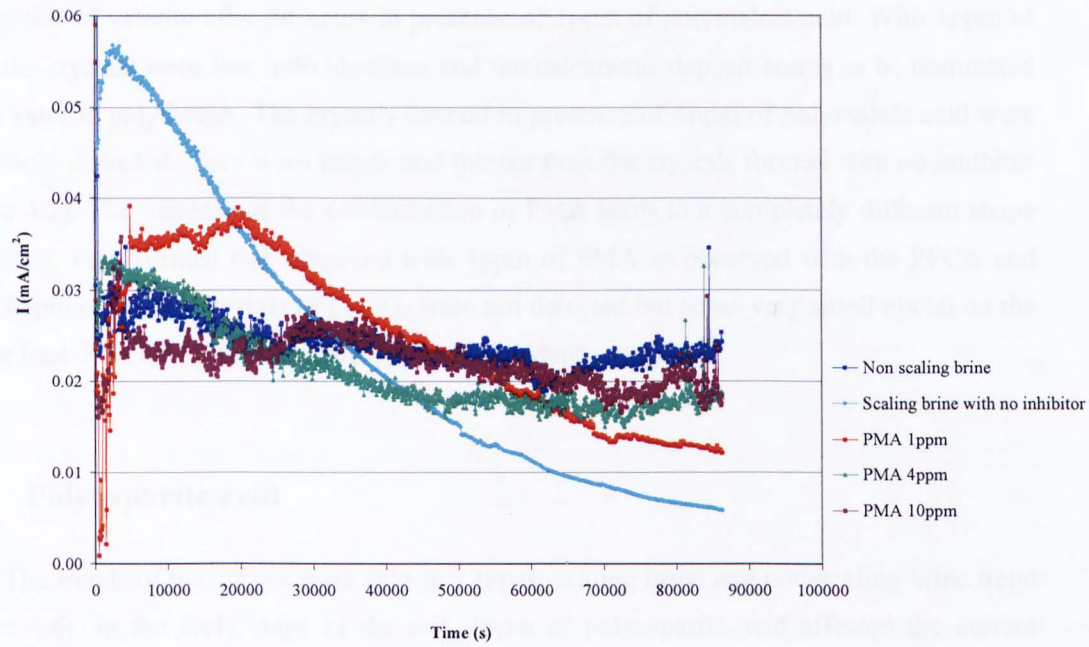

Figure 4.4: Assessment of the variation of the current density for a 24 hour duration in presence of polymaleic acid during calcium carbonate electrocrystallization.

The characteristics of the deposit formed in presence of 1ppm of Polymaleic acid were modified: it was more porous. The changes in the morphology of the crystals were visually detectable (Figure 4.5) from the concentration 1ppm contrary to what was observed with the PPCA. The crystals formed with 4ppm were strongly distorted but the deposit still generated the decrease of the current density. The interactions occurring on the surface with 10ppm of PMA generated a difference in the baseline current compared to the non-scaling brine but not constant as the differences were not significant during the 24 hour test.

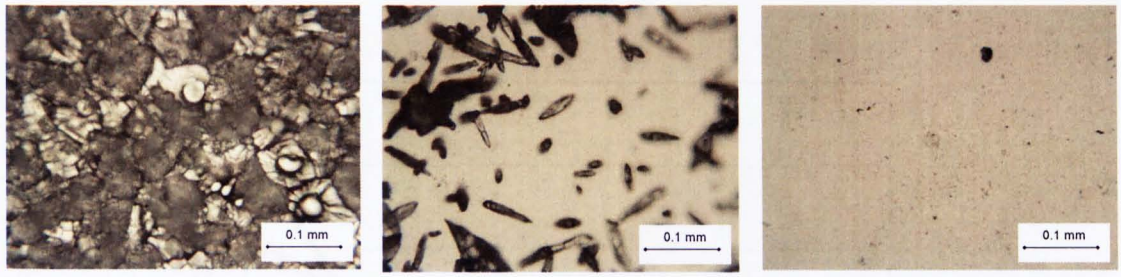

(a) (b) (c)

Figure 4.5: Calcium carbonate deposit obtained by electrocrystallization after 24 hours with 1ppm (a), 4ppm (b), 15ppm (c) of polymaleic acid

Figure 4.5 shows some modifications in the shape of the crystals and the presence of big crystals of vaterite after 24 hours in presence of 1ppm of polymaleic acid. With 1ppm of PMA the crystals were less individualised and the calcareous deposit seems to be dominated by the vaterite polymorph. The crystals formed in presence of 4ppm of polymaleic acid were completely distorted. They were longer and thinner than the crystals formed with no inhibitor (Figure 4.2). The increase of the concentration of PMA leads to a completely different shape of crystals. Free surface was observed with 4ppm of PMA as observed with the PPCA and with 10ppm of PMA. Crystals of $CaCO_3$ were not detected but some very small nuclei on the surface (not detected by light microscopy) were evident.

4.2.3 Polyaspartic acid

The trends of the curves were split in 2 types: scaling brine and non-scaling brine trend (Figure 4.6). In the early stage of the test, 1ppm of polyaspartic acid affected the current density; the initial increase observed with no inhibitor was reduced. From 20000s the current density changes were similar with or without 1ppm of PA. The curve representing 4ppm of polyaspartic acid was similar to the one observed for the non-scaling brine whereas the curve representing 10ppm had the same trend but the values of the current were lower. The modifications of the characteristics of the deposit appeared in the presence of 4ppm of Polyaspartic acid. The residual current at 1ppm was similar to that of the non-inhibited brine (0.0050 and 0.0051mA/cm^2 respectively) but at 4ppm the residual current increased significantly (0.0180mA/cm^2).

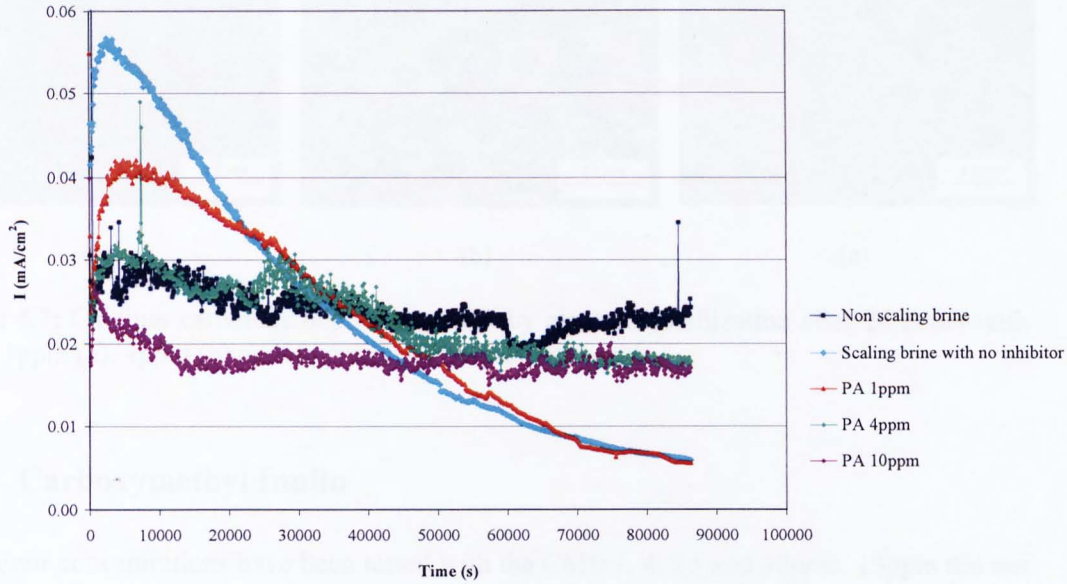

Figure 4.6: Assessment of the variation of the current density for a 24 hour duration in presence of polyaspartic acid during calcium carbonate electrocrystallization

The thick calcareous layer observed with 1ppm of polyaspartic acid after 24 hours had the same characteristics as the layer observed with no inhibitor and 1ppm of PPCA: the morphology of the crystals was similar (no changes have been detected with the light microscope) and a comparable residual current was measured for these 2 inhibitors (Figure 4.7).

Some important modifications were observed with 4ppm of polyaspartic acid and a lot of crystals of vaterite were observed (Figure 4.7). The number of crystals largely decreased with the addition of 4ppm of polyaspartic acid as free surface was observed between the big crystals of vaterite. Almost no crystals were observed with 10ppm of polyaspartic acid but the residual current observed at this concentration was the same as for 4ppm and different to the uninhibited case. Interactions on the surface were occurring at 10ppm but it was not calcium carbonate formation (Figure 4.7). Polyaspartic acid was surface active and generated changes in the crystal morphology from 4ppm. Vaterite was formed at this concentration. These observations are relevant to a previous study in which the authors found that one of the ways by which polyaspartic acid affect the formation of calcium carbonate is by adsorbing onto the calcium carbonate crystals promoting the vaterite form of $CaCO_3$ [54, 151]. A full explanation of the mechanism of inhibition is presented in chapter 7.

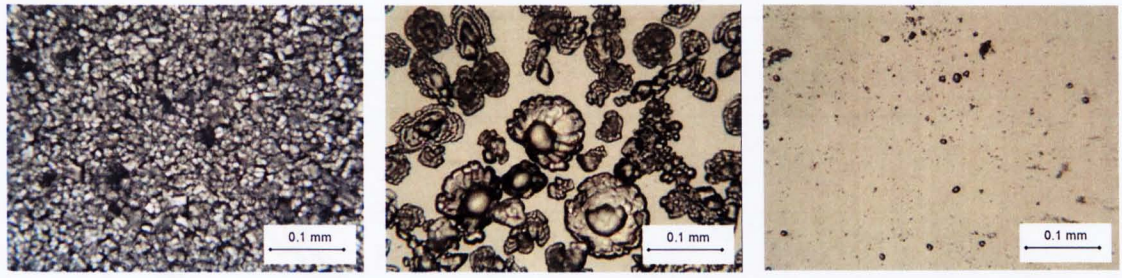

(a) (b) (c)

Figure 4.7: Calcium carbonate deposit obtained by electrocrystallization after 24 hours with 1ppm (a), 4ppm (b) and10ppm (c) of polyaspartic acid

4.2.4 Carboxymethyl Inulin

Four concentrations have been tested with the CMI: 1, 4, 15 and 30ppm. 15ppm did not block calcium carbonate formation therefore a much higher concentration (30ppm) has been tested in order to compare the chronoamperometric curves obtained with the four scale inhibitors when the concentration used effectively inhibited calcium carbonate deposition.

Two generic behaviours were observed when CMI was added as shown in Figure 7: for 1 and 4ppm the trend followed was the trend of the uninhibited scaling brine and for 15ppm and 30ppm the curve was similar to the non scaling brine. A difference of efficiency between the CMI and the PPCA was observed for the concentration of 4ppm. Nevertheless, an increase of the residual current at this concentration (0.0051mA/cm^2 and 0.0138mA/cm^2 for 1 and 4ppm respectively) showed a modification in the properties of the deposit. The trend of the curve and the baseline current for 30ppm of CMI (when no crystals were observed) were similar to what was observed when no carbonate was added to the brine whereas differences in magnitude of current were recorded with 10ppm of the PPCA, the PMA and the PA as previously shown.

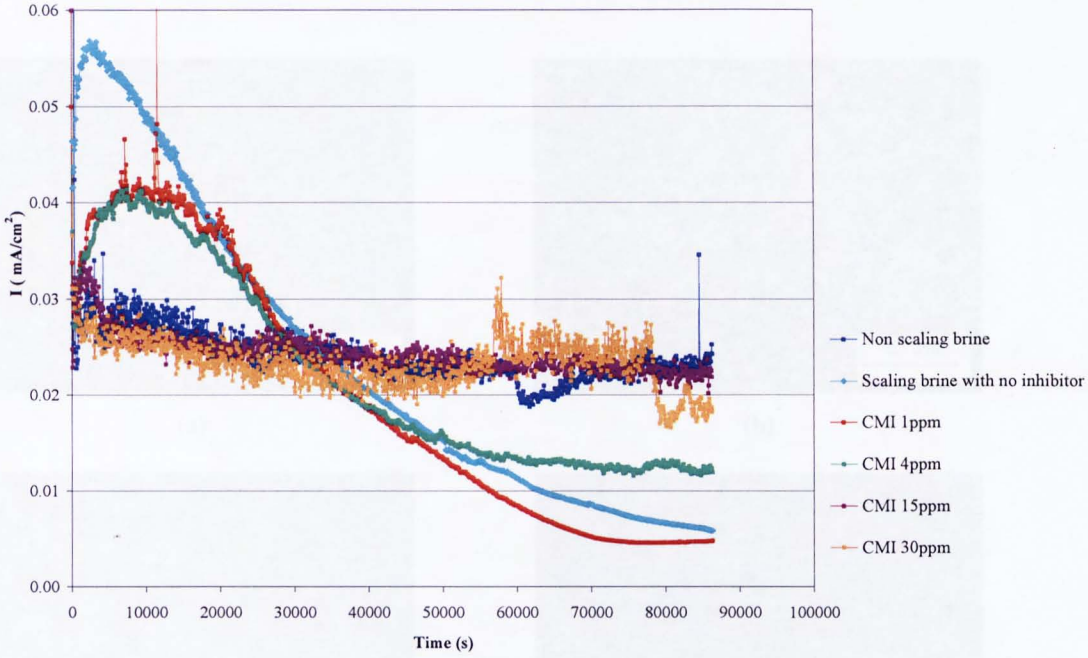

Figure 4.8: Assessment of the variation of the current density for a 24 hour duration in presence of Carboxymethyl Inulin during calcium carbonate electrocrystallization.

For CMI the baseline current was the same as the non scaling brine (at 30ppm). No interactions between the CMI and the metal surface were detected through current variations. Nevertheless the increase of the current in the early stages changed when 1 and 4ppm of CMI were present compared to the uninhibited case. But these changes were only seen at the early stages of the electrodeposition; both concentrations affected the mechanisms of calcium carbonate formation at the early stages.

The study of the chronoamperometric curves (Figure 4.8) has shown a variation of the residual current for 4ppm. The characteristics of the deposit have changed. It was more porous at 4ppm but these changes were not visually detectable with a light microscope (Figure 4.9). Some distorted crystals of calcium carbonate were still observed with 15ppm of CMI but the small amount of crystals did not generate any significant variations of the current density.

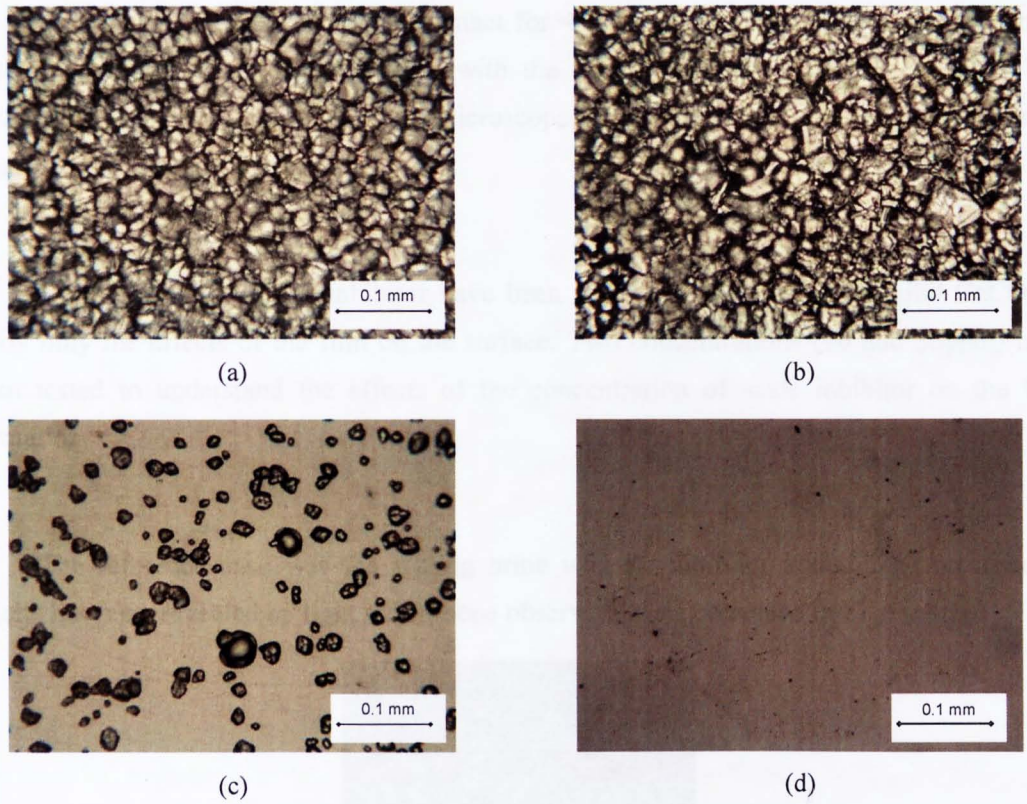

Figure 4.9: Calcium carbonate deposit obtained by electrocrystallization after 24 hours with 1ppm (a), 4ppm (b), 15ppm (c) and 30ppm (d) of CMI

4.3 Modifications of the surface properties

In order to better understand the different mechanisms by which the scale inhibitors studied act on calcium carbonate formation, the changes in the surface properties have been studied. Contact angle measurements have been made to determine the effects of the inhibitors on the wettability of the surface. It has been found that the scaling tendency of a surface is closely related to the surface energy of the surface [183, 184]. As the chronoamperometry study showed *some* interactions between the inhibitors and the metal surface, the contact angle measurements will show if the inhibitors act by changing the surface energy in order to decrease the scaling tendency. The interactions between the surface and the inhibitors could result in a film formation onto the metal surface [185] and this point will be discussed in Chapter 7. The presence of a such film has been studied by Fourier Transformed Infra Red spectroscopy (FT-IR).

The metal surface has been in contact for 4 hours with the brines (scaling and non-scaling) under polarization conditions (with the same characteristics as previously). The surface has been observed with a light microscope, studied by FT-IR and then contact angle measurements have been done.

High concentrations of inhibitor have been used in order to totally inhibit $CaCO_3$ to study only the effects of the film on the surface. Two concentrations (10 and 30ppm) have been tested to understand the effects of the concentration of scale inhibitor on the film formation.

The reference case was the scaling brine with no inhibitor added. The presence of calcite has been revealed by light microscope observations as presented in Figure 4.10.

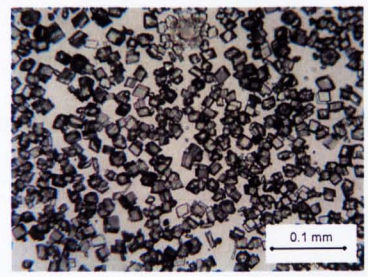

Figure 4.10: Calcium carbonate deposit obtained by electrocrystallization after 4 hours with no inhibitor

4.3.1 PPCA

The variation of the current density and the baseline current were similar when 10ppm and 30ppm of PPCA were added to a scaling brine (Figure 4.11). For this range of concentrations, the concentration of PPCA did not affect the current density. If a film of PPCA was present on the surface it had the same properties with regard to the blockage of the oxygen diffusion. Nevertheless the contact angle measurements showed a significant difference between 10 and 30ppm (Figure 4.12). The contact angle increased with the increase of the inhibitor concentration.

The absence of carbonate ions influenced the variation of the current density in the presence of 30ppm of PPCA. The trend of the curve (NSB PPCA 30ppm Figure 4.11) was linear but the baseline current was lower than that observed in the presence of carbonate ions.

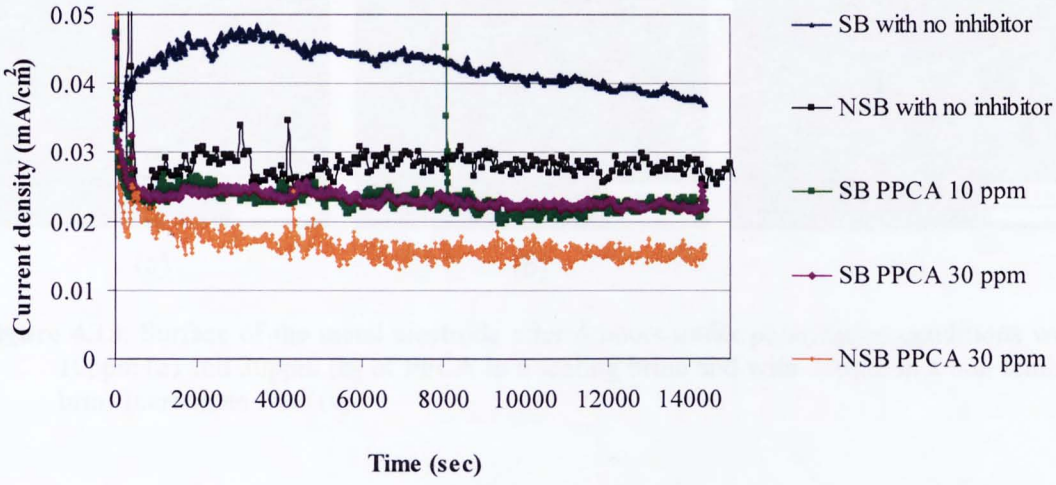

Figure 4.11: Effects of different concentrations of PPCA on the current density for 4 hours

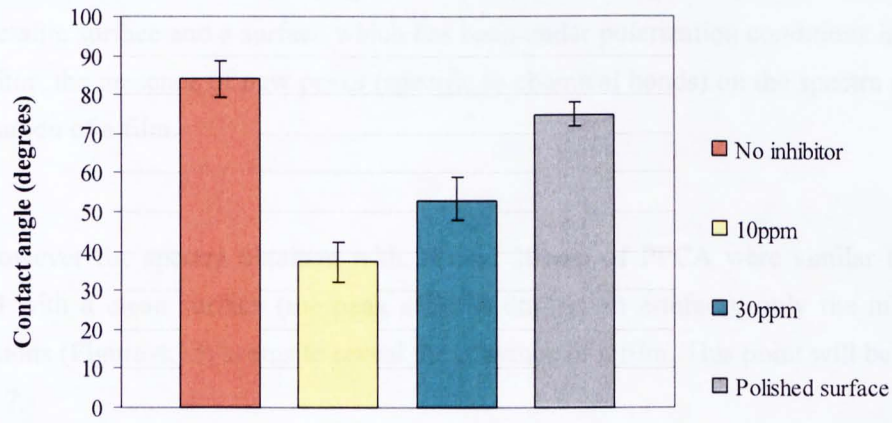

Figure 4.12: Influence of the concentration of PPCA on the contact angle

Figure 4.13 shows the surface after 4 hours under polarization. It has been seen previously that 10ppm of PPCA completely blocked calcium carbonate formation under the same experimental conditions (after 24 hours) and an inhibitor film was detected on the surface (with the variations of the current density, Figure 4.1). At 30ppm in a scaling brine the pattern obtained was really heterogeneous; some areas were fully covered and some parts of the sample seems free of film.

In the absence of carbonate ions with 30ppm of PPCA, heterogeneous patterns were present on the surface of the electrode (Figure 4.13c). This could be the film formed by PPCA. This film had an effect on the current density. The film formation occurred quickly as the baseline current value was reached at 6000 seconds.

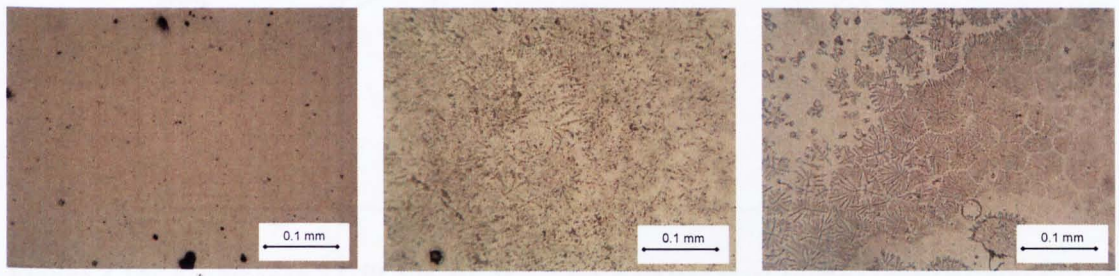

(a) (b) (c)

Figure 4.13: Surface of the metal electrode after 4 hours under polarization conditions with 10ppm (a) and 30ppm (b) of PPCA in a scaling brine and with 30ppm in a non scaling brine (carbonate free) (c).

Infra-red absorbance spectra have been studied in order to determine the presence of the inhibitor on the metallic surface (Figure 4.14). By comparing the spectra obtained with a clean metallic surface and a surface which has been under polarization conditions in presence of inhibitor, the presence of new peaks (specific to chemical bonds) on the spectra can reveal the formation of a film.

However the spectra obtained with 10 and 30ppm of PPCA were similar to the one obtained with a clean surface (the peak at 2350 cm^{-1} is an artefact); only the microscopic observations (Figure 4.13) seems to reveal the presence of a film. This point will be discussed Chapter 7.

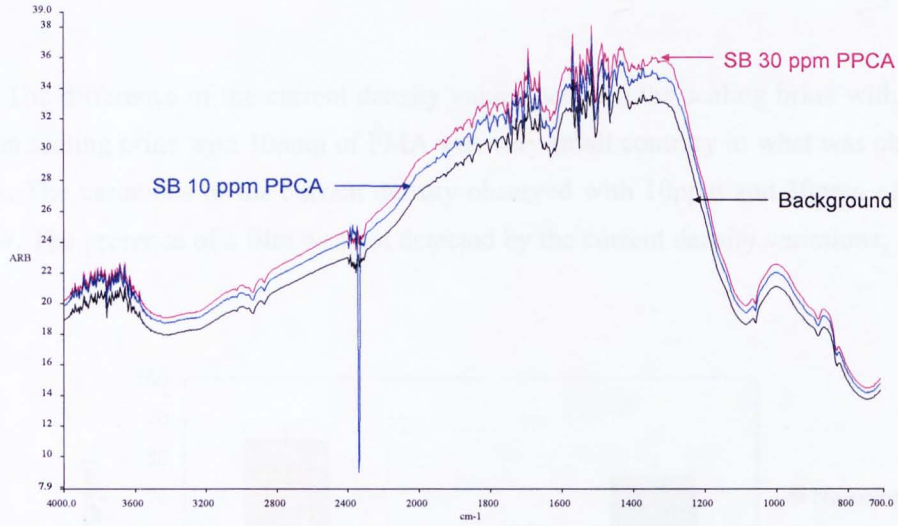

Figure 4.14: Absorbance FT-IR spectra of a clean stainless steel surface (background) and of the layer present on the metallic surface after 4 hours of electrodeposition with PPCA

4.3.2 PMA

The variation of the current density was the same with 10 and 30ppm of PMA (Figure 4.15). However the measurements of the contact angle showed the same variations as with PPCA (ie. increase of the contact angle with the increase of the concentration) (Figure 4.16).

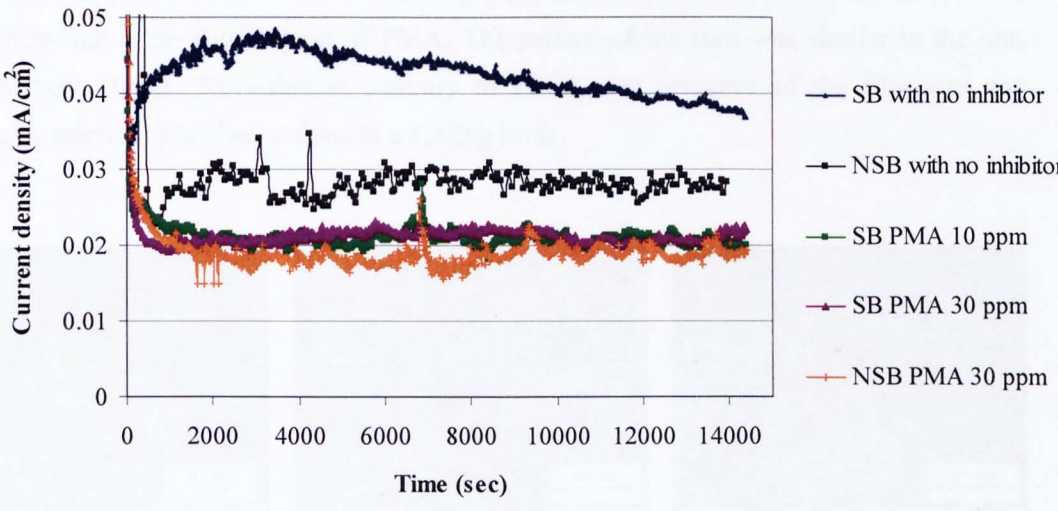

Figure 4.15: Effects of different concentrations of PMA on the current density for 4 hours

The difference of the current density values between the scaling brine with 30ppm and the non scaling brine with 30ppm of PMA was very small contrary to what was observed with PPCA. The variations of the current density observed with 10ppm and 30ppm of PMA were similar. The presence of a film was not detected by the current density variations.

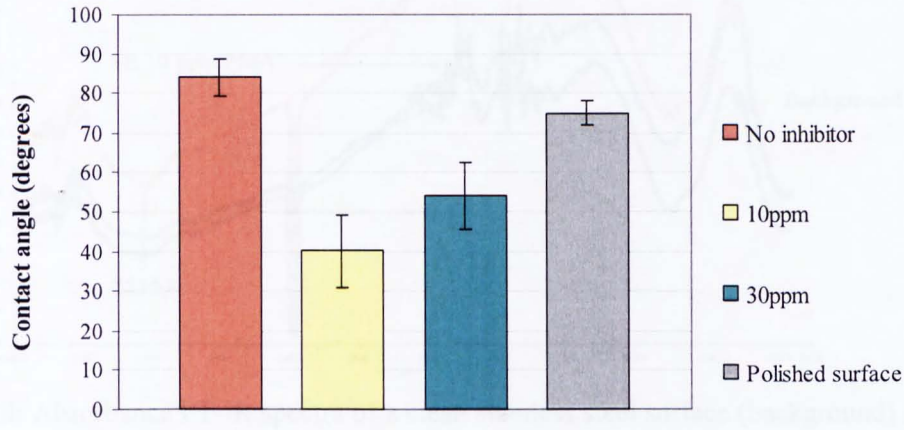

Figure 4.16: Influence of the concentration of PMA on the contact angle

The microscopic observations (Figure 4.17) show the absence of calcium carbonate with 10 and 30ppm of PMA added to a scaling brine and the presence of the inhibitor film in a carbonate-free brine with 30ppm of PMA. The pattern of the film was similar to the one observed with PPCA. Nevertheless contrary to PPCA, the presence of the film was not obvious by microscopic observations in a scaling brine.

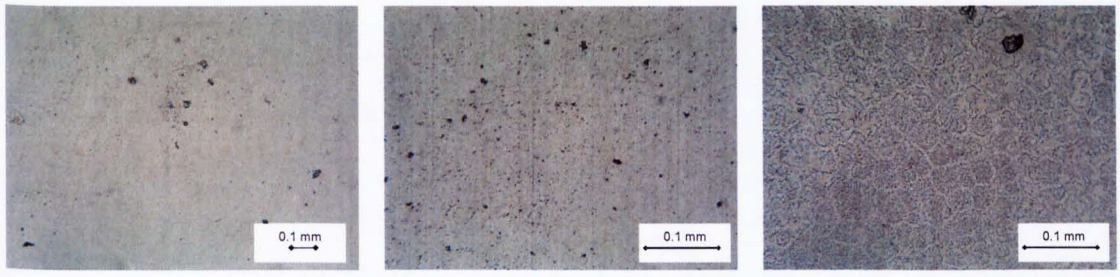

(a) (b) (c)

Figure 4.17: Surface of the metal electrode after 4hours under polarization conditions with 10ppm (a) and 30ppm (b) of PMA in a scaling brine and with 30ppm in a non scaling brine (carbonate free) (c).

A weak peak was detected by FT-IR at the wavelength of 3215.8 cm^{-1}, for the concentration 30ppm, which is specific to the carboxyl function (Figure 4.18) and PMA is a polycarboxylic acid.

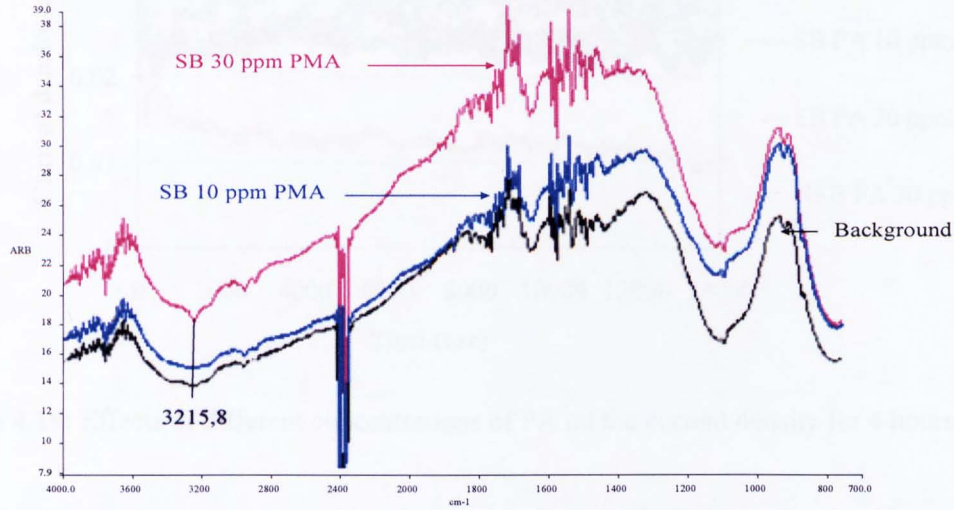

Figure 4.18: Absorbance FT-IR spectra of a clean stainless steel surface (background) and of the layer present on the metallic surface after 4hours of electrodeposition with PMA

4.3.3 PA

10 and 30ppm of PA had the same effects on the current density (same trend and same baseline current) (Figure 4.19). But there was a difference in the contact angle: as seen with the PPCA and the PMA, the increase of the concentration of PA generated an increase in the contact angle (Figure 4.20). The modification promoted by the increase of the concentration was not detected by the variation of the current density.

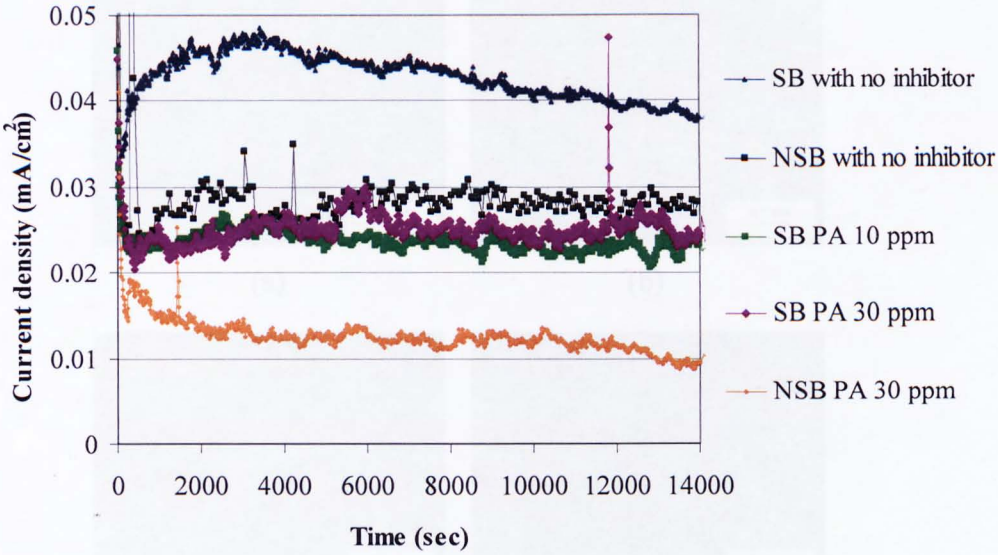

Figure 4.19: Effects of different concentrations of PA on the current density for 4 hours

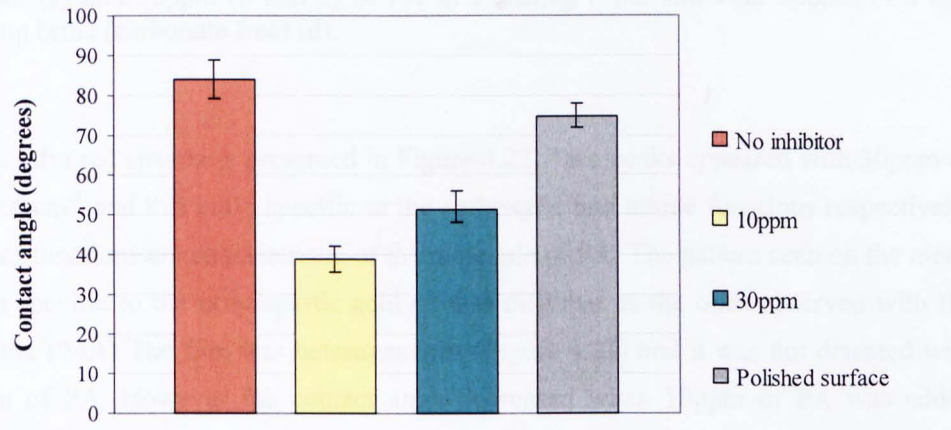

Figure 4.20: Influence of the concentration of PA on the contact angle

A large decrease in the current density values was observed with 30ppm of PA in absence of carbonate ions (Figure 4.19) probably due to the presence of the inhibitor film. Figure 4.21 shows the presence of a film when 30ppm of PA was present in the scaling and non scaling brines.

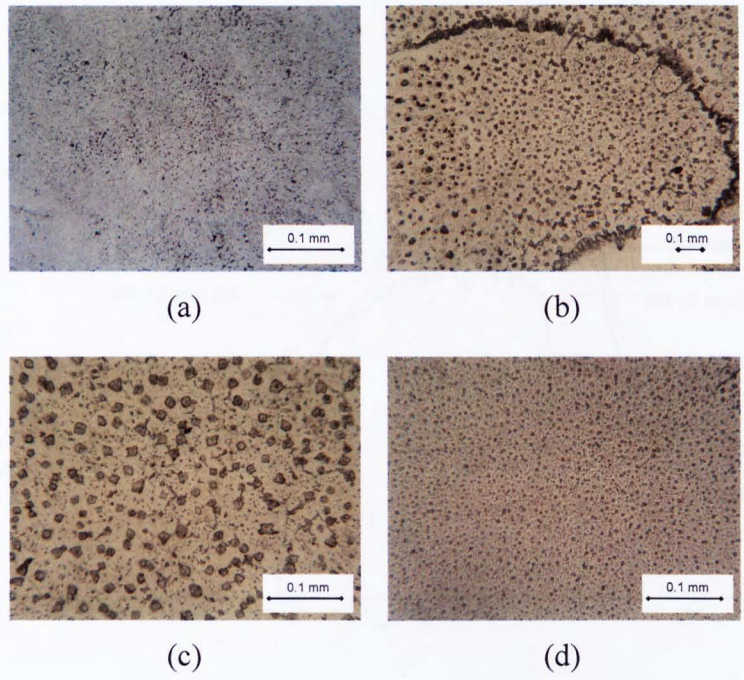

Figure 4.21 : Surface of the metal electrode after 4hours under polarization conditions with 10ppm (a) and 30ppm (b and c) of PA in a scaling brine and with 30ppm in a non scaling brine (carbonate free) (d).

The infra red spectra is presented in Figure 4.22. Two peaks appeared with 30ppm of PA at 1399.4 cm^{-1} and 875 cm^{-1}, specific to the carboxylic and amide functions respectively. Both of these functions are characteristic of the molecule of PA. The pattern seen on the metal surface was specific to the polyaspartic acid (it was different as the ones observed with the PPCA and the PMA) The film was heterogeneous (Figure 4.21) and it was not detected with only 10ppm of PA. However the contact angle increased when 10ppm of PA was added compared to the non inhibited case.

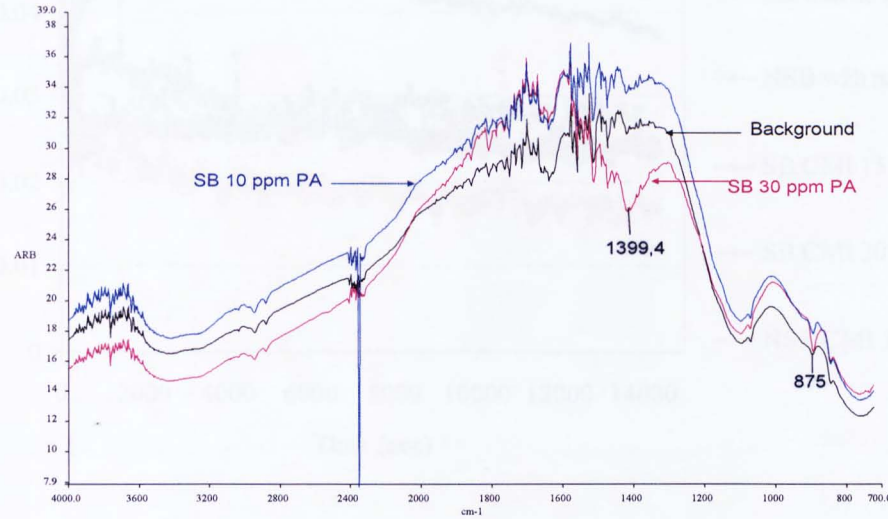

Figure 4.22: Absorbance FT-IR spectra of a clean stainless steel surface (background) and of the layer present on the metallic surface after 4hours of electrodeposition with PA

4.3.4 CMI

15 and 30ppm of CMI generated the same changes in the variation of the current density (as seen with PPCA) except at the beginning of the tests (until 4000 seconds) (Figure 4.23). 15ppm of CMI generated a slight increase and then a decrease of the current density. From 4000 seconds the two curves had the same trend and the same baseline current. In the inhibited brines in absence of carbonate ions, the trend of the curve was almost linear and the values of the current density were lower than in the inhibited scaling brine. The microscopic observations show the presence of a film when carbonate ions were removed from the solution (Figure 4.24) and the pattern of the film was similar to the film obtained with PPCA. A great difference in the pattern between the scaling brine and non scaling brine both containing 30ppm were revealed.

As observed with PPCA, the inhibitor film was heterogeneous (Figure 4.24b and 7c). Some areas of the samples seemed free of films and some others were fully covered by the film.

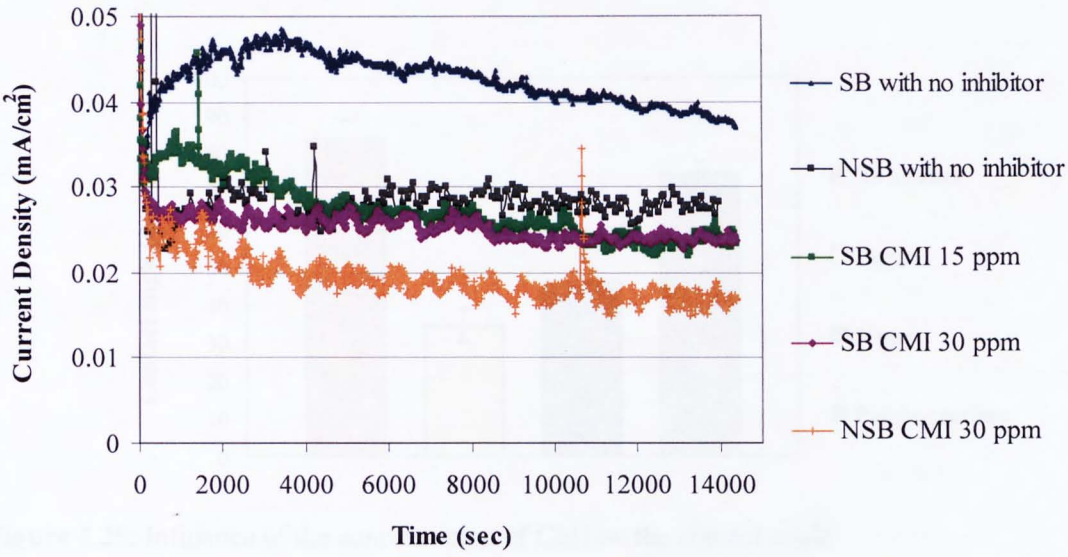

Figure 4.23: Effects of different concentrations of CMI on the current density for 4 hours

The contact angle increased with the increase of the concentration (Figure 4.25). The increase of the concentration generated changes on the surface (shown by the variation of the contact angles values) but these changes were not detected by the variation of the current density.

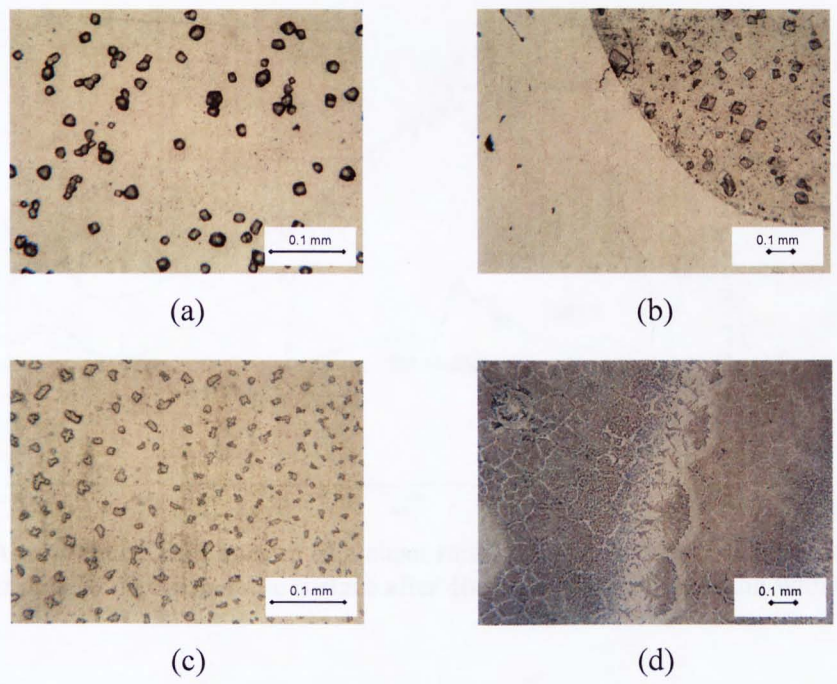

Figure 4.24: Surface of the metal electrode after 4hours under polarization conditions with 15ppm (a) and 30ppm (b and c) of CMI in a scaling brine and with 30ppm in a non scaling brine (carbonate free) (d).

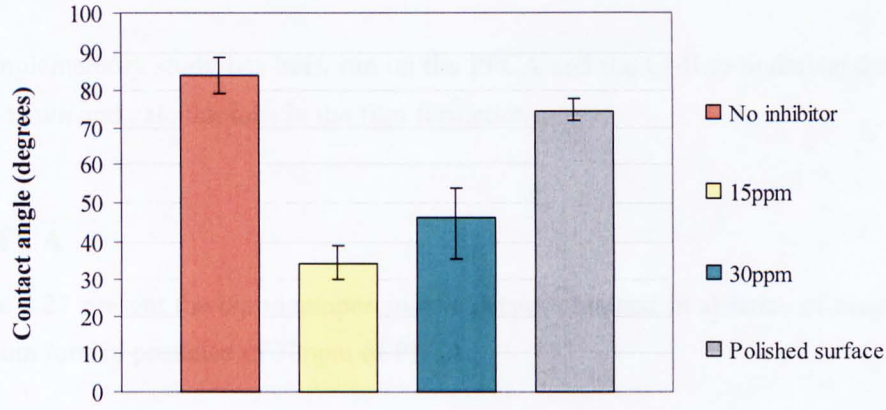

Figure 4.25: Influence of the concentration of CMI on the contact angle

The IR spectra obtained with 30ppm of CMI presents three more peaks than the one obtained with a clean stainless steel surface (Figure 4.26) at the wavelengths 3225.8, 1347.5 and 873cm^{-1} specific to the chemical bonds of the alcohol function, aromatic alcohols and oxygen bond respectively. The molecular structure shows that CMI is composed of these three chemical structures. CMI was bound onto the metal surface when present at 30ppm.

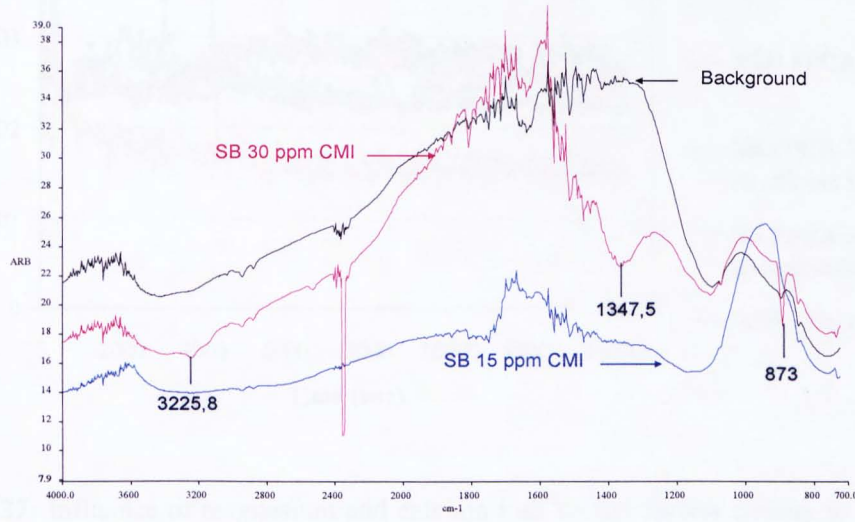

Figure 4.26: Absorbance FT-IR spectra of a clean stainless steel surface (background) and of the layer present on the metallic surface after 4hours of electrodeposition with CMI

4.3.5 Effects of the calcium and magnesium ions on film formation (PPCA and CMI)

A complementary study has been run on the PPCA and the CMI to understand the role of the magnesium and calcium ions in the film formation.

4.3.5.1 PPCA

Figure 4.27 present the chronoamperometric curves obtained in absence of magnesium and/or calcium ions in presence of 30ppm of PPCA.

The chronoamperometric curves obtained with a calcium-free and magnesium-free brine generated the same variations of the current density (Figure 4.27). The layer formed on the surface seemed to be less adherent for the magnesium-free brine as the oscillations of the signal are greater [75].

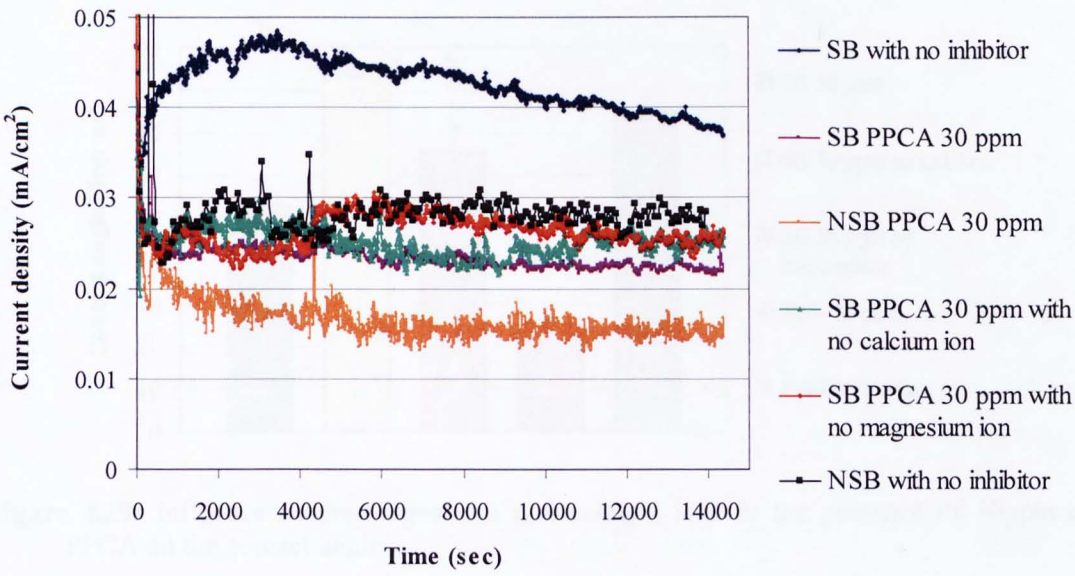

Figure 4.27: Influence of magnesium and calcium ions on the current density in presence of 30ppm of PPCA

No inhibitor film nor calcium carbonate crystals were observed on the surface of the electrode (Figure 4.28) in absence of Ca^{2+} or Mg^{2+}. Magnesium and/or calcium seem to have an important role in the film formation as no pattern was observed in the absence of these cations.

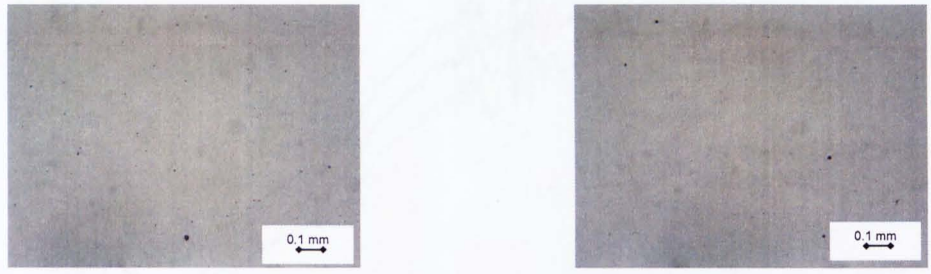

(a) (b)

Figure 4.28: Surface of the metal electrode after 4hours under polarization conditions with no calcium ion (a) and no magnesium ion (b) in a scaling brine and in presence of 30ppm of PPCA.

An increase of the contact angle was generated by the absence of magnesium in the brines and the increase was greater for the calcium-free brines. The influence of carbonate ions was important as a decrease of the contact angle was promoted. The calcium ions have a greater effect on the contact angle than the magnesium ions (Figure 4.29).

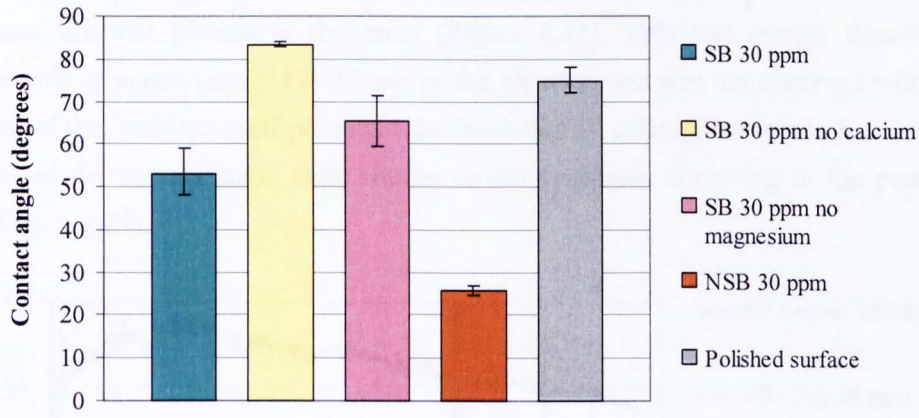

Figure 4.29: Influence of the magnesium and calcium ions in the presence of 30ppm of PPCA on the contact angle

No changes in the IR spectra were observed for the calcium-free and magnesium-free brines (Figure 4.30). The film was still not detected as observed when the cations were present in the brines.

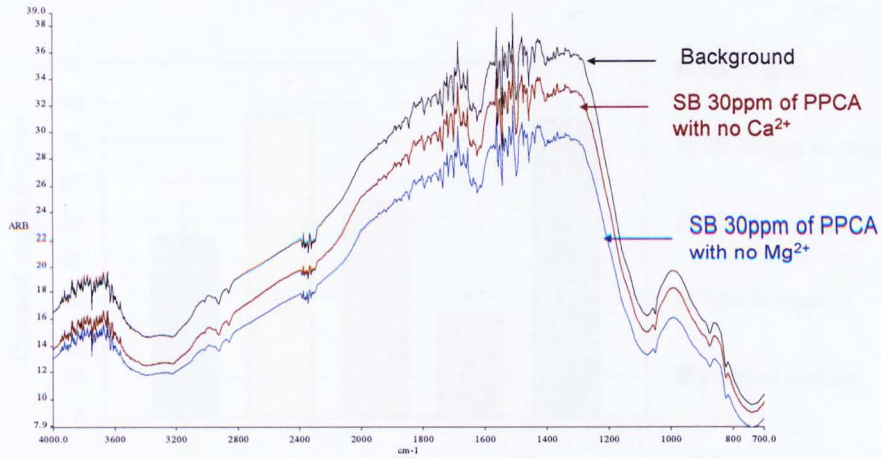

Figure 4.30: Absorbance FT-IR spectra of a clean stainless steel surface (background) and of the layer present on the metallic surface after 4hours of electrodeposition with 30ppm of PPCA in the absence of magnesium and calcium ions

4.3.5.2 CMI

The absence of both magnesium and calcium generated a slight increase of the baseline current values (Figure 4.31). In the calcium-free brine there was no film formation observed with a light microscope and there were some crystals of calcium carbonate formed when magnesium was not present in the brine (Figure 4.33). This last remark illustrated the inhibition role of magnesium [112]. However this phenomenon was not observed with PPCA; the action of the inhibitor itself permitted the inhibition of calcium carbonate formation. The variations of the contact angle were similar as the variations occurring in the presence of PPCA (Figure 4.29).

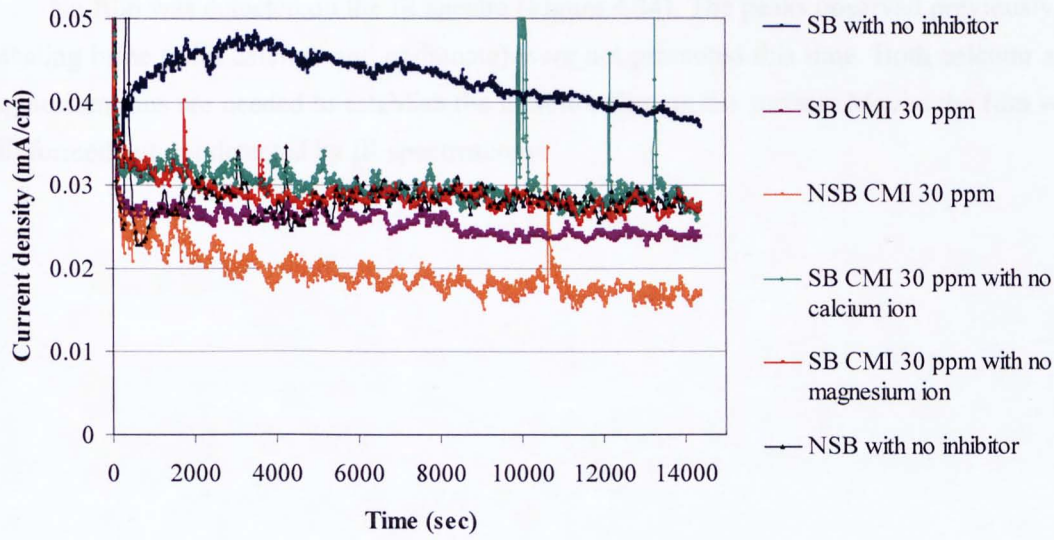

Figure 4.31: Influence of magnesium and calcium ions on the current density in the presence of 30ppm of CMI

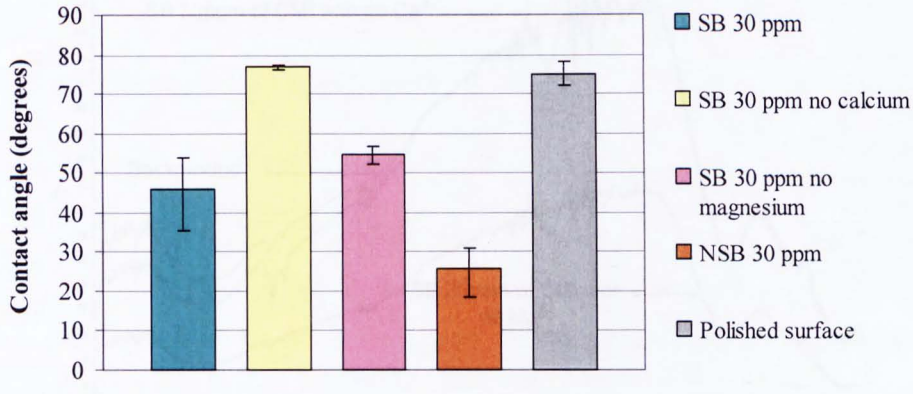

Figure 4.32: Influence of the magnesium and calcium ions in presence of 30ppm of CMI on the contact angle

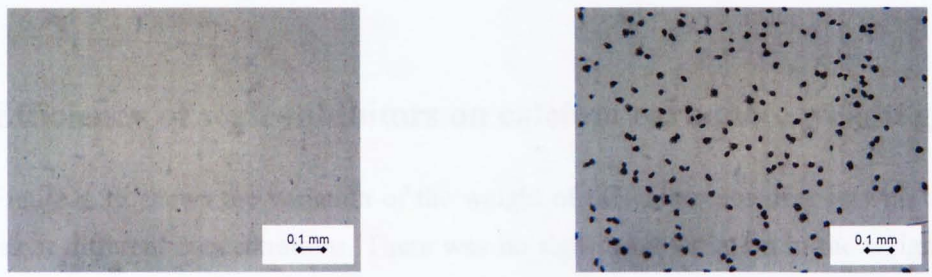

Figure 4.33: Surface of the metal electrode after 4hours under polarization conditions with no calcium ion (a) and no magnesium ion (b) in a scaling brine and in presence of 30ppm of CMI.

No film was detected on the IR spectra (Figure 4.34). The peaks observed previously in a scaling brine (with calcium and carbonate) were not promoted this time. Both calcium and magnesium ions are needed to establish the inhibitor film on the surface. Maybe the film was still formed but not detected by IR spectroscopy.

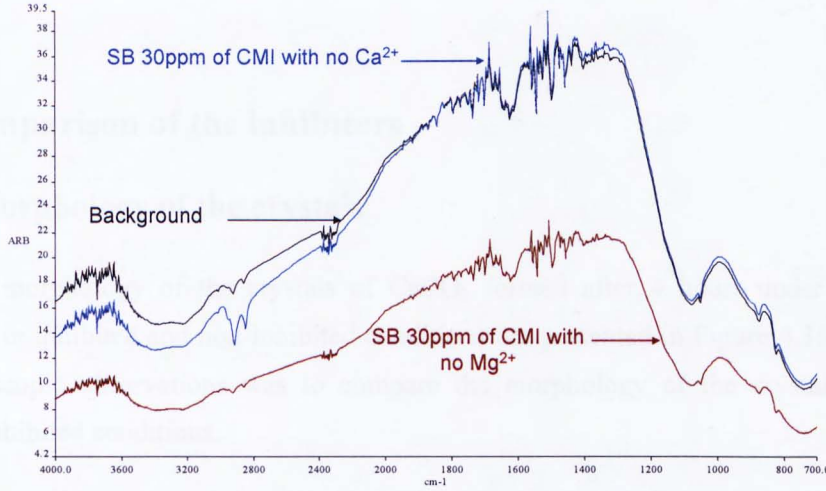

Figure 4.34: Absorbance FT-IR spectra of a clean stainless steel surface (background) and of the layer present on the metallic surface after 4hours of electrodeposition with 30ppm of CMI in the absence of magnesium and calcium ions

4.4 Efficiency of scale inhibitors on calcium carbonate weight gain

Figure 4.35 shows the variation of the weight of the calcareous deposit with different additives at different concentrations. There was no significant variation in the weight of the deposit when 1ppm of inhibitor was added. A large decrease of the weight gain was observed for 4ppm of PPCA and Polymaleic acid. For the concentrations 10ppm and 15ppm, the weight was reduced by such an extent that weight measurement was no longer accurate. It is interesting to note that PPCA significantly affected the weight of the deposit after 4 hours compared to the other inhibitors. Only an increase of 0.19mg was observed with 4ppm of PMA (between 4 and 24 hours) whereas for the PA and the CMI the weight of the calcareous layer had considerably increased (0.67 and 1.3mg for the PA and the CMI respectively).

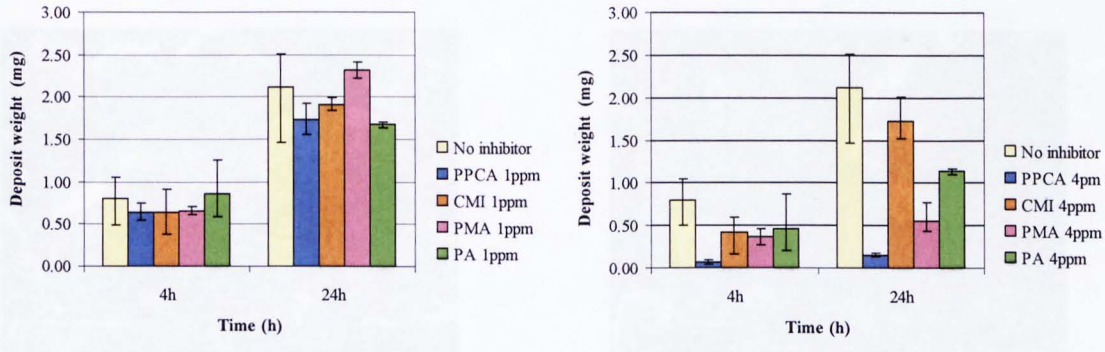

Figure 4.35: Variation of the weight of the calcareous deposit after 4 and 24 hours in presence of scale inhibitors at different concentrations

4.5 Comparison of the inhibitors

4.5.1 Morphology of the crystals

The morphology of the crystals of $CaCO_3$ formed after 4 hours under polarization conditions in inhibited and non-inhibited conditions are presented in Figure 4.36. The aim of the microscopic observations was to compare the morphology of the crystals formed in different inhibited conditions.

Cubical calcite and leaf-like vaterite are formed in the non-inhibited brine. The addition of inhibitors modified clearly the morphology of the crystals. 4ppm of PPCA leaded to the formation of rounded and small crystals, the crystals formed with 4ppm of PMA were elongated and distorted crystals of $CaCO_3$ were formed with 4ppm of PA and CMI (Figure 4.36). 1ppm of PPCA and PMA modified the morphology of the crystals whereas for PA and CMI 4ppm is needed to see some changes of the morphology. Crystals of vaterite are observed with 1ppm of CMI.

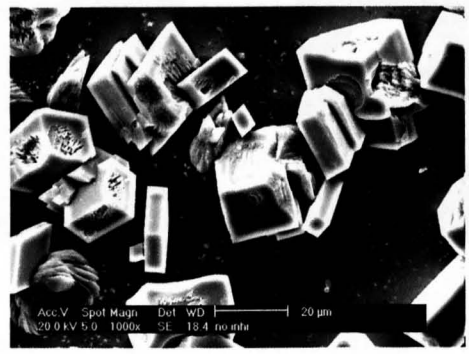

(a)

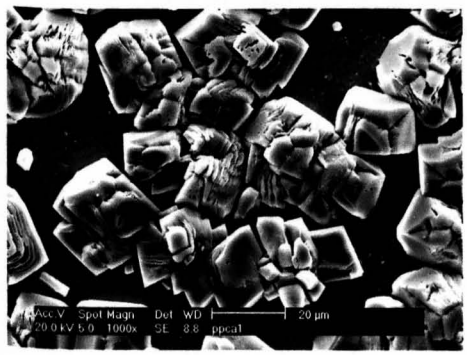

(b)

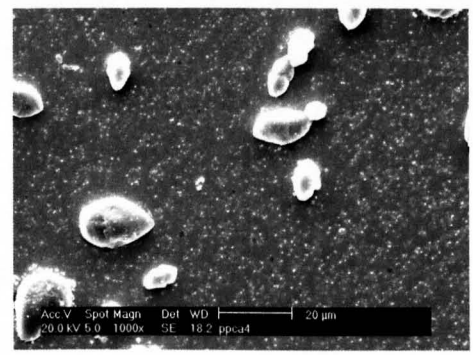

(c)

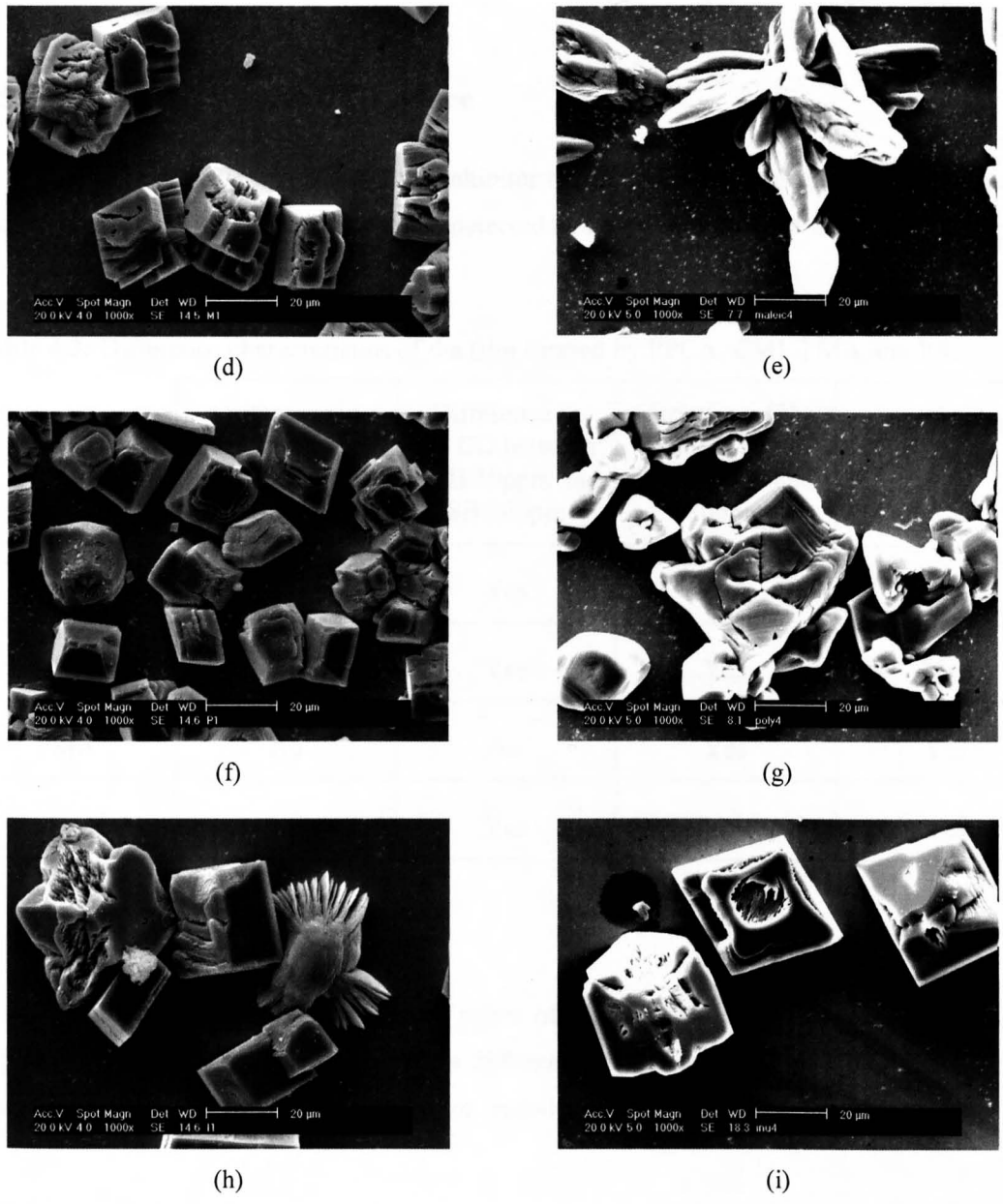

Figure 4.36: SEM observations of crystals of $CaCO_3$ formed on a metal surface in (a) a non-inhibited brine, with (b) 1 and (c) 4ppm of PPCA, with (d) 1 and (e) 4ppm of PMA, with (f) 1 and (g) 4ppm of PA, with (h) 1 and (i) 4ppm of CMI after 4 hours under polarization and static conditions.

4.5.2 Interactions with the surface

The different characteristics of the inhibitor film on the variations of the current density and the contact angle and the ability to be detected by IR are summarised Table 4.3.

Table 4.3: Difference characteristics of the film formed by PPCA, CMI, PMA and PA.

	Difference in the CD between SB 10 and SB 30ppm	Difference in the CD between NSB 30ppm and SB 30ppm	Variation of the contact angle between 10 and 30ppm	Detection of a film with FT-IR
PPCA	No	Yes	Yes	No
CMI	No	Yes	Yes	Yes
PMA	No	No	Yes	Yes
PA	No	Yes	Yes	Yes

(CD: Current Density)

For the 4 inhibitors, there was no effect of the increase of the concentration (10 to 30ppm) on the current density whereas a difference in the contact angle was detected; an increase of the concentration of the inhibitor leaded to an increase of the contact angle.

The absence of the carbonate ions seems to be important in the film formation with the PPCA and the PA as the baseline current was lower in a carbonate-free brine (NSB) with 30ppm of PPCA or PA. The chronoamperometry showed two different characteristics in the mechanism of the inhibitor film. It is appreciated that the carbonate ions could have an effect on the establishment of the inhibitor film with the CMI and the PMA but this was not detected by chronoamperometry.

The film formed with the PA and the CMI were detected by infra red spectroscopy whereas only the film formed with the PA was detected by chronoamperometry. It is interesting to note that the film obtained with the PPCA was well detected by the study of the current density variation whereas it was not by Fourier Transform Infra Red. Only one additional small peak was observed in presence of PMA.

The baseline current observed with 4ppm was lower than the one observed with 10ppm of PMA. At 4ppm, the surface was covered by the inhibitor and by some crystals of calcium carbonate whereas at 10ppm there were no crystals observed. The same remark can be made for the CMI: the baseline current at 15ppm was lower than the baseline current with 30ppm whereas for PPCA and PA, the baseline current at 10ppm was lower than at 4ppm. $CaCO_3$ was still formed with 4ppm of PMA and 15ppm of CMI. The current density was mostly due to the calcareous layer present on the surface (and not due to the presence of a film of inhibitor) as at higher concentration (when no crystals were formed) the baseline current was similar to that seen for the non scaling brine. The inhibitor had a smaller effect on the oxygen diffusion than PPCA and PA. For these two inhibitors, a high concentration of inhibitor (blocking calcium carbonate formation) had a greater effect on the oxygen diffusion.

The oscillations of the chronoamperometric curves obtained at high concentrations make the interpretation of the curves more difficult. It has been shown that the oscillations of a chronoamperometric curve is a function of the adherence of the material present on the surface [75]. It is clear that a homogeneous thick and non-porous calcium carbonate layer will generate a smoother curve than a curve obtained from a surface covered by a thin and heterogeneous film.

It is interesting to note that the effect of PPCA on scaling was efficient inhibition even if a film was not detected by IR spectroscopy. The percentage of inhibition efficiency based on weight measurements at 4ppm showed that PPCA was the most efficient after 4 hours under polarization (CMI, PA and PMA had almost the same efficiency, between 42 and 55%) and after 24 hours PPCA had still the greatest effects on calcium carbonate inhibition but the efficiency of the PMA was largely increased when studied for 24 hours (55% to 75% after 4 and 24 hours respectively). However the IR spectra did not detect as well as with PA and CMI the presence of the film on the surface. It seems that even if different inhibitors act with the same mechanism, their effects on calcium carbonate inhibition can be still quite different. The detection of a film did not show a greater inhibition property.

These different remarks lead to the fact that the film formed on a metal surface have different characteristics according to the inhibitor used. The characterisation of the film and the mechanism of its formation will be discussed in Chapter 7.

Chapter 5
Characterisation of $CaCO_3$ deposit with an *in-situ* flow cell and its interactions with the additives

5.1 Introduction

As seen in the previous chapter, the scale inhibitors studied in this thesis have a large effect on the morphology of the crystals of calcium carbonate. The use of an *in-situ* flow cell coupled with a video assembly and a microscope permits the determination of morphometric characteristics (in real time) of the crystals such as the diameter and the shape factor of the crystals. The number of crystals has been determined and the surface coverage of the calcareous deposit on the metal surface. This technique permitted the detection of crystals of calcium carbonate bigger than 1μm. When no crystals (or a few) were detected, electronic microscopic observations (with a Scanning Electron Microscope, SEM) were done in order to see if some crystals were present but were too small to be seen with the light microscope used in this set-up.

In order to study the effects of the scale inhibitors on the nucleation and growth of calcium carbonate, they were added into the brine before the start of the experiments for a large part of the study. The inhibitors were therefore present in the brines during the nucleation process. A complementary study has been carried out to study the effects of inhibitors on a calcareous layer already formed on the metal surface so on the growth of the crystals present on the surface (nucleated in a non inhibited brine). In this case the inhibitors were added after 10 minutes of crystallization.

The nature of the nucleation (instantaneous or progressive) has been determined. The determination of the morphometric characteristics allows the calculation of the lateral growth rate.

This chapter presents the results obtained with the same four additives as in Chapter 4 (PPCA, PMA, PA and CMI). The characteristics of the crystals formed in the inhibited brines were compared with the crystals formed in a non inhibited brine. The structure of this chapter follows the same model for each inhibitor. Firstly, the effects of the inhibitors were studied when the inhibitors were added before the start of the test and secondly when they were added after 10 minutes of polarization.

For both cases, the calcareous deposit was characterised and then the crystals of calcium carbonate were studied (morphometric characteristics of individual crystals). When the inhibitors were added 10 minutes after the creation of the supersaturation, some crystals of $CaCO_3$ were formed during the 10 minutes and grew on the metal surface. A complementary study has been realised for the PPCA, the PMA and the PA to determine the interactions between the surface of the calcium carbonate and the inhibitors and is reported at the end of the part characterising the inhibitors. The CMI has not been tested as Demadis *et al.* already showed the interactions of the CMI and $CaCO_3$ [155] and a summary of the findings are given instead.

5.2 Experimental details

The experiments were carried out in University of Franche-Comté (Besançon, France) in the UTINAM Institute in the team "Materials and Structured Surfaces".

5.2.1 Experimental set-up

The electrochemical cell integrated 3 electrodes in 2 parallel PMMA (poly(methyl methacrylate) plates as presented in (Figure 3.6). The potential applied was -0.8V/Ag/AgCl and each test was run for 60 minutes. The flow rate of the solution is $40ml.min^{-1}$ and the Reynolds number is nil suggesting that the system is in laminar conditions. The electrochemical cell was combined with an optical and measurement set-up (Figure 3.7). This system provided the following data: number of particles and diameter of the particles, shape factor and surface coverage.

5.2.2 Brines composition

The composition of the brines used in this study are summarized in Table 5.1 and Table 5.2.

Table 5.1: Composition of the brines used in the study with the *in-situ* flow cell

	NaCl	KCl	$MgCl_2$	$CaCl_2$	$NaHCO_3$
Brine 1	64.10g.l^{-1}	2.25g.l^{-1}	5.75g.l^{-1}	28.45g.l^{-1}	0
Brine 2	63.00g.l^{-1}	0	0	0	1.55g.l^{-1}

Table 5.2: Final ionic concentrations of the different elements containing in the brine used for the study with the *in-situ* flow cell

Ions	**Concentration (mg/l)**
Na^+	25188
K^+	590
Sr^{2+}	221
Mg^{2+}	345
Ca^{2+}	2614
Cl^-	44248
HCO_3^-	556

5.2.3 Experiment overview

The inhibitors have been added in the brine at different time:

- Before the start of the experiment (t=0)
- After 10 minutes from the start of the experiment (t=10). In order to have a correct observation at the 10th minute (with no perturbation of the system due to the addition of the inhibitors), the inhibitors were added at the exact time 9'30sec.

The experiment overview is presented Table 5.3.

Table 5.3: Experiments overview with the *in-situ* flow cell.

Inhibitors	Added at **t=0**	Added at **t=10minutes**
PPCA	1&4ppm	4ppm
PA	1&4ppm	4ppm
PMA	1&4ppm	4ppm
CMI	1&4ppm	4ppm

5.3 Characterisation of crystals of calcium carbonate formed in an uninhibited brine

5.3.1 Morphometric characteristics of the crystals of $CaCO_3$

Two parameters have been determined to characterise the crystals of calcium carbonate: their diameter and their shape factor. The mean values are summarized in Table 5.4. After 40 minutes, the agglomeration of crystals meant that the characterisation of the single crystals was no longer possible. The diameter of the crystals increased as a function of time which demonstrates that the crystals were growing during the entire duration of the experiment. The shape of the crystals was constant as indicated by the constant shape factor. The deposit seems to be composed of leaf-like vaterite and especially cubic calcite as shown in Figure 5.1 (d).

The nucleation occurs quickly after the start of the polarization as crystals were observed after only 2 minutes (Figure 5.1 (a)). It was found some black dots present before the start of the polarization therefore it could not be some calcium carbonate crystals but impurities on the surface of the lens of the microscope. They were not taking into account in the calculations of the surface coverage.

Table 5.4: Morphometric characteristics of crystals of calcium carbonate formed in absence of inhibitors

Time (minutes)	**5**	**10**	**20**	**40**	**60**
Shape factor	0.5	0.4	0.4	0.4	Formation of aggregates
Diameter (µm)	4.1	5.3	7.5	11.6	

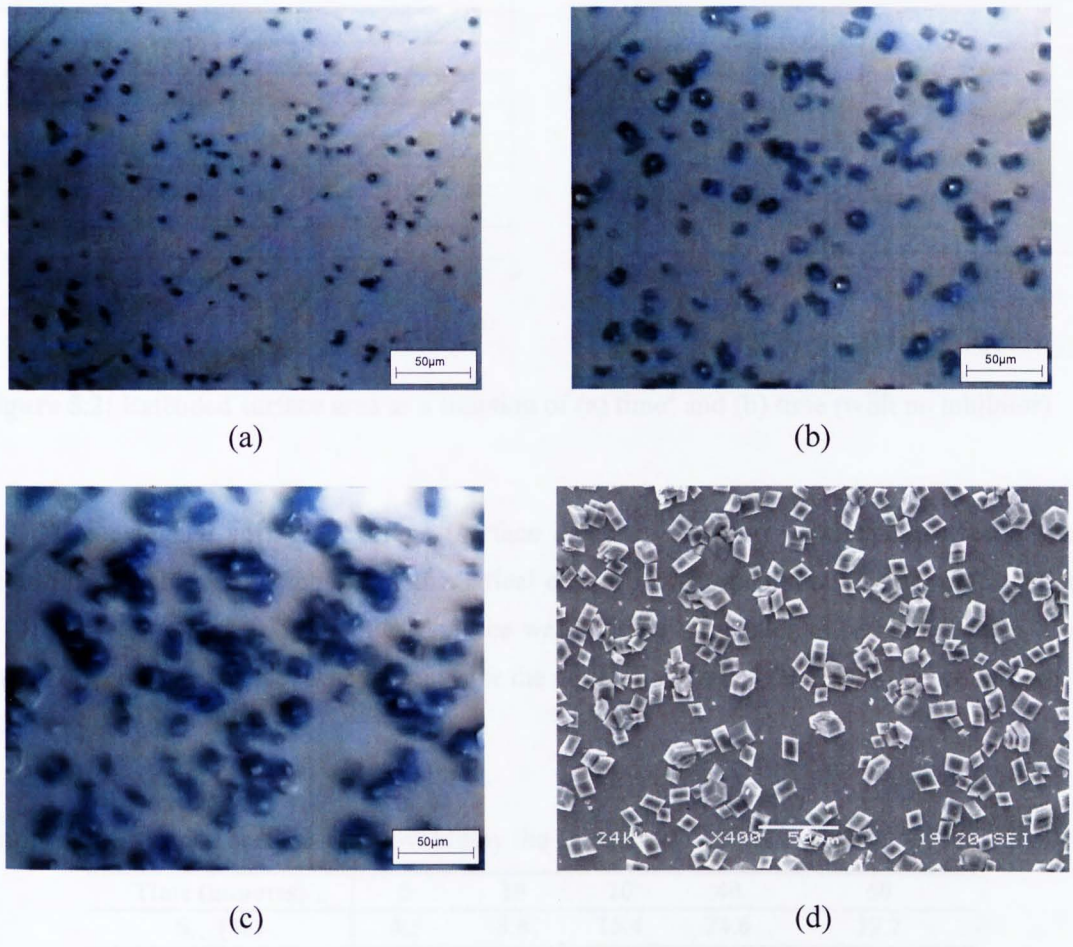

Figure 5.1: Microscopic observations of crystals of calcium carbonate (realised with a light microscope (a), (b) and (c) and with a SEM (d)) formed under polarization conditions and in a non-inhibited brine after (a) 5, (b) 20 and (c) and (d) 60 minute experiment

5.3.2 Surface coverage of the calcareous deposit

The nucleation was instantaneous as the extended surface coverage is a linear function of the time (Figure 5.2).

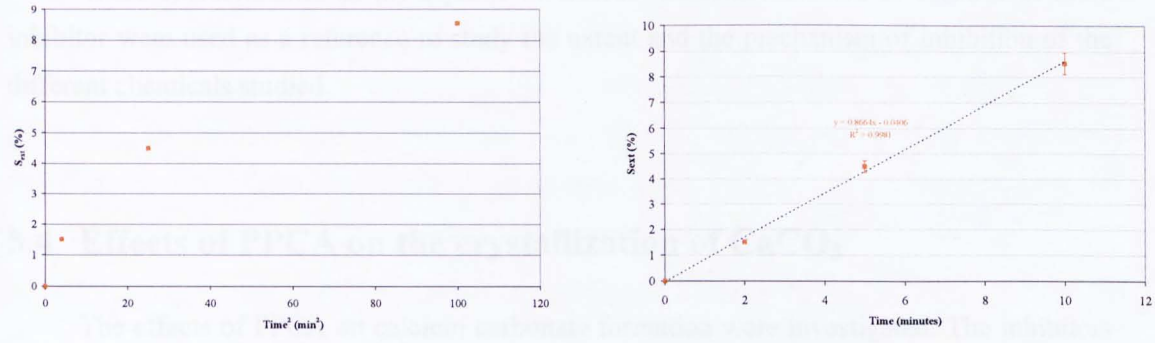

(a) (b)

Figure 5.2: Extended surface area as a function of (a) time^2 and (b) time (with no inhibitor)

The extended surface coverage (surface coverage with no overlapping effects) was determined (Table 5.5) using the mathematical expression developed in Chapter 3 (Equation 3.13). After 60 minutes 39.7% of the surface was covered with calcium carbonate scale. The rate of covering the surface was constant for the entire duration of the test as shown in Figure 5.3

Table 5.5: Extended surface area covered by the calcareous deposit in absence of inhibitor

Time (minutes)	5	10	20	40	60
S_{ext} (%)	4.5	8.6	15.4	24.6	39.7

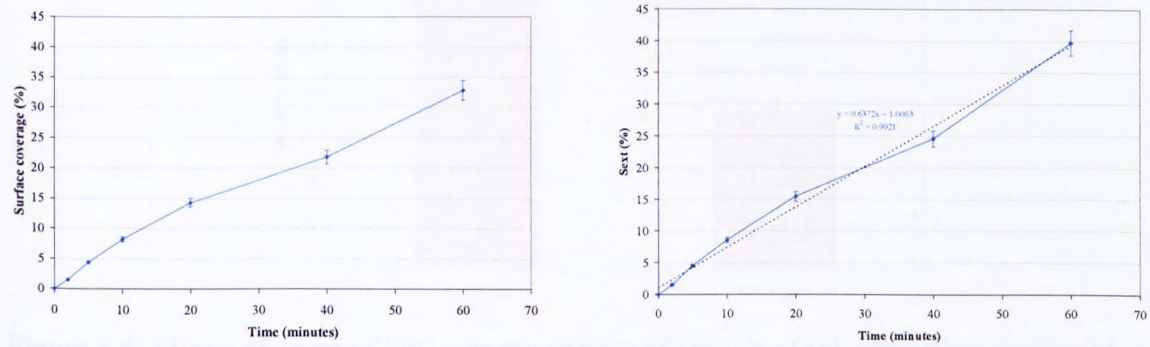

(a) (b)

Figure 5.3: Assessment of (a) the surface coverage by crystals of $CaCO_3$ observed and (b) on the extended surface area for 60 minute in absence of inhibitor

These characteristics of the crystals of calcium carbonate formed in absence of scale inhibitor were used as a reference to study the extent and the mechanism of inhibition of the different chemicals studied.

5.4 Effects of PPCA on the crystallization of $CaCO_3$

The effects of PPCA on calcium carbonate formation were investigated. The inhibitors have been added into the brine at t=0 (at the start of the experiment) in order to study the impact on the nucleation and growth process and at t=10 minutes to determine the effects of the inhibitors on the growth of crystals of calcium carbonate already formed.

5.4.1 Effects of 1 and 4ppm of PPCA on the nucleation and growth of $CaCO_3$

5.4.1.1 Surface coverage of the calcareous deposit

The number of crystals formed onto the metal surface (the observed surface area is 600μm^2) has been determined for each time studied (2, 5, 10, 20, 40 and 60 minutes). It was maintained constant during the 60 minute experiment. The number of crystals formed on the surface largely decreased (46%) with the addition of 1ppm of PPCA. No crystals were observed when 4ppm of PPCA was added (Figure 5.4).

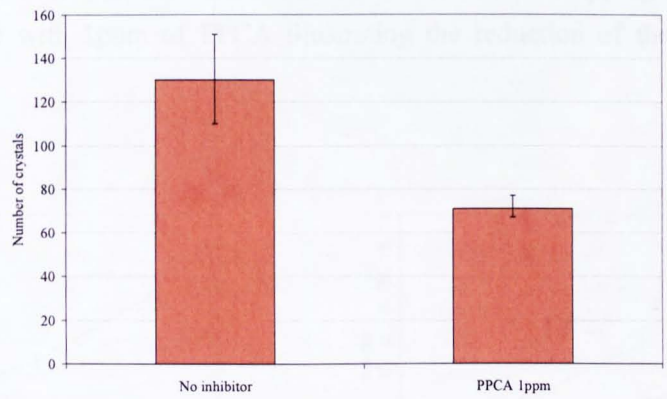

Figure 5.4: Effects of 1ppm of PPCA on the number of crystals of calcium carbonate formed onto a metal surface (600μm^2) after 60 minutes

The decrease in the number of crystals resulted in a decrease in the surface coverage (Figure 5.6).

The surface coverage is a linear function of time when no inhibitor was added. In the inhibited brine (1ppm of PPCA) a decrease was observed even in the early stage of calcium carbonate deposition and it was slowed down after the 5th minute. In both cases, the nucleation was instantaneous as the extended surface is a linear function of the time during the first minutes of the experiment (Figure 5.5). Two linear portions are defined in the inhibited case as it seems that the growth occurs according to two regimes (Figure 5.6).

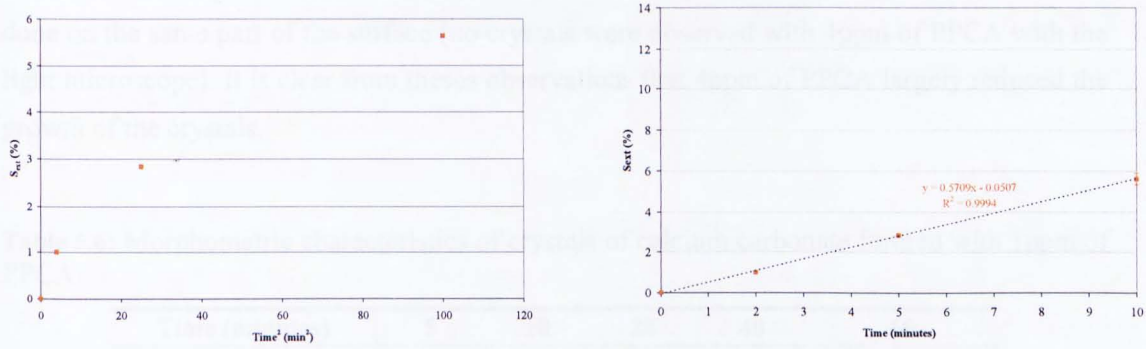

(a) (b)

Figure 5.5: Extended surface area as a function of (a) time^2 and (b) time (1ppm of PPCA)

The comparison of the surface coverage with (Figure 5.6a) and without overlapping effects (Figure 5.6b) in the uninhibited case shows that a difference in the surface coverage was observed from the 20th minute. The difference due to the overlapping effect was seen from the 40th minute with 1ppm of PPCA illustrating the reduction of the growth of the crystals (Figure 5.6).

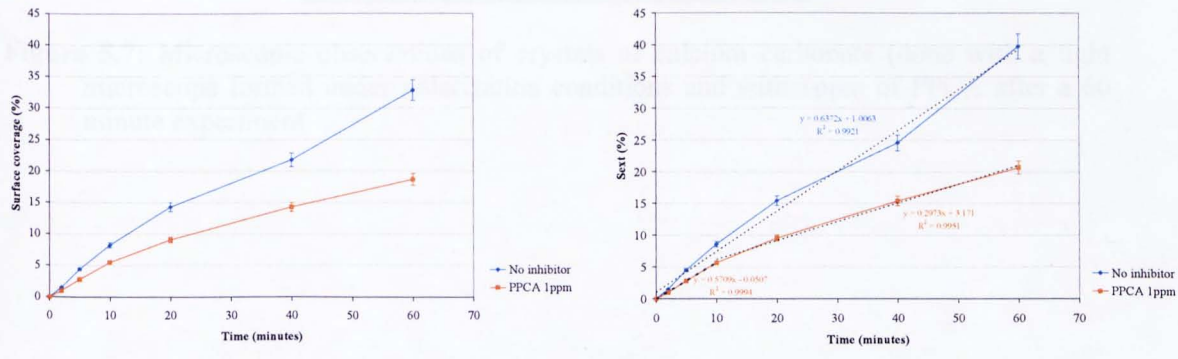

(a) (b)

Figure 5.6: Effects of (a) 1ppm of PPCA on the surface coverage observed and (b) on the extended surface area

5.4.1.2 Morphometric characteristics of the crystals of $CaCO_3$

The surface and the diameter of the crystals increased as a function of time during the 60 minute experiment (Table 5.6). The growth of the crystals occurred with 1ppm of PPCA for 1 hour (Figure 5.7). The metal surface was kept free of crystals with 4ppm of PPCA during the entire experiment: no crystals of $CaCO_3$ were detected on the surface. As the limit of the observation of the crystals is 1µm it is possible that some crystals form that are less than 1µm in size and therefore not detectable (Figure 5.8). A large particle is seen on the Figure 5.8. It could be a crystal of $CaCO_3$ as the observation realised with the SEM was not done on the same part of the surface (no crystals were observed with 4ppm of PPCA with the light microscope). It is clear from theses observations that 4ppm of PPCA largely reduced the growth of the crystals.

Table 5.6: Morphometric characteristics of crystals of calcium carbonate formed with 1ppm of PPCA

Time (minutes)	5	10	20	40	60
Shape factor	0.5	0.4	0.4	0.4	Formation of aggregates
Diameter (µm)	3.5	5.1	6.8	11.4	

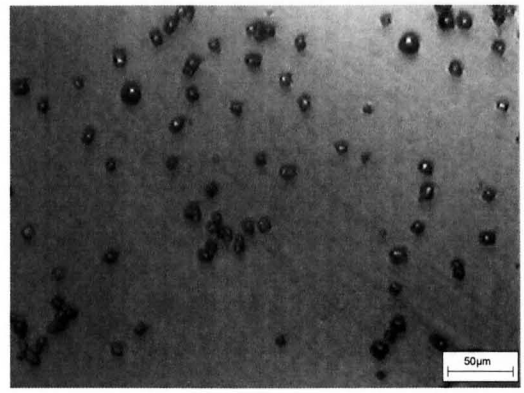

Figure 5.7: Microscopic observations of crystals of calcium carbonate (done with a light microscope formed under polarization conditions and with 1ppm of PPCA after a 60 minute experiment

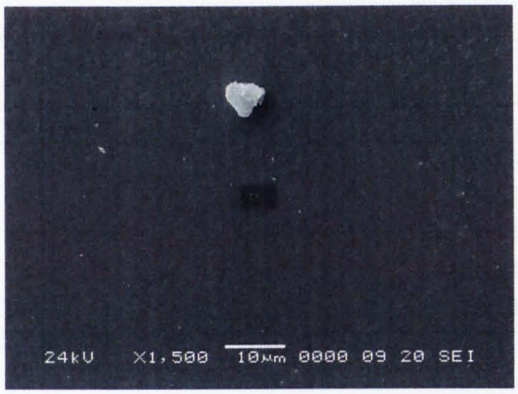

Figure 5.8: SEM observations of crystals of calcium carbonate formed under polarization conditions with 4ppm of PPCA after a 60 minute experiment

The diameter of the crystals was not significantly affected by 1ppm of PPCA (Figure 5.9). The growth of the diameter (Figure 5.9) of the crystals can be split into 2 parts: 0-5 minutes and 5-40 minutes. During the first 5 minutes, the mean diameter of the crystals increased rapidly and slowed after the 5th minute.

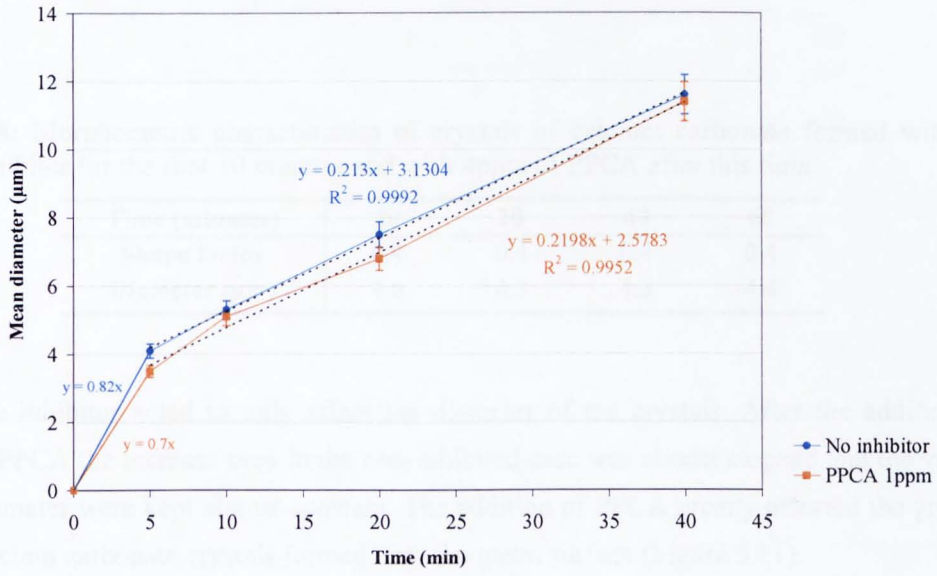

Figure 5.9: Effects of 1ppm of PPCA on the mean diameter of the crystals of $CaCO_3$

According to these results, the growth of the crystals does not seem to be influenced by 1ppm of PPCA. It was confirmed by the calculations of the lateral growth rate; the values were similar as calculated in the non-inhibited case (Table 5.7).

Table 5.7: Lateral growth rate (mol/μm/s) of the crystals of $CaCO_3$ with 1ppm of PPCA in function of time

Time (seconds)	No inhibitor	PPCA 1ppm
120	$1.4x10^{-15}$	$1.7x10^{-15}$
300	$1.6x10^{-15}$	$1.9x10^{-15}$
600	$1.6x10^{-15}$	$1.9x10^{-15}$
1200	$1.4x10^{-15}$	$1.6x10^{-15}$
2400	$1.1x10^{-15}$	$1.3x10^{-15}$

5.4.2 Effects of 4ppm of PPCA on crystals of $CaCO_3$ already formed

The crystals of $CaCO_3$ were formed in a non-inhibited brine and then 4ppm of PPCA was added to study the effect on the crystals already formed.

5.4.2.1 Morphometric characteristics of the crystals of $CaCO_3$

The shape factor was maintained constant (0.4). The increase of the diameter of the crystals was considerably changed after the addition of 4ppm of PPCA (Table 5.8 and Figure 5.10).

Table 5.8: Morphometric characteristics of crystals of calcium carbonate formed with no inhibitor for the first 10 minutes and with 4ppm of PPCA after this time

Time (minutes)	10	20	40	60
Shape factor	0.4	0.4	0.4	0.4
Diameter (μm)	4.0	4.3	4.3	4.4

The inhibitor acted to only affect the diameter of the crystals. After the addition of 4ppm of PPCA the increase seen in the non-inhibited case was almost stopped and the values of the diameter were kept almost constant. The addition of PPCA greatly affected the growth of the calcium carbonate crystals formed onto the metal surface (Figure 5.11).

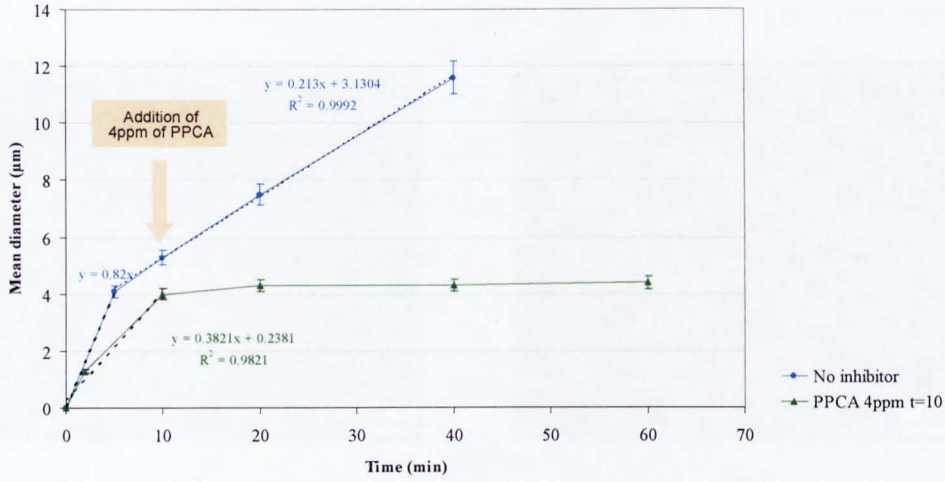

Figure 5.10: Effects of 4ppm of PPCA on the mean diameter of the crystals of $CaCO_3$ nucleated and grown for 10 minutes in absence of inhibitor

The surface coverage has not been determined as the number of crystals formed in these conditions were not similar enough from one test to another. A small difference in the growth of the crystals was observed between 0 and 10 minutes. One important point is that the inhibitors were added at the time 9.5 minutes (in order to have a correct measurement at 10 minutes). The difference could be due to complementary effects of the standard error of the tests, the error occurring during the image analyses and the early effects of the inhibitors.

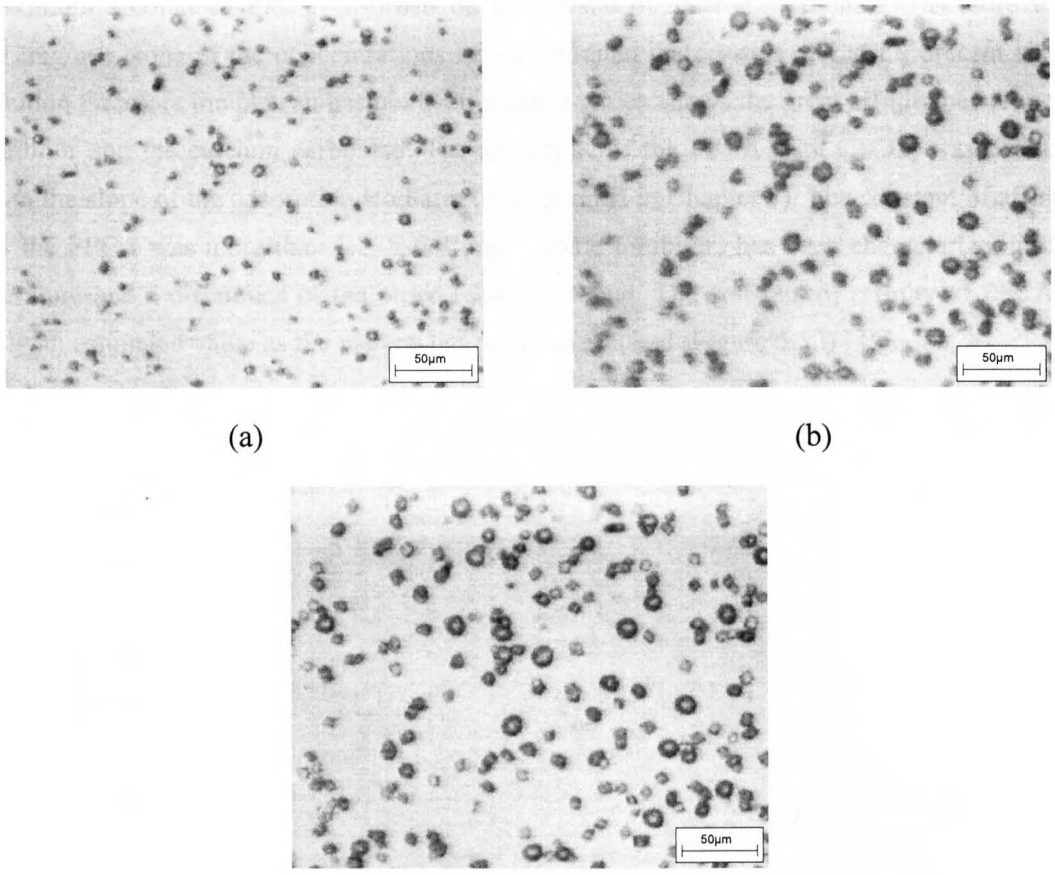

(a) (b)

(c)

Figure 5.11: Microscopic observations of crystals of calcium carbonate (done with a light microscope) formed under polarization conditions and with 4ppm of PPCA (added after 10minutes from the start of the experiment) after (a) 10, (b) 20 and (c) 60 minute experiment

5.4.3 Interactions between the PPCA and the crystals of $CaCO_3$ – Adsorption measurements

In order to determine if there were some interactions between the additives and the calcium carbonate formed on the surface, some adsorption tests were conducted. The scale inhibitors were placed in a solution containing a known quantity of calcium carbonate crystals and the affinity of the additives to the crystals of $CaCO_3$ has been studied. It is clear from Figure 5.12 that the PPCA interacts with the surface of the crystals of calcium carbonate. Ce is the solution equilibrium concentration of the PPCA (not adsorbed on $CaCO_3$).

Figure 5.12 and Figure 5.13 present the results obtained from the adsorption study. The maximum amount of PPCA adsorbed on the crystal of calcium carbonate was more than $0.12mg/m^2$. None of the concentrations tested saturated the crystals of $CaCO_3$ present in the solution therefore the plateau has not been reached which shows the great affinity between the inhibitor and the calcium carbonate. The affinity K of the PPCA with $CaCO_3$ was deduced from the slope of the adsorption isotherm (as explained in Chapter 3). The constant of affinity for the PPCA was more than $1.27E\text{-}04L.mg^{-1}$. Some inhibitors has been characterized in the literature and a difference of the order 1.E-02 is found. The constant of affinity of PPCA is only an estimated value as the plateau has not been reached (Figure 5.12) [46].

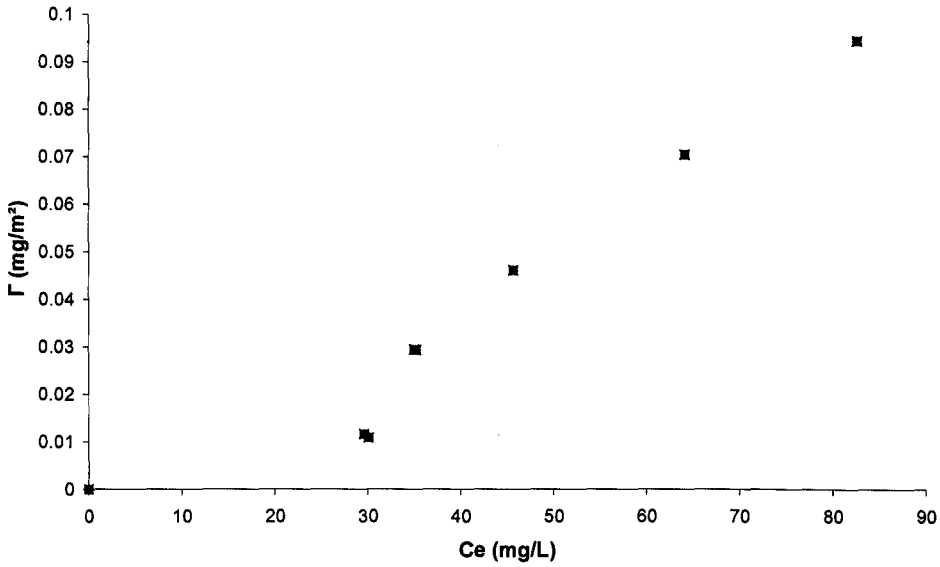

Figure 5.12: Quantity of PPCA adhered on the crystals of calcium carbonate as a function of the solution equilibrium concentration of PPCA.

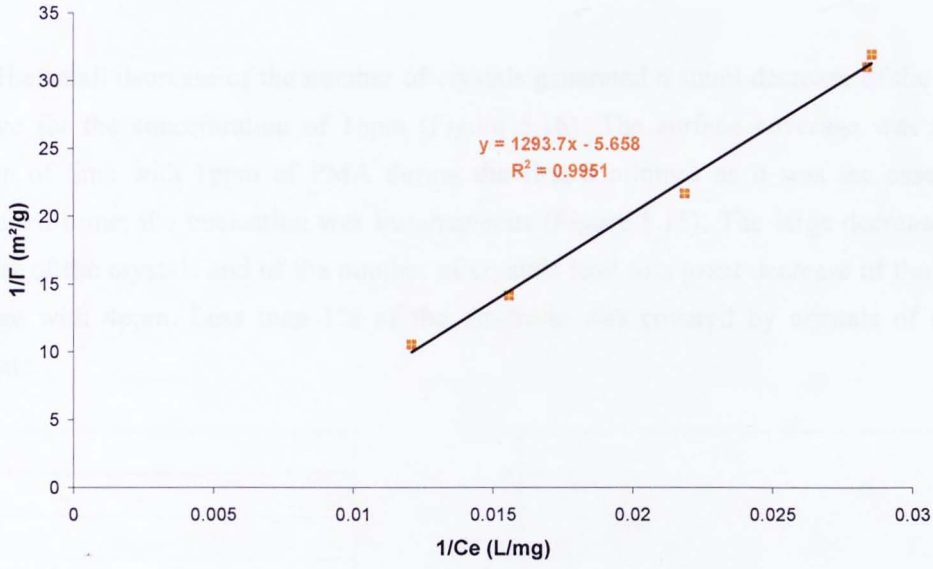

Figure 5.13: Adsorption isotherm of the PPCA

5.5 Effects of the PMA on the crystallization of $CaCO_3$

5.5.1 Effects of 1 and 4ppm of PMA on the nucleation and growth of $CaCO_3$

5.5.1.1 Surface coverage of the calcareous deposit

The number of crystals slightly decreased (20%) with the addition of 1ppm of PMA compared to the 46% decrease observed when 1ppm of PPCA were present in the solution (Figure 5.4 and Figure 5.14). A decrease of 87% was observed when 4ppm of PMA was added. The nucleation was strongly reduced.

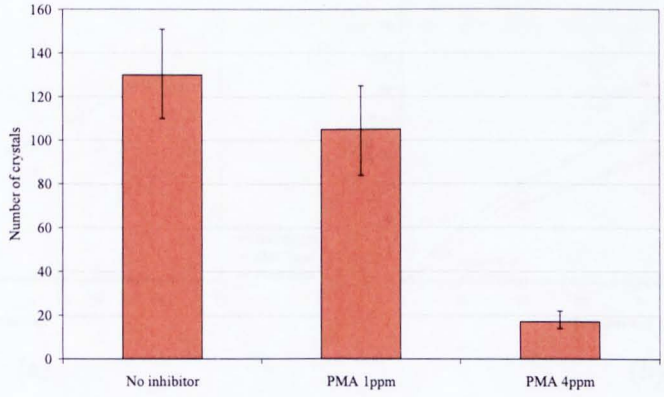

Figure 5.14: Effects of 1 and 4ppm of PMA on the number of crystals of calcium carbonate formed onto a metal surface (600μm^2) after 60 minutes

The small decrease of the number of crystals generated a small decrease of the surface coverage for the concentration of 1ppm (Figure 5.16). The surface coverage was a linear function of time with 1ppm of PMA during the first 5 minutes as it was the case for an uninhibited brine; the nucleation was instantaneous (Figure 5.15). The large decrease of the diameter of the crystals and of the number of crystals lead to a great decrease of the surface coverage with 4ppm. Less than 1% of the electrode was covered by crystals of calcium carbonate.

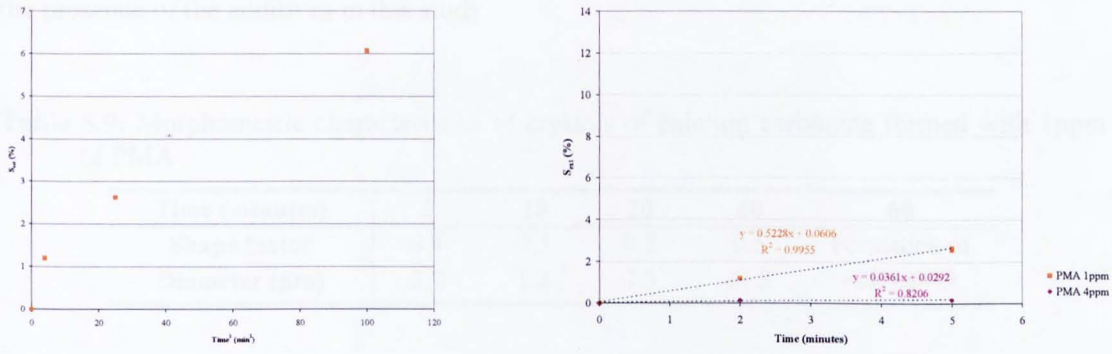

(a) (b)

Figure 5.15: Extended surface area as a function of (a) time^2 and (b) time (1 and 4ppm of PMA)

By comparing the surface coverage measured with the overlapping effects (Figure 5.16a) and without (Figure 5.16b), a difference in the surface coverage values appears after the 20th minute with 1ppm of PMA (as observed in the uninhibited brine). The crystals overlapped from the same time as seen with no inhibitor showing a similar growth process with 1ppm of PMA.

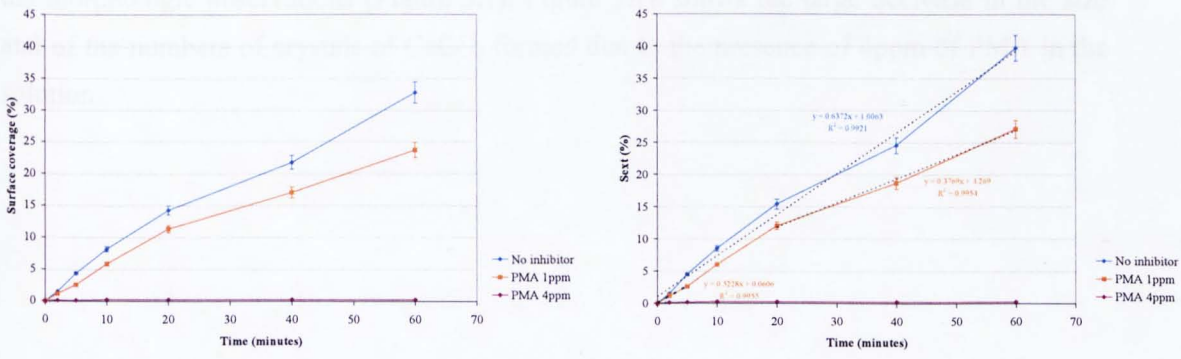

(a) (b)

Figure 5.16: Effects of 1 and 4ppm of PMA on the surface coverage observed (a) and on the extended surface area (b)

5.5.1.2 Morphometric characteristics of the crystals of $CaCO_3$

The surface and the diameter of the crystals of $CaCO_3$ formed in the presence of 1ppm of PMA kept increasing during the 60 minute test whereas they were strongly affected by the addition of 4ppm of PMA (Table 5.9 and Table 5.10). The formation of aggregates did not permit the determination of the morphometric characteristics of the crystals at 60 minutes with 1ppm. The shape factor was kept constant for both concentrations and it was similar to the shape factor obtained with a non-inhibited brine; it seems the shape was not affected by the presence of the additives in this study.

Table 5.9: Morphometric characteristics of crystals of calcium carbonate formed with 1ppm of PMA

Time (minutes)	5	10	20	40	60
Shape factor	0.4	0.5	0.5	0.5	Formation of
Diameter (µm)	3.7	5.3	7.3	11.2	aggregates

Table 5.10: Morphometric characteristics of crystals of calcium carbonate formed with 4ppm of PMA

Time (minutes)	5	10	20	40	60
Shape factor	0.4	0.4	0.4	0.5	0.5
Diameter (µm)	2.2	2.6	2.9	2.8	2.7

The crystals formed with 1ppm of PMA were mostly calcite and vaterite (Figure 5.17). No significant variation of the number of crystals was observed over time. The crystals were not distorted. Their shape was well defined. They were comparable to the crystals observed in the non-inhibited brine as indicated by the similar shape factor between these two cases and the morphologic observations (Figure 5.1). Figure 5.18 shows the large decrease in the size and of the numbers of crystals of $CaCO_3$ formed due to the presence of 4ppm of PMA in the solution.

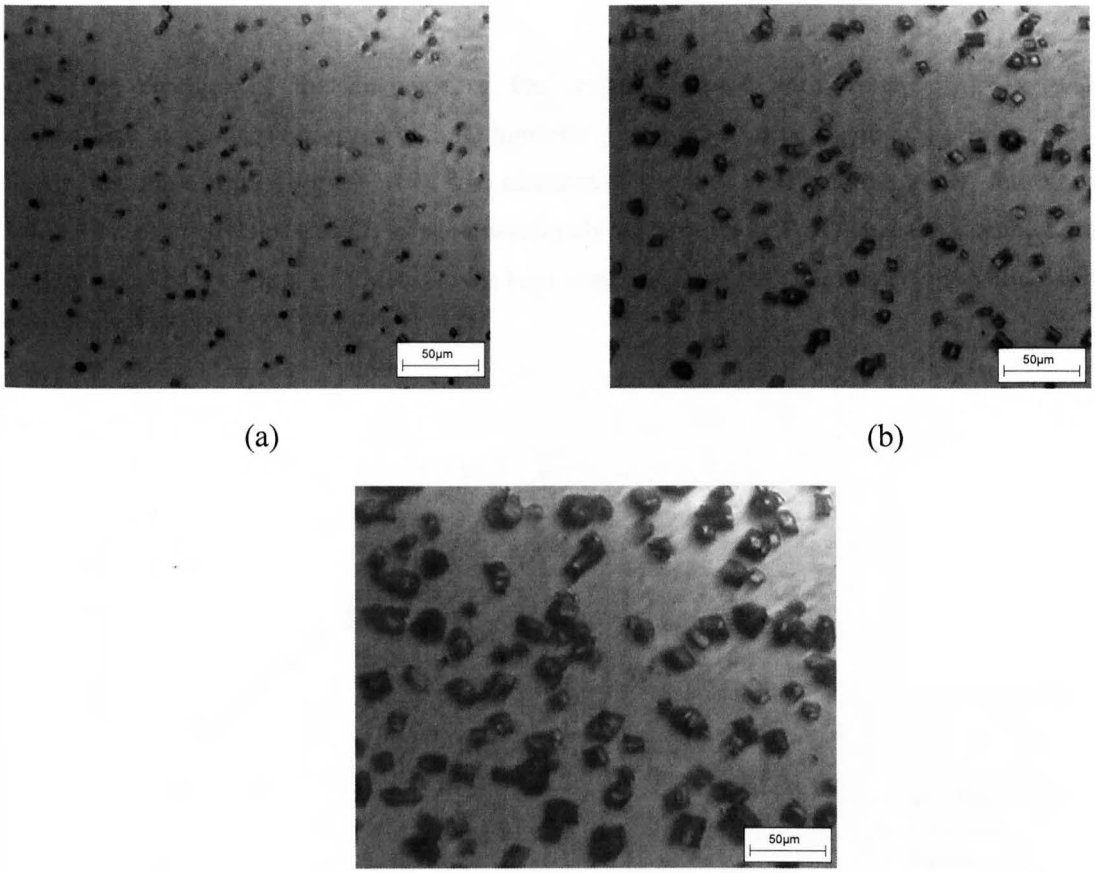

(a) (b)

(c)

Figure 5.17: Microscopic observations of crystals of calcium carbonate (made with a light microscope) formed under polarization conditions and with 1ppm of PMA, after (a) 5, (b) 20 and (c) 60 minute experiment

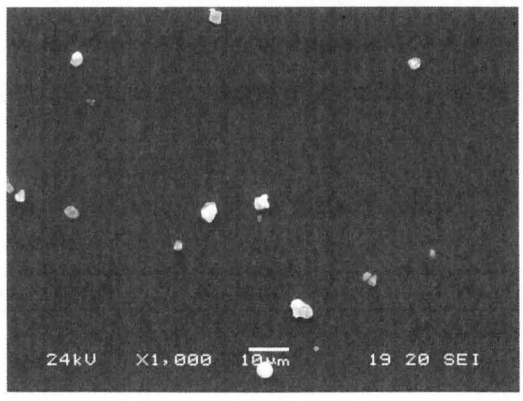

Figure 5.18: SEM microscopic observations of crystals of calcium carbonate formed under polarization conditions with 4ppm of PMA after a 60 minute experiment

The changes of the diameter of the crystals formed with 1ppm of PMA were comparable to the ones observed with no inhibitor. From the 5th minute the mean diameter is a linear function of time (Figure 5.19). The addition of 4ppm of PMA did not totally inhibit the nucleation of crystals of $CaCO_3$ as seen previously with 4ppm of PPCA but the diameter was largely affected by 4ppm of PMA. It was kept constant from the 5th minute to the end of the test.

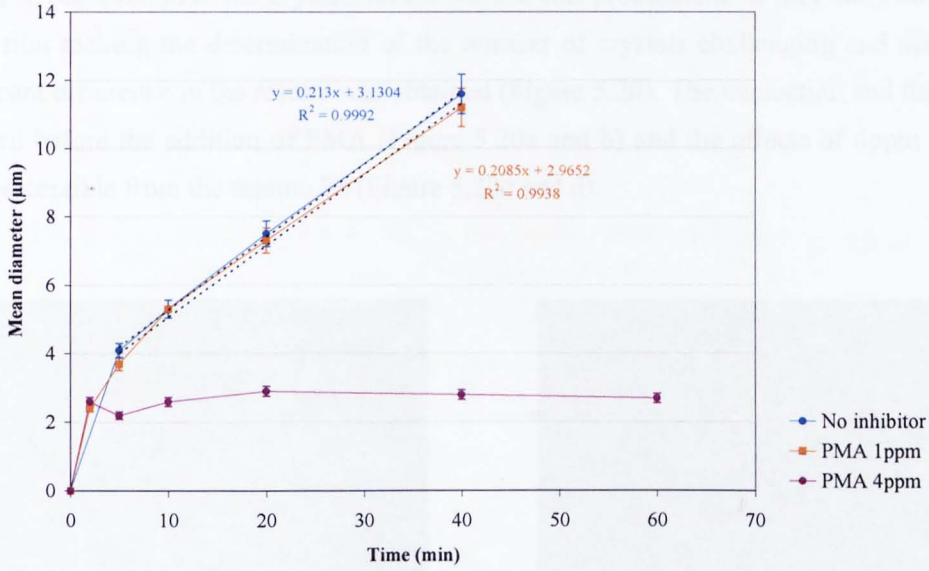

Figure 5.19: Effects of 1 and 4ppm of PMA on the mean diameter of the crystals of $CaCO_3$

The lateral growth rate was constant over time. 1ppm of PMA did not affect the rate. The lateral growth was similar with and without 1ppm of PMA but the addition of 4ppm lead to blockage of the crystal growth thus the lateral growth rate was nil (Table 5.11).

Table 5.11: Lateral growth rate (mol/µm/s) of the crystals of $CaCO_3$ with 1 and 4ppm of PMA in function of time

Time (seconds)	No inhibitor	PMA 1ppm
120	$1.4x10^{-15}$	$1.4x10^{-15}$
300	$1.6x10^{-15}$	$1.2x10^{-15}$
600	$1.6x10^{-15}$	$1.4x10^{-15}$
1200	$1.4x10^{-15}$	$1.4x10^{-15}$
2400	$1.1x10^{-15}$	$1.4x10^{-15}$

A large difference between 1 and 4ppm of PMA were recorded in the morphometric characteristics of the crystals of calcium carbonate and the difference occurred at the early stage of the growth process (from the 2nd minute).

5.5.2 Effects of 4ppm of PMA on crystals of $CaCO_3$ already formed

The inhibitor was added 10 minutes after the start of the polarization.

5.5.2.1 Morphology of the crystals of $CaCO_3$

The observation of the crystals on the surface was problematic as they were covered by a thin film making the determination of the number of crystals challenging and therefore a significant difference in the results was obtained (Figure 5.20). The nucleation and the growth occurred before the addition of PMA (Figure 5.20a and b) and the effects of 4ppm of PMA were perceptible from the minute 20 (Figure 5.20c and d).

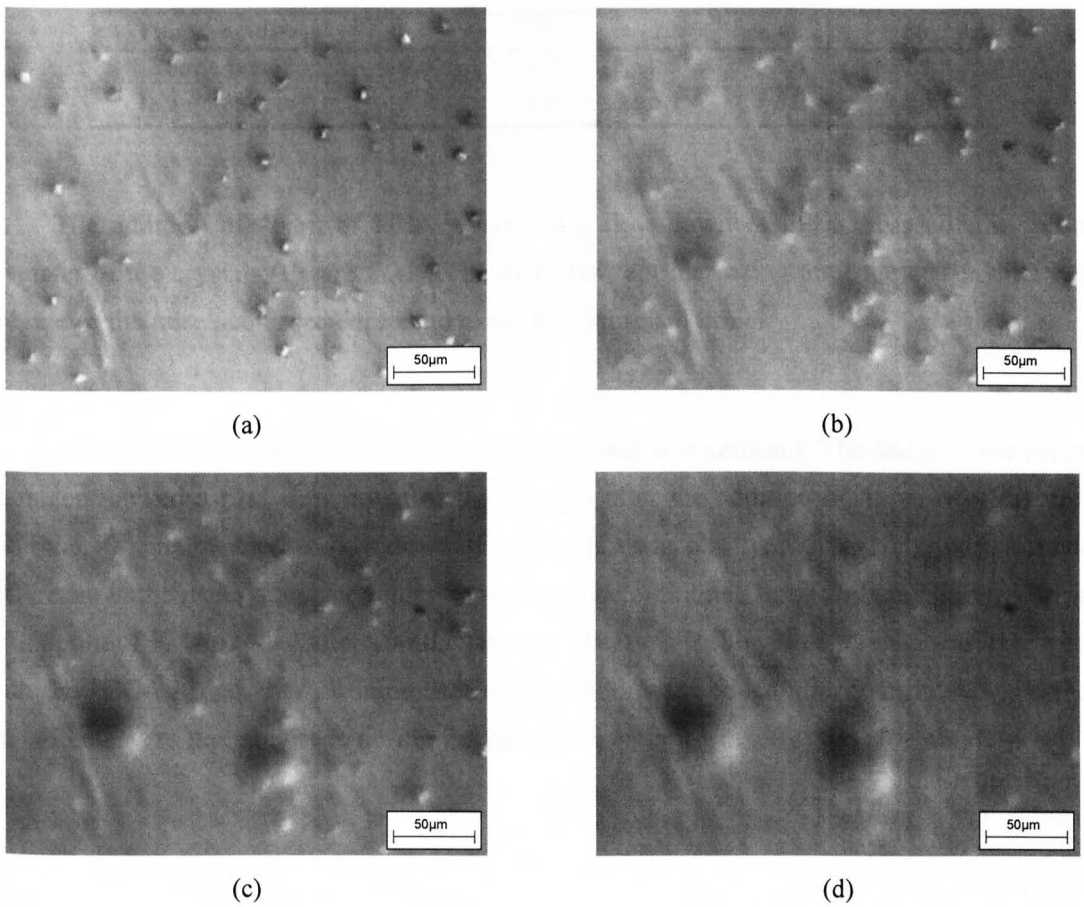

(a) (b)

(c) (d)

Figure 5.20: Microscopic observations of crystals of calcium carbonate (done with a light microscope) formed under polarization conditions with 4ppm of PMA (added after 10 minutes from the start of the experiment) after (a) 5, (b) 10, (c) 40 and (d) 60 minute experiment

PMA seems to cover the metal surface and the coverage was greater at the 60th minute than the 20th as the detection of the crystals were harder at the minute 60. The outline of the crystals was less apparent over time. The size of the crystals did not vary significantly from the 20th minute but some single crystals grew extensively round-shaped.

5.5.2.2 Morphometric characteristics of the crystals of $CaCO_3$

The morphometric characteristics presented in Table 5.12 shows that the growth process was still occurring after the addition of 4ppm of PMA. The shape factor was constant during all the test.

Table 5.12: Morphometric characteristics of crystals of calcium carbonate formed with no inhibitor for the first 10 minutes and with 4ppm of PMA after this time

Time (minutes)	5	10	20	40	60
Shape factor	0.5	0.5	0.5	0.5	0.5
Diameter (µm)	3.9	4.6	5.1	6.2	6.0

The addition of 4ppm of PMA generated a slow down of the increase of the mean diameter of the crystals (Figure 5.21). The diameter kept increasing until the 40th minute but the rate of the raise decreased compared to the non-inhibited brine.

After this time in the inhibited case, the diameter was constant. The study of the mean diameter showed a first slow down of the kinetics after the addition of 4ppm of PMA and from the 40th minute another slow down of the kinetics was observed. At t=10minutes, a small difference in the mean diameter values between the non inhibited brine and the inhibited brine with 4ppm of PMA (added after 10 minutes) was observed. A bigger difference was observed with the PPCA added after 10 minutes. The inhibitors were added after 9.5 minutes and the first effects were probably seen during the measurement being made at the 10th minute.

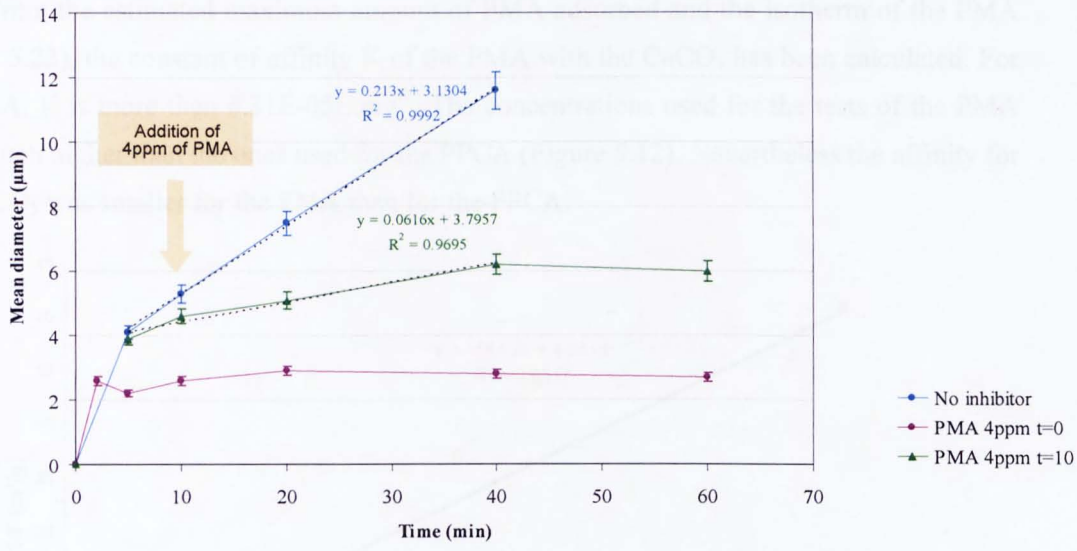

Figure 5.21: Effects of 4ppm of PMA on the mean diameter of the crystals of $CaCO_3$ nucleated and grown for 10 minutes in absence of inhibitor

5.5.3 Interactions between the PMA and the crystals of $CaCO_3$ – Adsorption measurements

As observed with PPCA, none of the concentrations tested saturated the adsorption sites of the crystals of calcium carbonate added in the solution (Figure 5.22). The maximum amount of polymaleic acid has therefore not been determined but estimated. More than 6.85E-02mg/m^2 can adhere on the $CaCO_3$ crystals present in the solution.

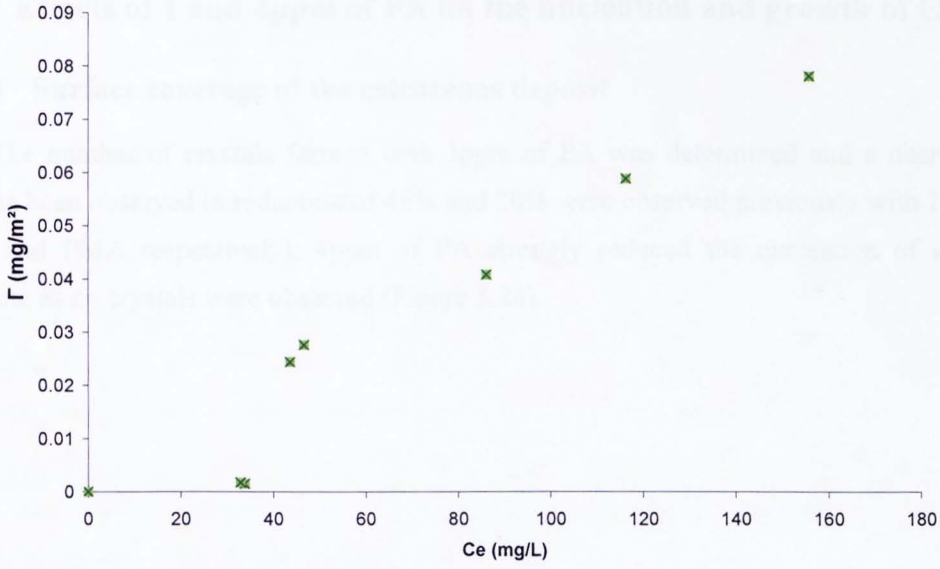

Figure 5.22: Quantity of PMA adhered on the crystals of calcium carbonate as a function of the solution equilibrium concentration of PMA.

From the estimated maximum amount of PMA adsorbed and the isotherm of the PMA (Figure 5.23), the constant of affinity K of the PMA with the $CaCO_3$ has been calculated. For the PMA, K is more than 6.31E-05L.mg^{-1}. The concentrations used for the tests of the PMA were much higher than the ones used for the PPCA (Figure 5.12). Nevertheless the affinity for the $CaCO_3$ was smaller for the PMA than for the PPCA.

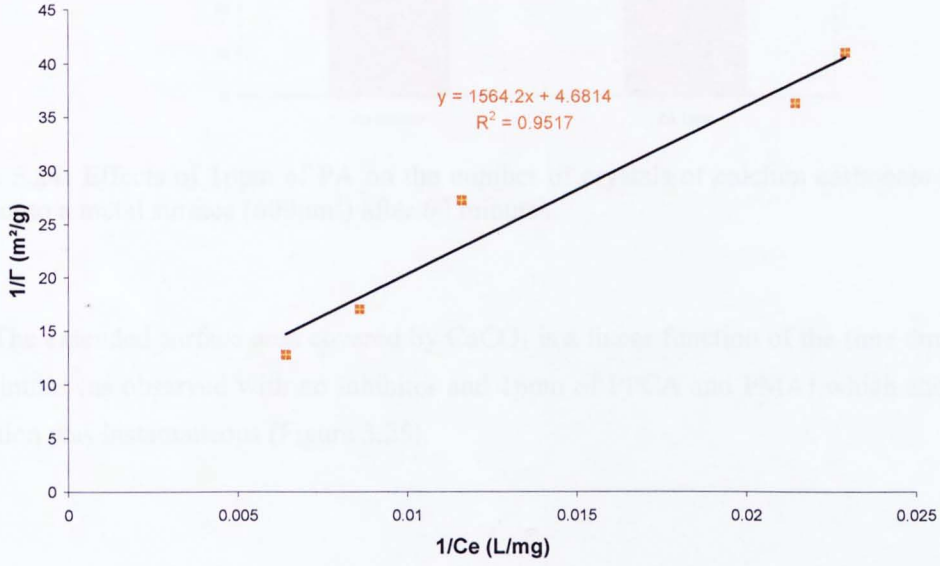

Figure 5.23: Adsorption isotherm of the PMA

5.6 Effects of the PA on the crystallization of $CaCO_3$

5.6.1 Effects of 1 and 4ppm of PA on the nucleation and growth of $CaCO_3$

5.6.1.1 Surface coverage of the calcareous deposit

The number of crystals formed with 1ppm of PA was determined and a decrease of 33% has been observed (a reduction of 46% and 20% were observed previously with 1ppm of PPCA and PMA respectively). 4ppm of PA strongly reduced the nucleation of calcium carbonate as no crystals were observed (Figure 5.24).

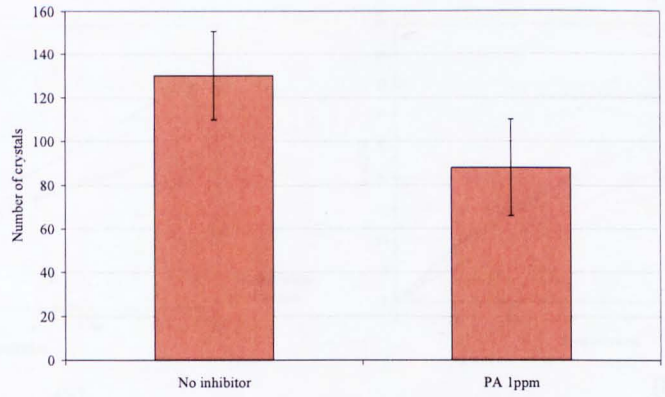

Figure 5.24: Effects of 1ppm of PA on the number of crystals of calcium carbonate formed onto a metal surface (600μm^2) after 60 minutes

The extended surface area covered by $CaCO_3$ is a linear function of the time during the first minutes (as observed with no inhibitor and 1ppm of PPCA and PMA) which shows the nucleation was instantaneous (Figure 5.25).

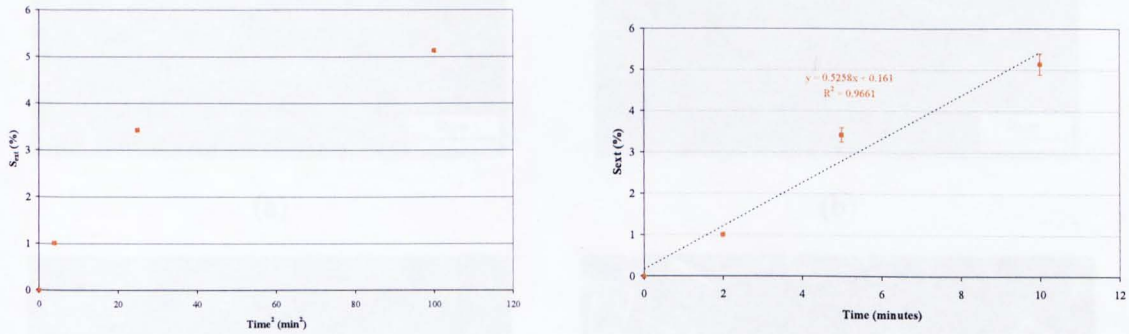

(a) (b)

Figure 5.25: Extended surface area as a function of (a) time^2 and (b) time (1 and 4ppm of PMA)

The difference between the surface coverage observed and the extended surface area was observed from the 40th minute (Figure 5.26). The extended surface area was a linear function of time during the entire duration of the test (as observed with no inhibitor and 1ppm of PMA) and a slight decrease of the rate was observed. A reduction of 12% of the extended surface coverage was observed when 1ppm of PA was added in the solution. As no crystals were detected with 4ppm of PA, the surface coverage was nil.

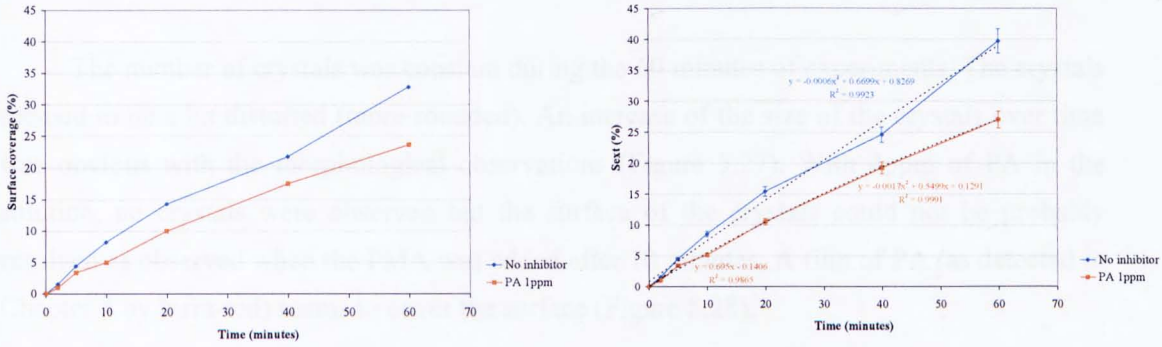

(a) (b)

Figure 5.26: Effects of 1ppm of PA on the surface coverage observed (a) and on the extended surface area (b)

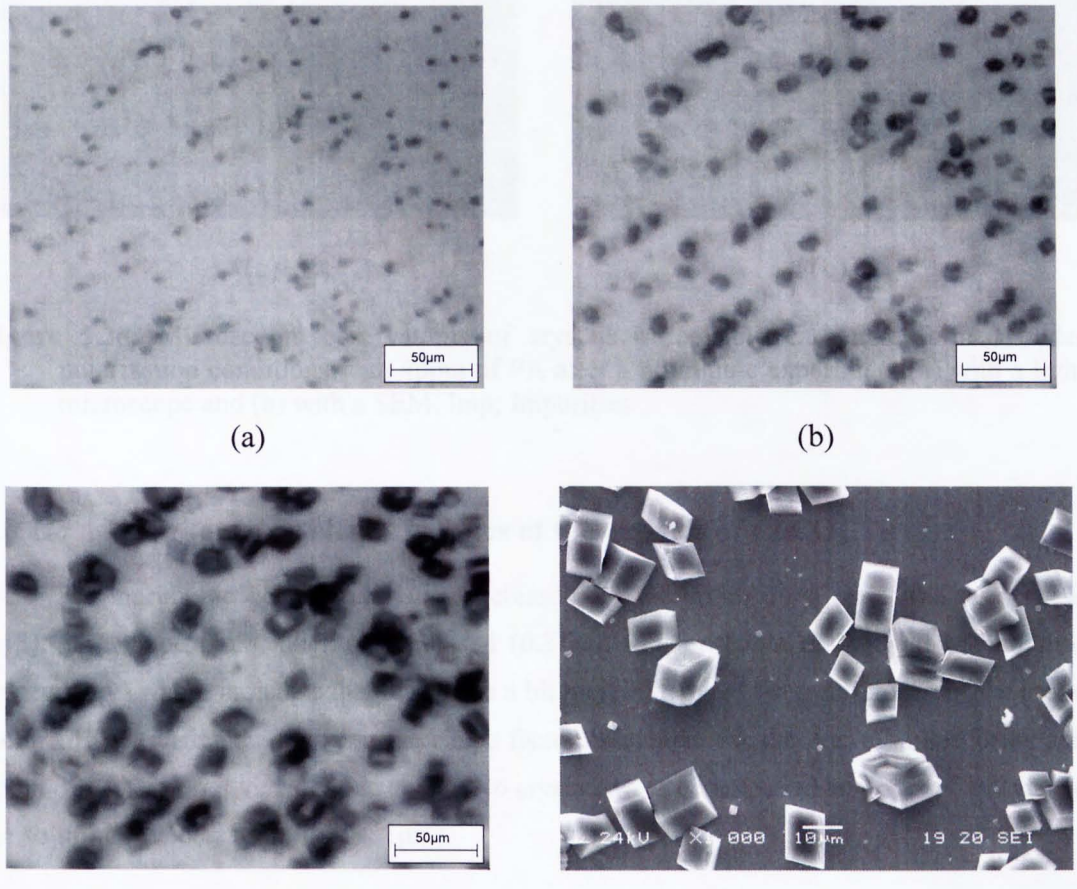

(a) (b)

(c) (d)

Figure 5.27: Microscopic observations of crystals of calcium carbonate (realised with a light microscope (a), (b) and (c) and with a SEM (d)) formed under polarization conditions and with 1ppm of PA after (a) 5, (b) 20 and (c) and (d) 60 minute experiment

The number of crystals was constant during the 60 minutes of experiments. The crystals seemed to be a bit distorted (more rounded). An increase of the size of the crystals over time was obvious with the morphological observations (Figure 5.27). With 4ppm of PA in the solution, no crystals were observed but the surface of the crystals could not be probably resolved as observed when the PMA was added after 10 minutes. A film of PA (as detected in Chapter 4 by infra-red) seems to cover the surface (Figure 5.28).

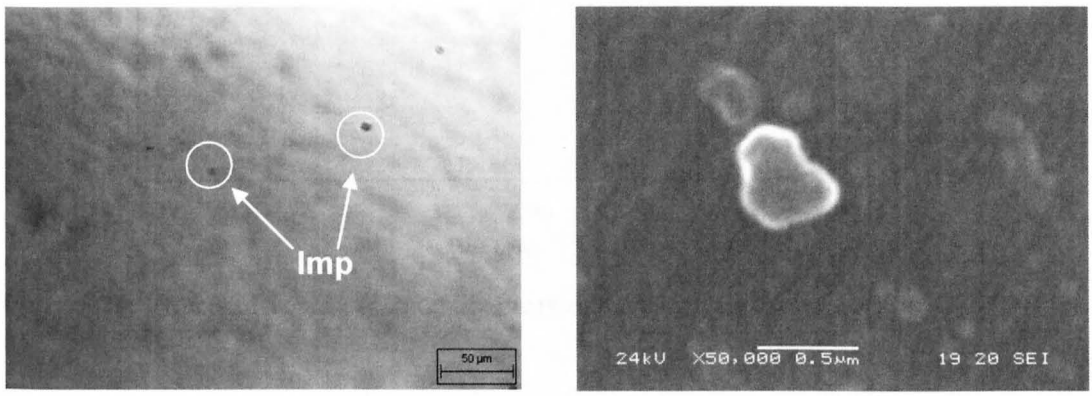

(a) (b)

Figure 5.28: Microscopic observations of crystals of calcium carbonate formed under polarization conditions with 4ppm of PA after a 60 minute experiment (a) with a light microscope and (b) with a SEM. Imp; Impurities

5.6.1.2 Morphometric characteristics of the crystals of $CaCO_3$

The morphometric characteristics increased for the entire duration of the test (Table 5.13). The shape factor slightly decreased (0.3 and 0.5 for 1ppm of PA and no inhibitor respectively) which indicates that they were a bit more elongated but a difference of the shape factor of 0.2 (difference between the shape factor calculated for the non-inhibited brine and 1ppm of PA) was not visually detectable. No crystals were observed when 4ppm of PA was in the solution (the detection limit is 1µm).

Table 5.13: Morphometric characteristics of crystals of calcium carbonate formed with 1ppm of PA

Time (minutes)	5	10	20	40	60
Shape factor	0.3	0.3	0.3	0.3	0.3
Diameter (µm)	3.7	5.1	7.2	10.4	12.2

The assessment of the mean diameter followed the same trend as in the non-inhibited brine (Figure 5.29). A small slow down of the kinetics was observed at the 40th minute.

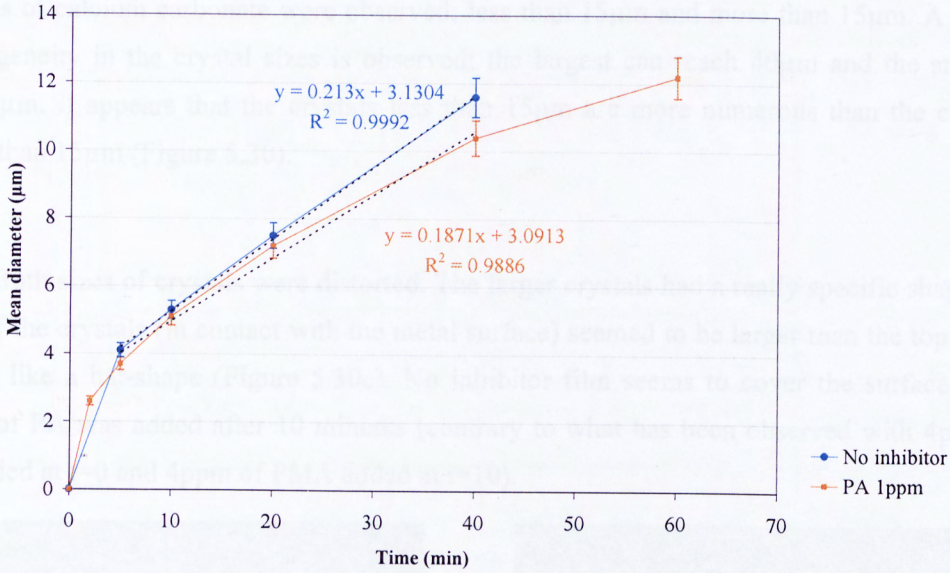

Figure 5.29: Effects of 1ppm of PA on the mean diameter of the crystals of $CaCO_3$

The lateral growth rate was calculated and the results are presented in Table 5.14. The values were constant over time and similar to the values obtained with the non-inhibited brine (as observed with 1ppm of PPCA and PMA) so 1ppm of PA did not affect the growth of the crystals.

Table 5.14: Lateral growth rate (mol/µm/s) of the crystals of $CaCO_3$ with 1ppm of PA in function of time

Time (seconds)	No inhibitor	PA 1ppm
120	$1.4x10^{-15}$	$1.4x10^{-15}$
300	$1.6x10^{-15}$	$1.9x10^{-15}$
600	$1.6x10^{-15}$	$1.4x10^{-15}$
1200	$1.4x10^{-15}$	$1.5x10^{-15}$
2400	$1.1x10^{-15}$	$1.3x10^{-15}$

5.6.2 Effects of 4ppm of PA on crystals of $CaCO_3$ already formed

5.6.2.1 Surface coverage of the calcareous deposit

The shape factor was a bit increased at 10 minutes which showed that the crystals were more circle-like. These changes were more obvious on big crystals (from 20 minutes) (Figure 5.30).

4ppm of PA affected the morphology of the crystals to a great extent. Two sizes of crystals of calcium carbonate were observed; less than 15µm and more than 15µm. A strong heterogeneity in the crystal sizes is observed; the largest can reach 40µm and the smallest only 5µm. It appears that the crystals less than 15µm are more numerous than the crystals larger than 15µm (Figure 5.30).

Both sizes of crystals were distorted. The larger crystals had a really specific shape: the base of the crystals (in contact with the metal surface) seemed to be larger than the top of the crystal like a hat-shape (Figure 5.30c). No inhibitor film seems to cover the surface when 4ppm of PA was added after 10 minutes (contrary to what has been observed with 4ppm of PA added at t=0 and 4ppm of PMA added at t=10).

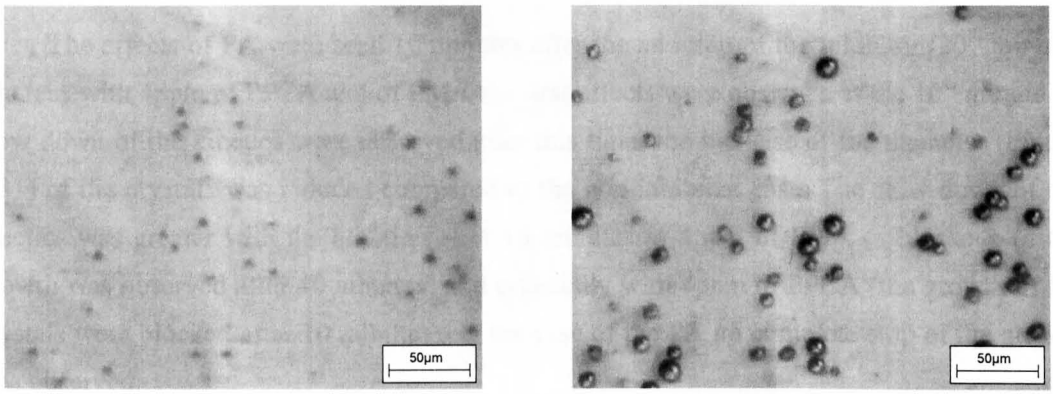

(a) (b)

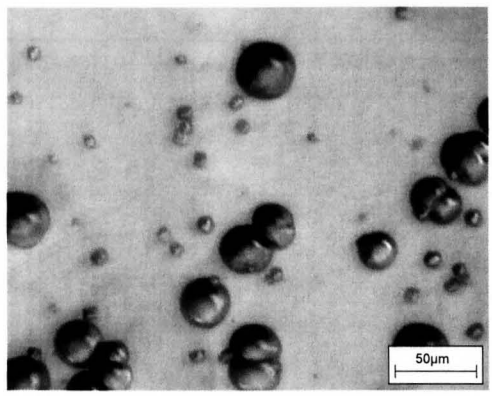

(c)

Figure 5.30: Microscopic observations of crystals of calcium carbonate (realised with a light microscope) formed under polarization conditions and with 4ppm of PA (added after 10minutes from the start of the experiment) after (a) 5, (b) 20 and (c) 60 minute experiment

5.6.2.2 Morphometric characteristics of the crystals of $CaCO_3$

The addition of 4ppm of PA in the solution when the nucleation and growth process has started for 10 minutes lead to an increase of 0.2 of the shape factor which indicated that the crystals formed were more circle-like (Table 5.15). The surface and the diameter of the crystals kept increasing after the addition of the inhibitor.

Table 5.15: Morphometric characteristics of crystals of calcium carbonate formed with no inhibitor for the first 10 minutes and with 4ppm of PA after this time

Time (minutes)	5	10	20	40	60
Shape factor	0.5	0.6	0.6	0.6	0.6
Diameter (µm)	3.6	5.1	7.1	7.8	9.7

The effects of PA were seen 10 minutes after the addition of the inhibitor (20th minute) whereas with 4ppm of PPCA and of PMA the first effects were observed at the 10th minute. A slow down of the kinetics were observed after this time: the increase of the diameter (Figure 5.31) of the crystals was reduced compared to the non-inhibited case. The slow down of the kinetics was greater with the addition after 10 minutes of 4ppm of PMA (a blockage of the growth was observed after 40 minutes) and especially with 4ppm of PPCA (the growth of the crystals were blocked after 10 minutes). In the case of the PA no complete stop of the growth was observed.

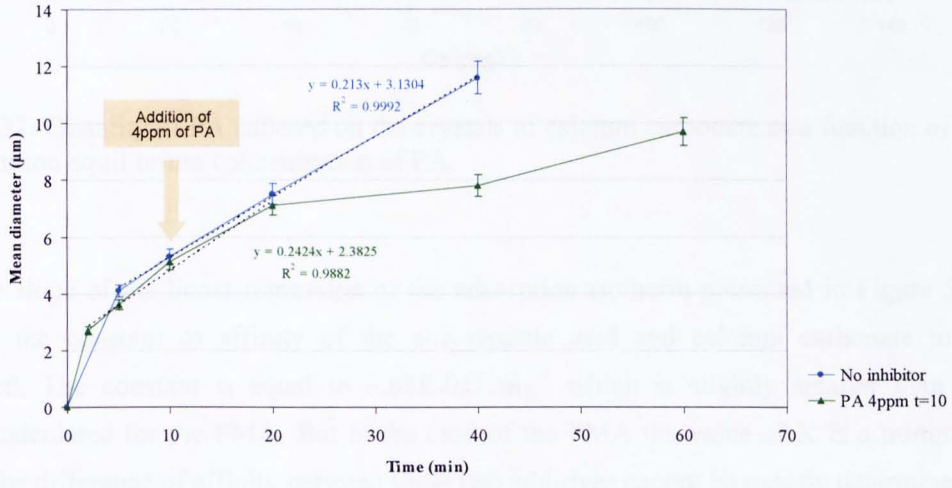

Figure 5.31: Effects of 4ppm of PA on the mean diameter of the crystals of $CaCO_3$ nucleated and grown for 10 minutes in absence of inhibitor

PA affected the growth of the crystals of calcium carbonate formed and grown in a non-inhibited solution but the effects of 4ppm PA occurred later than the effects seen with 4ppm of PMA and PPCA.

5.6.3 Interactions between the polyaspartic acid and the crystals of $CaCO_3$ – Adsorption measurements

Contrary to what was observed for the PPCA and the PMA, the amount of PA adsorbed is not linear from 40mg/L. The concentrations tested almost saturated the adsorption sites of the crystals of $CaCO_3$. (Figure 5.32). The maximum amount of polyaspartic acid which can adsorb on the crystals of calcium carbonate was 5.81E-02mg.m^{-2}.

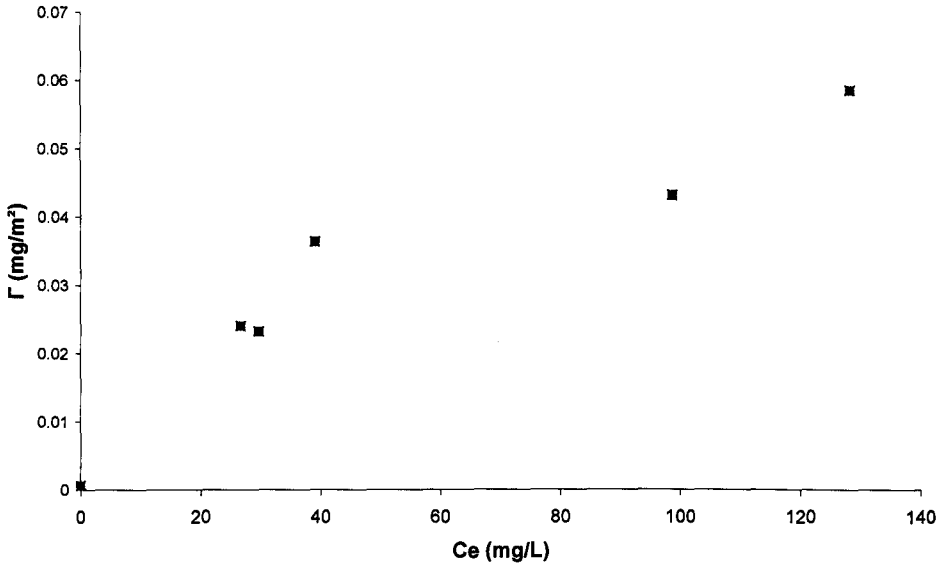

Figure 5.32: Quantity of PA adhered on the crystals of calcium carbonate as a function of the solution equilibrium concentration of PA.

The slope of the linear regression of the adsorption isotherm presented in Figure 5.33 permitted the constant of affinity of the polyaspartic acid and calcium carbonate to be determined. The constant is equal to 6.63E-05L.mg^{-1} which is slightly smaller than the constant calculated for the PMA. But in the case of the PMA the value of K is a minimum value so the difference of affinity between these two additives cannot be exactly determined.

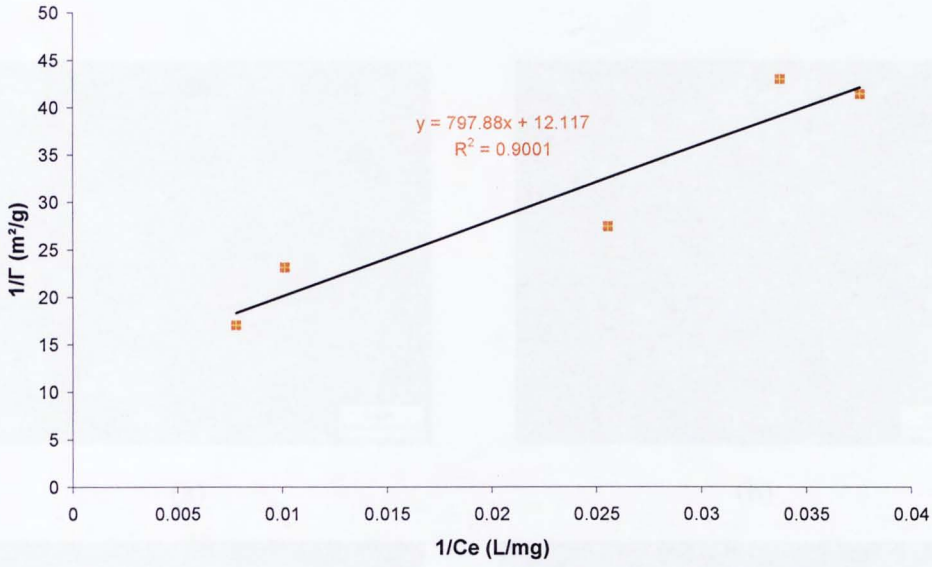

Figure 5.33: Adsorption isotherm of the PA

5.7 Effects of the CMI on the crystallization of $CaCO_3$

5.7.1 Effects of 1 and 4ppm of CMI on the nucleation and growth of $CaCO_3$

5.7.1.1 Surface coverage of the calcareous deposit

The number of crystals could not be determined as the number detected in the repeatability tests were too different. The surface coverage was therefore non-reproducible except for the late part of the test. The mean surface coverage directly estimated from the image analysis (with the overlap effects) was of about 19.5% at 60 minute. Nevertheless the morphometric characteristics were reproducible.

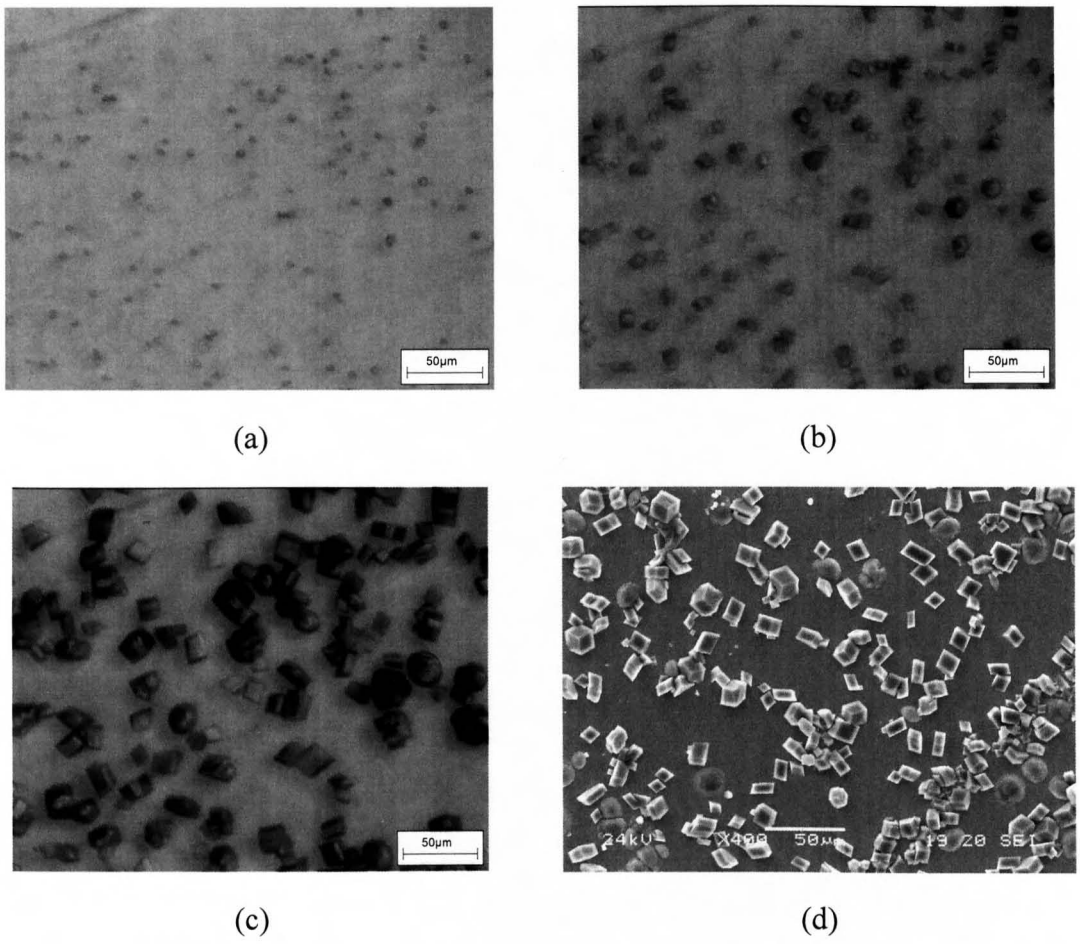

(a) (b)

(c) (d)

Figure 5.34: Microscopic observations of crystals of calcium carbonate (realised with a light microscope (a), (b) and (c) and with a SEM (d)) formed under polarization conditions and with 1ppm of CMI after (a) 5, (b) 20 and (c) and (d) 60 minute experiment

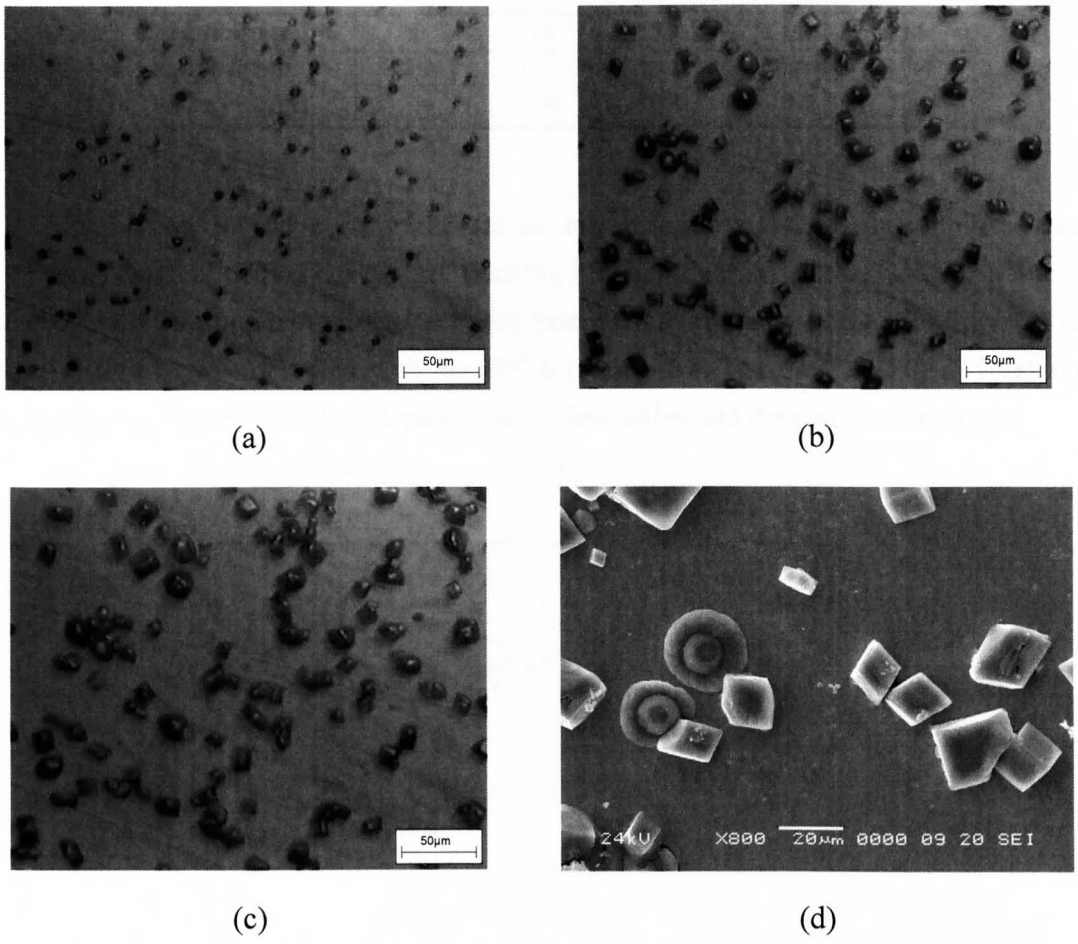

(a) (b)

(c) (d)

Figure 5.35: Microscopic observations of crystals of calcium carbonate (realised with a light microscope (a), (b) and (c) and with a SEM (d)) formed under polarization conditions and with 4ppm of CMI after (a) 5, (b) 20 and (c) and (d) 60 minute experiment

5.7.1.2 Morphometric characteristics of the crystals of $CaCO_3$

CMI has been tested at 1 and 4ppm and the morphometric characteristics are summarised in Table 5.16 and Table 5.17. The shape factor was similar for both concentrations indicated that the shape of the crystals were not different as the shape of the crystals formed in the non-inhibited brine (Table 5.4). The diameter of the crystals kept increasing over time for 1 and 4ppm.

Table 5.16: Morphometric characteristics of crystals of calcium carbonate formed with 1ppm of CMI

Time (minutes)	5	10	20	40	60
Shape factor	0.4	0.4	0.4	0.4	0.4
Diameter (µm)	3.8	5.4	7.6	10.5	12.1

Table 5.17: Morphometric characteristics of crystals of calcium carbonate formed with 4ppm of CMI

Time (minutes)	5	10	20	40	60
Shape factor	0.4	0.5	0.5	0.4	0.4
Diameter (µm)	3.4	4.6	7.1	10.7	12.4

The diameter of the crystals followed the same variations as in the non-inhibited case with 1 and 4ppm of CMI (Figure 5.36). With the PPCA, the PMA and the PA the increase of the diameter were similar to the non-inhibited case but only for the concentration 1ppm. With 4ppm no crystal was observed with the PPCA (Figure 5.8) and the PA (Figure 5.6a) and 4ppm of PMA (Figure 5.18) had large effects on the number and the size of the crystals.

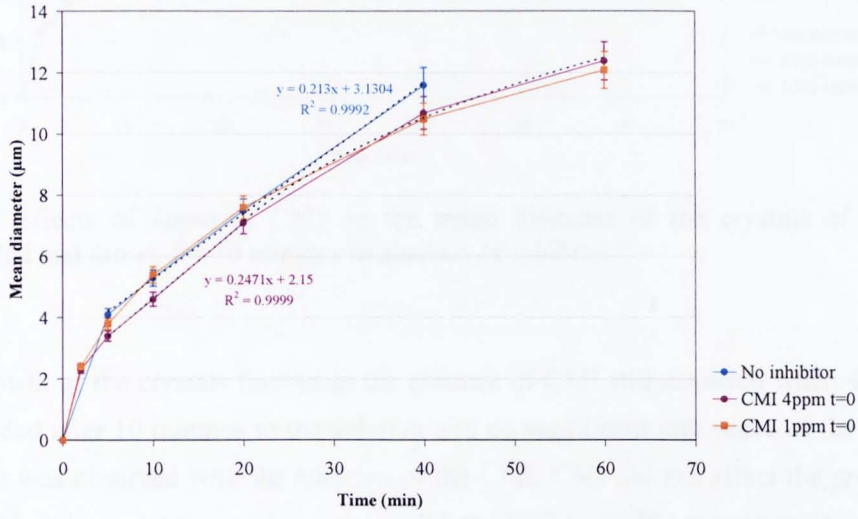

Figure 5.36: Effects of 1 and 4ppm of CMI on the mean diameter of the crystals of $CaCO_3$

5.7.2 Effects of 4ppm of CMI on crystals of $CaCO_3$ already formed

The addition of 4ppm of CMI did not stop the growth of the crystals as the increase of the morphometric characteristics increased during the 60 minute test (Table 5.18). Adding the inhibitor after 10 minutes did not affect the shape factor (0.4 and 0.5 for the non-inhibited case and for 4ppm added at t=0 respectively).

Table 5.18: Morphometric characteristics of crystals of calcium carbonate formed with no inhibitor for the first 10 minutes and with 4ppm of CMI after this time

Time (minutes)	5	10	20	40	60
Shape factor	0.5	0.5	0.5	0.5	Formation of
Diameter (µm)	3.6	5.3	7.1	10.5	aggregates

The assessment of the mean diameter of the crystals when the CMI was added after 10 minutes did not lead to any difference compared to the case where no inhibitor was added and when CMI was added at t=0 (Figure 5.37). The increase rate of the diameter was similar in these 3 different conditions.

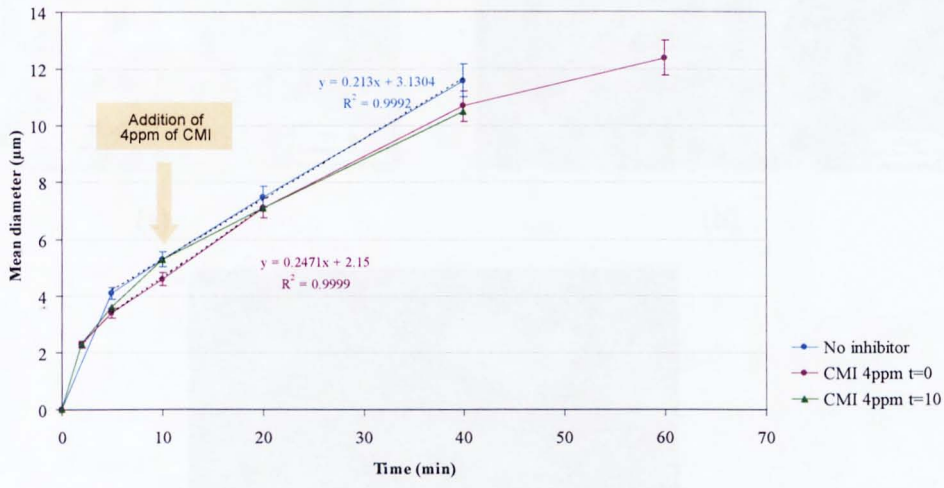

Figure 5.37: Effects of 4ppm of CMI on the mean diameter of the crystals of $CaCO_3$ nucleated and grown for 10 minutes in absence of inhibitor

The growth of the crystals formed in the absence of CMI still occurred when 4ppm of CMI were added after 10 minutes to the solution and no significant difference of the growth of the crystals was observed with the addition of the CMI. CMI did not affect the growth of the crystals; this is in contrast to what was seen with the PPCA, the PMA and the PA.

Nevertheless the morphology of the crystals was affected by the addition of the CMI as shown in Figure 5.38.

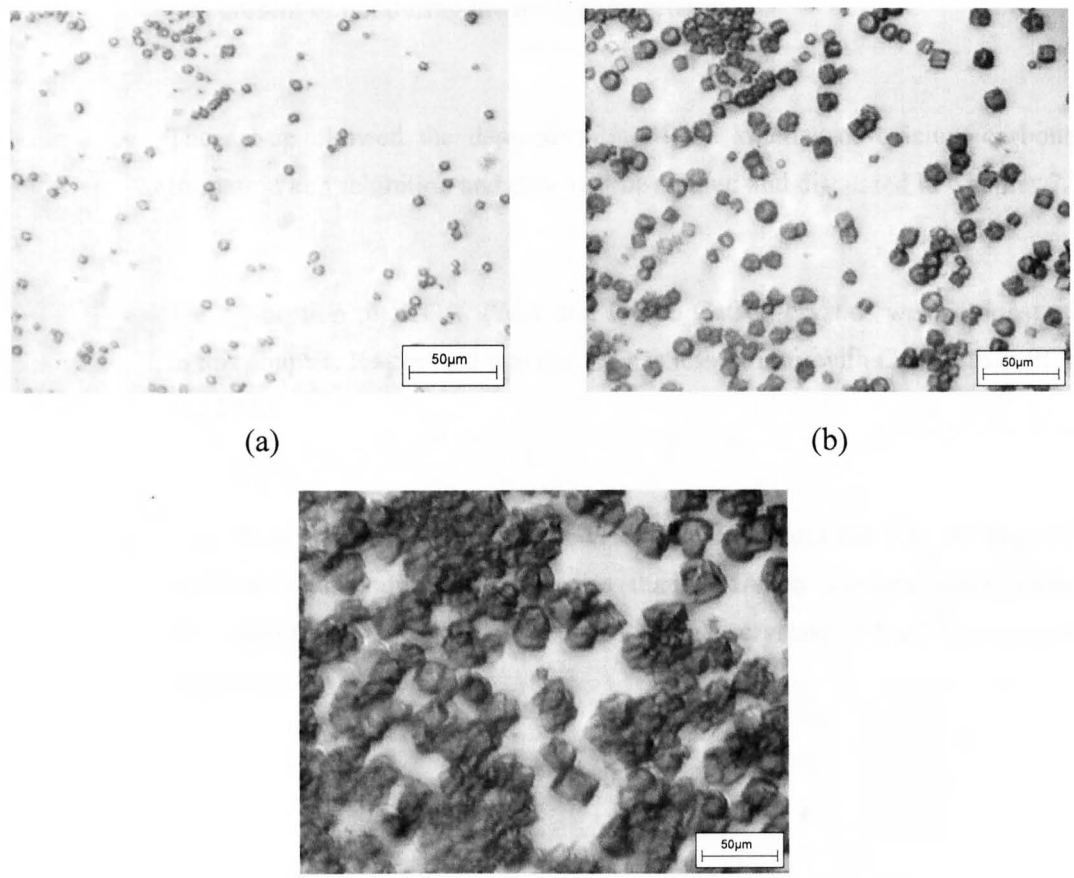

(a) (b)

(c)

Figure 5.38: Microscopic observations of crystals of calcium carbonate formed under polarization conditions with 4ppm of CMI (added after 10 minutes from the start of the experiment) after 5, 20, and 60 minute experiment ((a), (b) and (c) respectively)

5.8 Concluding remarks

The study with the *in-situ* electrochemical cell enabled some significant findings relating to $CaCO_3$ deposition and inhibition to be determined:

- The nucleation was instantaneous (realised in a really short time) in all the different conditions tested;

- This method permitted the effects on the nucleation and the growth processes of the scale inhibitors to be assessed separately (with a detection limit of 1µm for the number of nuclei);

- The mechanism of inhibition was different for a specific inhibitor whether it was present or not during the nucleation process;

- The set-up allowed the determination of the kinetics of calcium carbonate formation and inhibition and they will be studied and discussed in Chapter 7.

- The adsorption of PPCA, PMA and PA on $CaCO_3$ crystals was demonstrated in this chapter. It appeared that the PA has less affinity with $CaCO_3$ than PPCA and PMA.

- This study shown a difference between the PMA and the PA: At 4ppm PA presents better inhibition properties than PMA on a clean metal surface whereas PMA is more efficient than PA when crystals of $CaCO_3$ are already formed on the surface.

Chapter 6
Synchrotron X-Ray Diffraction: *in-situ* study of $CaCO_3$ formation and inhibition

6.1 Introduction

In this chapter calcium carbonate was generated by mixing two supersaturated brines with respect of $CaCO_3$ and as such the driving force for the deposition of scale is not assessed with electrochemical potential as in Chapter 4 and 5. The main objective of this chapter is to determine the crystal characteristics of the $CaCO_3$ formed in an uninhibited brine and to assess the effects of scale inhibitors (PPCA, PMA, PA and CMI) on the relative dominance of certain crystal planes of calcium carbonate. Synchrotron X-Ray diffraction has been used to study the mechanisms of calcium carbonate formation and inhibition [7] but this thesis presents the first results focussing on the mechanisms of green inhibitors. An *in-situ* flow cell allows the application of realistic conditions in term of temperature and pressure. These two parameters can reach 250°C and 34MPa respectively.

Chen et *al.* used a silicon and PMMA cell in a similar set-up. These two substrates were chosen for their weak X-Ray diffraction pattern [7, 73, 186]. In this study a stainless steel cell was used in order to have a surface which is more realistic in terms of completion materials used in the oil and gas sector.

The intensity of the peaks, characteristic of $CaCO_3$, has been assessed over time in order to understand the mechanism of inhibition of PPCA, PMA, PA and CMI. The total intensity of the three different polymorphs has been assessed to see the effects of the scale inhibitors tested on the general morphology of the crystals. Scale inhibitors were added at the beginning of each experiment when scale deposition occurred on a clean metal surface. A complementary study has been carried out with two inhibitors (PPCA and PMA) in order to determine the mechanism of inhibition when a calcareous layer was already formed on the substrate.

The aim of this study was not to determine the lattice parameters of the crystal cell. The initial objective was to characterise the scale formed in terms of polymorphs and to compare the effects of different scale inhibitors on the composition of the deposit (calcite, aragonite and vaterite). The challenge was to identify the crystal planes despite the strong background due to the substrate of deposition (stainless steel). The main objectives were to characterise the effects of the scale inhibitors on the different polymorphs and specific crystal planes in terms of inhibition of the nucleation, inhibition of the growth, the kinetics of inhibition, the nature of the deposit and to point out any significant differences of the mechanisms of inhibition of the different scale inhibitors studied.

This technique is the only way reported in the literature to permit the in-depth characterisation in depth of the crystals of $CaCO_3$ formed (at the crystal planes level) to be determined. The study of a relevant substrate for industry and of green inhibitors are novel features of this study.

6.2 Experimental details

6.2.1 Experimental set up

The experiments with Synchrotron X-Ray Diffraction have been carried out in the Brookhaven National Laboratory (US) in the NSLS department with the collaboration of Dr Zhong Zhong. A monochromatic beam is needed in this study as the sample studied is polycrystalline (the use of a white radiation would not lead to the determination of specific planes as the different radiations would be reflected by all the different planes). The most important characteristic of the beam is its high energy as the beam has to penetrate into the substrate and into the polycrystalline sample. The energy of the beam decreases when it penetrates some materials and to be detected, the diffracted beam needs to have a sufficient energy. Thus the initial energy of the beam has to be high enough to go through the substrate and the $CaCO_3$ crystals and to be detected. The beam used is the X17B1 with a wavelength of 0.17712Å (70keV).

Calcium carbonate has been formed by mixing 2 brines in the *in-situ* cell (Figure 3.11). The supersaturation index (which corresponds to the decimal logarithm of the supersaturation ratio, S) of the brine resulting from the mixing is 1.91 at 80°C (calculated with ScaleSoftPitzer™, version 4.0). The tests have been performed at 80°C and at 1atm.

A flow rate of 10ml/min (5ml/min for brine 1 and 5ml/min for brine 2) has been set up for the brines to go through the system. The flow regime is laminar (Re=291). 500ml of each brine were prepared for each test. The temperature has been maintained at 80°C with an oven placed before the *in-situ* cell. The pH of brine 2 was buffered to 6.8 by adding acetic acid. The brine composition is presented Table 6.1.

Table 6.1: Composition (ppm) of the brine used to study calcium carbonate formation by SXRD

Ca^{2+}	HCO_3^-	Na^+	Cl^-
1440	2196	6873	11871

The mixing of the two brines occured in the mixing chamber (Figure 3.11) and calcium carbonate was formed in the capillary (2mm bore) cell. The beam penetrated the cell and was diffracted giving structural information on the crystals present in the cell when the measurement was realised. The tests were set up for 60 minutes with a data collection every 2 minutes (30 frames). The tests were stopped when the pressure in the system reached 400psi as the calcium carbonate deposit were blocking the cell.

6.2.2 Experiment overview

The experiment overview is presented Table 6.2. For the four scale inhibitors tested they were added at the start of the experiments to study their effects on $CaCO_3$ deposition on a metal surface. In order to determine their effects on a calcareous layer already formed PPCA and PMA were added after 5 minutes; during the first 5 minutes a layer of calcium carbonate was built on the metal surface and then the inhibitors were added.

Table 6.2: Experiment overview; t=0 means inhibitor added at the start of the experiment, t=5 minutes means the inhibitor added after 5 minutes

Inhibitors	Concentration tested **t=0**	Concentration tested **t=5minutes**
PPCA	1-4ppm	4ppm
PA	4ppm	-
PMA	1-4ppm	4ppm
CMI	4ppm	-

6.3 Calcium carbonate formation in a non-inhibited brine

The cell was blocked after 44 minutes when no inhibitor was present. The scale formed in absence of inhibitor was dominated by the aragonite polymorph; 6 crystal faces of aragonite were observed for a total intensity of 544a.u (Figure 6.1). The total intensity of the vaterite crystal planes was much higher than for the calcite (460 and 154 a.u respectively). The main peaks were mostly vaterite (planes (110) and (300)) and aragonite (planes (032), (111), (031), (200)). In the main peaks only one was characteristic of calcite (the calcite (006) plane).

Most of the crystal planes were observed after 8 minutes. V(300) was the last plane to emerge (after 20 minutes). After emergence of a crystal plane, the intensity increased with time except for the aragonite plane A(012). For this plane, the intensity was maintained constant after the emergence (at 2 minutes). This point will be discussed in chapter 7.

For the d-spacing of 2.58Å a peak was observed. According to the database there is no crystal plane characteristic of $CaCO_3$. This peak could be due to the overlapping of two diffraction peaks of different known crystal planes resulting in an unknown characteristic d-space value. This plane was called "X".

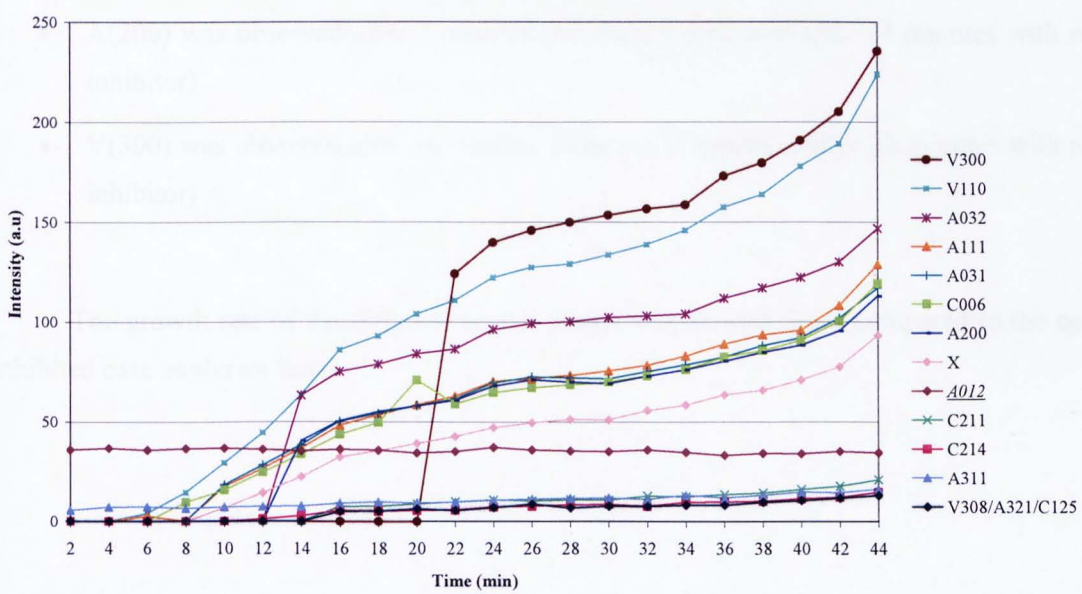

Figure 6.1: Assessment of the intensity of the diffracted beam reflecting the growth of the main crystal planes formed on a metallic surface with no inhibitor at 80°C

6.4 Effects of the PPCA on calcium carbonate formation

6.4.1 Effects of the PPCA on $CaCO_3$ deposition on a clean metal surface

PPCA was added in the brine at the beginning of the tests in order to determine the characteristic of the crystals of calcium carbonate formed under the experimental conditions chosen. This part presents the results obtained with 1 and 4ppm of PPCA on the crystals of $CaCO_3$ formed onto the clean stainless steel capillary.

6.4.1.1 Effects of 1ppm of PPCA

With 1ppm of PPCA the cell was not blocked after 60 minutes and so there was clearly some inhibition at 1ppm. The crystal planes A(311), C(214), C(211) and A(012) observed with no inhibitor were not observed anymore (Figure 6.2). Nevertheless the main peaks present in the non inhibited case were still present but with a smaller intensity.

There was the emergence of the aragonite plane A(221) with a weak intensity and a second unknown crystal plane was present corresponding to the 2-theta value 3.15°. This plane was called "Y". The induction time was generally the same as in the uninhibited case except for the aragonite plane A(200) and the vaterite plane V(300):

- A(200) was observed after 2 minutes (whereas it appeared after 14 minutes with no inhibitor)
- V(300) was observed after 16 minutes (whereas it appeared after 22 minutes with no inhibitor)

The growth rate of the different crystal planes was slowed down compared to the non inhibited case as shown later.

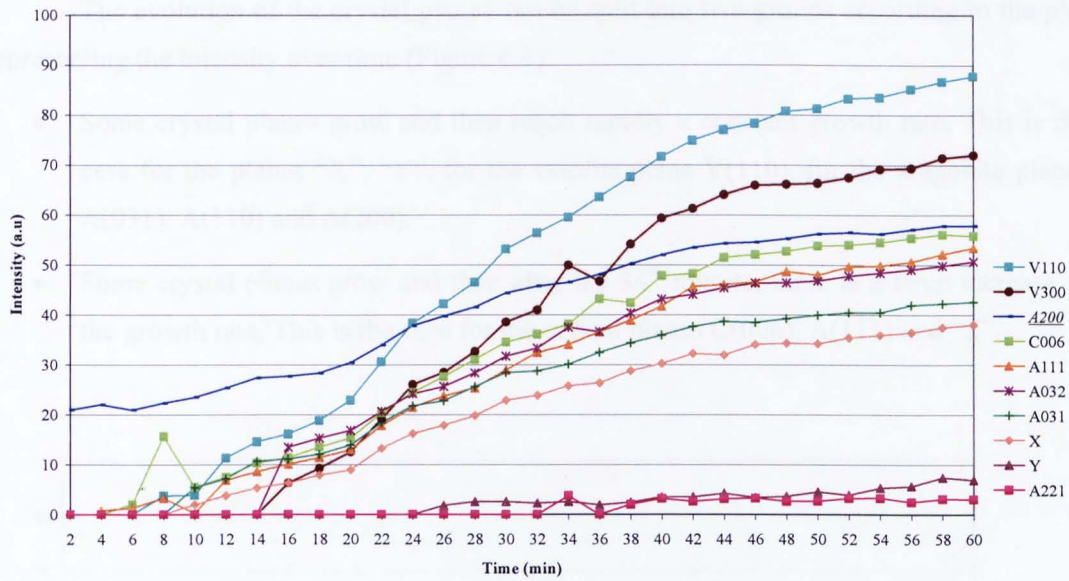

Figure 6.2: Assessment of the intensity of the diffracted beam reflecting the growth of the main crystal planes formed on a metallic surface with 1ppm of PPCA at 80°C

6.4.1.2 Effects of 4ppm of PPCA

The dominant vaterite plane V(300) was not observed with 4ppm of PPCA. There was a total inhibition for this plane. The aragonite plane A(032) was totally inhibited as well. The plane "Y" was present with a higher intensity and a smaller induction time (26 and 2 minutes for 1 and 4ppm respectively) and a new plane corresponding to the d-space value 3.71Å was observed after 14 minutes. This plane was called "Z".

The aragonite plane A(200) appeared after 2 minutes. It is interesting to note that its intensity was greater than the other crystal plane formed and that the intensity value at 2 minutes was almost the same at the end of the test.

For all the crystal planes the induction time was greater with 4ppm of PPCA except for the aragonite A(111) and the plane "Y".

The evolution of the crystal planes can be split into two groups according to the plot representing the intensity over time (Figure 6.3):

- Some crystal planes grow and then reach rapidly a constant growth rate. This is the case for the planes "X", "Y", for the vaterite plane V(110), for the aragonite planes A(031), A(110) and A(200).
- Some crystal planes grow and then after the 34th minute, there is a large increase of the growth rate. This is the case for the crystal planes C(006), A(111) and "Z".

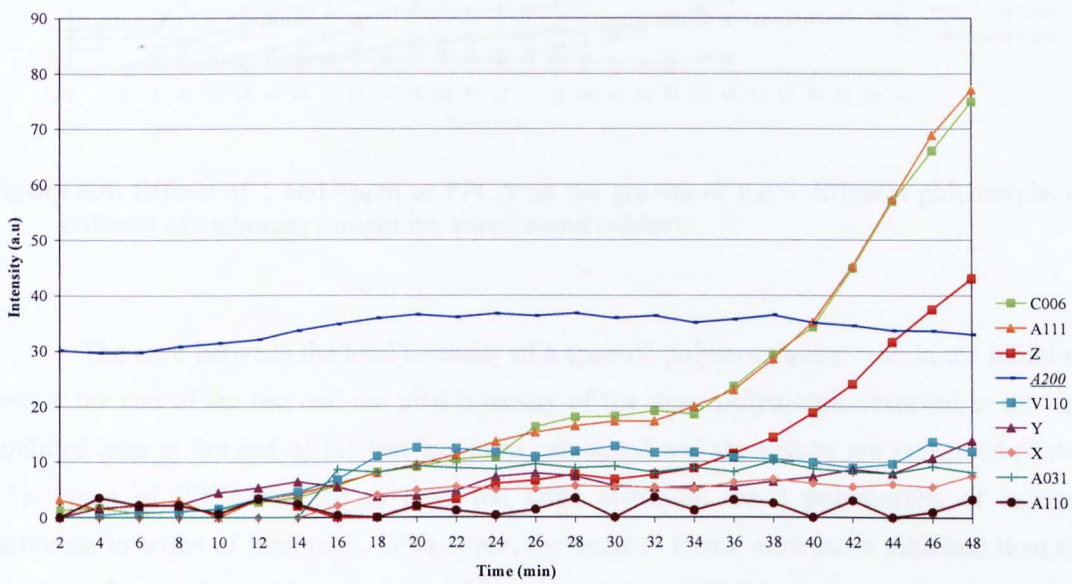

Figure 6.3: Assessment of the intensity of the diffracted beam reflecting the growth of the main crystal planes formed on a metallic surface with 4ppm of PPCA at 80°C

The evolution of the total intensity for the specific polymorph has been assessed (Figure 6.4). The aragonite, vaterite and calcite forms were reduced with 1ppm of inhibitor and the reduction was greater with 4ppm; the intensity of the aragonite and of the calcite was not kept constant in the second part of the test (an increase of the intensity is observed from the 34th minute) compared to the intensity of the vaterite (due to the increase of the intensity of the calcite (006) and the aragonite (032)).

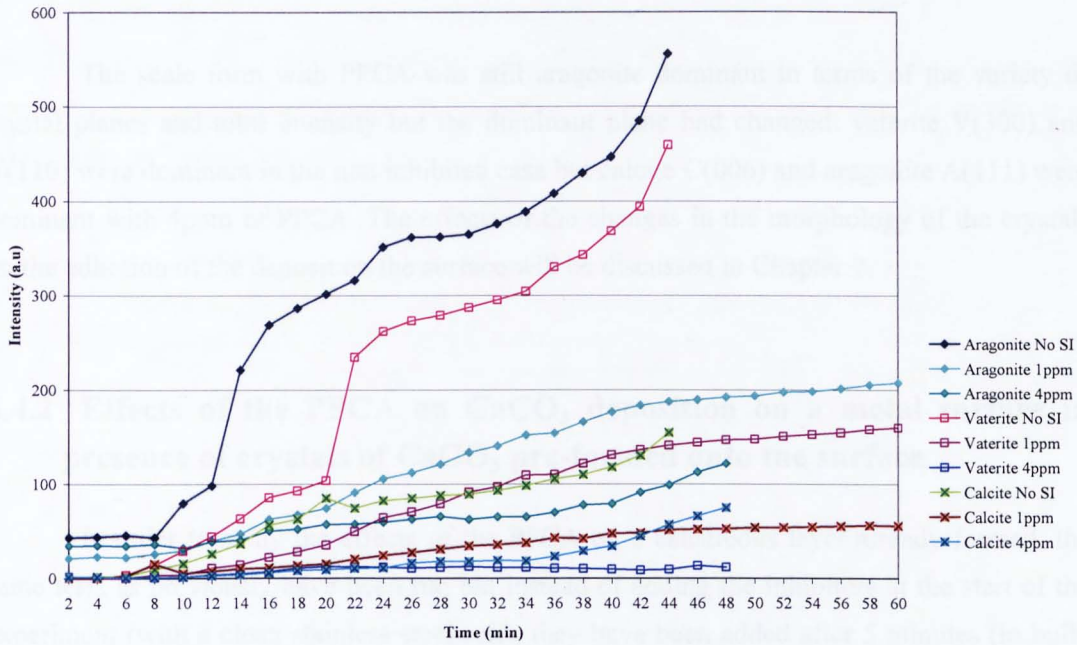

Figure 6.4: Effects of 1 and 4ppm of PPCA on the growth of the 3 different polymorphs of calcium of carbonate (aragonite, vaterite and calcite)

The ratio between the total intensity of a specific polymorph observed in the inhibited case at the end of the test and the total intensity of the same polymorph observed in the non inhibited case at the end of the test has been calculated and the results are presented (Table 6.3). 1ppm of PPCA seemed to have the same effect on the 3 polymorphs of calcium carbonate in terms of inhibition. With 4ppm, the vaterite forms were more inhibited than the aragonite forms. The calcite was least inhibited by 4ppm of PPCA (due to the increase of the growth rate of the plane C(006)).

Table 6.3: Inhibition ratio (*Total intensity of a specific polymorph/Total intensity of the same polymorph in the non inhibited case*) calculated for the inhibited brines with PPCA.

Polymorph	1ppm PPCA	4ppm PPCA t=0
Calcite	0.36	0.48
Vaterite	0.34	0.02
Aragonite	0.39	0.22

The number of aragonite crystal planes was always greater than the vaterite and calcite even with the increase of the concentration of PPCA (Figure 6.2 and Figure 6.3).

The scale form with PPCA was still aragonite dominant in terms of the variety of crystal planes and total intensity but the dominant plane had changed: vaterite V(300) and V(110) were dominant in the non inhibited case but calcite C(006) and aragonite A(111) were dominant with 4ppm of PPCA. The effects of the changes in the morphology of the crystals on the adhesion of the deposit on the surface will be discussed in Chapter 7.

6.4.2 Effects of the PPCA on $CaCO_3$ deposition on a metal surface in presence of crystals of $CaCO_3$ pre-formed onto the surface

In order to study the effects of the PPCA on a calcareous layer already formed, the same tests as previously have been run but instead of adding the inhibitors at the start of the experiment (with a clean stainless steel cell), they have been added after 5 minutes (to build up a calcium carbonate layer on the surface of the cell). The time t=0 of the graph corresponds to the time at which the inhibitors have been added. No measurement has been done during the first 5 minutes, during the building up of the calcareous layer, as it is impossible to reach the system once the beam is on. The calcareous layer was probably thin as the intensity at 5 minutes was small when no inhibitor was added (Figure 6.1) nevertheless it modified the mechanism of inhibition as shown the different variations of the intensity depending on when the inhibitors were added (Figure 6.5).

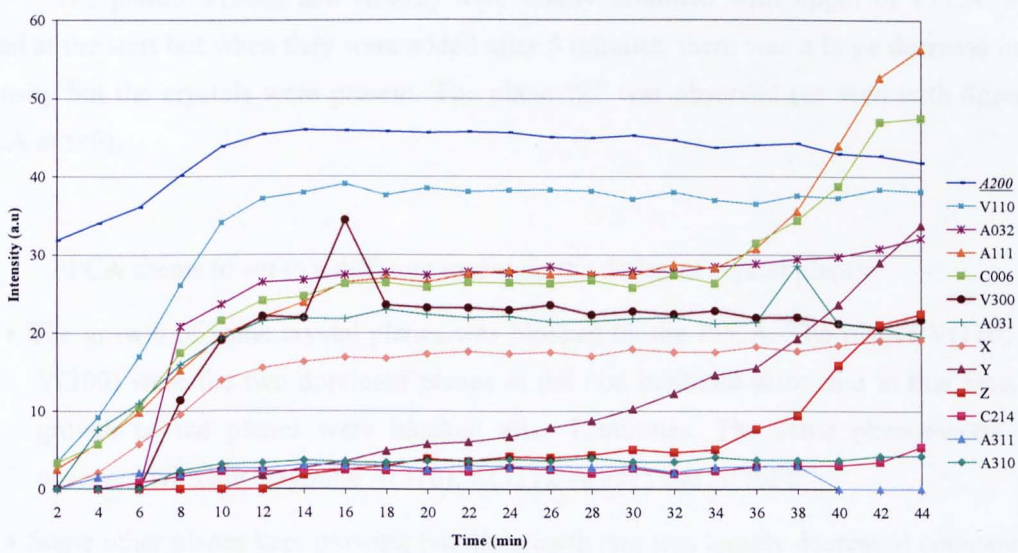

Figure 6.5: Assessment of the intensity of the diffracted beam reflecting the growth of the main crystal planes formed on a metallic surface with 4ppm of PPCA added after 5 minutes after the start of the scale formation at 80°C

The scale formed was still aragonite dominant in terms of intensity and variety of crystal planes (153a.u and 5 crystal planes) (Figure 6.5). The intensity of the peaks was generally smaller than the intensity of the non inhibited case. The inhibition was the greatest on the vaterite forms (Table 6.3).

Table 6.4: Inhibition ratio (*Total intensity of a specific polymorph/Total intensity of the same polymorph in the non inhibited case*) calculated for the inhibited brines with PPCA added 5minutes after the creation of the supersaturation.

Polymorph	4ppm PPCA t=5
Calcite	0.34
Vaterite	0.13
Aragonite	0.28

Some crystal planes with a weak intensity were missing (as observed when PPCA was added at the start of a test) like the plane A(321)/V(308)/C(125) (the same d-space value characterises these 3 different planes). A new aragonite plane A(310) appeared.

The planes V(300) and A(032) were totally inhibited with 4ppm of PPCA when added at the start but when they were added after 5 minutes, there was a large decrease in the intensity but the crystals were present. The plane "Z" was observed (as seen with 4ppm of PPCA at t=0).

PPCA seems to act to a different extent on the different crystal planes:

- The growth of some crystal planes was blocked by the PPCA. The planes V(110) and V(300) were the two dominant planes in the non inhibited brine and in this case, the growth of the planes were blocked after 12minutes. The same phenomenon was observed with the aragonite A(310), A(311), A(031) and A(200).
- Some other planes kept growing but the growth rate was largely decreased compared to the non inhibited case. The growth of the planes A(032), C(214) and "X" was drastically slowed down but the intensity kept increasing.

The growth rate of the calcite C(006), the aragonite A(111) and the plane "Z" was first slowed down and almost constant and at the 34th minute was largely increased (as observed when the PPCA was added at t=0). The plane "Y" was following the same trend as these ones but the growth was always increasing, there was no stable stage before the great increase.

6.5 Effects of the PMA on calcium carbonate formation

6.5.1 Effects of the PMA on $CaCO_3$ deposition on a clean metal surface

6.5.1.1 Effects of 1ppm of PMA

The cell was not blocked after 60 minutes as observed with 1ppm of PPCA. The crystal planes A(321)/V(308)/C(125), A(213), A(311) and A(012) were totally inhibited. There was no emergence of new crystal planes at this concentration (Figure 6.6). The crystal growth was slowed down for all the crystal planes.

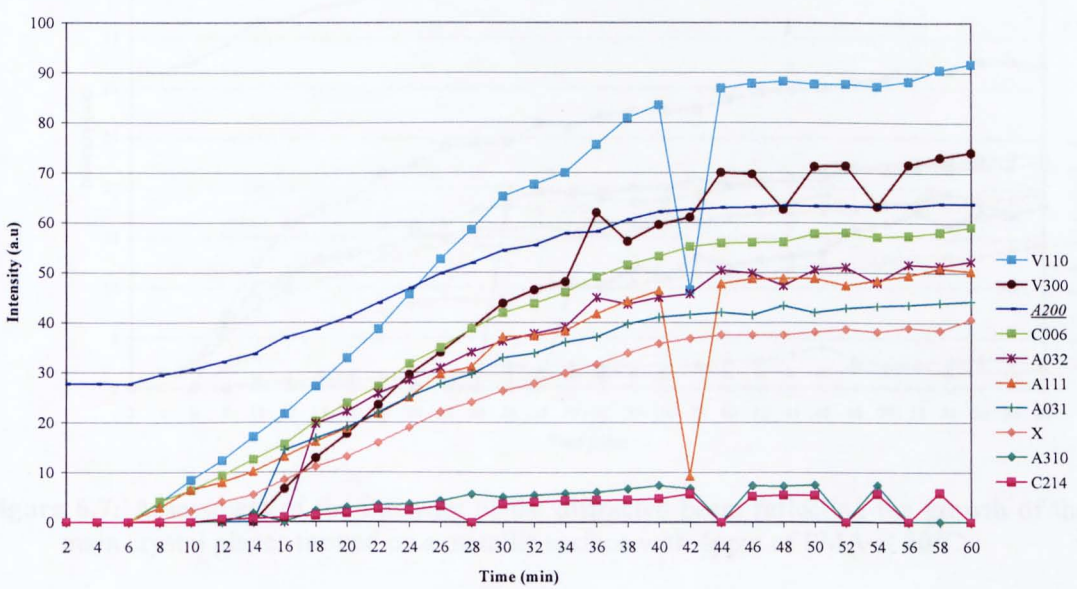

Figure 6.6: Assessment of the intensity of the diffracted beam reflecting the growth of the main crystal planes formed on a metallic surface with 1ppm of PMA at 80°C

The effects of 1ppm of PMA on the induction time differs according to the crystal planes considered: the emergence of the crystal plane A(200) occurs earlier than in the non inhibited case whereas it is delayed for the aragonite A(031) and A(032). The early emergence of the aragonite A(200) will be discussed in Chapter 7. The induction time of the other crystal planes was not affected by the inhibitor.

6.5.1.2 Effects of 4ppm of PMA

At this concentration there was no more disappearance of crystal planes present in the non inhibited case but the plane "Y" found with 1ppm of PPCA was formed as well with 4ppm of PMA (Figure 6.7). Its presence was not detected in all the frames and the intensity of the peak was small so it has not been reported .

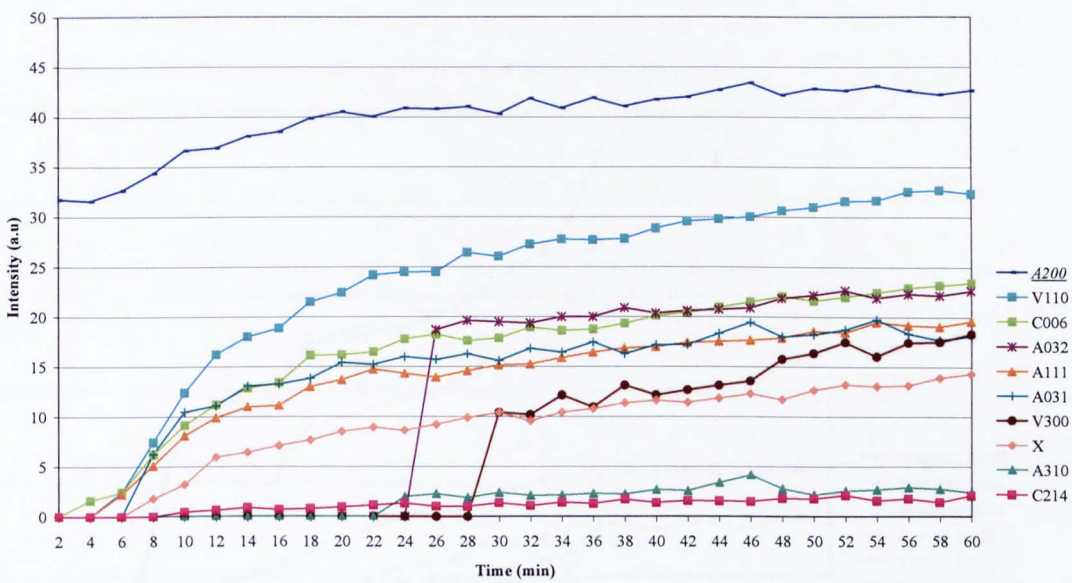

Figure 6.7: Assessment of the intensity of the diffracted beam reflecting the growth of the main crystal planes formed on a metallic surface with 4ppm of PMA at 80°C

4ppm had a greater effect (more planes were affected) on the induction time and as observed with the PPCA and 1ppm of PMA they were different according to the crystal planes:

- It was increased for the aragonite A(032) and A(310) and the vaterite V(300).
- The calcite C(006) were formed earlier than in the non inhibited case.

The growth was largely decreased with the use of 4ppm of PMA. Nevertheless 4ppm of PMA only totally blocked the growth of two crystal planes, the calcite C(214) and aragonite A(310). The retardation of the growth occurred just after the emergence of the planes. For the other crystal planes the growth was strongly reduced but there were still growth of the crystal planes.

The scale formed in the presence of 4ppm of PMA was aragonite dominant in terms of intensity and crystalline variety. The vaterite form V(300) was not the dominant crystal plane as observed in the non inhibited case but the aragonite A(200) was.

Figure 6.8 presents the effects of the PMA on the different polymorphs of calcium carbonate. A large reduction in the intensity was observed with 1ppm and especially with 4ppm of PMA. Contrary to what was seen with the PPCA, the total intensity of the aragonite and calcite was almost steady.

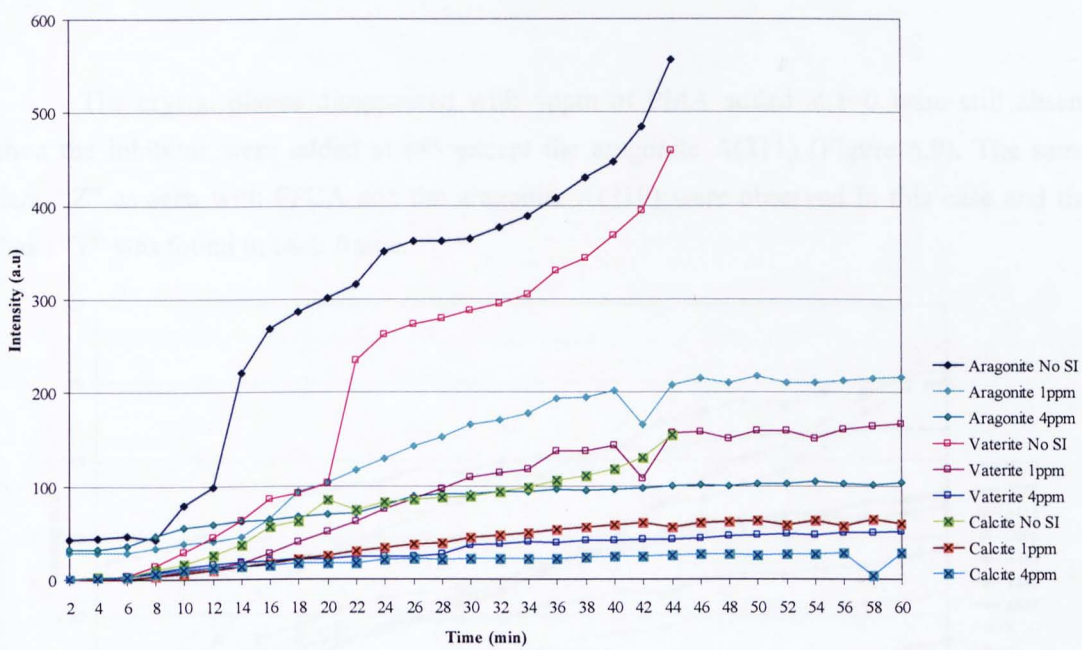

Figure 6.8: Effects of 1 and 4ppm of PMA on the growth of the 3 different polymorphs of calcium of carbonate (aragonite, vaterite and calcite)

PMA affected more the vaterite forms than the aragonite or calcite forms but the difference in the inhibition was not as great as the difference seen with the PPCA. It is interesting to note that the efficiency of PMA on the calcite and the aragonite was similar (Table 6.5).

Table 6.5: Inhibition ratio (*Total intensity of a specific polymorph/Total intensity of the same polymorph in the non inhibited case*) calculated for the inhibited brines with PMA.

Polymorph	1ppm PMA	4ppm PMA t=0
Calcite	0.42	0.18
Vaterite	0.35	0.11
Aragonite	0.40	0.18

6.5.2 Effects of the PMA on $CaCO_3$ deposition on a metal surface in presence of crystals of $CaCO_3$ pre-formed onto the surface

Like previously for the PPCA, the effects of 4ppm of PMA on a calcareous layer already formed have been studied. The time t=0 of the graph corresponds to the time at which the inhibitors have been added (5 minutes after the start of a run).

The crystal planes disappeared with 4ppm of PMA added at t=0 were still absent when the inhibitor were added at t=5 except the aragonite A(311) (Figure 6.9). The same plane "Z" as seen with PPCA and the aragonite A(310) were observed in this case and the phase "Y" was found in each frame.

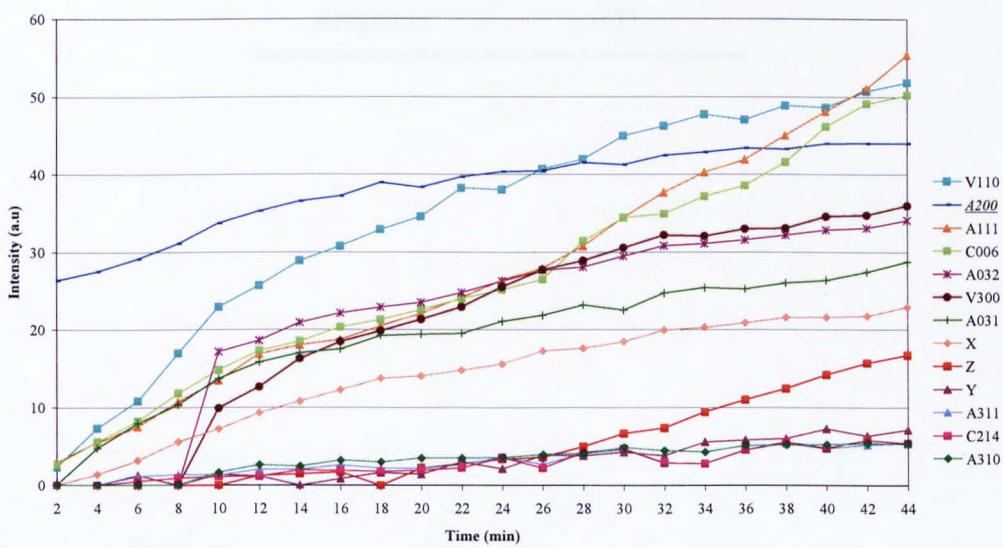

Figure 6.9: Assessment of the intensity of the diffracted beam reflecting the growth of the main crystal planes formed on a metallic surface with 4ppm of PMA added after 5 minutes after the start of the scale formation at 80°C

The majority of the crystal planes seem to follow the same growth trend: after the emergence of the planes the growth rate slowed down. Three different crystal planes did not follow this trend: at the 28th minute the growth rate of the calcite C(006), the aragonite A(111) and the plane "Z" increased as observed with the PPCA.

The plane A(311), A(310), C(214) and "Y" had a more linear growth compared to the other planes but the intensity of these planes was small (the final intensity was around 5).

The scale formed was still aragonite dominant in term of intensity and crystalline variety and even on a calcareous layer already formed the PMA was more efficient on the vaterite forms (Table 6.6).

Table 6.6: Inhibition ratio (*Total intensity of a specific polymorph/Total intensity of the same polymorph in the non inhibited case*) calculated for the inhibited brines with 4ppm of PMA added 5minutes after the creation of the supersaturation.

Polymorph	**4ppm PMA t=5**
Calcite	0.35
Vaterite	0.19
Aragonite	0.31

6.6 Effects of the PA on calcium carbonate formation

As observed with the other inhibitor, the crystal planes A(321)/V(308)/C(125) and A(012) were absent with 4ppm of PA (Figure 6.10). But contrary to what was seen with the PPCA and the PMA there was no emergence of new crystal planes (The plane "Y" and the aragonite (310)). The induction time was increased for the aragonite A(311).

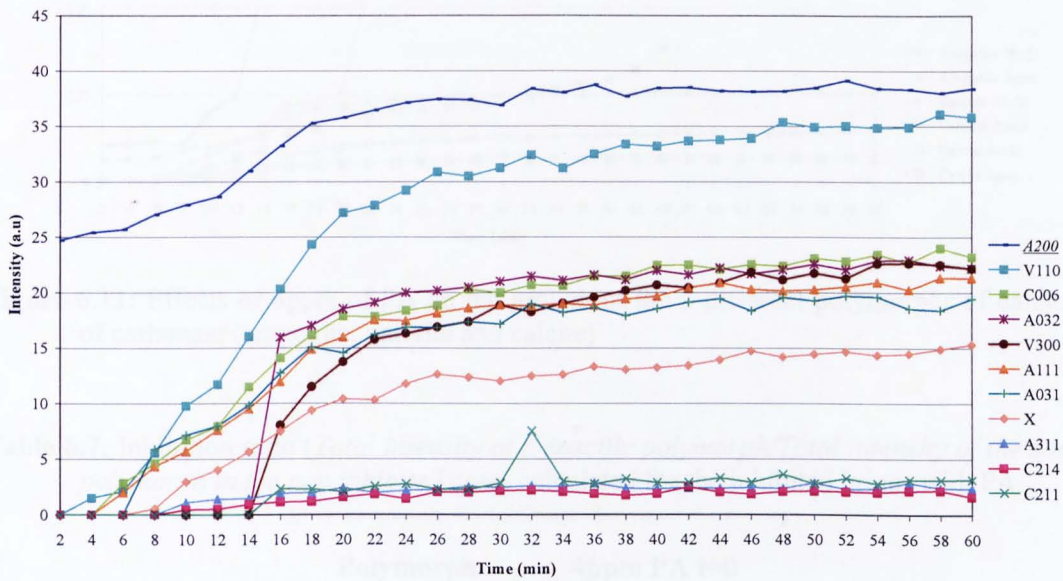

Figure 6.10: Assessment of the intensity of the diffracted beam reflecting the growth of the main crystal planes formed on a metallic surface with 4ppm of PA at 80°C

The growth of the crystal planes with low intensity (C(214), C(211), A(311)) was blocked rapidly (less than 10 minutes after the emergence of the plane). For the other planes they all grew until the 24th minute and then:

- There was a drastic slowing down of the growth for vaterite V(300) and V(110), the calcite C(006), the aragonite A(111) and the crystal plane "X".
- Or the growth was totally blocked; A(031), A(032) and A(200).

The inhibition effects of 4ppm of PA were stronger on the vaterite form of calcium carbonate (Table 6.7) and the total intensity of the aragonite, the vaterite and the calcite was almost constant (Figure 6.11).

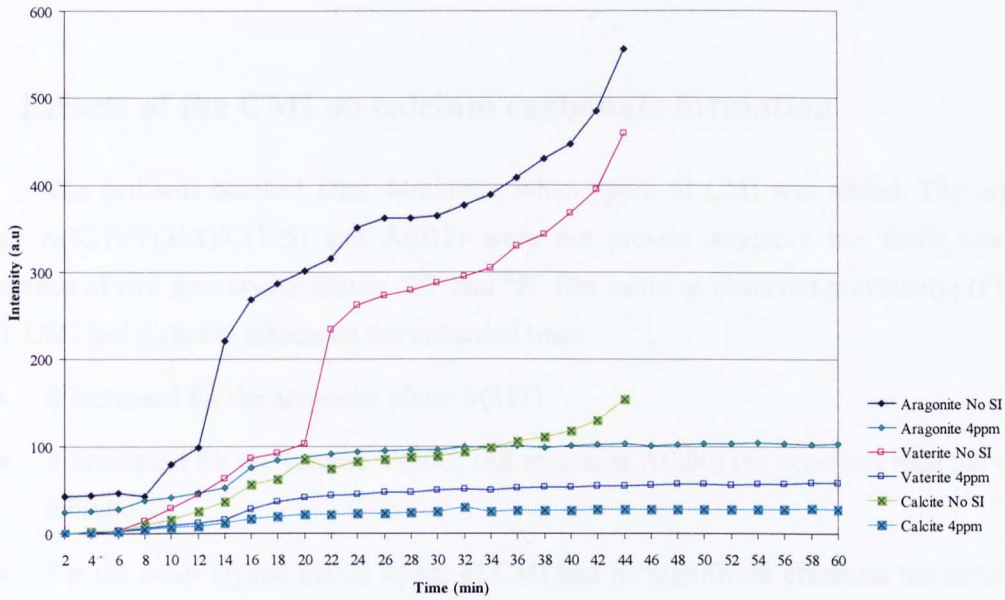

Figure 6.11: Effects of 4ppm of PA on the growth of the 3 different polymorphs of calcium of carbonate (aragonite, vaterite and calcite)

Table 6.7: Inhibition ratio (*Total intensity of a specific polymorph/Total intensity of the same polymorph in the non inhibited case*) calculated for the inhibited brines with PA.

Polymorph	4ppm PA t=0
Calcite	0.22
Vaterite	0.12
Aragonite	0.19

6.7 Effects of the CMI on calcium carbonate formation

The cell was blocked after 44minutes when 4ppm of CMI was added. The crystal planes A(321)/V(308)/C(125) and A(012) were not present anymore but there was the emergence of two new crystal planes "Y" and "Z" (the same as observed previously) (Figure 6.12). CMI had different effects on the induction time:

- It increased for the aragonite plane A(311)
- It decreased for the vaterite V(300) and aragonite A(200) (as observed with the other inhibitors)
- For the other crystal planes 4ppm of CMI had no significant effect on the induction time

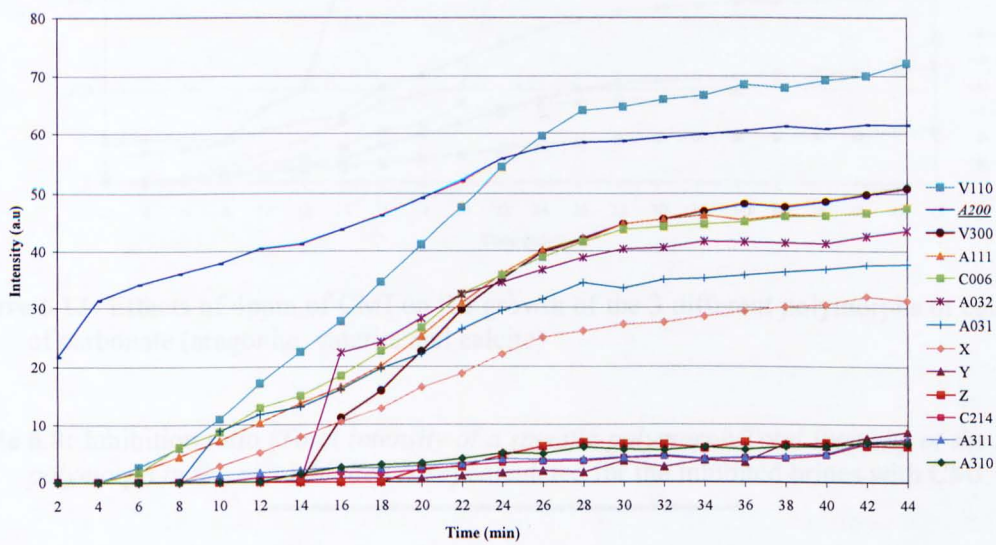

Figure 6.12: Assessment of the intensity of the diffracted beam reflecting the growth of the main crystal planes formed on a metallic surface with 4ppm of CMI at 80°C

A decrease in the intensity of the peaks was observed for all the crystal planes and except for the plane "Z", the growth of the planes increase; there was no total blockage of the growth.

It is interesting to note that the growth rate was significantly slowed down from the 28^{th} minute for almost all the crystal planes (except A(200)).

CMI seems to act more on the vaterite form but the difference in the ratio between the 3 polymorphs was not as great as observed with PPCA (Table 6.8) and Figure 6.13 shows that the total intensity of the three polymorphs of calcium carbonate was still increasing during the test.

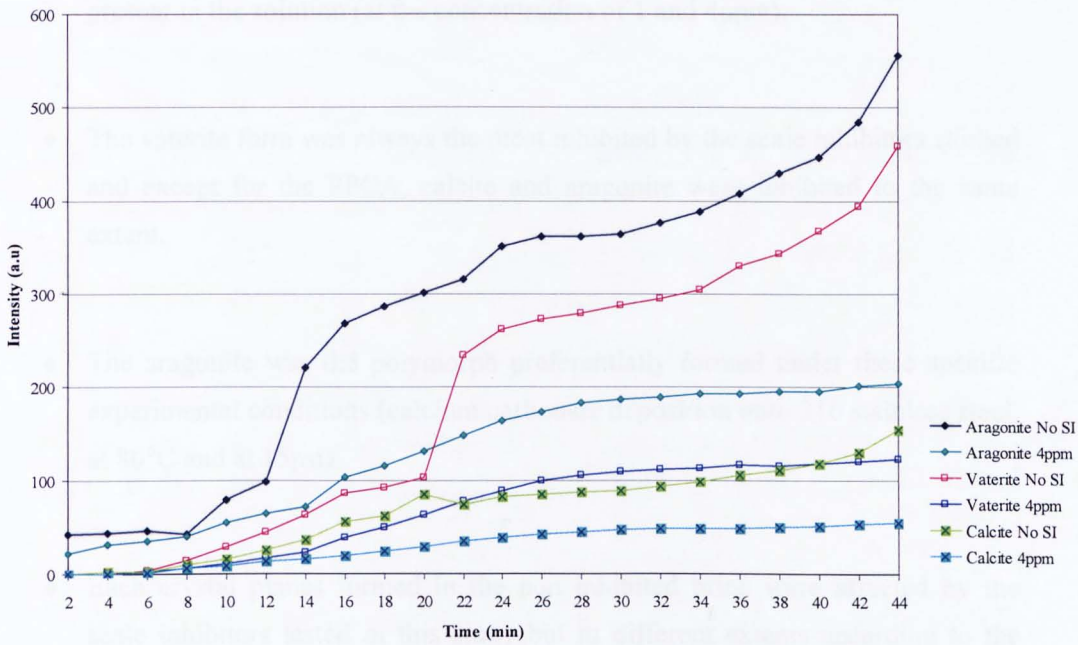

Figure 6.13: Effects of 4ppm of CMI on the growth of the 3 different polymorphs of calcium of carbonate (aragonite, vaterite and calcite)

Table 6.8: Inhibition ratio (*Total intensity of a specific polymorph/Total intensity of the same polymorph in the non inhibited case*) calculated for the inhibited brines with CMI.

Polymorph	4ppm CMI t=0
Calcite	0.35
Vaterite	0.26
Aragonite	0.35

6.8 Concluding remarks

The main concluding remarks arising from this chapter are:

- The intensity of the peaks decreased when any scale inhibitor tested were present in the solution (at the concentration of 1 and 4ppm).

- The vaterite form was always the most inhibited by the scale inhibitors studied and except for the PPCA, calcite and aragonite were inhibited to the same extent.

- The aragonite was the polymorph preferentially formed under these specific experimental conditions (calcium carbonate deposition onto 316 stainless steel, at 80°C and at 15psi).

- Each crystal planes formed in the non inhibited brine were affected by the scale inhibitors tested in this study but to different extents according to the nature and the concentration of the inhibitor.

- PMA and PA at 4ppm showed similar behaviour.

- Different effects were observed on the induction time according to the inhibitor and the crystal planes considered.

Chapter 7
Discussion

7.1 Introduction

The objectives of the work presented in this thesis were to provide a new understanding of calcium carbonate formation and inhibition directly onto a surface by combining different methodologies. To improve the use of these inhibitors or to design better ones, it is important to understand the mechanisms of calcium carbonate formation and then the mechanisms of inhibition of the additives studied. The use of different methodologies meant that several aspects of their mechanisms could be probed. Each methodology had its own specificity and some important conclusions were raised from these results. In this chapter, four key points are discussed and these four points were determined in a way to present the main aspects of the inhibitor mechanisms. The main contribution of this work to the scaling community is therefore able to be extracted from the following discussion.

First of all, the *inhibition properties* of the different additives studied are discussed. The results pointed out that each chemical used acted to a different extent on calcium carbonate formation. The second part is focused on the *interactions between the inhibitors and the metal surface and the inhibitors and the calcium carbonate crystals*. The effects of the inhibitors on the morphology and on the crystallography of the crystals are discussed in the third part of this chapter. The inhibitors have different effects on the different polymorphs and on the different crystal planes. Then, the *kinetics* of calcium carbonate formation and inhibition were investigated. A comparative study was made between two different methods (*in-situ* flow cell combined with electrodeposition and *in-situ* SXRD measurements) to determine the kinetics of formation and the effects of the four scale inhibitors on the kinetics of the different polymorphs of $CaCO_3$.The findings provided by these four parts of the discussion were arisen from the data obtained when the inhibitors were present during all the different steps of calcium carbonate formation (the inhibitors were added before the supersaturation was created). The last part of the discussion relates to one part of the study which has not received any attention in the literature this far; *the determination of the effects of the scale inhibitors on crystals of calcium carbonate already formed on a surface.*

7.2 Inhibition properties of the different chemicals studied

The efficiency of scale inhibitors has already been widely studied but most of the works were based on the inhibition of scale in the bulk solution by titration of Ca^{2+} [153, 187], ICP (Inductively Coupled Plasma spectroscopy) measurements of selective elements [57, 145, 188], ion chromatography [57], conductivity [189] and turbidity measurements [59]. Most of the studies conducted on the inhibition properties of the scale inhibitors on the scale deposition on a surface were conducted on the variations of the mass of the deposit [78, 84, 152, 190-192] or of the pressure of during tube blocking tests [67, 188].

In this study, the efficiency of the additives to inhibit calcium carbonate formation *on a surface* was determined from two different parameters:

- the mass of the deposit formed in presence of different concentrations of inhibitors after 4 and 24 hours under polarizations in static tests (Chapter 4)
- the surface coverage by the crystals of calcium carbonate determined with the *in-situ* flow cell after 1 hour under polarization conditions (Chapter 5).

This two techniques give complementary information on the mechanisms of inhibition: the measurements after 4 and 24 hours show the effects of the inhibition on the late steps of crystal formation whereas the value of the surface coverage after 1 hour of electrodeposition indicates how the inhibitors affect the scale formation during the early stages of calcium carbonate formation.

7.2.1 Effects of the scale inhibitors on the mass of calcium carbonate deposited

A potential has been applied to create the supersaturation at the vicinity of the electrode and the weight of the deposit has been measured after 4 and 24 hours (Figure 4.35). Table 7.1 presents the percentage of efficiency calculated from the weight measurements. The PPCA was the inhibitor presenting the best ability to decrease the weight of the deposit with 93% efficiency with 4ppm. The PMA was the most efficient green inhibitor tested in these experimental conditions (74% with 4ppm after 24 hours). The CMI showed the poorest inhibition properties with only 19% of efficiency.

The time is an important factor for the study of the inhibition efficiency of chemicals. The weight measurements have been made after 4 and 24 hours under polarization conditions and the conclusions raised can be different according to the duration of electrodeposition considered. 1ppm of PMA had the same effect on the weight of the deposit as PPCA and CMI (21%, 20% and 18% of efficiency respectively) but the PA did not generate any significant decrease after 4 hours whereas the contrary was observed after 24 hours, the PMA had no more effect and the efficiency of the PA reached 21%.

The PA interacts more with the metal surface than with the crystals of $CaCO_3$ (Table 7.1) contrary to the PMA. The reduction of scale deposition due to the formation of an inhibitor film increased with time whereas the efficiency of the PMA which interacts with the crystals of $CaCO_3$ decreases over time at low concentration. At high concentration the inhibitor presenting a higher affinity with $CaCO_3$ has the greater inhibition efficiency. The blockage of the growth sites of the crystals of $CaCO_3$ seems to be a better strategy to reduce scale deposition. The slower kinetics of adsorption of PA on the metal surface than PMA on $CaCO_3$ crystals could explain the different efficiency at different times.

Table 7.1: Correlation between the adsorption (on the metal surface and on $CaCO_3$) and the efficiency of the inhibitors. The efficiency was calculated from the weight measurements $((W_{No\ SI}-W_{SI})/W_{No\ SI})*100$ of the inhibitors studied at 1ppm and 4ppm and after 4 and 24 hours.

Time	4 hours		24 hours		Adsorption	
Concentration	1ppm	4ppm	1ppm	4ppm	Surface	$CaCO_3$
PPCA	21%	91%	18%	93%		
CMI	20%	48%	10%	19%		
PMA	18%	55%	0%	74%	+	+++
PA	0%	42%	21%	46%	+++	+

The different efficiency of the inhibitor according to the duration of electrodeposition lead to some hypothesis. The kinetic and the strength of adsorption is likely to be specific to the chemical considered. The concentration of carboxylate groups contained by the different chemicals tested is unknown. It has been proved that this function plays a key role in the adsorption properties of a chemical [193] which partly explained the different inhibiting behaviour observed of the inhibitors. A rapid adsorption but with weak strength would provide an early inhibition but not constant in time. A slow and strong adsorption would result in a progressive but constant inhibition.

The effects of 4ppm of PMA were more constant over time than what was observed with the PA and the CMI (Figure 4.35). This statement does not take into account the efficiency of the inhibitors. It is based only on the variations of mass between 4 and 24 hours. The greatest difference was observed with 4ppm of CMI whereas at 4 hours the efficiency was similar as the efficiency calculated for the PA and the PMA (Table 7.1) illustrating the effects of the time on the inhibition properties; the CMI lost its ability to inhibit $CaCO_3$.

7.2.2 Effects of the scale inhibitors on the surface coverage detected in *in-situ* cell

Contrary to the observations from the weight measurements, the study of the surface coverage (without overlapping effects) showed inhibiting effects of PPCA, PMA and PA from the concentration 1ppm. The results were summarised in Table 7.2. A strong inhibition was observed with 4ppm of PPCA, PA and PMA. This is consistent with the study of the mass of the deposit as the best results were obtained with these three inhibitors. Even though the techniques differ, the trend of the inhibition efficiency are the same.

Table 7.2: Extended surface coverage of the electrode after 60 minutes under polarization in the *in-situ* flow cell in presence with 1 and 4ppm of inhibitors

Time	**1 hour**	
No SI	39.7%	
Concentration	**1ppm**	**4ppm**
PPCA	20.7%	No crystals
CMI	n.d	19.5%
PMA	27.2%	0.3%
PA	27.1%	No crystals

The weight measurements and the surface coverage were determined with different set-up and the main difference was the test run for 4 and 24 hours were in static conditions whereas the tests run for 1 hour have been run with the *in-situ* flow cell. Nevertheless it is interesting to note that for both PPCA and PA no crystals were detected with 4ppm after 1 hour but after 4 hours in the static tests there were some crystals of calcium carbonate on the surface (Figure 4.3 and Figure 4.7). The efficiency of the PPCA was much greater than the efficiency of the PA (91% and 42% respectively) (Table 7.1).

It seems that the time factor is very important for the study of the inhibition properties of an additive: it can show very good inhibition properties in the early beginning of calcium carbonate formation (like the PA) and then the same inhibitor can reach only 50% of efficiency after 24 hours of test. A ranking of the efficiency of the inhibitors studied is presented in Table 7.3. The ranking is realised for the three different measurements done:

- After *1 hour*, in-situ electrochemical flow cell (surface coverage)
- After *4 hours*, static electrodeposition (weight measurement)
- After *24 hours*, static electrodeposition (weight measurement).

Table 7.3: Ranking of the efficiency of the scale inhibitors studied at 4ppm *(the efficiency at 1 hour was obtained with a different set-up than the efficiency at 4 and 24 hours)*

Duration of the scaling conditions	PPCA	PMA	PA	CMI
1 hour	1	2	1	4
4 hours	1	2	2	2
24 hours	1	2	3	4

PPCA and PA seems to be efficient to inhibit the nucleation process and early growth as they are efficient at the beginning of the scaling process. The ranking of the efficiency of the PMA to inhibit $CaCO_3$ is constant and PMA seems to interact more with growth process of $CaCO_3$ formation. The ability of PPCA to inhibit the nucleation step has already been pointed out [145]. The decrease of the number of crystals results in a decrease of the weight of the deposit. The extent of the growth inhibition cannot be determined by assessing the mass of the deposit. It has been reported that the green inhibitors mechanisms operate principally as nucleation inhibitors on $BaSO_4$ [194]. It seems to be the same trend for the $CaCO_3$ except for the CMI.

7.3 Different level of interactions with scale inhibitors

To inhibit the scale deposition on a surface, the inhibitors can act either on the crystals of $CaCO_3$ or on the substrate or both. As has been seen in the previous part, the inhibitors have a different affinity with the crystals of $CaCO_3$ resulting in different inhibition properties. The inhibitors can also interact with the substrate leading to the modifications of the surface properties.

7.3.1 Interactions between scale inhibitors and the substrate of deposition

The electrochemical tests conducted in static mode for 24 hours pointed out some interactions between the inhibitors and the metal surface. No quantification can be realised from chronoamperometry studies as the variations of the current density depend on the free access of the surface and not on the quantity of scale present onto the metal surface: a thick and porous calcareous layer can lead to the same current density variations as a thin but compact layer. Some further analyses was carried out (infra-red spectroscopy and contact angle measurements) to characterise these interactions. The contact angle measurements pointed out for the four inhibitors the presence of a film of inhibitor at 10 and 30ppm.

The discussion is focused on the methodology used to detect the inhibitor film in order to characterise the film according to the nature of the inhibitor.

7.3.1.1 Behaviour of the inhibitor film regarding O_2 diffusion

A large increase of the current density was observed in the early stages for the scaling brine with no inhibitor (Figure 4.1). This increase has been observed in previous studies. As soon as a potential was applied, the system needed a few seconds to reach the dynamic equilibrium to permit the diffusion layer of O_2 to be established [173]. This increase was not observed with the non scaling brine for the following reason. The formation of calcium carbonate (with the scaling brine) generated a local decrease of the pH at the surface/brine interface [18, 195] which leaded to the rise of the kinetics of the oxygen reduction as OH^- ions were produced to increase the pH again. The amount of electrons (the current) was therefore increased. In the absence of carbonate ions (for NSB), the local drop of pH was not taking place since no scale occurred and, as such, the reaction was slowed as the OH^- concentration at the metal/solution interface reached a steady value. The current density was therefore steady.

The scale inhibitors affected to a different extent (according to the concentration used) the establishment of the diffusion layer. Two phenomena could explain the trend of the curve at the early stages (both could occur simultaneously) :

- The presence of the scale inhibitor film limits the oxygen access on the surface at low concentrations and at high concentrations the surface is blocked (for the the PPCA for example) as no increase was observed by forming a film on the surface of the electrode as previously shown for carboxylic acids [185] and phosphonates [196].

- The presence of scale inhibitor in the solution decreases the kinetics of calcium carbonate formation and the local pH drop resulting in the reduction of $CaCO_3$ formation and thus causing a decrease in the kinetics of oxygen reduction.

An inhibitor film onto the metal surface were detected by the current density variations for the concentrations 10 and 30ppm with the PPCA and the PA. Magnesium and calcium ions play an important role in the formation of the film as when they were removed from the solution (especially the magnesium), the baseline of the current density increased (showing less interactions between the metal surface and the inhibitors) (Figure 4.27).

The non detection of the film of PMA by the study of the variations of the current density shows that its property to isolate a metal surface from the oxygen diffusion is weaker than the film of PA. This could come from its porosity and its compactness explaining as well the weak detection by infra-red spectroscopy of the film of PMA as seen with the PPCA. Moreover Nagayasu *et al.* showed that carboxylic acids with plural carboxyl groups had much higher affinity with the surface [197]. Another important factor is the immersion time in the brine. Compere *et al.* studied the kinetics of formation of an organic layer formed after immersion in sea water [198]. The presence of the film of PMA was revealed by light microscopy and by the changes of the contact angle of the surface. It has been found that the deposit is extremely heterogeneous and that the overall coverage increases with immersion time. 4 hours of immersion might not be sufficient enough to form a detectable film of PMA by chronoamperometry.

The presence of a film of CMI on the surface was not as well detected as the film present with the PPCA as the current density variations were the same for the scaling brine with 30ppm of CMI and the non-scaling brine from 4000s. The baseline of the current density observed for the carbonate-free solution containing 30ppm of CMI strongly decreased showing a blockage of the diffusion of the oxygen to the surface. A film was deposited on the surface but as mentioned for the PMA the heterogeneity of the film [198] or its porosity and compactness [75] allowed the oxygen to diffuse to the surface. Moreover the film of CMI formation was probably disturbed by the high affinity of the CMI with Ca^{2+} and small nuclei of calcium carbonate most likely present at the vicinity of the surface [154, 155].

7.3.1.2 Thickness of the film

The film of PPCA has not been detected on the IR spectra. The limit of detection of the thickness of a film is 1µm. Kellner et *al.* shown that the absorbance is a function of the layer thickness [199]. Moreover when a beam impinges on the film, a reflected beam is generated and also a transmitted beam; a first diffracted beam is generated when the beam impinges the surface of the film (in contact with the air) and a second when the transmitted beam reached the metal surface [200]. If the film of inhibitor is too thin the diffracted beam from the metal surface interfere with the diffracted beam from the film itself. The film of PPCA might be too thin to be detected by FT-IR.

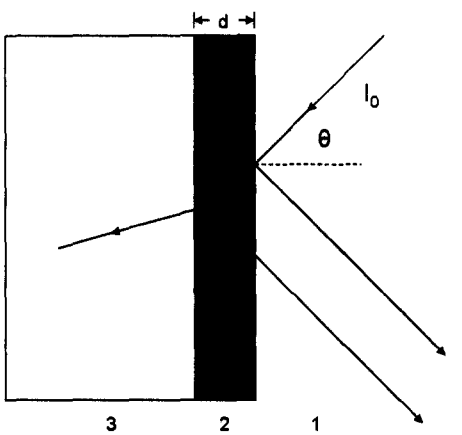

Figure 7.1: A schematic representation of the paths which a beam of light takes when impinging on a thin film sample.

The film formed by the polyaspartic acid has been visualised with the *in-situ* electrochemical cell (Figure 5.28). The presence of the film has been easily detected with the different methodology used in this study. Estievenart et *al.* showed by reflectometry that polyaspartic acid adsorbs on metallic surfaces [151]. An inhibitor film is present on the surface and limits the oxygen access. It has been shown that the molecular weight of polyaspartic acid had an effect on its ability to be adsorbed on a metallic surface: the higher the molecular weight, the less molecules are adsorbed. The polymer used in this study had a low molecular weight, so its adsorption on the surface was favoured [151].

The infra red spectra showed the presence of the CMI onto the surface for the concentration 30ppm with the detection of 3 peaks characteristic of the CMI. Moreover the observation of the surface showed some small and rounded particles which are probably the inhibitor film as no peak characteristic of $CaCO_3$ [201] was revealed.

7.3.1.3 Characterisation of the film and efficiency

Table 7.4 summarises the properties of the inhibitor film and a correlation with the efficiency is presented. The film on the surface was detected for the PA and the CMI with the three techniques whereas they present the lower efficiency after 4 and 24 hours of scale deposition. This shows that the formation of a film on the surface explains only partly the reduction of scale deposition.

Table 7.4: Ranking (best being the PPCA) of the efficiency of the scale inhibitors studied at 4ppm according to the detection of the inhibitor film by chronoamperometry, FT-IR spectroscopy and contact angle measurements

Chronoamperometry	FT-IR	Contact angle	Efficiency		
			1 hour	4 hours	24 hours
PPCA	-	PPCA	PPCA	PPCA	PPCA
PA	PA	PA	PA	PMA	PMA
CMI	CMI	CMI	PMA	CMI	PA
-	PMA	PMA	CMI	PA	CMI

7.3.1.4 General scheme of the inhibitor film formation

Imamura et *al.* have shown the good adsorption properties of aspartic acid on stainless steel surface at low pH [202]. This was explained by electrostatic interactions between the ionized groups of the aspartic acid (—COO^-) and the ionized groups on the stainless steel surface (—OH_2^+). Every inhibitor studied are negatively charged at high pH and behaved as negative particles. The pH at the vicinity of the electrode in this study is likely to be between 10.4 and 10.7 [203] and the surface charge at high pH is negative due to the presence of —O- groups [202]. Direct interactions between the negatively charged inhibitors and the metal surface does not seem possible and the hypothesis that the inhibitors interact with a positive charge like calcium and magnesium ions which interact with the negative charges of the surface is presented (Figure 7.2).

In general, the scale tendency is favoured for a substrate with a high surface energy [183]. The contact angle increases with the decrease of the surface energy. The changes in the contact angle followed the same trend for the four inhibitors and the variations were to the same extent from one inhibitor to another (Figures 4.12, 4.16, 4.20 and 4.24). The decrease of the contact angle observed for 10ppm of inhibitors means according to [183] the scale tendency should increase but it was not the case as no crystal of $CaCO_3$ were observed.

This last point shows that the changes of the surface energy are a consequence of the action of the inhibitors on the surface and not the reason of the absence of scale deposition. Moreover Förster et *al.* and Cheong et *al.* showed that the changes of the surface energy were not enough to explain the inhibition properties of a surface but parameters like surface roughness and chemical properties were essential as well to take into account [184, 204]. At higher concentration of inhibitors, the contact angle increased leading to less favourable scaling conditions. At 30ppm the inhibition of $CaCO_3$ was not only due to the changes of the contact angle onto the surface as a good inhibition efficiency were already observed at 10ppm (no weight gain were measured). Nevertheless it could be an alternative way to inhibit $CaCO_3$ deposition on a surface; the inhibitor strategy could be not to interact with the ions but to interact with the substrate directly leading to less favourable scaling conditions.

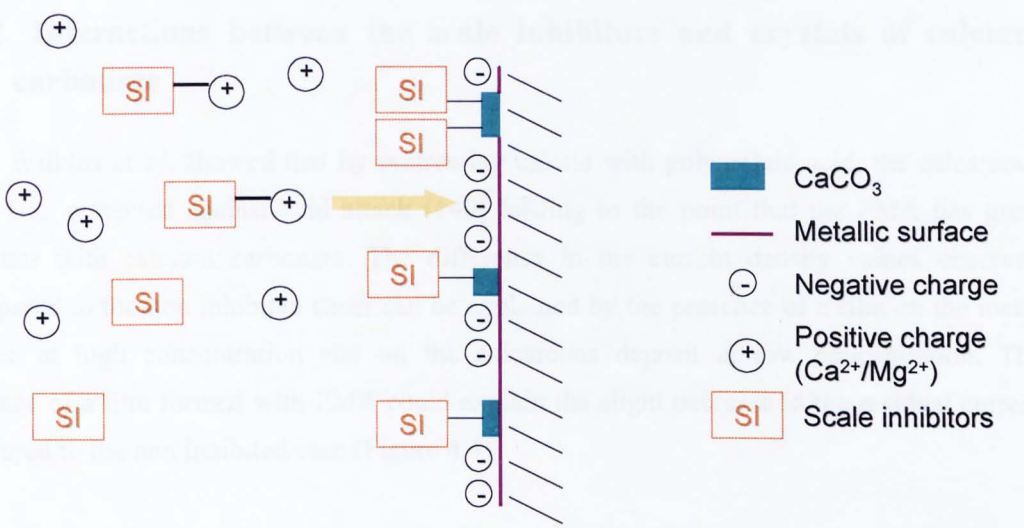

Figure 7.2: Scheme of the interactions between the scale inhibitors and the metal surface occurring under polarization conditions

In the absence of the carbonate ions, the film had greater properties regarding the oxygen diffusion (Figures 4.27 and 4.31). This point has been confirmed with the great decrease of the contact angle for the four inhibitors and the current density for the PPCA, PA and CMI. The light microscopy limits the detection of the small nuclei which could be present on the metal surface. Calcium ions can either binds the surface or the carbonate ions. The large decrease of the baseline of the current density in the carbonate-free solution suggests that the affinity of the calcium ions is greater for the carbonate ions than for the metal surface. It is well known that in the initial stage of $CaCO_3$ formation onto a surface, a Mg-containing film is deposited on the surface and this layer has a poisoning effects on $CaCO_3$ deposition [88]. In the absence of magnesium, the calcium carbonate formation occurs directly on the metal surface.

The increase of the baseline of the current density illustrated the absence of this thin layer. The availability of the calcium and magnesium ions was greater in the absence of carbonates thus the film formation was favoured in the absence of this anion. Moreover the calcium ions affected more the film formation than the magnesium ions as shown by the difference of the contact angle values in the absence of Ca^{2+} and Mg^{2+} (Figures 4.29 and 4.32).

The results showed that the mechanism of the inhibitor film formation for the four inhibitors was similar. Nevertheless there is no doubt that they all have different properties as different results were obtained with the current density study and the IR spectra (Table 4.3).

7.3.2 Interactions between the scale inhibitors and crystals of calcium carbonate

Wilkins et *al.* showed that by pretreating calcite with polymaleic acid, the calcareous layer was protected against acid attack [149] leading to the point that the PMA has great affinities with calcium carbonate. The difference in the current density values observed (compared to the non inhibited case) can be explained by the presence of a film on the metal surface at high concentration and on the calcareous deposit at low concentration. The presence of a film formed with PMA could explain the slight decrease in the residual current compared to the non inhibited case (Figure 4.4).

The microscopic observations realised *in-situ* (Figure 5.20) with 4ppm of PMA added 10 minutes after the creation of the supersaturation showed the presence of a film onto the crystals. This was not observed when the inhibitor was added before the mixing of the two brines. This indicates that PMA strongly interacts with $CaCO_3$.

In the absence of crystals on the surface, the film of PMA was not easily detected whereas when crystals of $CaCO_3$ were already formed onto the metal surface, the film was observed in a more obvious way.

The polyaspartic acid showed better affinities with the metal surface than with $CaCO_3$. The Langmuir isotherm illustrated the smaller affinity of the PA to the $CaCO_3$ compared to the PMA and the PPCA (Figure 7.3). It was seen previously that the PA had better inhibiting effects when it was added before the mixing of the brines and the PMA showed better growth inhibition than the PA when it was added 10 minutes after the supersaturation was created. These facts are explained with the different affinities of the PMA and the PA with metal surface and $CaCO_3$; the film of PA formed on the metal surface without $CaCO_3$ largely disturbed the nucleation and growth process whereas when $CaCO_3$ is already present the film on the metal surface, the crystals disturbed the film formation and therefore the inhibition of $CaCO_3$. The contrary occurred with the PMA. The PMA has strong affinity with $CaCO_3$ so when some crystals are present on the surface, the adsorption of the PMA is favoured and the inhibition properties are strong (as seen with the total blockage of the growth rate in Figure 5.21).

Wada et *al.* showed the high affinity of the carboxylic acids for $CaCO_3$ [193] leading to a inhibition of the growth of the crystals. Two carboxylates of the inhibitors interact with the adsorption site $-Ca(H_2O)^+$ by a mechanism of complexation. The strength of the binding depends on the geometry of the adsorbing molecules (distance between the two carboxylates) and on their substitution [181] which would explain the different affinities of the inhibitors with $CaCO_3$.

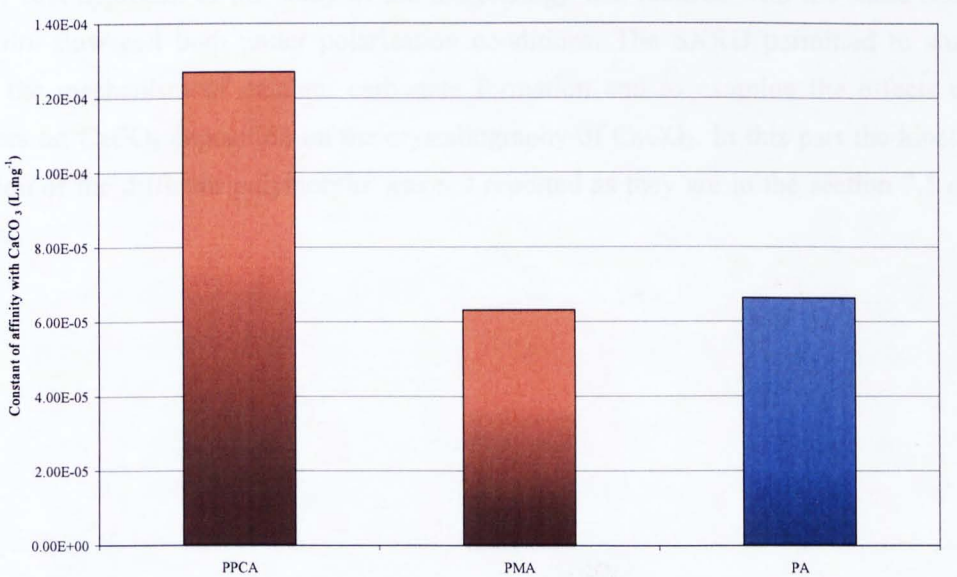

Figure 7.3: Constant of affinity of the inhibitors (K) with $CaCO_3$. *The values determined for the PPCA and the PMA are estimated meaning that the values presented are the minimum value of K.*

The carboxylic acids did not influence the nucleation stage, only the growth process showing a better affinity for the adsorption on $CaCO_3$ than for complexation for the free calcium ions in the solution [193]. Wada and co-workers were focused on the inhibition occurring in the bulk solution. In this study, the focus is the processes occurring on the surface. The formation of a film onto the metal surface probably disturbed more the nucleation process. The ability of the inhibitors to adsorb on the crystals of $CaCO_3$ is responsible of the variations of the growth. It is likely to think that a molecule act more specifically on one process of $CaCO_3$ formation but all the different stages of the mechanism are affected.

From this study, specific affinities have been pointed out:

- PPCA interacts with both the *metal surface* and the *crystals of $CaCO_3$*.
- PMA acts mainly by blocking the *growth sites of the crystals of $CaCO_3$*.
- PA affects greatly the *surface of deposition* resulting in a reduction of scaling.

7.4 Effects of SI on the morphology and on the crystallography of calcium carbonate

A first approach of the study of the morphology was realised with the static tests and the *in-situ* flow cell both under polarization conditions. The SXRD permitted to study in details the mechanism of calcium carbonate formation and to examine the effects of the inhibitors on $CaCO_3$ deposition on the crystallography of $CaCO_3$. In this part the kinetics of formation of the different polymorphs was not reported as they are in the section 7.5 of this chapter.

7.4.1 Morphology of the crystals in the presence of scale inhibitors

It has been largely reported that the presence of additives in the scaling solution affects the morphology of the crystals [44, 100, 205-213].

The average diameter of a single crystal of $CaCO_3$ formed under polarization conditions with the *in-situ* cell flow after 60 minutes was 11.6μm. The addition of 4ppm of PPCA, PMA and PA was needed to observe a significant decrease of the diameter of the crystals. Some crystals were probably affected by 1ppm of inhibitor but they were too small to be detected. The concentrations of CMI tested in this study did not lead to any significant change of the size of the crystals. A large decrease of the size of the crystals was observed with the PPCA, the PA and the PMA with a respective diameter of less than 0.5μm for PPCA and PA and of 2.7μm for the PMA.

Table 7.5: Summary of the changes of the morphology of the crystals of $CaCO_3$ formed after 60minutes with the in-situ flow cell under polarization conditions.

	1ppm	4ppm
No Inhibitor	Cubical calcite and leaf-like vaterite	
PPCA	Distorted calcite ++	Distorted calcite +++
PMA	Distorted calcite+	Distorted calcite +++
PA	Cubical calcite	Distorted calcite +++
CMI	Cubical calcite and Vaterite	Cubical calcite and Vaterite

+, ++, +++: *from a bit to strongly*

The PPCA has strongly affected the morphology of the crystals from 1ppm and the CMI did not change the morphology but an increase of the vaterite forms of $CaCO_3$ was observed. It seems that the changes of the morphology of the crystals are related to the inhibition properties discussed in the first part of this chapter; the greater the changes of the morphology, the better the inhibition properties (both studies have been realised under polarization conditions leading to a better comparison). It is difficult to conclude about the PA and the PMA regarding the link between the morphology of the crystals and the inhibition efficiency as their effects on these parameters were not as distinguished as the effects of the PPCA (greatest effects) and the CMI (poorest effects).

It is clear the addition of the inhibitors influenced the general shape of the crystals of calcium carbonate. The morphology changes could be promoted by the adsorption of the inhibitors on specific crystal planes leading to a complete modified general shape or they could act non-specifically and alter all the crystal planes. The use of the SXRD with the *in-situ* flow cell was an efficient tool in the determination of the effects of the additives on the crystallography of $CaCO_3$.

7.4.2 Effects of SI on the crystallography of $CaCO_3$

Kjellin studied the effects of two different organic compounds and pointed out that they affected differently the growth of $CaCO_3$: one was inhibited the vaterite growth and the second one affected the growth of the crystals of calcite [190]. It has been previously seen that the different inhibitors studied, affected differently the kinetics of formation of the three polymorphs thus this part is not treated of the kinetics but only of the morphology of the crystals of $CaCO_3$ formed.

The morphology of the deposit formed in the non-scaling brine was especially dominated by the aragonite, then the vaterite and at last the crystals of calcite were the least present in the cell. This order has not been modified with the addition of inhibitors except for the PPCA and the PMA at the concentration 4ppm. For these two cases, the deposit was still mostly composed of aragonite but the quantity of the vaterite forms decreased such as the calcite forms dominated the vaterite crystals in terms of quantity. These conclusions have been raised from the study of the total intensity for each polymorph as the intensity is proportional of the amount of crystals deposited on the substrate [214]. For the four inhibitors studied, the vaterite forms were the most inhibited. The PMA affected to the same extent the aragonite and the calcite crystals as well as the PA and the CMI. Nevertheless the inhibition of the vaterite was greater with the two carboxylic acids than the CMI. The PPCA affected the aragonite crystals to a greater extent than the calcite crystals. It appears that the PMA, the PA and the CMI act according to one selective inhibition (vaterite) and the PPCA according to two (first the vaterite and then the calcite).

Table 7.6 summarizes the main crystal planes of calcium carbonate formed in inhibited and non-inhibited conditions. The mechanisms of inhibition seems common to the four inhibitors. First of all, each crystal planes have been affected by the inhibitors present to different extent.

Secondly, they act by decreasing the volume quantity of the different crystal planes; either the size or the number of the crystals (most probably both). There was no emergence of new crystalline planes formed as it has been seen by SXRD *in-situ* measurement but on different substrate (PMMA and silicon, [73, 186]). Only the PPCA at the concentration 4ppm inhibited completely two main planes: the aragonite (032) and the vaterite (300). The inhibition of these two planes was probably linked to the sudden increase of the growth rate (as seen in the above kinetics study) of the calcite (006) and of the aragonite (111): the absence of two main crystal planes allowed the growth of the other two crystal planes. The system was in a sensitive zone as 4ppm was close to the MIC of the PPCA; the inhibition was strong as shown by the absence of the aragonite (032) and the vaterite (300) but not enough to maintain the inhibition on all the crystal planes.

Table 7.6: Review of the main crystal planes of calcium carbonate formed in the uninhibited brines and in presence of scale inhibitors and comparison of the total intensity (I_{total} in a.u).

		Calcite	I_{total}	Aragonite	I_{total}	Vaterite	I_{total}
Uninhibited brines		**006** 214, 211	154	**032, 111 031, 200**	555	**300, 110**	459
PPCA	1ppm	**006**	55	**200, 111 032, 031**	207	**110, 300**	159
	4ppm	**<u>006</u>**	74	**<u>111</u>**, 200 031, ~~032~~	121	**110,** ~~**300**~~	11
PMA	1ppm	**006** 214	59	**200, 032 111, 031**	216	**110, 300**	165
	4ppm	**006** 214	28	**200, 032 111, 031**	103	**110, 300**	51
PA	4ppm	**006** 214, 211	28	**200, 032, 111, 031**	103	**110, 300**	58
CMI	4ppm	**006** 214	54	**200, 111 032, 031**	204	**110, 300**	123

(006: crystal plane formed with a low intensity; ***006****: dominant crystal plane;* ***<u>006</u>****: take off of the crystal plane intensity after reduction;* ~~300~~*: suppression of the crystal plane.)*

Some differences of behaviour of the inhibitors regarding the calcite forms with a low intensity (calcite (214) and (111)) were seen: the PPCA acts as a nucleation inhibitor both, the PA acts as a growth inhibitor on both and the PMA and the CMI as a growth inhibitor on the calcite (214) and as a nucleation inhibitor on the calcite (111). The aragonite (310) emerged with 4ppm of PMA. The 2-theta values of the aragonite (310) and the calcite (111) are very close (1.61° and 1.62° respectively). Therefore it is hard to conclude about the effects of the scale inhibitors on these two crystal planes.

Table 7.7: Summary of the effects of 4ppm of PPCA, PMA, PA and CMI on the growth rate of the different crystal planes formed.

Crystal Planes	Totally Inhibited	Growth rate blocked	Growth rate strongly reduced	Growth rate reduced
C(211)/A(310)	PPCA	PMA/PA	-	CMI
C(006)	-	-	PMA/PA	CMI/PPCA*
C(214)	PPCA	PMA/PA	CMI	-
V(300)	PPCA	-	PMA/PA	CMI
V(110)	-	PPCA	PMA/PA	CMI
X	-	PPCA	PMA/PA	CMI
A(032)	PPCA	PMA/PA	-	CMI
A(031)	-	PPCA/PMA/PA	-	CMI
A(111)	-	-	PMA/PA/CMI	PPCA*
A(200)	-	PPCA/PMA PA/CMI	-	-
A(311)	PMA	PPCA/PA	CMI	-

(PPCA: first a reduction of the growth rate is observed and then a great increase)*

The inhibitors affected more the growth of the crystals than the nucleation process as most of the crystal planes formed in the non-inhibited case were found in the inhibited case (Table 7.7). They act by reducing or blocking the growth of the crystals. The PPCA showed in this entire study the best inhibition properties and only the PPCA inhibited the nucleation of two main planes. The inhibition of these planes results in a significant reduction of scale deposition as it was seen with the electrodeposition study. It seems that some specific crystal planes play an important role in the extent of inhibition of $CaCO_3$ deposition. The determination of the characteristics of these specific crystal planes could lead to a strategy of inhibition which would consist to design molecules to inhibit the growth of these key planes resulting in a reduction of the scale deposition. Nevertheless the PMA and the PA presented interesting effects on the calcium carbonate deposition too but none of the main crystal planes were totally inhibited showing that a chemical does not have to totally inhibit the crystal plane to show good inhibition properties but the blockage of the growth is one good alternative.

The changes of the growth of some different crystal planes can lead to the formation of a complete different crystal. The inhibitors affected all the crystal planes but to a different extent resulting in a different morphology of the deposit as it has been observed in the electrodeposition study. The effects of the chemicals on one specific crystal plane can be either due to the direct interactions between the inhibitor and the plane or it can be the consequence of the interactions with another crystal plane disturbing the growth of the considered plane.

The study of the effects of the inhibitors on the different polymorphs showed a selective inhibition of the vaterite forms of $CaCO_3$ but it did not appear any selective inhibition at the crystal plane level.

Table 7.8 summarises the crystal planes formed in different conditions and the length of the cell is proportional to the final intensity measured: comparing the size of the cell returns to compare the extent of the growth of the crystal planes. It is clear that 4ppm of PMA and PA have very similar effects on $CaCO_3$ growth. In both cases the same crystal planes are formed with a close final intensity. It is interesting to note that the crystal planes formed with 4ppm of PPCA are different from the planes formed with 4ppm of PMA but these two inhibitors seem to affect the $CaCO_3$ deposition to the same extent with 1ppm. A general trend can be draw. Under low inhibition conditions (PPCA 1ppm, PMA 1ppm, CMI 4ppm), the same crystal planes as in the non-inhibited case are formed with a reduced intensity. Under great inhibition conditions, two mechanisms are observed:

- Total inhibition of some main crystal planes and increase of the growth of other crystal planes (PPCA 4ppm),
- The same crystal planes formed in the non-inhibited case are formed with a smaller intensity (PMA and PA 4ppm). This mechanism is similar as the inhibition process occurring at low inhibition conditions mentioned above.

Table 7.8: Summary of the crystal planes detected by SXRD formed under non-inhibited and inhibited conditions in flowing conditions (laminar flow). The length of the cells are proportional to the final intensity measured.

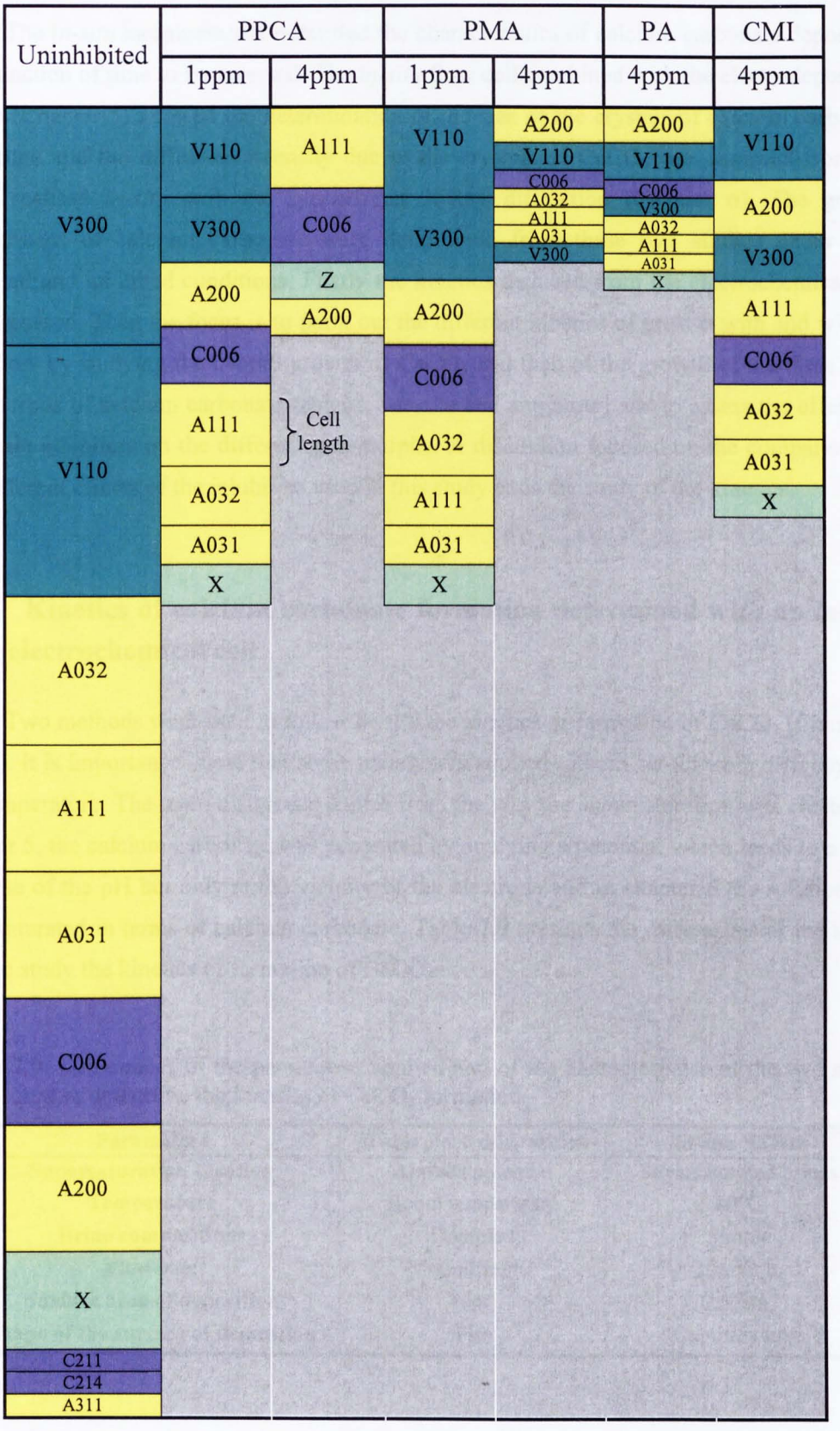

7.5 Kinetics of formation and inhibition of $CaCO_3$

The *in-situ* measurements permitted the characteristics of calcium carbonate deposition as a function of time to be assessed. The *in-situ* flow cell combined with the electrodeposition set-up (Chapter 5) allowed the determination of the size of the crystals of calcium carbonate over time and the diffracted intensity due to the crystals of $CaCO_3$ was assessed from the study realised *in-situ* with the synchrotron X-Ray diffraction (Chapter 6). The growth mechanisms of calcium carbonate were determined from these two studies under non-inhibited and inhibited conditions. Firstly the kinetics deduced from the electrochemical cell are discussed. Then the focus is to point out the different kinetics of growth with and without inhibitors by studying the overall growth of $CaCO_3$ and then of the growth of the three main polymorphs of calcium carbonate (calcite, vaterite and aragonite) and to assess the effects of the scale inhibitors on the different polymorphs. A discussion focused on the comparison of the different effects of the inhibitors used in this study ends the study of the kinetics.

7.5.1 Kinetics of calcium carbonate formation determined with an *in-situ* electrochemical cell

Two methods were used to follow *in-situ* the kinetics of formation of $CaCO_3$ (Chapter 5 and 6). It is important to note that some parameters applied to both set-up were different like the temperature. The main difference comes from the way the supersaturation was created. In chapter 5, the calcium carbonate was generated by applying a potential which leads to a large increase of the pH but only at the vicinity of the electrode and in chapter 6 the solution was supersaturated in terms of calcium carbonate. Table 7.9 presents the differences of the set-up used to study the kinetics of formation of $CaCO_3$.

Table 7.9: Differences of the parameters applied and of the characteristics of the two set-up used to determine the kinetics of $CaCO_3$ formation

Parameters	*In-situ* electrodeposition	*In-situ* SXRD
Supersaturation creation	Applied potential	Supersaturated brines
Temperature	Room temperature	80°C
Brine compositions	Complex	Simple
Flow rate	40ml/min	10ml/min
Surface area of deposition	$1cm^2$	$0.56cm^2$
Shape of the surface of deposition	Flat	Capillary tube

The estimation of the rate of the linear part of the curve assessing the changes of the size of the crystals as a function of time was considering as the growth rate of calcium carbonate as shown in Figure 7.4.

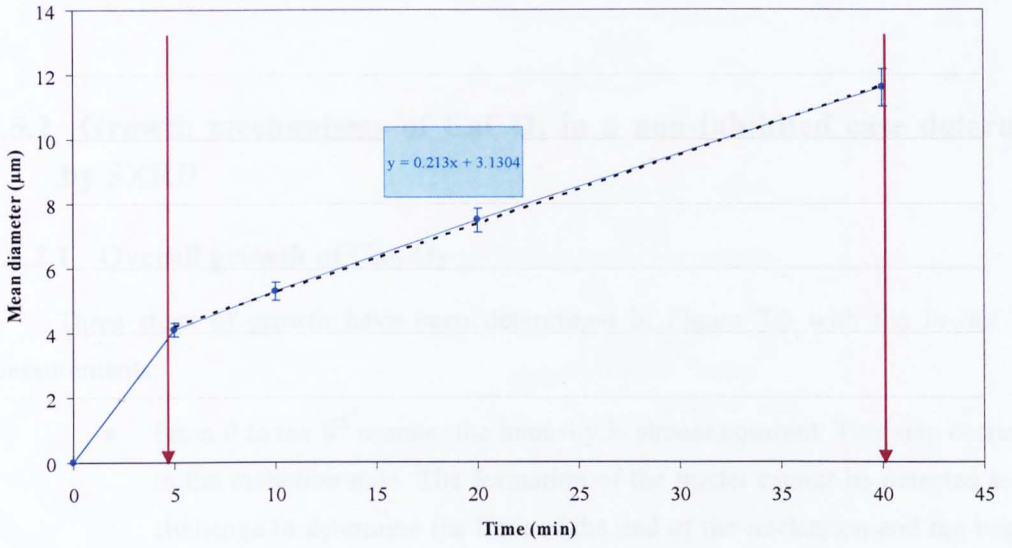

Figure 7.4: Illustration of the calculation of the growth rate measured with the *in-situ* electrochemical cell

The results are summarised in Table 7.10.

Table 7.10: Growth rate determined from the variations of the size of the diameter ($\mu m.min^{-1}$) of calcium carbonate (5 minutes after the creation of the supersaturation) determined with the *in-situ* flow cell combined with electrodeposition

Concentration	1ppm	4ppm
No Inhibitor	0.21	
PPCA	0.22	-
PMA	0.21	nil
PA	0.19	-
CMI	0.20	0.25

As the growth rate was a linear function of time from the 5th minute (similar for the non inhibited and inhibited case), Table 7.10 gives a summary of the growth rate measured from the 5th minute with the *in-situ* electrochemical flow cell. During the first 5 minutes the growth rates in the non-inhibited and inhibited case were similar (for the concentration 1ppm) ($0.82\mu m.min^{-1}$ for the non-inhibited case). The difference observed with 1ppm of inhibitor came only from the surface coverage and the number of crystals not from the growth rate. At this concentration the inhibitors only inhibit the growth of some crystals (in such an extent that they were not observed) but the crystals detected grew as in the non-inhibited case.

4ppm of inhibitors affect the overall of the deposition of $CaCO_3$ (except the CMI). Dawe *et al.* assessed the size of the crystals of calcium carbonate and established that the size was a linear function of the time. The first linear portion was not pointed out as the first measurements were done after 5 minutes [215].

7.5.2 Growth mechanisms of $CaCO_3$ in a non-inhibited case determined by SXRD

7.5.2.1 Overall growth of $CaCO_3$

Three steps of growth have been determined in Figure 7.5 with the *in-situ* SXRD measurements:

- From 0 to the 8th minute: the intensity is almost constant. This step corresponds to the *induction time*. The formation of the nuclei cannot be detected as it is a challenge to determine the limit of the end of the nucleation and the beginning of the growth process. It is likely to think that the growth of a nucleus occurs before the end of the nucleation process. Therefore only the growth steps are studied (the start of the nucleation probably occurs before the first measurement). The presence of the aragonite A(012) since the first measurement explains the value (not nil) of the intensity during the induction time. This point will be discussed later.

- From the 8th to the 26th minute: the total intensity largely increased and the increase is *linear*. This step is characterized by the emergence and the growth of new crystals planes. Nancollas and Reddy showed that a high growth rate may reflect a high surface area for growth produced by the nucleation process [29]. In our case, the slow down of the growth could be due to the saturation of the growth site of calcium carbonate.

- From the 26th minute to the 44th: the growth increases *slowly and then rapidly* The growth of calcium carbonate (leading to a decrease of calcium ions concentrations in the bulk) did not generate any decrease of the supersaturation in the capillary tube as 1l of brines were prepared for each test and only 600ml were pumped into the system. Therefore the stock of calcium and carbonate ions was always regenerated.

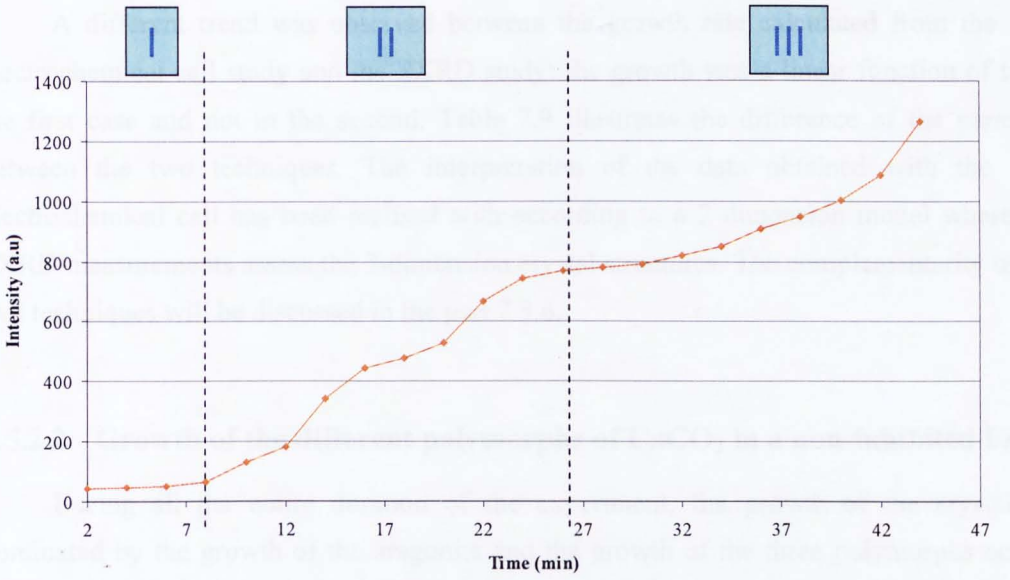

Figure 7.5: Different steps of growth of calcium carbonate determined from the Synchrotron X-Ray Diffraction study, in absence of inhibitors

The general growth trend (not linear) has already been reported in the literature as shown in [216]. The late increase of the growth has not been observed in this particular example. The growth of the crystals formed in a non-inhibited brine is characterized by (as shown in Figure 7.6):

- An induction time: intensity constant and nil (I)
- A 1st step of growth: linear (II)
- A 2nd step of growth: parabolic (III)

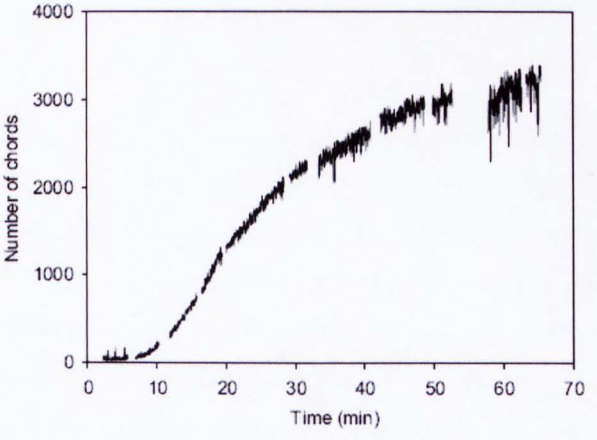

Figure 7.6: Example of a similar general trend of the kinetics of $CaCO_3$ precipitation [216]

A different trend was observed between the growth rate calculated from the *in-situ* electrochemical cell study and the SXRD study: the growth was a linear function of time in the first case and not in the second. Table 7.9 illustrates the difference of the parameters between the two techniques. The interpretation of the data obtained with the *in-situ* electrochemical cell has been realised with according to a 2-dimension model whereas the SXRD measurements assess the 3-dimension crystal structures. The complementarity of these two techniques will be discussed in the part 7.5.6.

7.5.2.2 Growth of the different polymorphs of $CaCO_3$ in a non-inhibited brine

During all the entire duration of the experiment, the growth of the crystals was dominated by the growth of the aragonite and the growth of the three polymorphs occurred under the same three regimes (I, II, III) (Figure 7.7). The main difference is observed during the second step: the growth of the dominant polymorphs (aragonite and vaterite) is not linear whereas the overall growth was. The emergence of the aragonite A(111) and A(031) first and then of the aragonite A(032) and A(200) lead to an increase of the total intensity of aragonite. Each emergence is followed by a great increase of the intensity illustrating an increase of the growth (Figure 7.7). The last step of growth is characterised by an increase of the growth according two different regimes. The growth first slows down and then rapidly increases.

The limit between the second and third step for the calcite growth trend is not as clear as for the aragonite and the vaterite as the calcite C(006) is the main calcite plane and the contribution of the two other calcite crystal planes (C(211) and C(214)) of the total intensity is small.

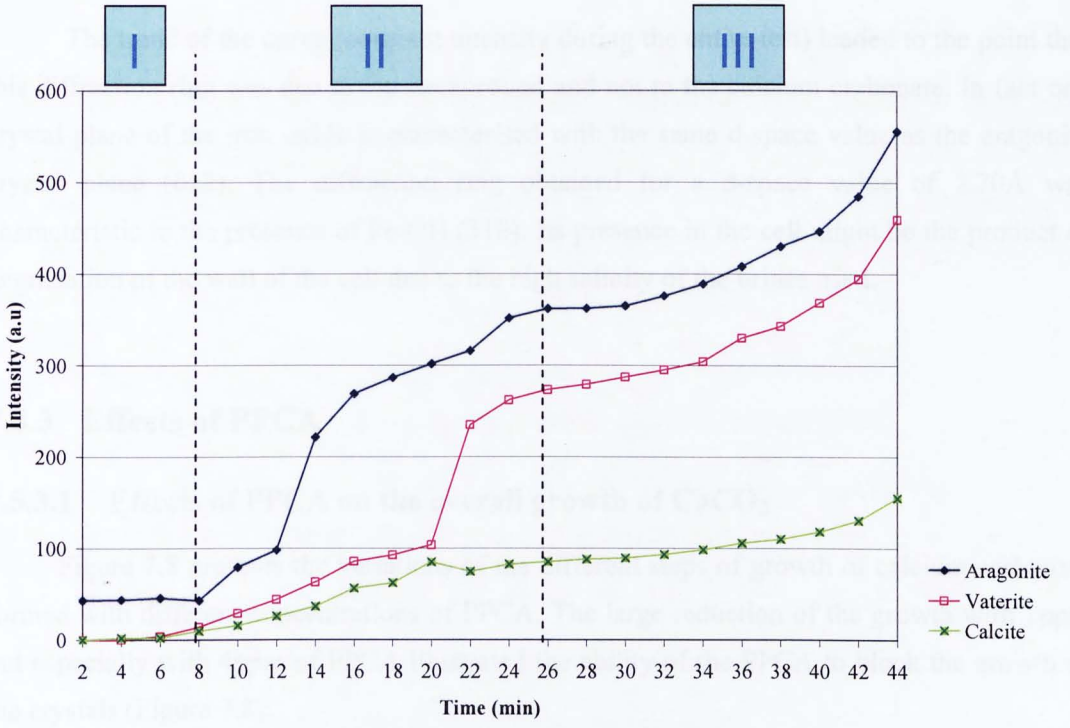

Figure 7.7: Different steps of growth of aragonite, vaterite and calcite determined from the Synchrotron X-Ray Diffraction study, in absence of inhibitors

The vaterite crystal planes growth is similar to the aragonite growth. Three steps characterised the growth mechanism. The induction time (until the 6th minute), the growth of the existing and the emergence of new planes (until the 24th minute) and the growth of all existing planes with the same two regimes as observed with aragonite.

A comparison of the different growth steps with and without inhibitors will be discussed after the review of the results obtained for the different inhibited cases.

Every crystal plane followed the same growth trend (Figure 6.1) with different characteristics (emergence time, growth rate, final intensity) except for the aragonite crystal plane (012). The diffraction ring corresponding to the d-space value (2.70Å) characteristic of the aragonite plane (012) was maintained constant during the entire duration of the experiment. The cell (stainless steel) used for the tests without inhibitors have been changed (for maintenance reason) and a new cell (hastelloy) was used when the inhibitors have been tested. This fact explains why this peak was only found for the non-inhibited case.

The trend of the curve (constant intensity during the entire test) leaded to the point that this diffraction ring was due to the background and not to the calcium carbonate. In fact one crystal plane of the iron oxide is characterised with the same d-space value as the aragonite crystal plane (012). The diffraction ring obtained for a d-space value of 2.70Å was characteristic to the presence of Fe-OH (310). Its presence in the cell might be the product of degradation of the wall of the cell due to the high salinity of the brines used.

7.5.3 Effects of PPCA

7.5.3.1 Effects of PPCA on the overall growth of $CaCO_3$

Figure 7.8 presents the variations of the different steps of growth of calcium carbonate formed with different concentrations of PPCA. The large reduction of the growth with 1ppm but especially with 4ppm of PPCA illustrated the ability of the PPCA to block the growth of the crystals (Figure 7.8):

- The growth with 1ppm of PPCA occurred under the three steps determined with the non-inhibited case. The difference between step II and step III is the decrease of the growth rate (there is no parabolic growth)
- The growth with 4ppm is more regular over time. The three steps are not observed.

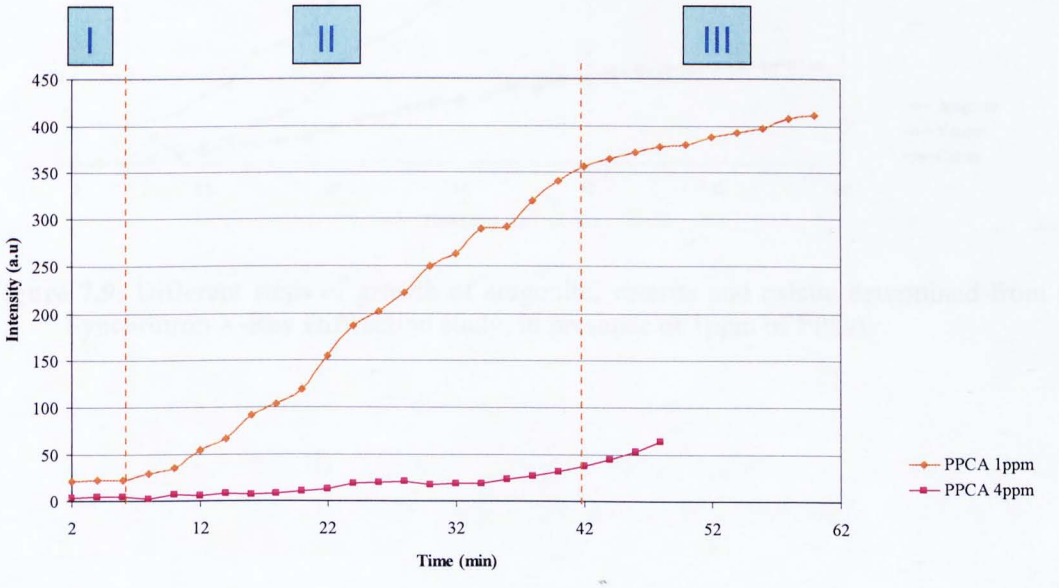

Figure 7.8: Different steps of growth of calcium carbonate determined from the Synchrotron X-Ray Diffraction study, in presence of PPCA

4ppm of PPCA delayed the growth of calcium carbonate. The nucleation might have been affected by the presence of PPCA but it is a real challenge to separate the nucleation step to the growth step. As soon as the nuclei are formed, the growth process starts leading to the fact that the limit of these two processes is hard to be determined and it is not possible with this technique.

7.5.3.2 Effects of PPCA on aragonite, vaterite and calcite growth

The growth of aragonite, vaterite and calcite follow the same trend (steps I, II and III) as seen with the overall growth of calcium carbonate with the non-inhibited case (Figure 7.9):

- Step I: induction time
- Step II: emergence and growth of new crystal planes
- Step III: Growth of existing crystal planes.

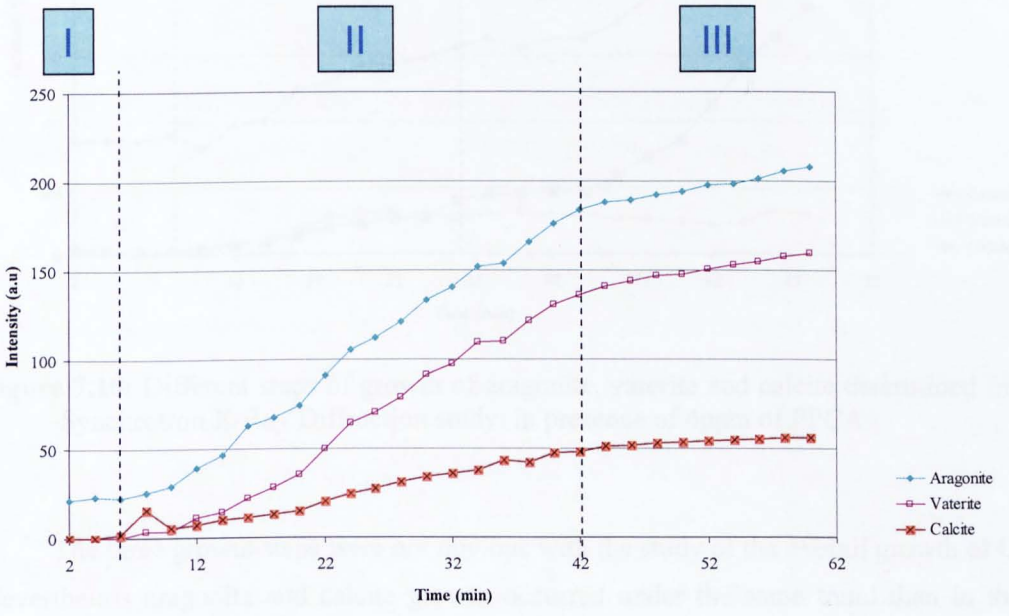

Figure 7.9: Different steps of growth of aragonite, vaterite and calcite determined from the Synchrotron X-Ray Diffraction study, in presence of 1ppm of PPCA

Only the crystals of aragonite and calcite were responsible of the late increase of the growth of the deposit. PPCA had stronger effects on the crystals of vaterite (blockage of the growth from the 17th minute) (Figure 7.10). This finding was confirmed by the ratio of the final intensity calculated in Table 6.3. According to these ratios, the PPCA was the least efficient on the calcite crystals although the large effects on the growth of the crystals were obvious (Table 7.8). The crystals of calcite were the least dominating of the deposit of calcium carbonate so even with a reduced growth the effects were not as great as the ones observed on the crystals of aragonite (which was the dominated polymorph).

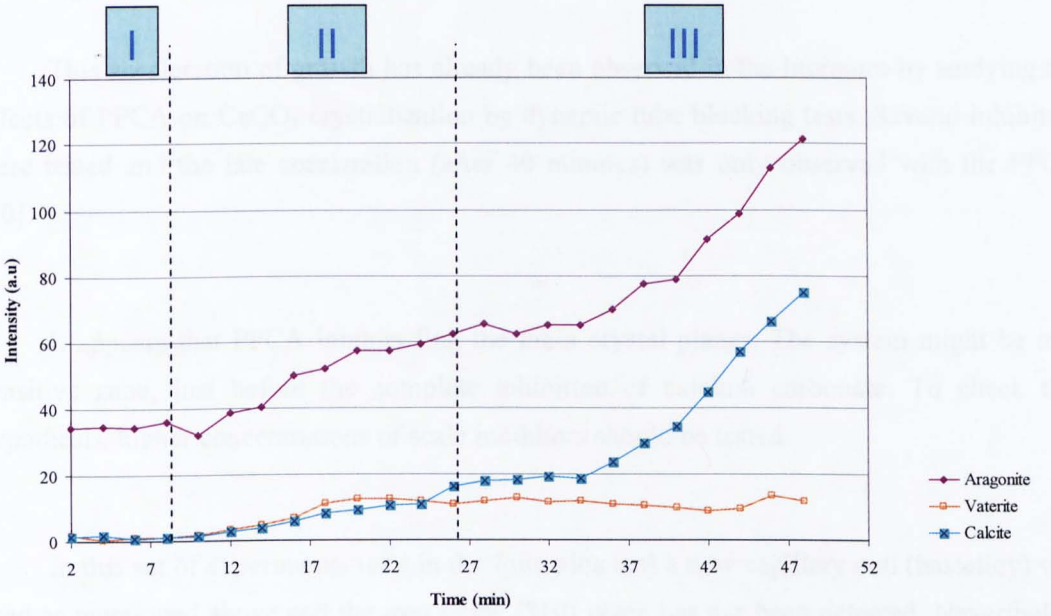

Figure 7.10: Different steps of growth of aragonite, vaterite and calcite determined from the Synchrotron X-Ray Diffraction study, in presence of 4ppm of PPCA

The three growth steps were not obvious with the study of the overall growth of $CaCO_3$. Nevertheless aragonite and calcite growth occurred under the same trend than in the non-inhibited case and with same duration of each step:

- Step I: Induction time
- Step II: 1st growth step
- Step III: 2nd growth step (parabolic), due to the calcite (006), the aragonite (111) crystal planes and the two unknown Y and Z plane

For 4ppm of PPCA, two major crystal planes (the vaterite (300) and the aragonite (032)) were totally suppressed and the intensity of the calcite (006) and the aragonite (111) crystal planes largely increased after the 34th minute. The concentration (4ppm) is probably really close to the MIC (Minimum Inhibitor Concentration) of the PPCA that is why there is no total inhibition of calcium carbonate formation; the suppression of some main crystal planes could enable the calcite (006) and the aragonite (111) to grow or because of the growth of these two crystal planes the vaterite (300) and the aragonite (032) are suppressed. One hypothesis is that PPCA does not favour the formation of specific crystal planes but the inhibition of some main planes leads to the growth of others. The increase of the growth could be a consequence of the inhibition of some main crystal planes.

This acceleration of growth has already been observed in the literature by studying the effects of PPCA on $CaCO_3$ crystallization by dynamic tube blocking tests. Several inhibitors were tested and the late acceleration (after 40 minutes) was only observed with the PPCA [70].

It appears that PPCA inhibits first the main crystal planes. The system might be in a sensitive zone, just before the complete inhibition of calcium carbonate. To check this hypothesis, higher concentrations of scale inhibitors should be tested.

In this set of experiments (and in the following set) a new capillary cell (hastelloy) was used as mentioned above and the iron oxide (310) plane has not been detected. Nevertheless the initial intensity of the aragonite (200) crystal plane was unexpectedly high compared to the other crystal planes. Contrary to what was observed with the Fe-OH (310) crystal plane, the growth rate of the aragonite (200) increased as a function of time for the concentration 1ppm. However for the concentration 4ppm, the growth rate was almost nil during the entire duration of the test.

The intensity of the aragonite (200) was in fact the combination of the diffracted beam due to the aragonite (200) and to another Fe-OH plane ((222) crystal plane) as the d-space value of these two planes are the same. At 4ppm of PPCA the intensity was high and constant therefore the diffracted beam was due to the cell itself; it was part of the background.

The pressure of the cell reached $2.8.10^6$ Pa (400psi) with 4ppm of PPCA after the 48th minute. The scale deposition in the capillary cell blocked the cell leading to an increase of the pressure. The total intensity of the diffracted beams due to $CaCO_3$ strongly decreased with the addition of 4ppm therefore the blockage of the cell was probably due to a big single crystal or an agglomerate formed, blocking off the cell.

Previously the results on the inhibition properties of the PPCA showed that no crystals were observed with 4ppm whereas in this study crystals of calcium carbonate were detected by SXRD. The divergence of the two techniques is discussed in the section 7.5.6.

PPCA (4ppm) leads to a large reduction of the growth of the vaterite, calcite and especially of the aragonite (Figure 7.10). The effects of the PPCA were observed since the early beginning of the process of calcium carbonate especially the vaterite and calcite crystals planes. The growth of the vaterite was almost blocked for the 45 minute test whereas the crystals of calcite and aragonite started growing after the 32nd minute. The growth of the vaterite crystals was small and rapidly kept constant.

PPCA enabled the blockage of the growth of the three polymorphs at the early stage of calcium carbonate formation. After 30 minutes, 4ppm of PPCA did not block the growth of the crystals of calcite and aragonite anymore even though the growth seems to become constant. The effects were time limited.

7.5.4 Effects of green carboxylic acids

7.5.4.1 Effects of PMA and PA on the overall growth of $CaCO_3$

Two different carboxylic acids were studied: the polymaleic acid and the polyaspartic acid. Both inhibitors had similar effects on the growth rate of calcium carbonate (Figure 7.11 and Figure 7.12). In both cases the growth occurs according to the three steps previously seen (Figure 7.5):

- Step I: induction time, the growth of the crystals is not detected
- Step II: emergence and growth of the new crystal planes
- Step III: 2nd step of growth (change of the growth rate, from linear to parabolic)

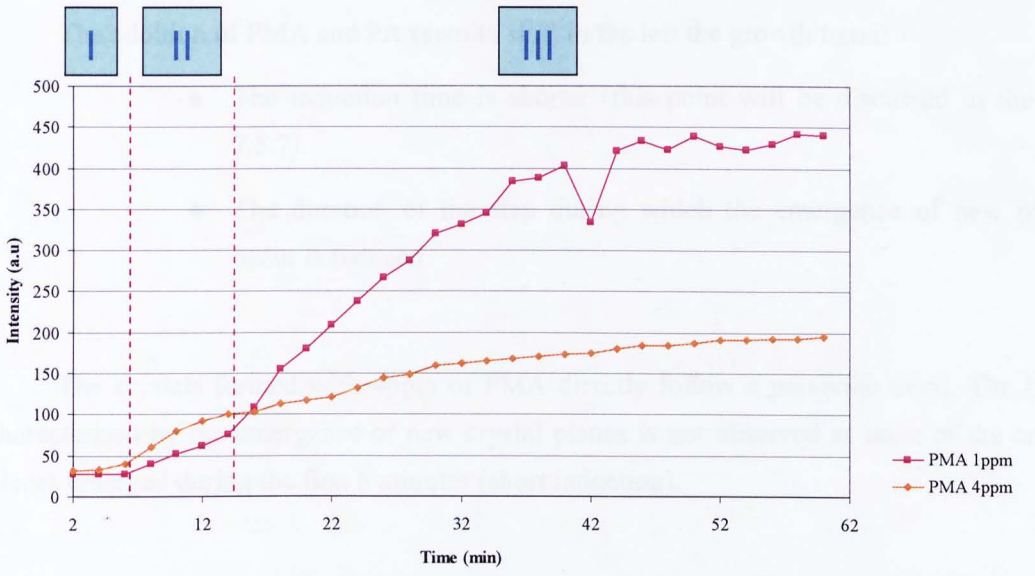

Figure 7.11: Different steps of growth of calcium carbonate determined from the Synchrotron X-Ray Diffraction study, in presence of PMA

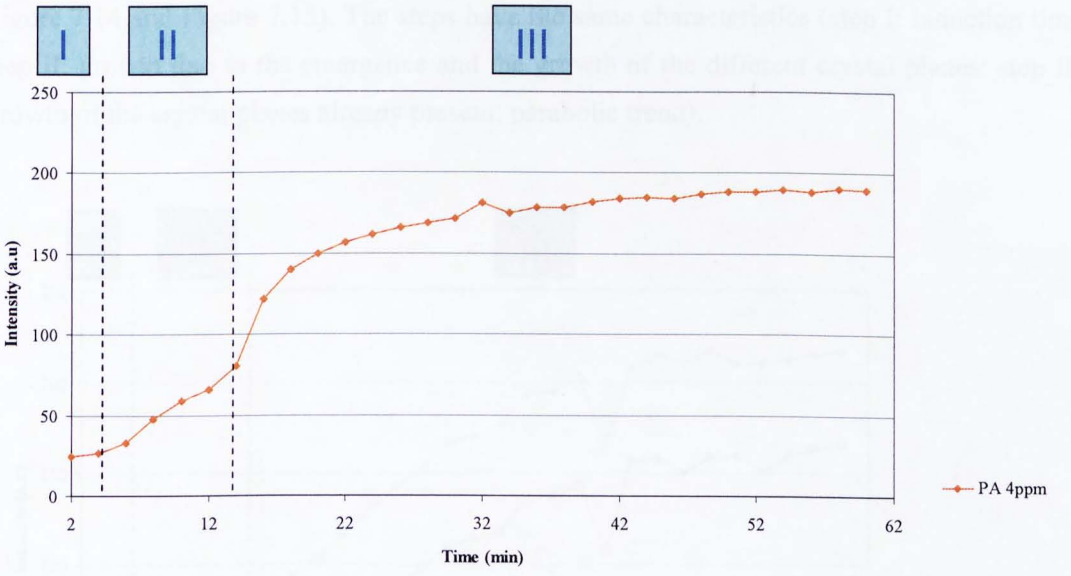

Figure 7.12: Different steps of growth of calcium carbonate determined from the Synchrotron X-Ray Diffraction study, in presence of PA

It seems that PMA had affected the induction time of some crystal planes to a greater extent than the PA. The induction time of the aragonite A(032) and the vaterite V(300) were increased with the addition of 4ppm of PMA resulting probably in the decrease of the induction time of the calcite (006). The delay of the emergence of two main crystal planes (A(032) and V(300)) was in favour of the early emergence of the calcite C(006).

The addition of PMA and PA seem to shift to the left the growth trend:

- The induction time is shorter (this point will be discussed in the part 7.5.7).
- The duration of the step during which the emergence of new planes occur is reduced.

The crystals formed with 4ppm of PMA directly follow a parabolic trend. The linear characterised by the emergence of new crystal planes is not observed as most of the crystal planes emerged during the first 6 minutes (short induction).

7.5.4.2 Effects of PMA and PA on the growth of aragonite, vaterite and calcite

The growth of the crystals of $CaCO_3$ with 1 and 4ppm of PMA and 4ppm of PA occurs according to the 3 growth step observed with no inhibitor and 1ppm of PPCA (Figure 7.13, Figure 7.14 and Figure 7.15). The steps have the same characteristics (step I: induction time; step II: growth due to the emergence and the growth of the different crystal planes; step III: growth of the crystal planes already present, parabolic trend).

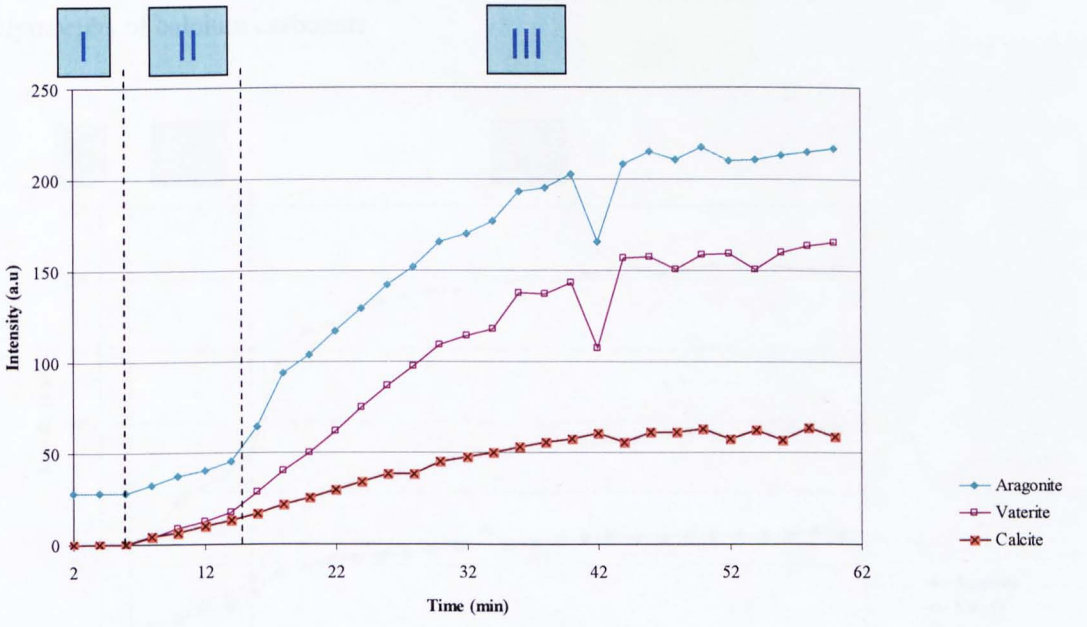

Figure 7.13: Different steps of growth of aragonite, vaterite and calcite determined from the Synchrotron X-Ray Diffraction study, in presence of 1ppm of PMA

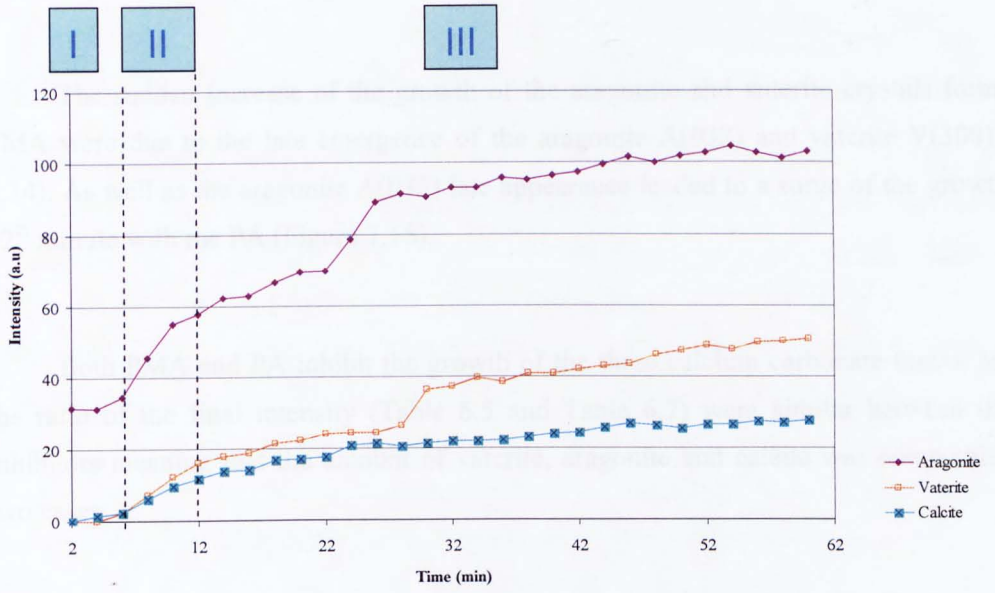

Figure 7.14: Different steps of growth of aragonite, vaterite and calcite determined from the Synchrotron X-Ray Diffraction study, in presence of 4ppm of PMA

4ppm of PMA and PA inhibited the growth of the three polymorphs of calcium carbonate. Both inhibitors strongly inhibited the growth of the aragonite, vaterite and calcite from the 30th minute as shown by the almost constant intensity (Figure 7.14 and Figure 7.15). The late increase observed with the PPCA was not seen with these two inhibitors. Once the crystal growth has been stopped, the blockage was maintained and this for the three polymorphs of calcium carbonate.

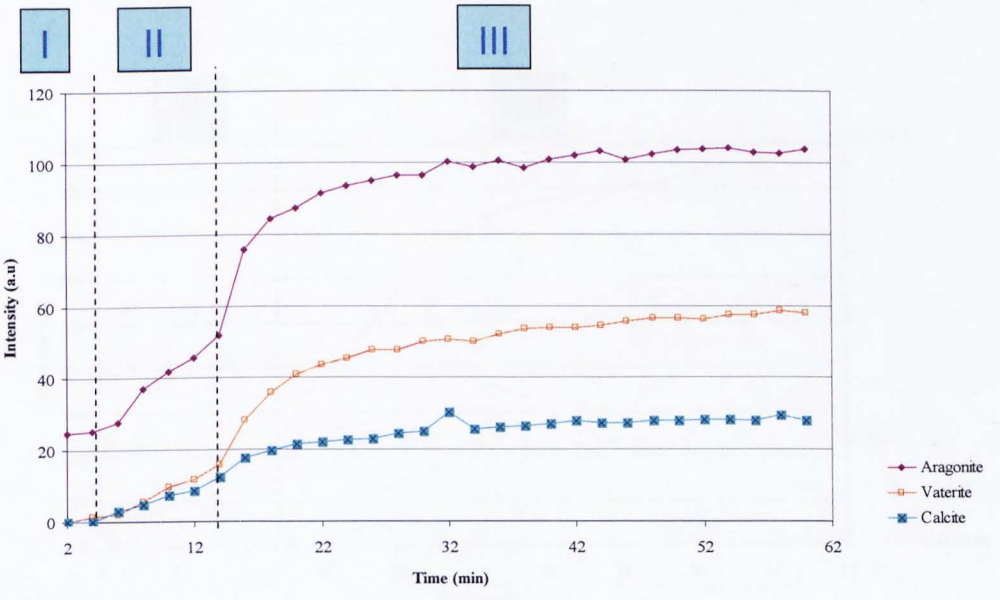

Figure 7.15: Different steps of growth of aragonite, vaterite and calcite determined from the Synchrotron X-Ray Diffraction study, in presence of 4ppm of PA

The sudden increase of the growth of the aragonite and vaterite crystals formed with PMA were due to the late emergence of the aragonite A(032) and vaterite V(300) (Figure 7.14). As well as the aragonite A(032) late appearance leaded to a surge of the growth rate at 12th minute with the PA (Figure 7.15).

Both PMA and PA inhibit the growth of the three calcium carbonate forms. Moreover the ratio of the final intensity (Table 6.5 and Table 6.7) were similar between these two inhibitors meaning that the amount of vaterite, aragonite and calcite was comparable in the two cases.

The shift observed for the overall growth of $CaCO_3$ is seen with the polymorphs with both PA and PMA. These two inhibitors decrease the induction time and the time of emergence of the new crystal planes.

7.5.5 Effects of CMI

7.5.5.1 Effects of CMI on the overall growth of $CaCO_3$

The induction time (step I) is too short to be determined with 4ppm of CMI therefore only two growth steps are determined. The first step is therefore step II compared to the other inhibitors. The emergence of the new crystal planes occurs during step II (Figure 7.16).

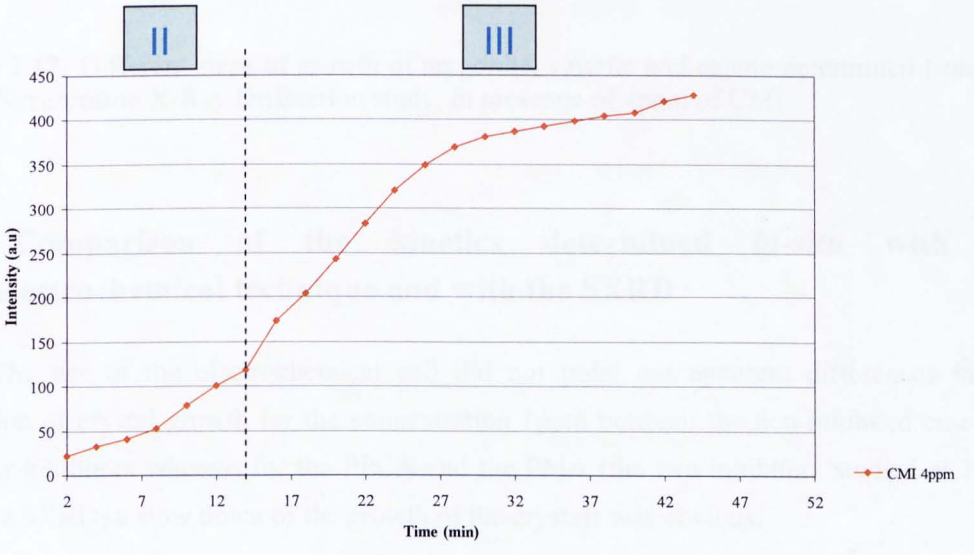

Figure 7.16: Different steps of growth of calcium carbonate determined from the Synchrotron X-Ray Diffraction study, in presence of CMI

7.5.5.2 Effects of the CMI on the growth of aragonite, vaterite and calcite

CMI affected the kinetics of growth of the three polymorphs to a different extent (Figure 7.17). The growth of the aragonite and the vaterite forms were less reduced than seen for the other inhibitors. The growth of the three polymorphs followed the same trend as observed in the non inhibited case but in a smaller extent. The early emergence of the aragonite A(200) explains why the induction time is not detected with the study of the total intensity: the aragonite A(200) was present in the cell during the first measurements (at 2 minutes). The growth of the vaterite and the calcite crystal planes occurs according to the three step model described previously. As observed with the PMA and the PA, the growth was strongly reduced from the 36th minute (slow increase of the intensity).

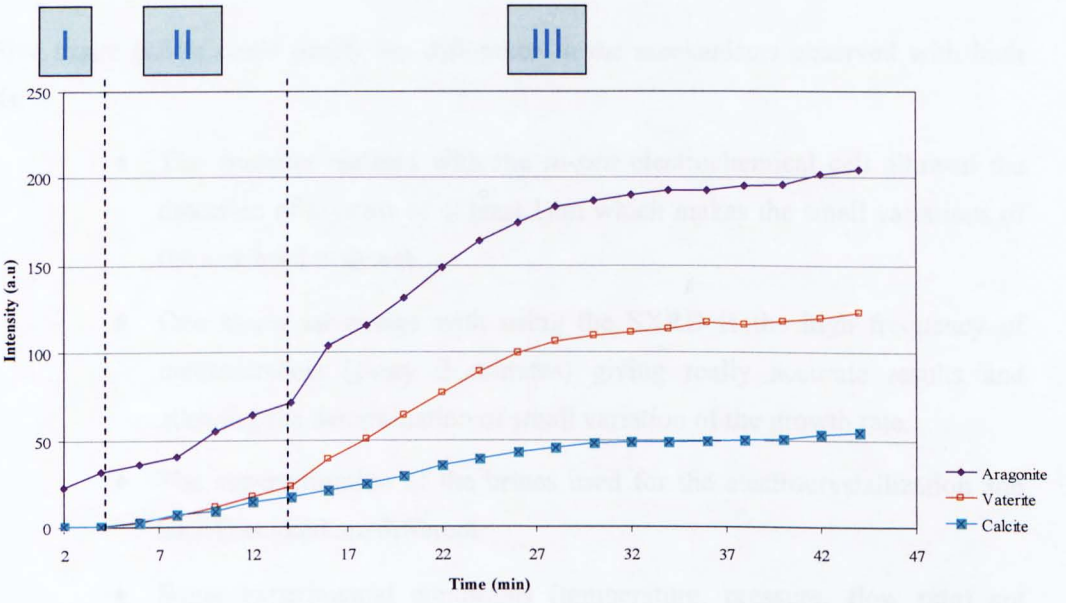

Figure 7.17: Different steps of growth of aragonite, vaterite and calcite determined from the Synchrotron X-Ray Diffraction study, in presence of 4ppm of CMI

7.5.6 Comparison of the kinetics determined *in-situ* with an electrochemical technique and with the SXRD

The use of the electrochemical cell did not point out apparent differences in the inhibition of crystal growth for the concentration 1ppm between the non-inhibited case and the four inhibitors whereas for the PPCA and the PMA (the two inhibitors studied at 1ppm with the SXRD) a slow down of the growth of the crystals was obvious.

1ppm is too low to affect all the crystals formed in the electrochemical cell thus it is likely to think that 1ppm of PPCA and PMA affected the growth of some crystals and their detection was not possible because of their resulting small size.

The main difference came from the tests conducted at 4ppm. No crystals of $CaCO_3$ were observed with the addition of PPCA and of PA with the electrochemical cell whereas a deposit of calcium carbonate was detected by SXRD. It is likely to find some crystals but too small to be detected on the SEM pictures. Both techniques illustrated the ability of the PMA to block the growth of the crystals. A large difference was observed with the CMI: in one case no growth inhibition property was noticed whereas the study by SXRD pointed out a reduction of the growth rate (but smaller to that observed with the other inhibitors).

Five major points could justify the difference in the mechanisms observed with both methods:

- The analyses realised with the *in-situ* electrochemical cell allowed the detection of crystals of at least 1µm which makes the small variations of the size hard to detect.
- One major advantage with using the SXRD is the high frequency of measurements (every 2 minutes) giving really accurate results and allowing the determination of small variation of the growth rate.
- The supersaturation of the brines used for the electrocrystallization and SXRD studied are different.
- Some experimental conditions (temperature, pressure, flow rate) are different (Table 7.9).
- A 2-dimension model is applied to extract the data from the electrochemical cell technique whereas 3-dimension information are obtained from the SXRD measurements. The use of a 2-dimension model can lead to the simplification of the mechanisms.

This shows the merits of using different techniques to quantify the amount of scale (electrochemical cell) and to get to the bottom of the mechanisms of the inhibition (SXRD).

7.5.7 Mechanisms of the growth inhibition of the scale inhibitors

Table 7.11 summarises the effects of the inhibitors on the induction time of the main crystal planes. It is difficult to classify the inhibitors according to their effects on the induction time as they act differently on the crystal planes. The induction time of the vaterite V(110) is almost unaffected by the presence of 4ppm of the scale inhibitors tested. The inhibitors decrease the induction time of the aragonite A(111) whereas they increase the induction time of the aragonite A(032) (except the PPCA which completely inhibit this plane). The effects of the inhibitors are not specific to the polymorph considering but to the crystal planes.

It has been seen during this study that the PMA and the PA have similar effects but it is interesting to note that they affect in an opposite manner the induction time of the vaterite V(300).

It is surprising to observe a decrease of the induction time of some main crystals whereas a delay of the growth is often combined with an increase of the induction time. Drach *et al.* showed that organic polymers can significantly inhibit the crystallization of calcium oxalate dehydrate by paradoxically enhancing the nucleation [217]. The hypothesis presented is that the inhibitors act as nucleation substrates. Once the nuclei are formed on the polymers their growth is then delayed. The PMA seems to act by delaying the growth for the vaterite V(300) and the aragonite A(032) but it seems to enhance the growth (and maybe the nucleation) of the aragonite A(111) and A(031) and of the calcite C(006).

The PA generates a decrease of the induction time for most of the main crystal planes. PA seems to act by enhancing the nucleation and then the growth rate is retarded (Table 7.11).

The CMI generally decreases the induction time whereas Demadis *et al.* pointed out the prolongation of the induction time with the addition of CMI [156]. Two main reasons could explain this contradiction. First of all, the crystallization of $CaCO_3$ has been assessed by absorbance measurements and maybe the presence of small nuclei could not be detected. Secondly, the range of concentrations used was much higher: 100 to 300ppm of CMI was used (whereas 4ppm was studied with the SXRD).

The PPCA presents various behaviour according to the crystal planes considered:

- Total inhibition of the vaterite V(300) and the aragonite A(032),
- No effect on the induction time for the vaterite V(110),
- Delay of the growth of the calcite C(006) and the aragonite A(031),
- Enhancement of the nucleation for the aragonite A(111).

Table 7.11: Summary of the effects of 4ppm of the scale inhibitors studied on the induction time of the main crystal planes formed. *(Green and orange: decrease and increase of the induction time respectively)*

	No inhibitor	PPCA	PMA	PA	CMI
V(300)	20	-	28	14	14
V(110)	4	4	4	2	4
A(032)	12	-	24	14	14
A(111)	8	2	4	4	4
C(006)	6	8	2	4	4
A(031)	8	16	6	6	8

For the three green inhibitors, the third step of growth is characterised by a constant growth. A small and constant growth of the crystals occurred whereas the growth measured for the non-inhibited case strongly increased. The effects of these inhibitors were the same but to a different extent. The growth sites of the crystals were blocked probably by the adsorption of the scale inhibitors on the $CaCO_3$ formed in the cell thus the creation of free growth sites did not occur as seen in the non-inhibited case [29].

The four inhibitors showed some growth inhibition properties, different according to the inhibitors used. Both carboxylic acid studied (PMA and PA) had similar effects on the inhibition of $CaCO_3$. Four different kinds of molecules were studied and they showed some difference in the inhibition of calcium carbonate. Each inhibitor has a specific affinity with calcium carbonate depending on many factors (like the molecular structure, the molecular weight, the conformation etc.) resulting in different inhibition properties.

7.6 Effects of SI on a calcareous layer already formed

This last part treats about the effects of the scale inhibitors when they have been added 5 or 10 minutes (according to the set-up and the method) after the creation of the supersaturation. Thus the nucleation process and the early growth occurred in a non-inhibited solution. This aims to understand how the inhibitors affect the crystals of $CaCO_3$ already formed and in a growing process and to point out any difference of the mechanisms of inhibition according to the presence or not of a calcareous layer to optimise their use.

7.6.1 Kinetics of inhibition

7.6.1.1 Effects of the PPCA

The study with the *in-situ* electrochemical cell illustrated the growth inhibition of the PPCA, the PMA and the PA on calcareous layer already formed (Table 7.12). The effects with PA were delayed of 10 minutes whereas the PPCA and the PMA affected the growth of the crystals as soon as they have been added.

Table 7.12: Growth rate ($\mu m.min^{-1}$) of calcium carbonate with and without inhibitors added at t= 0 and t=10minutes after the creation of the supersaturation determined with the *in-situ* flow cell combined with electrodeposition

Concentration	4ppm t=0	4ppm t=10min
No Inhibitor	0.21	
PPCA	no crystals	nil
PMA	nil	0.06
PA	no crystals	0.065
CMI	0.21	0.25

No SXRD measurement have been done during the 5minutes of the building-up of the calcareous layer as it was impossible to reach the system (to add the inhibitors) once the beam was on. The same experimental conditions as before were applied thus a measurement every 2 minutes was taken meaning that the first measurement was realised at the 7^{th} minute compared to the non-inhibited brine. The values of the intensity were not comparable as the inhibitors were already in the solution when the first measurement was done. Nevertheless a similar or lower value for a same crystal plane was expected when the inhibitor was added after 5 minutes than the intensity measured in the non-inhibited brine.

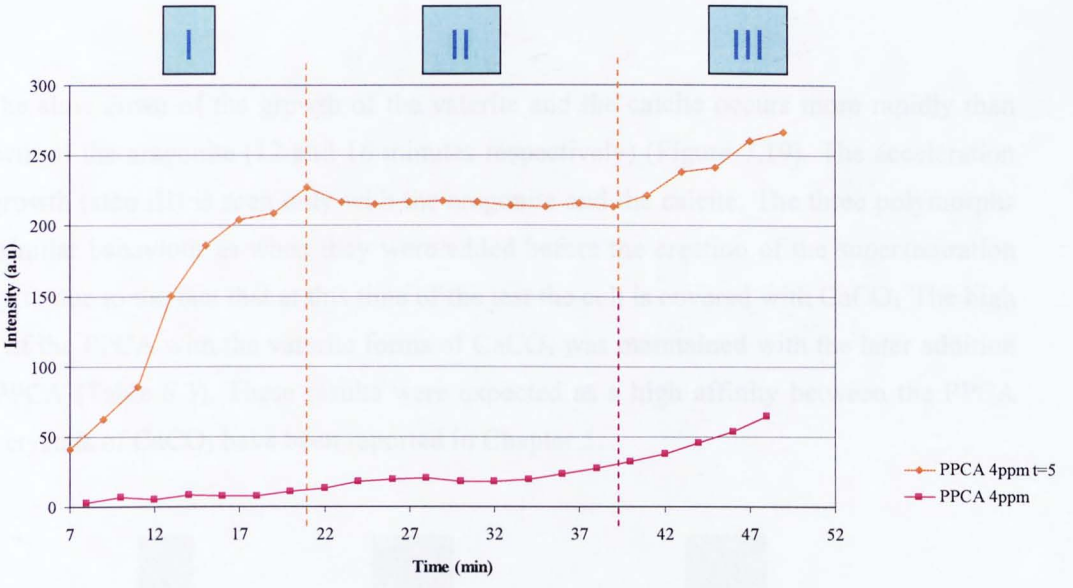

Figure 7.18: Different steps of growth of calcium carbonate determined from the Synchrotron X-Ray Diffraction study, in presence of 4ppm of PPCA added before and 5minutes after the creation of the supersaturation

The step I previously characterised the induction time when the inhibitors were added before the creation of the supersaturation. In this part, the induction time could not be measured for the reasons mentioned above. Step I in this case is characterised by a large increase of the growth of the crystals of $CaCO_3$. There is a delay in the ability of the PPCA to inhibit the growth of the crystals when they are added after 5 minutes (Figure 7.18). This shows that the PPCA interfere at the beginning of the crystallisation process which is in a good accordance with the fact that PPCA is a nucleation inhibitor [145].

Then the growth is slowed down and kept constant during the second step (step II). The same late acceleration of the growth is observed after 40 minutes as observed previously (step III).

The intensity depends on the volume quantity of crystals [177]. A chemical can either act on the size or the number of crystals. The nucleation process is likely to be finish after 5 minutes (as seen in Chapter 5) so the PPCA can only act on the growth process in the experimental conditions.

The slow down of the growth of the vaterite and the calcite occurs more rapidly than the growth of the aragonite (12 and 16 minutes respectively) (Figure 7.19). The acceleration of the growth (step III) is seen only with the aragonite and the calcite. The three polymorphs have a similar behaviour as when they were added before the creation of the supersaturation probably to due to the fact that at this time of the test the cell is covered with $CaCO_3$. The high affinity of the PPCA with the vaterite forms of $CaCO_3$ was maintained with the later addition of the PPCA (Table 6.3). These results were expected as a high affinity between the PPCA and the crystals of $CaCO_3$ have been reported in Chapter 5.

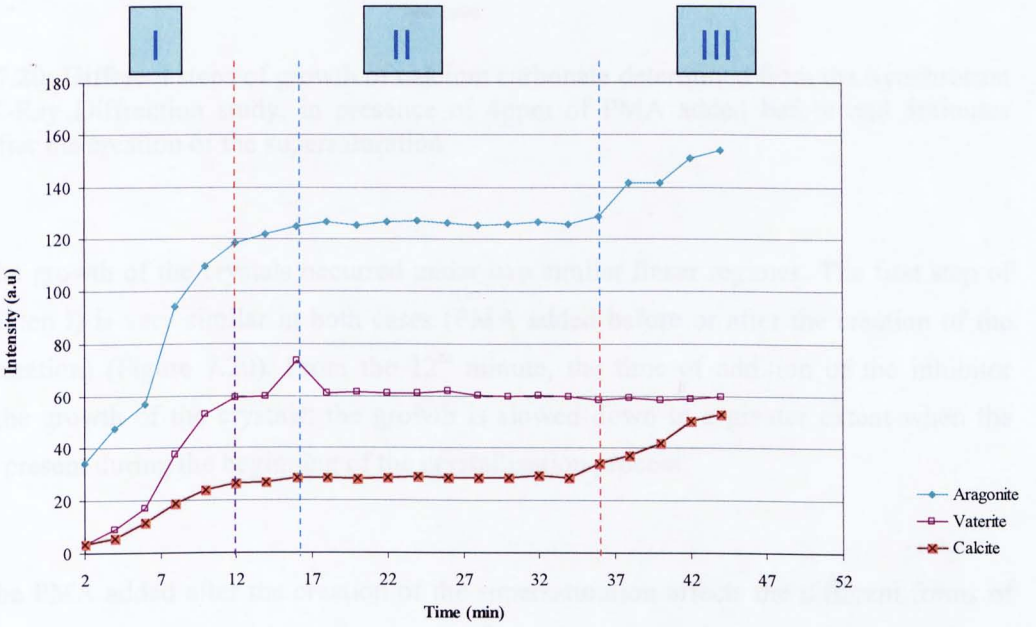

Figure 7.19: Different steps of growth of aragonite, vaterite and calcite determined from the Synchrotron X-Ray Diffraction study, in presence of 4ppm of PPCA added 5minutes after the creation of the supersaturation

7.6.1.2 Effects of PMA

It was previously found that PMA acted more as a growth inhibitor thus the difference between added the inhibitor after or before the creation of the supersaturation had fewer effects than for the PPCA (Figure 7.20). This illustrates the higher affinity of the PMA with the crystals of $CaCO_3$ than with the metal surface (as seen in Chapter 5).

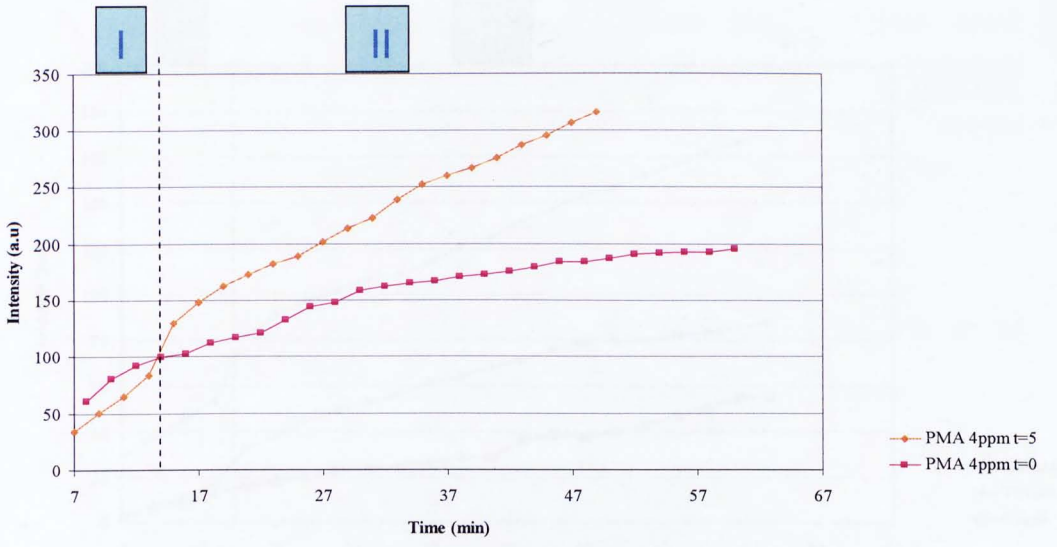

Figure 7.20: Different steps of growth of calcium carbonate determined from the Synchrotron X-Ray Diffraction study, in presence of 4ppm of PMA added before and 5minutes after the creation of the supersaturation

The growth of the crystals occurred under two similar linear regimes. The first step of growth (step I) is very similar in both cases (PMA added before or after the creation of the supersaturation) (Figure 7.20). From the 12th minute, the time of addition of the inhibitor affects the growth of the crystals: the growth is slowed down in a greater extent when the PMA is present during the beginning of the crystallization process.

The PMA added after the creation of the supersaturation affects the different forms of calcium carbonate (Figure 7.21). The three polymorphs follow the same two-step model previously seen whereas the growth trend of the vaterite formed with PPCA was different as the aragonite and calcite growth trend. An acceleration of the growth of the aragonite A(111) and the calcite C(006) is observed at the 26th minute as seen with the PPCA but not with the PMA when it was added before the creation of the supersaturation. These two planes seem to be very sensitive at the concentration (close to the MIC) of the inhibitors added. The change of the growth rate at the 14th minute is due to the emergence of the aragonite (032) and the vaterite (300).

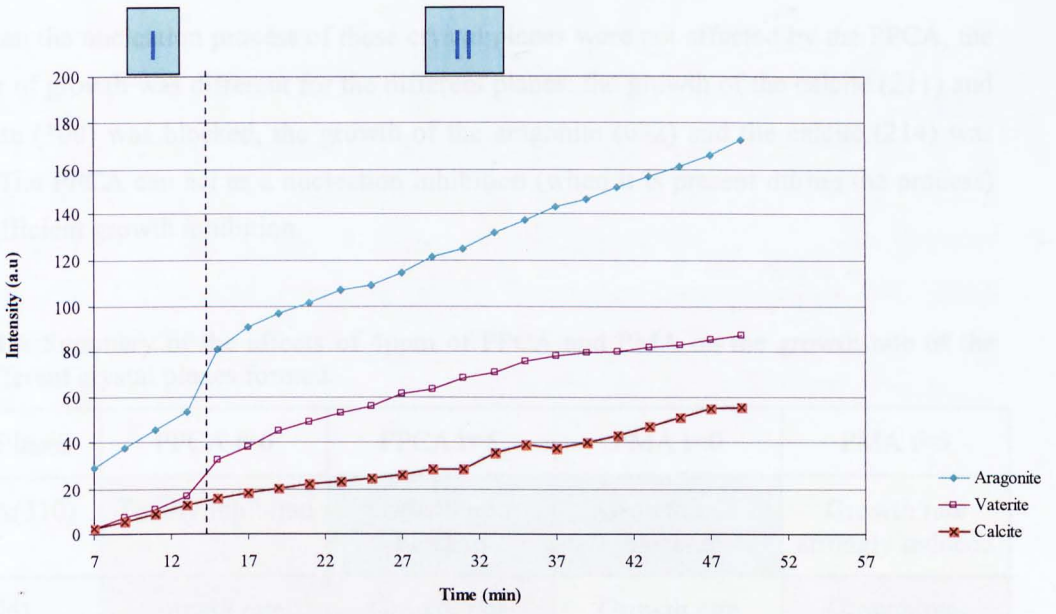

Figure 7.21: Different steps of growth of aragonite, vaterite and calcite determined from the Synchrotron X-Ray Diffraction study, in presence of 4ppm of PMA added 5minutes after the creation of the supersaturation

A complete different mechanism of inhibition is observed between PPCA and PMA added after the creation of the supersaturation:

- PPCA blocks temporarily the growth of the crystals and then the growth occurs again (the second point has not been revealed with the *in-situ* electrochemical cell).
- PMA reduced the growth (without blocking) of the crystals first (a blockage of the growth was observed with the *in-situ* electrochemical cell).

7.6.2 Inhibition of the different crystal planes

The late addition of the PMA affected the growth of the crystals of $CaCO_3$ by strongly reducing the growth for all the crystal planes (Table 7.13). They were not different behaviour as observed when the PMA was added before the creation of the supersaturation. It exists a correlation between the inhibition behaviour with the addition of the PPCA regarding the time of addition; the PPCA acted by blocking the growth rate of some crystal planes when it was added before and after the mixing of the two brines (V(110), X, A(031), A(200) and A(311)). The crystals had the same behaviour whether the PPCA was added before or after the creation of the supersaturation. The PPCA acted as a nucleation inhibitor for the calcite (211) and (214), for the vaterite (300) and for the aragonite (032).

When the nucleation process of these crystal planes were not affected by the PPCA, the behaviour of growth was different for the different planes: the growth of the calcite (211) and the vaterite (300) was blocked, the growth of the aragonite (032) and the calcite (214) was reduced. The PPCA can act as a nucleation inhibition (when it is present during the process) or as an efficient growth inhibition.

Table 7.13: Summary of the effects of 4ppm of PPCA and PMA on the growth rate of the different crystal planes formed.

Crystal Planes	PPCA t=0	PPCA t=5	PMA t=0	PMA t=5
C(211)/A(310)	Totally Inhibited	Growth rate blocked	Growth rate blocked	Growth rate strongly reduced
C(006)	Growth rate reduced*	Growth rate reduced*	Growth rate strongly reduced	Growth rate reduced*
C(214)	Totally Inhibited	Growth rate strongly reduced	Growth rate blocked	Growth rate strongly reduced
V(300)	Totally Inhibited	Growth rate blocked	Growth rate strongly reduced	Growth rate strongly reduced
V(110)	Growth rate blocked	Growth rate blocked	Growth rate strongly reduced	Growth rate strongly reduced
X	Growth rate blocked	Growth rate strongly reduced	Growth rate strongly reduced	Growth rate strongly reduced
A(032)	Totally Inhibited	Growth rate strongly reduced	Growth rate blocked	Growth rate strongly reduced
A(031)	Growth rate blocked	Growth rate blocked	Growth rate blocked	Growth rate strongly reduced
A(111)	Growth rate reduced*	Growth rate reduced*	Growth rate strongly reduced	Growth rate reduced*
A(200)	Growth rate blocked	Growth rate blocked	Growth rate blocked	Growth rate strongly reduced
A(311)	Growth rate blocked	Growth rate blocked	Totally Inhibited	Growth rate strongly reduced

(Growth rate reduced: first a reduction of the growth rate is observed and then a great increase)*

It is interesting to note that the intensity of the calcite (006) and aragonite (111) largely increased from the 34th minute with 4ppm of PPCA added before and after the creation of the supersaturation. This phenomenon was only observed when the PMA was added when a calcareous layer was pre-formed but in a smaller extent. The growth of the calcite (006) and of the aragonite (111) was blocked with the PPCA and then enhanced whereas the PMA reduced only the growth of the crystal planes. These two planes had similar growth as the other planes in the non-inhibited solution. The inhibition of both crystal planes was limited in time.

7.7 Implications for industry

In this part the contributions of this thesis to the industry associated with scale control and scale management is presented.

It has been reported in this thesis that different mechanisms of inhibition exist according to the affinity of the chemicals with either the metal surface or the crystals of $CaCO_3$. The environment where the scaling deposition occurs can lead to the choice of the inhibitor to use. Some inhibitors like the PPCA and the PMA interact strongly with the crystals of $CaCO_3$. Some surfaces are difficult to reach and the removal of scale can be cost effective (like in the pipes for example). In that case, the PPCA and the PMA are two potential inhibitors to use as they interact with the calcareous layer already formed onto the surfaces resulting in a reduction of the deposition. On the contrary, the PA can be used preferentially on clean equipment to prevent any scale deposition as the film of inhibitor formed reduced more efficiently the scaling deposition.

In the SXRD study the deposit was aragonite dominant with and without the addition of inhibitors. The inhibitors did not block completely the growth of the crystals of aragonite and often a late increase of the growth was observed. It seems that reducing only the aragonite crystals or specific crystal planes of aragonite would result in a general reduction of the deposition. The target of the inhibitors could be the aragonite in order to block the growth of the dominant polymorph therefore the growth of the deposit would be reduced.

The two different *in-situ* techniques used in this thesis revealed new features to understand the mechanisms of inhibition. For the field applications, the electrochemical cell gives interesting data about the kinetics of $CaCO_3$ and a quick estimation of the potential scaling risks could be determined. The disadvantage is the difficulty to reproduce realistic conditions. The *in-situ* cell used with the SXRD is easily applicable to realistic conditions (ie. substrate, high temperature and pressure, composition of the water) and the accuracy of the results provides reliable data. The process of the data and the complex use of this tool make it difficult to apply it directly to the field.

For industry the suggestion in this thesis that the inhibitors have selective preference to inhibit certain planes more strongly is important and could help to lead ultimately to the molecular design of new inhibitor molecules.

Chapter 8
Conclusions

8.1 Introduction

This section gives a summary of the different conclusions raised from this thesis. Different approaches have been used to study the formation and the inhibition by green chemicals of $CaCO_3$ deposition on a metal surface. The conclusions are given according to five key points of this study. First the conclusions about the *interactions* of the inhibitors and the metal surface are summarised. Then, the findings related to the *adsorption* of the chemicals on the $CaCO_3$ are given. The *mechanisms of inhibition* and the effects on the *morphology* of the crystals are then proposed for the different inhibitors. The contribution of the *in-situ* methodologies are reviewed. Finally, the Synchrotron X-Ray Diffraction as a tool to study scale formation is considered.

8.2 Interactions between the inhibitors and the metal surface

It was known that some inhibitors interact with the surface to inhibit $CaCO_3$. This study permitted the detection of an inhibitor film on a metal surface . The principal conclusions related to the interactions between the inhibitors and the metal surface are raised below.

- The presence of an inhibitor film on a metal surface has been detected by chronoamperometry and/or by Fourier Transform Infra-Red spectroscopy. PPCA, PMA, PA and CMI inhibit partly calcium carbonate formation by forming a film on the surface.

- The inhibitors interact with the surface via cations (Ca^{2+}/Mg^{2+}). The properties of the film formed onto the surface is specific to the inhibitor as different techniques (showing different characteristics of the film) were needed to point out the presence of the film.

- The changes of the contact angle of the surface is a consequence of the presence of the inhibitors and not the strategy to inhibit calcium carbonate formation. Nevertheless both approaches (chemical treatment and physical modification of the surface) are potential strategies to inhibit $CaCO_3$ deposition.

8.3 Adsorption of the inhibitors on $CaCO_3$

The inhibitors not only interact with the substrate of deposition but with crystals of $CaCO_3$. The different adsorption properties on $CaCO_3$ of the inhibitors results in different abilities to inhibit $CaCO_3$ when a calcareous layer is already formed on the surface. This illustrates the significance of characterising the scale inhibitors in order to optimize their conditions of use. The scale inhibitor used in the industry in a system already affected by scale can be different than the inhibitor used in a clean system, for a prevention treatment for example. PMA and PPCA present a great affinity with $CaCO_3$ and an inhibitor film was detected with the addition of 4ppm of PMA added 10 minutes after the beginning of the crystallization process. PA interact more with the surface metal.

8.4 Mechanisms of inhibition

The mechanisms of $CaCO_3$ formation and inhibition was investigated by chronoamperometry, *in-situ* electrochemical flow cell and *in-situ* SXRD.

- $CaCO_3$ formation occurs under three steps of growth. First there is an induction time, then the total growth largely increases due to the emergence of new crystal planes. In the last step, the growth slows down and then an acceleration of the growth occurs.

- The growth of most of the crystal planes in a inhibited system depends on the moment the inhibitors are added. The aragonite A(032) is completely inhibited when PPCA is added before the creation of the supersaturation whereas it is only reduced when the PPCA is added 5 minutes after the start of the crystallization. The PPCA can act as a nucleation inhibitor when it is present at the early stage of $CaCO_3$ formation.

- PPCA presented the greatest inhibition efficiency of $CaCO_3$ deposition during the different studies. PMA and PA affect the $CaCO_3$ formation in a very similar way. A common trend of calcium carbonate inhibition was observed for both carboxylic acids. The effects of CMI were less significant than for the other inhibitors.

- PPCA and PA seems to affect the nucleation and the growth of the crystals whereas the effects of PMA are predominant during the growth process.

8.5 Effects on the morphology

The morphology was studied with the *in-situ* electrochemical cell and the Synchrotron X-Ray Diffraction.

- The electrochemical flow cell showed that 1ppm PPCA, PMA and PA affected the morphology of the crystals of $CaCO_3$.

- The SXRD showed that the aragonite is the dominant form of $CaCO_3$ crystallized under the specific experimental conditions (SXRD study). Vaterite and calcite were formed as well in the cell.

- The same crystal planes formed in the non-inhibited case were formed in the inhibited cases and the growth of all the crystal planes were affected by the presence of the scale inhibitors.

- The PMA, PA and CMI inhibit $CaCO_3$ formation by reducing the growth of all the crystal planes whereas the PPCA totally inhibits two main crystal planes (aragonite (032) and vaterite (300)).

- The acceleration of the growth of the calcite C(006) and of the aragonite A(111) was only observed with the PPCA.

- The 4 inhibitors seem to inhibit preferentially the vaterite forms.

8.6 *In-situ* methodologies

The *in-situ* methodologies provided important information in the mechanism of $CaCO_3$. The inhibitors usually affect both the nucleation and the growth processes but one mechanism of inhibition often predominates.

- The ability of PPCA and PA to affect the $CaCO_3$ formation during the early stage has been pointed out with the *in-situ* electrochemical cell.

- The inhibitor film has been detected by *in-situ* visualization for the PMA added 10 minutes after the start of the crystallization.

- The assessment of the size of the crystals over time permitted to point out different inhibition mechanisms.

8.7 Synchrotron X-Ray Diffraction

The Synchrotron X-Ray Diffraction is a very accurate tool to study scale formation under different conditions (temperature, pressure, flow rate, water composition, nature of the substrate etc.). Its use is a novelty in the scale area and it brought in the past new findings about $CaCO_3$ formation. The study of the effects of green inhibitors with the SXRD determined the different steps of growth and the difference of the mechanisms of inhibition of the different chemicals used.

This technique provided information on the growth of the different polymorphs and on the preferentially formed crystal planes. A deep study is necessary to understand the mechanisms of inhibition as the four inhibitors tested exhibit different behaviour according to the crystal planes considered.

Chapter 9
Future work

9.1 Introduction

This thesis was focused on the mechanisms of inhibition of green and non-green chemicals and some new conclusions have been raised from this work. Nevertheless some aspects need to be given some attention to fully understand the mechanism of calcium carbonate formation and inhibition. This chapter aims to introduce some studies which could be conducted to improve the solutions brought to the industry to reduce calcium carbonate formation.

9.2 Calcareous surfaces

It has been shown in this thesis that the behaviour of a chemical can vary according to the presence of crystals of calcium carbonate on the surface. This aspects of this study is important as the industrial surfaces can be very hard to clear from any calcareous layer already present before applying an anti-scaling treatment. The scale inhibitors studied showed great interactions with calcium carbonate. The formation of film of inhibitor onto a surface covered of a calcareous deposit could be a strategy to reduce the scaling problems especially when the risk of scale deposition occurs in a natural environment.

9.3 Combination of different inhibitors

Calcium carbonate occurs according to two main steps: nucleation and growth of the crystals. This study confirmed that the scale inhibitors act generally during both steps but it appears that PMA acts more on the growth of the crystals rather than the PA which showed interesting nucleation inhibition properties. The combination of inhibitors with different strategies (either nucleation inhibitor or growth inhibitor) could offer a better inhibition and it might exist a concentration for which the scale inhibition is optimum. The study of the synergic effects of different chemicals could bring new inhibition properties from additives which are already used in the field.

9.4 Kinetics model

The SXRD is a great tool to study the kinetics of scale formation and inhibition. Some *ex-situ* analyses could help to build a kinetic model. Some parameters like the weight of the deposit formed could give important data to link to the increase of the diffracted intensity with the amount of scale. Microscopic observations of the scale produced could provide important information on the changes of morphology and disposition of the crystals. The set-up used allows the variations of some key parameters in the calcium carbonate formation like the temperature, the flow rate and the pressure. This would lead to conditions closer to the field.

A kinetics model taking into account more realistic conditions would provide a great tool to the industry to predict the scale formation and therefore more adapted treatment could be planned.

9.5 Anti-scaling surfaces

The significant role of the interactions between the surface of deposition and the scale inhibitors has been pointed out in this study. Inhibition of $CaCO_3$ formation results from the coverage of the substrate by an inhibitor film. The modifications of the surface properties either physical or chemical could be an efficient strategy to inhibit scale formation even though the design of anti-scaling surfaces remains a major challenge. The changes of the surface properties could lead to a variation of the adhesion of the crystals on the surface and therefore the flow rate applied in the pipes for example could be sufficient to reduce the problems of flow assurance. The addition of a chemical treatment to these anti-scaling surface could be an efficient and environmental friendly (if combined with a green chemical) way to inhibit scale. The anti-scaling surfaces would be very interesting to study with the SXRD as a full mechanism of calcium carbonate formation could be obtained.

References

1. www.eia.doe.gov/oiaf/ieo/index.html.
2. Uren, L.C., *Petroleum Production Engineering; Oil field Exploitation.* Third ed, ed. M.-H.B. Company. 1953.
3. Wilson, D. and B.J. Hepburn, *An Alternative Polymer for Squeeze Treatments.* Corrosion, NACE conference, 1997. paper no 172.
4. http://www.pipetech.no/aquamilling.asp.
5. http://www.pet.hw.ac.uk/research/fast1/reasearch/squeeze.htm.
6. Stamatakis, E., C. Chatzichristos, J. Sagen, A.K. Stubos, I. Palyvos, J. Muller, and J.A. Stokkan, *An integrated radiotracer approach for the laboratory evaluation of scale inhibitors performance in geological environments.* Chemical Engineering Science, 2006. 61(21): p. 7057-7067.
7. Chen, T., *New Insights into the Mechanisms of Calcium Carbonate Mineral Scale Formation and Inhibition.* Thesis, 2005.
8. Jordan, M., K. Sjuraether, I.R. Collins, N. Feasey and D. Emmons. *Life cycle management of scale control within subsea fields and its impact on flow assurance, Gulf of Mexico and the North Sea basin.* in *Chemistry in the oil industry VII.* 2001. Manchester, UK: The Royal Society of Chemistry.
9. Al-Anezi, K. and N. Hilal, *Scale formation in desalination plants: effect of carbon dioxide solubility.* Desalination, 2007. 204(1-3): p. 385-402.
10. Devos, O., C. Gabrielli, M. Tlili and B. Tribollet, *Nucleation-growth process of scale electrodeposition - Influence of the supersaturation.* Journal Of The Electrochemical Society, 2003. 150(7): p. C494-C501.
11. Hui, F. and J. Ledion, *Evaluation methods for the scaling power of water.* Journal European of Water Quality, 2002. T 33: p. Fasc. 1.
12. Luft, J.R. and G.T. DeTitta, *A method to produce microseed stock for use in the crystallization of biological macromolecules.* Acta crystallographica, 1999. D55: p. 988-993.
13. Dalas, E. and P.G. Koutsoukos, *The effect of magnetic fields on calcium carbonate scale formation.* Journal of Crystal Growth, 1989. 96(4): p. 802.
14. Sohnel, O. and J.W. Mullin, *Precipitation of calcium carbonate.* Journal of Crystal Growth, 1982. 60(2): p. 239.
15. Sohnel, O. and J.W. Mullin, *Interpretation of crystallization induction periods.* Journal of Colloid and Interface Science, 1988. 123(1): p. 43.
16. Gill, J.S. and G.H. Nancollas, *Kinetics of growth of calcium sulfate crystals at heated metal surfaces.* Journal of Crystal Growth, 1980. 48(1): p. 34-40.
17. Mullin, J.W., *Crystallization.* 1961: Butterworth & Co. 268.
18. Tomson, M.B., *Effect of precipitation inhibitors on calcium carbonate scale formation.* Journal of Crystal Growth, 1983. 62(1): p. 106-112.
19. Davis, R.V., P.W. Carter, M.A. Kamrath, D.A. Johnson and P.E. Reed, *The Use of Modern Methods in the Development of Calcium Carbonate Inhibitors for Cooling Water Systems.* Mineral Scale Formation and Inhibition, 1995.
20. Dirksen, J.A. and T.A. Ring, *Fundamental of crystallization: Kinetic effects on particle size distributions and morphology.* Chemical Engineering Sciences, 1991 46(10): p. 2389-2427.

21. Gabrielli, C., G. Maurin, G. Poindessous and R. Rosset, *Nucleation and growth of calcium carbonate by an electrochemical scaling process.* Journal of Crystal Growth, 1999. 200(1-2): p. 236.
22. Sohnel, O. and J. Garside, *Precipitation_Basic principles and industrial applications.* 1992.
23. Packter, A., *The Precipitation of Sparingly Soluble Alkaline-earth Metal and Lead Salts : Nucleation and Growth Orders during the Induction Period.* Journal of Chemsitry Society (A), 1968: p. 859-862.
24. Euvrard, M., F. Membrey, C. Filiatre and A. Foissy, *Crystallization of calcium carbonate at a solid/liquid interface examined by reflection of a laser beam.* Journal of crystal growth, 2004. 265( ): p. 332-330.
25. Vere, A.W., *Crystal growth: principles and progree*, ed. P.J. Dobson. 1987: Plenum Press. 258.
26. Nancollas, G.H., *The growth of crystals in solution.* Advances in Colloid and Interface Science, 1979. 10(1): p. 215-252.
27. Stumm, W. and J.J. Morgan, *Aquatic chemistry : an introduction emphasizing chemical equilibria in natural waters* 1970: p. 233.
28. Nancollas, G.H., *Kinetics of crystal growth from solution.* Journal of Crystal Growth, 1968. 3-4: p. 335-339.
29. Nancollas, G.H. and M.M. Reddy, *The crystallization of calcium carbonate. II. Calcite growth mechanism.* Journal of Colloid and Interface Science, 1971. 37(4): p. 824.
30. Barrett, C.S., *Structure of metals:crystallographic methods, principles and data.* 2nd edition ed. 1952: New York; London: Mc Graw Hill.
31. Graf, D.L., *Crystallographic tables for the rhombohedral carbonates.* The american mineralogist, 1961. 46: p. 1283-1316.
32. Villiers, J.P.R.d., *Crystal structure of aragonite, strontianite and witherite.* The american mineralogist, 1971. 56: p. 758-767.
33. Kahmi, S.R., *On the structure of vaterite $CaCO_3$.* Acta Crystallographica, 1963. 16: p. 770-772.
34. http://webmineral.com.
35. Peric, J., M. Vucak, R. Krstulovic, L. Brecevic and D. Kralj, *Phase transformation of calcium carbonate polymorphs.* Thermochimica Acta, 1996. 277: p. 175-186.
36. Chakraborty, D., V.K. Agarwal, S.K. Bhatia and J. Bellare, *Steady-State Transitions and Polymorph Transformations in Continuous Precipitation of Calcium Carbonate.* Ind. Eng. Chem. Res., 1994. 33(9): p. 2187-2197.
37. Altay, E., T. Shahwan and M. Tanoglu, *Morphosynthesis of CaCO3 at different reaction temperatures and the effects of PDDA, CTAB, and EDTA on the particle morphology and polymorph stability.* Powder Technology, 2007. 178(3): p. 194-202.
38. Han, Y.S., G. Hadiko, M. Fuji and M. Takahashi, *Factors affecting the phase and morphology of CaCO3 prepared by a bubbling method.* Journal of the European Ceramic Society, 2006. 26(4-5): p. 843-847.
39. Chen, P.-C., C.Y. Tai and K.C. Lee, *Morphology and growth rate of calcium carbonate crystals in a gas-liquid-solid reactive crystallizer.* Chemical Engineering Science, 1997. 52(21-22): p. 4171-4177.
40. Clifford Y. Tai, F.B.C., *Polymorphism of CaCO3, precipitated in a constant-composition environment.* AIChE Journal, 1998. 44(8): p. 1790-1798.

41. Park, W.K., S.-J. Ko, S.W. Lee, K.-H. Cho, J.-W. Ahn, and C. Han, *Effects of magnesium chloride and organic additives on the synthesis of aragonite precipitated calcium carbonate.* Journal of Crystal Growth, 2008. 310(10): p. 2593-2601.
42. Xie, A.-j., Y.-h. Shen, X.-y. Li, Z.-w. Yuan, L.-g. Qiu, C.-y. Zhang, and Y.-f. Yang, *The role of Mg2+ and Mg2+/amino acid in controlling polymorph and morphology of calcium carbonate crystal.* Materials Chemistry and Physics, 2007. 101(1): p. 87-92.
43. Gutjahr, A., H. Dabringhaus and R. Lacmann, *Studies of the growth and dissolution kinetics of the CaCO3 polymorphs calcite and aragonite II. The influence of divalent cation additives on the growth and dissolution rates.* Journal of Crystal Growth, 1996. 158(3): p. 310.
44. Meldrum, F.C. and S.T. Hyde, *Morphological influence of magnesium and organic additives on the precipitation of calcite.* Journal of Crystal Growth, 2001. 231(4): p. 544-558.
45. Marin-Cruz, J., E. Garcia-Figueroa, M. Miranda-Hernandez and I. Gonzalez, *Electrochemical treatments for selective growth of different calcium carbonate allotropic forms on carbon steel.* Water Research, 2004. 38(1): p. 173.
46. Westin, K.J. and A.C. Rasmuson, *Crystal growth of aragonite and calcite in presence of citric acid, DTPA, EDTA and pyromellitic acid.* Journal of Colloid and Interface Science, 2005. 282(2): p. 359.
47. Jaouhari, R., A. Benbachir, A. Guenbour, C. Gabrielli, J. Garcia-Jareno, and G. Maurin, *Influence of Water Composition and Substrate on Electrochemical Scaling.* Journal of The Electrochemical Society, 2000. 147(6): p. 2151-2161.
48. Wang, Z., *Mineral scale formation - Aspects of surface energy and adhesion,* School of Mechanical Engineering, University of Leeds, PhD, 2006, 272
49. Kralj, K.D. and N. Vdović, *The influence of some naturally occuring minerals on the precipitation of calcium carbonate polymorphs.* Water Research 2000. 34(1): p. 179-184.
50. Chen, T., A. Neville and M. Yuan, *Calcium carbonate scale formation--assessing the initial stages of precipitation and deposition.* Journal of Petroleum Science and Engineering, 2005. 46(3): p. 185.
51. Grases, F. and J.G. March, *Determination of phosphate based on inhibition of crystal growth of calcite.* Analytica Chimica Acta, 1990. 229: p. 249-254.
52. Lin, Y.-P. and P.C. Singer, *Inhibition of calcite crystal growth by polyphosphates.* Water Research, 2005. 39(19): p. 4835-4843.
53. Lin, Y.-P. and P.C. Singer, *Inhibition of calcite precipitation by orthophosphate: Speciation and thermodynamic considerations.* Geochimica et Cosmochimica Acta, 2006. 70(10): p. 2530.
54. Manoli, F., J. Kanakis, P. Malkaj and E. Dalas, *The effect of aminoacids on the crystal growth of calcium carbonate.* Journal of Crystal Growth, 2002. 236(1-3): p. 363-370.
55. Ross, R.J., K.C. Low and J.E. Shannon, *Polyaspartate Scale Inhibitors - Biodegradable alternatives to polyacrylates.* Corrosion, NACE conference, 1996. paper no 162.
56. Verraest, D.L., J.A. Peters, H. Van Bekkum and G.M. Van Rosmalen, *Carboxymethyl Inulin: A New Inhibitor for Calcium Carbonate Precipitation.* Journal Of the American Oil Chemists' Society, 1996. 73(1): p. 55-62.

57. Butt, F.H., F. Rahman and U. Baduruthamal, *Evaluation of SHMP and advanced scale inhibitors for control of CaSO4, SrSO4, and CaCO3 scales in RO desalination.* Desalination, 1997. 109(3): p. 323-332.
58. Abdel-Aal, N. and K. Sawada, *Inhibition of adhesion and precipitation of CaCO3 by aminopolyphosphonate.* Journal of Crystal Growth, 2003. 256(1-2): p. 188-200.
59. Tantayakom, V., T. Sreethawong, H.S. Fogler, F.F. de Moraes and S. Chavadej, *Scale inhibition study by turbidity measurement.* Journal of Colloid and Interface Science, 2005. 284(1): p. 57.
60. He, S., A.T. Kan and M.B. Tomson, *Inhibition of calcium carbonate precipitation in NaCl brines from 25 to 90[deg]C.* Applied Geochemistry, 1999. 14(1): p. 17.
61. Euvrard, M., P. Leroy and J. Ledion, *Effects and consequences of electric treatment in preventing scaling of drinking water system.* J Water SRT_Aqua, 1997. 46(2): p. 71-83.
62. O'Sullivan, C.K. and G.G. Guilbault, *Commercial quartz crystal microbalances - theory and applications.* Biosensors and Bioelectronics, 1999. 14(8-9): p. 663.
63. Abdel-Aal, N., K. Satoh and K. Sawada, *Study of the adhesion mechanism of CaCO3 using a combined bulk chemistry/QCM technique.* Journal of Crystal Growth, 2002. 245(1-2): p. 87.
64. Abdel-Aal, N., K. Satoh and K. Sawada, *Study of Adhesion of Mechanism of Calcareous Scaling by Using Quartz Crystal Microbalance Technique.* Analytical sciences, 2001. 17: p. i825-i828.
65. Yang, Q., Y. Liu, A. Gu, J. Ding and Z. Shen, *Investigation of Calcium Carbonate Scaling Inhibition and Scale Morphology by AFM.* Journal of Colloid and Interface Science, 2001. 240(2): p. 608.
66. Hasson, D., R. Semiat, D. Bramson, M. Busch and B. Limoni-Relis, *Suppression of CaCO3 scale deposition by anti-scalants.* Desalination, 1998. 118(1-3): p. 285.
67. Dyer, S.J. and G.M. Graham, *The effect of temperature and pressure on oilfield scale formation.* Journal of Petroleum Science and Engineering, 2002. 35(1-2): p. 95.
68. Bazin, B., N. Kohler, A. Zaitoun, T. Johnson and H. Raaijmakers, *A new class of green mineral scale inhibitors for squeeze treatments.* International Symposium on Oilfield Scale, Aberdeen., 2004. SPE 87453.
69. Yuan, M.D., E. Jamieson and P. Hammonds, *Investigation of scaling and inhibition mechanisms and the influencing factors in static and dynamic inhibition tests.* Corrosion, NACE conference, 1998. Paper No 67.
70. Smith, J.K., J. Hammons, G. Boyd and Q.F. Fu. *Performance of scale inhibitors under carbonate and sulfide scaling conditions.* in *SPE International Oilfield Scale Conference.* 2008. Aberdeen, UK.
71. Zhang, Y., H. Shaw, R. Farquhar and R. Dawe, *The kinetics of carbonate scaling--application for the prediction of downhole carbonate scaling.* Journal of Petroleum Science and Engineering, 2001. 29(2): p. 85.
72. Hennessy, A., G. Graham, J. Hastings, D.P. Siddons and Z. Zhong, *New pressure flow cell to monitor BaSO4 precipitation using synchrotron in situ angle-dispersive X-ray diffraction.* Journal of Synchrotron Radiation, 2002. 9: p. 323-324.

73. Chen, T., N. Anne, S. Ken and Z. Zhong, *Using synchroton radiation (WAXS) to study the inhibition effect of polyphoscarboxylic acid (PPCA) on CaCO3 scale formation.* CORROSION, 2006. Paper 06386(NACE).
74. Jones, F., P. Jones, R. De Marco, B. Pejcic and A.L. Rohl, *Understanding barium sulfate precipitation onto stainless steel.* Applied Surface Science, 2008. 254(11): p. 3459-3468.
75. Ledion, J., P. Leroy and J.P. Labbe, *Determination du Caractere Incrustant d'une Eau par un Essai d'Entartrage Accelere*
T.S.M., 1985. No 7-8 July-August: p. 323-328.
76. Barchiche, C., C. Deslouis, D. Festy, O. Gil, P. Refait, S. Touzain, and B. Tribollet, *Characterization of calcareous deposits in artificial seawater by impedance techniques: 3--Deposit of CaCO3 in the presence of Mg(II).* Electrochimica Acta, 2003. 48(12): p. 1645.
77. Barchiche, C., C. Deslouis, O. Gil, P. Refait and B. Tribollet, *Characterisation of calcareous deposits by electrochemical methods: role of sulphates, calcium concentration and temperature.* Electrochimica Acta, 2004. 49(17-18): p. 2833.
78. Gabrielli, C., M. Keddam and H. Perrot, *Characterization of the efficiency of antiscale treatments of water Part I: Chemical processes* Jounal of applied electrochemistry, 1996. 26(11): p. 1125-1132.
79. Devos, O., C. Gabrielli and B. Tribollet, *Simultaneous EIS and in situ microscope observation on a partially blocked electrode application to scale electrodeposition.* Electrochimica Acta, 2006. 51(8-9): p. 1413.
80. Deslouis, C., C. Gabrielli, M. Keddam, A. Khalil, R. Rosset, B. Tribollet, and M. Zidoune, *Impedance techniques at partially blocked electrodes by scale deposition.* Electrochimica Acta, 1997. 42(8): p. 1219.
81. Deslouis, C., D. Festy, O. Gil, V. Maillot, S. Touzain, and B. Tribollet, *Characterization of calcareous deposits in artificial sea water by impedances techniques: 2-deposit of Mg(OH)2 without CaCO3.* Electrochimica Acta, 2000. 45(11): p. 1837.
82. Devos, O., C. Gabrielli and B. Tribollet, *Nucleation-growth process of scale electrodeposition--Influence of the mass transport.* Electrochimica Acta, 2006. 52(1): p. 285.
83. Gabrielli, C., M. Keddam, A. Khalil, R. Rosset and M. Zidoune, *Study of calcium carbonate scales by electrochemical impedance spectroscopy.* Electrochimica Acta, 1997. 42(8): p. 1207.
84. Garcia, C., G. Courbin, F. Ropital and C. Fiaud, *Study of the scale inhibition by HEDP in a channel flow cell using a quartz crystal microbalance.* Electrochimica Acta, 2001. 46(7): p. 973-985.
85. Neville, A., T. Hodgkiess and A.P. Morizot, *Electrochemical assessment of calcium carbonate deposition using a rotating disc electrode (RDE).* Journal of Applied Electrochemistry, 1999. 29(4): p. 455.
86. Morizot, A., A. Neville and T. Hodgkiess, *Studies of the deposition of CaCO3 on a stainless steel surface by a novel electrochemical technique.* Journal of Crystal Growth, 1999. 198-199(Part 1): p. 738.
87. Morizot, A.P. and A. Neville, *Insights into Electrodeposition of an Inhibitor Film and Its Inhibitive Effects on Calcium Carbonate Deposition.* Journal of Colloid and Interface Science, 2002. 245(1): p. 40.

88. Neville, A. and A.P. Morizot, *Calcareous scales formed by cathodic protection--an assessment of characteristics and kinetics.* Journal of Crystal Growth, 2002. 243(3-4): p. 490.
89. Gabrielli, C., R. Jaouhari, M. Keddam and G. Maurin, *An electrochemical method for testing the scaling susceptibility of insulating materials.* Journal of Electrochemical Society, 2001. 148(12): p. B517-B521.
90. Euvrard, M., C. Filiatre and E. Crausaz, *A cell to study in situ electrocrystallization of calcium carbonate.* Journal of Crystal Growth, 2000. 216(1-4): p. 466.
91. Euvrard, M., F. Membrey, C. Filiatre, C. Pignolet and A. Foissy, *Kinetic study of the electrocrystallization of calcium carbonate on metallic substrates.* Journal of Crystal Growth, 2006. 291(2): p. 428.
92. Moussa, S.B., G. Maurin, C. Gabrielli and M.B. Armor, *Electrochemical precipitation of struvite.* Electrochemical and Solid-State Letters, 2006. 9(6): p. C97-C101.
93. Amor, M.B., D. Zgolli, M.M. Tlili and A.S. Manzola, *Influence of water hardness, substrate nature and temperature on heterogeneous calcium carbonate nucleation.* Desalination, 2004. 166: p. 79.
94. Teng, H.H., P.M. Dove and J.J. De Yoreo, *Kinetics of calcite growth: surface processes and relationships to macroscopic rate laws.* Geochimica et Cosmochimica Acta, 2000. 64(13): p. 2255-2266.
95. Pina, C.M., M. Enders and A. Putnis, *The composition of solid solutions crystallising from aqueous solutions: the influence of supersaturation and growth mechanisms.* Chemical Geology, 2000. 168(3-4): p. 195.
96. Hu, Z. and Y. Deng, *Supersaturation control in aragonite synthesis using sparingly soluble calcium sulfate as reactants.* Journal of Colloid and Interface Science, 2003. 266(2): p. 359-365.
97. Hu, Z. and Y. Deng, *Synthesis of needle-like aragonite from calcium chloride and sparingly soluble magnesium carbonate.* Powder Technology, 2004. 140(1-2): p. 10-16.
98. Cheng, B., M. Lei, J. Yu and X. Zhao, *Preparation of monodispersed cubic calcium carbonate particles via precipitation reaction.* Materials Letters, 2004. 58(10): p. 1565-1570.
99. Feng, B., A.K. Yong and H. An, *Effect of various factors on the particle size of calcium carbonate formed in a precipitation process.* Materials Science and Engineering: A, 2007. 445-446: p. 170-179.
100. Yu, J., M. Lei, B. Cheng and X. Zhao, *Effects of PAA additive and temperature on morphology of calcium carbonate particles.* Journal of Solid State Chemistry, 2004. 177(3): p. 681.
101. Helmut Cölfen, L.Q., *A Systematic Examination of the Morphogenesis of Calcium Carbonate in the Presence of a Double-Hydrophilic Block Copolymer.* Chemistry, 2001. 7(1): p. 106-116.
102. Weyl, P.K., *The change in solubility of calcium carbonate with temperature and carbon dioxide content.* Geochimica et Cosmochimica Acta, 1959. 17(3-4): p. 214.
103. Gryta, M., *Alkaline scaling in the membrane distillation process.* Desalination, 2008. 228(1-3): p. 128-134.
104. Karabelas, A.J., *Scale formation in tubular heat exchangers--research priorities.* International Journal of Thermal Sciences, 2002. 41(7): p. 682.

105. Andritsos, N., A.J. Karabelas and P.G. Koutsoukos, *Morphology and Structure of CaCO₃ Scale Layers Formed under Isothermal Flow Conditions.* Langmuir, 1997. 13(10): p. 2873-2879.
106. Lin, S.H. and S.C. Dexter, *Effects of temperature and magnesium ions on calcareous deposition.* Corrosion, 1988. 44(9): p. 615-622.
107. Berner, R.A., *The role of magnesium in the crystal growth of calcite and aragonite from sea water.* Geochimica et Cosmochimica Acta, 1975. 39(4): p. 489.
108. Dickinson, S.R., G.E. Henderson and K.M. McGrath, *Controlling the kinetic versus thermodynamic crystallisation of calcium carbonate.* Journal of Crystal Growth, 2002. 244(3-4): p. 369-378.
109. Deleuze, M. and S.L. Brantley, *Inhibition of calcite crystal growth by Mg2+ at 100°C and 100 bars: Influence of growth regime.* Geochimica et Cosmochimica Acta, 1997. 61(7): p. 1475-1485.
110. Damir Kralj, J.K.L.B., ccaron, evi, cacute and G.F.V. Nöthig-Laslo, *Effect of Inorganic Anions on the Morphology and Structure of Magnesium Calcite.* Chemistry - A European Journal, 2004. 10(7): p. 1647-1656.
111. Zhang, Y. and R.A. Dawe, *Influence of Mg2+ on the kinetics of calcite precipitation and calcite crystal morphology.* Chemical Geology, 2000. 163(1-4): p. 129.
112. Chen, T., A. Neville and M. Yuan, *Influence of Mg^{2+} on initial stages of $CaCO_3$ scale formed on metal surface.* Chemical Research in Chinese Universities, 2004. 20(4): p. 381-385.
113. Chen, T., A. Neville and M. Yuan, *Influence of Mg2+ on CaCO3 formation--bulk precipitation and surface deposition.* Chemical Engineering Science, 2006. 61(16): p. 5318.
114. Chen, T., A. Neville and M. Yuan, *Assessing the effect of Mg2+ on CaCO3 scale formation-bulk precipitation and surface deposition.* Journal of Crystal Growth, 2005. 275(1-2): p. e1341-e1347.
115. Roques, H., *Chemical Water Treatment: Principles adn Practice.* 1996: VCH Publishers. 620.
116. Hausner, D.B., R.J. Reeder and D.R. Strongin, *Humidity-induced restructuring of the calcite surface and the effect of divalent heavy metals.* Journal of Colloid and Interface Science, 2007. 305(1): p. 101-110.
117. Ghizellaoui, S., M. Euvrard, J. Ledion and A. Chibani, *Inhibition of scaling in the presence of copper and zinc by various chemical processes.* Desalination, 2007. 206(1-3): p. 185.
118. Lopez-Sandoval, E., C. Vazquez-Lopez, B.E. Zendejas-Leal, G. Ramos, E. San Martin-Martinez, N. Munoz Aguirre, and E. Reguera, *Calcium carbonate scale inhibition using the "allotropic cell" device.* Desalination, 2007. 217(1-3): p. 85-92.
119. Meyer, H.J., *The influence of impurities on the growth rate of calcite.* Journal of Crystal Growth, 1984. 66(3): p. 639-646.
120. Pernot, B., M. Euvrard and P. Simon, *Effects of iron and manganese on the scaling potentiality of water.* J Water SRT_Aqua, 1998. 47(1): p. 21-29.
121. Manoli, F., S. Koutsopoulos and E. Dalas, *Crystallization of calcite on chitin.* Journal of Crystal Growth, 1997. 182(1-2): p. 116-124.
122. Dalas, E., P.G. Klepetsanis and P.G. Koutsoukos, *Calcium Carbonate Deposition on Cellulose.* Journal of Colloid and Interface Science, 2000. 224(1): p. 56-62.

123. Dalas, E. and P.G. Koutsoukos, *The crystallization of vaterite on cholesterol.* Journal of Colloid and Interface Science, 1989. 127(1): p. 273-280.
124. Dalas, E., J. Kallitsis and P.G. Koutsoukos, *The crystallization of calcium carbonate on polymeric substrates.* Journal of Crystal Growth, 1988. 89(2-3): p. 287.
125. Sabbides, T.G. and P.G. Koutsoukos, *The crystallization of calcium carbonate in artificial seawater; role of the substrate.* Journal of Crystal Growth, 1993. 133(1-2): p. 13.
126. MacAdam, J. and S.A. Parsons, *Scaling on heat transfer surfaces: chemical versus non chemical control.* Corrosion 04073, 2004.
127. Doyle, J.D., K. Oldring, J. Churchley and S.A. Parsons, *Struvite formation and the fouling propensity of different materials.* Water Research, 2002. 36(16): p. 3971-3978.
128. Mantel, K.E., W.H. Hartt and T.Y. Chen, *Substrate, Surface Finish, and Flow Rate Influences on Calcareous Deposit Structure.* Corrosion, 1992. 48(6): p. 489-500.
129. Gunn, D.J., *Effect of surface roughness on the nucleation and growth of calcium sulphate on metal surfaces.* Journal of Crystal Growth, 1980. 50(2): p. 533.
130. Keysar, S., R. Semiat, D. Hasson and J. Yahalom, *Effect of Surface Roughness on the Morphology of Calcite Crystallizing on Mild Steel.* Journal of Colloid and Interface Science, 1994. 162(2): p. 311-319.
131. Quddus, A. and A.-H.L. M, *Influence of solution hydrodynamics on the deposition of CaSO4 scale on aluminium.* Desalination, 2007.
132. Quddus, A., *Effect of hydrodynamics on the deposition of CaSO4 scale on stainless steel.* Desalination, 2002. 142(1): p. 57-63.
133. Quddus, A. and I.M. Allam, *BaSO4 scale deposition on stainless steel.* Desalination, 2000. 127(3): p. 219-224.
134. Hasson, D., M. Avriel, W. Resnick, T. Rozenman and S. Windreich, *Mechanism of Calcium Carbonate Scale Deposition on Heat-Transfer Surfaces.* Ind. Eng. Chem. Fund., 1968. 7(1): p. 59-65.
135. Hasson, D., D. Bramson, B. Limoni-Relis and R. Semiat, *Influence of the flow system on the inhibitory action of CaCO3 scale prevention additives.* Desalination, 1997. 108(1-3): p. 67.
136. Freedman, A.J., *Cooling Water Technology in the Eighties.* Corrosion, NACE conference, 1983. No 273.
137. Jordan, M.M., K. Sjuraether, G. Seland and H. Gilje, *The use of scale inhibitor squeeze placement software to extend squeeze life and reduce operating cost in mature high temperature oilfields.* Corrosion 2000, 2000. Paper no 00106.
138. Morizot, A.P., *Electrochemically Based Study of Mineral Scale Formation and Inhibition.* Thesis, 1999: p. 351.
139. Cooper, K.G., L.G. Hanlon, G.M. Smart and R.E. Talbot, *The threshold scale inhibition phenomenon.* Desalination, 1979. 31(1-3): p. 257.
140. van der Leeden, M.C. and G.M. van Rosmalen, *Adsorption Behavior of Polyelectrolytes on Barium Sulfate Crystals.* Journal of Colloid and Interface Science, 1995. 171(1): p. 142-149.
141. Benton, W.J., I.R. Collins, I.M. Grimsey, G.M. Parkinson and S.A. Rodger, *Nucleation, growth and inhibition of barium sulfate-controlled modification with organic and inorganic additives.* Faraday Discussion, 1993. 95: p. 281-297.

142. http://www.chemtexcorp.com/docarchive/pub/TT-22%20How%20Polymers%20Work.DOC.
143. Schwamborn, M., *Chemical Synthesis of Polyaspartates: a biodegradable alternative to currently used polycarboxylate homo- and copolymers.* Polymer Degradation and Stability, 1998. 59: p. 39-45.
144. Reddy, M.M. and G.H. Nancollas, *Calcite crystal growth inhibition by phosphonates.* Desalination, 1973. 12(1): p. 61.
145. Graham, G.M., L.S. Boak and K. Sorbie. *The influence of formation calcium and magnesium on the effectiveness of generically different barium sulphate oilfield scale inhibitors.* in *International symposium on Oilfield Chemistry.* 1997. Houston, USA.
146. Rabaioli, M.R. and T.P. Lockhart, *Solubility and phase behavior of polyacrylate scale inhibitors.* Journal of Petroleum Science and Engineering, 1996. 15(2-4): p. 115-126.
147. Hess, A.N. and Y.-P. Chin, *Physical and chemical characteristics of poly(maleic acid), a synthetic organic colloid analog.* Colloids and Surfaces A: Physicochemical and Engineering Aspects, 1996. 107: p. 141.
148. Vdovic, N. and D. Kralj, *Electrokinetic properties of spontaneously precipitated calcium carbonate polymorphs: the influence of organic substances.* Colloids and Surfaces A: Physicochemical and Engineering Aspects, 2000. 161(3): p. 499-505.
149. Wilkins, S.J., R.G. Compton and H.A. Viles, *The Effect of Surface Pretreatment with Polymaleic Acid, Phosphoric Acid, or Oxalic Acid on the Dissolution Kinetics of Calcium Carbonate in Aqueous Acid.* Journal of Colloid and Interface Science, 2001. 242(2): p. 378.
150. Thompson, M., S.J. Wilkins, R.G. Compton and H.A. Viles, *Channel flow cell studies on the evaluation of surface pretreatments using phosphoric acid or polymaleic acid for calcite stone protection.* Journal of Colloid and Interface Science, 2003. 259(2): p. 338.
151. Estievenart, C., N. Kohler, F. Ropital and C. Fiaud, *Mechanisms of Scale and Corrosion Inhibition by Polyaspartate.* Corrosion, 2004. Paper no 04536.
152. Estievenart, C., N. Kohler, F. Ropital and C. Fiaud. *Polyaspartates: influence of synthetic routes on scale inhibition and biodegradability.* in *NACE Corrosion 2002 conference.* 2002. Denver, USA.
153. Li, H.-Y., W. Ma, L. Wang, R. Liu, L.-S. Wei, and Q. Wang, *Inhibition of calcium and magnesium-containing scale by a new antiscalant polymer in laboratory tests and a field trial.* Desalination, 2006. 196(1-3): p. 237-247.
154. Johannsen, F.R., *Toxicological profile of carboxymethyl inulin.* Food and Chemical Toxicology, 2003. 41(1): p. 49.
155. Demadis, K.D. and A. Stathoulopoulou, *Multifunctional, Environmentally Friendly Additives for Control of Inorganic Foulants in Industrial Water and Process Applications.* Materials sciences, 2006: p. 40-44.
156. Demadis, K.D., E. Neofotistou, E. Mavredaki, M. Tsiknakis, E.-M. Sarigiannidou, and S.D. Katarachia, *Inorganic foulants in membrane systems: chemical control strategies and the contribution of "green chemistry".* Desalination, 2005. 179(1-3): p. 281-295.
157. Anastas, P.T. and J.C. Warner, *Green Chemistry: Theory and Practice.* 1998: p. 11.
158. Darling, D. and R. Rakshpal, *Green Chemistry Applied to Corrosion and Scale Inhibitors.* Material Performance, 1998. 37(12): p. 42-45.

159. Commission, M.M.o.t.O., *2003 Strategies of the OSPAR Commission for the Protection of the Marine Environment of the North-East Atlantic.* Bremen: 25 june 2003. Reference Number:2003-21.
160. Killaars, J., J. Hall and D. Whitfill, *Step Change in Development of Environmentally Responsible Chemicals.* 10th Annual International Petroleum Environmental Conference 2003.
161. Lioliou, M.G., C.A. Paraskeva, P.G. Koutsoukos and A.C. Payatakes, *Heterogeneous nucleation and growth of calcium carbonate on calcite and quartz.* Journal of Colloid and Interface Science, 2007. 308(2): p. 421-428.
162. Veazey, M.V., *Green Corrosion Inhibitors Come of Age.* Materials Performance, 2002. 41(8): p. 17-20.
163. http://toxics.usgs.gov/definitions/biodegradation.html.
164. http://toxics.usgs.gov/definitions/bioaccumulation.html.
165. Thatcher, M. and G. Payne, *Impact of the OSPAR Decision on the Harmonised Mandatory Control Scheme on the Offshore Chemical Supply Industry.* 2001.
166. http://www.cefas.co.uk/offshore-chemical-notification-scheme-(ocns).aspx).
167. Glover, S. and I. Still, *HMCS (Harmonised Mandatory Control Scheme) and the Issue of Substitution.* Ninth Annual International Petroleum Environmental Conference, 2002.
168. Sheahan, D.A., A.J. Millais, P. Neall, R.J. Rycroft, S. Thompson, M.A. Tolhurst, and L. Weiss. *Evaluation of the hazard and risk of chemicals used by the UK offshore oil and gas industry and the management and reduction of use of those considered of greatest environmental concern. Forecasting trends in chemical use and impacts.* in *Chemistry in the Oil Industry X.* 2007. Manchester, UK: The Royal Society of Chemistry, EOSCA.
169. Jordan, M., N. Feasey, C. Johnston, D. Marlow and M. Elrick. *Biodegradable scale inhibitors. Laboratory and field evaluation of "Green" carbonate and sulphate scale inhibitors with deployment histories in the North Sea.* in *Chemistry in the Oil Industry X.* 2007. Manchester, UK: The Royal Society of Chemistry, EOSCA.
170. Association, O.T.N.O.I., *The environmental efforts of the petroleum industry Facts and trends*, E. Report, Editor. 2007. p. 63.
171. *Metals handbook, 9th Edition.* Howard E. Boyer, Timothy L.Gall ed. 1997.
172. Bard, A. and L. Faulkner, *Electrochemical methods, fundamentals and applications*, ed. J.W. Sons. 1980. 718.
173. Beaunier, L., C. Gabrielli, G. Poindessous, G. Maurin and R. Rosset, *Investigation of electrochemical calcareous scaling: Nuclei counting and morphology.* Journal of Electroanalytical Chemistry, 2001. 501(1-2): p. 41.
174. Dastillung, R., *In-situ Analysis of Electrodeposited scale.* MPhil thesis, December 2002.
175. Bockris, J.O.M., N. Bonciocat and F. Gutmann, *An introduction to electrochemical science*, ed. F.R.S. Prof Sir Nevill Mott and G.R. Noakes. 1974, London: Wykeham Publications (London) Ltd. 134.
176. Coppens, P., *Synchrotron radiation Crystallography.* 1992: Academic press inc. 316.
177. Guinebretiere, R., *Diffraction des rayons X sur echantillons polycrystallins.* lavoisier ed, ed. S. edition. 2006: Hermes science 361.
178. Zhong, Z., C.C. Kao, D.P. Siddons and J.B. Hastings, *Sagittal focusing of high-energy synchrotron X-rays with asymmetric Laue crystals. II. Experimental studies.* Journal of applied crystallography, 2001. 34: p. 646-653.

179. crystallographers, I.u.o., *Commission on powder diffraction.* (Newsletter Number 26).
180. http://cds.dl.ac.uk/cds/datasets/crys/icsd/llicsd.html.
181. Geffroy, C., A. Foissy, J. Persello and B. Cabane, *Surface Complexation of Calcite by Carboxylates in Water.* Journal of Colloid and Interface Science, 1999. 211(1): p. 45.
182. Ledion, J., P. Leroy and J.P. Labbe, *Determination du Caractere Incrustant d'une Eau par un Essai d'Entartrage Accelere.* T.S.M., Juillet-aout 1985. No 7-8: p. 323-328.
183. Müller-Steinhagen, H. and Q. Zhao, *Investigation of low fouling surface alloys made by ion implantation technology.* Chemical Engineering Science, 1997. 52(19): p. 3321-3332.
184. Förster, M., W. Augustin and M. Bohnet, *Influence of the adhesion force crystal/heat exchanger surface on fouling mitigation.* Chemical Engineering and Processing, 1999. 38(4-6): p. 449-461.
185. Morizot, A. and A. Neville. *A study of inhibitor film formation using an electrochemical technique.* in *NACE Corrosion 2000 conference.* 2000. Houston.
186. Chen, T., A. Neville, K. Sorbie and Z. Zhong, *Using in situ synchrotron radiation wide angle X-ray scattering (WAXS) to study CaCO3 scale formation at ambient and elevated temperature.* Faraday Discussion, 2007. 136: p. 355-365.
187. Li, H., W. Liu and X. Qi, *Evaluation of a novel CaSO4 scale inhibitor for a reverse osmosis system.* Desalination, 2007. 214(1-3): p. 193-199.
188. Fleming, N., B.H. M, S.C. J and B.A. S. *Developpement of an ecofriendly scale inhibitor for harsh scaling environment.* in *International symposium on Oilfield Chemistry.* 2001. Houston, USA.
189. Drela, I., P. Falewicz and S. Kuczkowska, *New rapid test for evaluation of scale inhibitors.* Water Research, 1998. 32(10): p. 3188-3191.
190. Kjellin, P., *X-ray diffraction and scanning electron microscopy studies of calcium carbonate electrodeposited on a steel surface.* Colloids and Surfaces A: Physicochemical and Engineering Aspects, 2003. 212(1): p. 19.
191. Parlaktuna, M. and E. Okandan, *The use of chemical inhibitors for prevention of calcium carbonate scaling.* Geothermics, 1989. 18(1-2): p. 241-248.
192. Khalil, A., R. Rosset, C. Gabrielli, M. Keddam and H. Perrot, *Characterization of the effiency of antiscale treatments of water. Part II: Physical processes.* Journal of Applied Electrochemistry, 1996. 29: p. 339-346.
193. Wada, N., K. Kanamura and T. Umegaki, *Effects of Carboxylic Acids on the Crystallization of Calcium Carbonate.* Journal of Colloid and Interface Science, 2001. 233(1): p. 65.
194. Inches, C.E., K.S. Sorbie and K.E. Doueiri. *Green inhibitors: Mechanisms in the control of barium sulphate.* in *NACE International.* 2006.
195. Gómez-Morales, J., J. Torrent-Burgués and R. Rodríguez-Clemente, *Nucleation of calcium carbonate at different initial pH conditions.* Journal of Crystal Growth, 1996. 169(2): p. 331-338.
196. Choi, D.-J., S.-J. You and J.-G. Kim, *Development of an environmentally safe corrosion, scale, and microorganism inhibitor for open recirculating cooling systems.* Materials Science and Engineering A, 2002. 335(1-2): p. 228-235.
197. Nagayasu, T., C. Yoshioka, K. Imamura and K. Nakanishi, *Effects of carboxyl groups on the adsorption behavior of low-molecular-weight substances on a*

stainless steel surface. Journal of Colloid and Interface Science, 2004. 279(2): p. 296.

198. Compere, C., B.-F. M.-N, P. Bertrand, D. Costa, P. Marcus, C. Poleunis, C.-M. Pradier, B. Rondot, and M.G. Walls, *Kinetics of conditioning layer formation on stainless steel immersed in sea water.* Biofouling, 2001. 17(2): p. 129-145.
199. Kellner, R. and C. Weigel, *Pushing the limits of quantitative FTIR-microscopy.* Microchimica Acta, 1988. 94(1): p. 163-166.
200. Ulman, A., *Characterization of organic thin films.* Materials characterization series, ed. C.R. Brundle and C.A. Evans. 1995. 275.
201. Jackson, K.D.O. (1998) *A Guide to Identifying Common Fillers and Activators Using Vibrational Spectroscopy.* The Internet Journal of Vibrational Spectroscopy **Volume**, DOI: www.ijvs.com/volume2/edition3/section3.html
202. Imamura, K., T. Mimura, M. Okamoto, T. Sakiyama and K. Nakanishi, *Adsorption Behavior of Amino Acids on a Stainless Steel Surface.* Journal of Colloid and Interface Science, 2000. 229(1): p. 237-246.
203. Deslouis, C., I. Frateur, G. Maurin and B. Tribollet, *Interfacial pH measurement during the reduction of dissolved oxygen in a submerged impinging jet cell.* Journal of Applied Electrochemistry, 1997. 27(4): p. 482.
204. Cheong, W.C., A. Neville, P.H. Gaskell and S. Abbott. *Using nature to provide solutions to calcareous scale deposition.* in *SPE International Oilfield Scale Conference.* 2008. Aberdeen, UK.
205. Kitamura, M., *Controlling factor of polymorphism in crystallization process.* Journal of Crystal Growth, 2002. 237-239(Part 3): p. 2205-2214.
206. Lei, M., W.H. Tang, L.Z. Cao, P.G. Li and J.G. Yu, *Effects of poly (sodium 4-styrene-sulfonate) on morphology of calcium carbonate particles.* Journal of Crystal Growth, 2006. 294(2): p. 358-366.
207. Nan, Z., Z. Shi, B. Yan, R. Guo and W. Hou, *A novel morphology of aragonite and an abnormal polymorph transformation from calcite to aragonite with PAM and CTAB as additives.* Journal of Colloid and Interface Science, 2008. 317(1): p. 77-82.
208. Mao, Z. and J. Huang, *Habit modification of calcium carbonate in the presence of malic acid.* Journal of Solid State Chemistry, 2007. 180(2): p. 453-460.
209. Hou, W. and Q. Feng, *A simple method to control the polymorphs of calcium carbonate in CO2-diffusion precipitation.* Journal of Crystal Growth, 2005. 282(1-2): p. 214-219.
210. Ouhenia, S., D. Chateigner, M.A. Belkhir, E. Guilmeau and C. Krauss, *Synthesis of calcium carbonate polymorphs in the presence of polyacrylic acid.* Journal of Crystal Growth. In Press, Corrected Proof.
211. Shivkumara, C., P. Singh, A. Gupta and M.S. Hegde, *Synthesis of vaterite CaCO3 by direct precipitation using glycine and l-alanine as directing agents.* Materials Research Bulletin, 2006. 41(8): p. 1455-1460.
212. Wang, C., *Control the polymorphism and morphology of calcium carbonate precipitation from a calcium acetate and urea solution.* Materials Letters. In Press, Corrected Proof.
213. Cölfen, H., *Precipitation of carbonates: recent progress in controlled production of complex shapes.* Current Opinion in Colloid & Interface Science, 2003. 8(1): p. 23-31.
214. Xu, S., M. C.A, P. J.H and M.A. Kamrath, *Structure andmorphology of electrodeposited $CaCO_3$: X-ray diffraction and microscopy studies.* Journal of The Electrochemical Society, 1999. 146(9): p. 3315-3323.

215. Dawe, R.A. and Y. Zhang, *Kinetics of calcium carbonate scaling using observations from glass micromodels.* Journal of Petroleum Science and Engineering, 1997. 18(3-4): p. 179-187.
216. Al Nasser, W.N., A. Shaikh, C. Morriss, M.J. Hounslow and A.D. Salman, *Determining kinetics of calcium carbonate precipitation by inline technique.* Chemical Engineering Science, 2008. 63(5): p. 1381-1389.
217. Drach, G.W., S. Sarig, A.D. Randolph and S. Thorson, *The paradox of inhibition and enhancement of the formation of urinary stones.* Urological Research, 1982. 10(4): p. 165-168.